

**Unified power flow controller: Modeling, Stability
analysis, Control strategy and Control system
Design**

by

Kannan Sreenivasachar

A thesis

presented to the University of Waterloo

in fulfillment of the

thesis requirement for the degree of

Doctor of Philosophy

in

Electrical and Computer Engineering

Waterloo, Ontario, Canada, 2001

© Kannan Sreenivasachar 2001



**National Library
of Canada**

**Acquisitions and
Bibliographic Services**

**395 Wellington Street
Ottawa ON K1A 0N4
Canada**

**Bibliothèque nationale
du Canada**

**Acquisitions et
services bibliographiques**

**395, rue Wellington
Ottawa ON K1A 0N4
Canada**

Your file Votre référence

Our file Notre référence

The author has granted a non-exclusive licence allowing the National Library of Canada to reproduce, loan, distribute or sell copies of this thesis in microform, paper or electronic formats.

The author retains ownership of the copyright in this thesis. Neither the thesis nor substantial extracts from it may be printed or otherwise reproduced without the author's permission.

L'auteur a accordé une licence non exclusive permettant à la Bibliothèque nationale du Canada de reproduire, prêter, distribuer ou vendre des copies de cette thèse sous la forme de microfiche/film, de reproduction sur papier ou sur format électronique.

L'auteur conserve la propriété du droit d'auteur qui protège cette thèse. Ni la thèse ni des extraits substantiels de celle-ci ne doivent être imprimés ou autrement reproduits sans son autorisation.

0-612-60570-1

Canada

The University of Waterloo requires the signatures of all persons using or photocopying this thesis. Please sign below, and give address and date.

Abstract

Unified power flow controller (UPFC) has been the most versatile Flexible AC Transmission System (FACTS) device due to its ability to control real and reactive power flow on transmission lines while controlling the voltage of the bus to which it is connected. UPFC being a multi-variable power system controller it is necessary to analyze its effect on power system operation.

To study the performance of the UPFC in damping power oscillations using PSCAD-EMTDC software, a de-coupled control system has been designed for the shunt inverter to control the UPFC bus voltage and the DC link capacitor voltage. The series inverter of a UPFC controls the real power flow in the transmission line. One problem associated with using a high gain PI controller (used to achieve fast control of transmission line real power flow) for the series inverter of a UPFC to control the real power flow in a transmission line is the presence of low damping. This problem is solved in this research by using a fuzzy controller. A method to model a fuzzy controller in PSCAD-EMTDC software has also been described. Further, in order to facilitate proper operation between the series and the shunt inverter control system, a new real power coordination controller has been developed and its performance was evaluated.

The other problem concerning the operation of a UPFC is with respect to transmission line reactive power flow control. Step changes to transmission line reactive power references have significant impact on the UPFC bus voltage. To reduce the adverse effect of step changes in transmission line reactive power references on the UPFC bus voltage, a new reactive power coordination controller has been designed.

Transient response studies have been conducted using PSCAD-EMTDC software to show the improvement in power oscillation damping with UPFC. These simulations include the real and reactive power coordination controllers.

Finally, a new control strategy has been proposed for UPFC. In this proposed control strategy, the shunt inverter controls the DC link capacitor voltage and the transmission line reactive power flow. The series inverter controls the transmission line real power flow and the UPFC bus voltage. PSCAD-EMTDC simulations have been conducted to show the viability of the control strategy in damping power oscillations.

Acknowledgements

I would like to thank Dr. Shesha Kamal Jayaram, one of my thesis supervisors, for her help in seeing this thesis through to its completion. Dr. Jayaram has always shown professionalism, dedication and enthusiasm, and I am grateful for having had the opportunity to study and work under her supervision. I would also like to thank her for the financial assistance given to me during the period of my stay at Waterloo. I consider myself fortunate to have worked with such a dedicated, understanding, knowledgeable and humble professor.

I would also like to thank Dr. Magady Salama, my other thesis supervisor, as well. I am extremely grateful for his confidence in my abilities, and his steady encouragement over the past few years. His encouragement during my depressive times has been a moral booster for me. Dr. Salama has been very professional and enthusiastic and has been of great help during the course of my stay at Waterloo. I find myself lucky to have known him and be associated with such a knowledgeable professor.

Ivan, Steven, Behdad, Srikanth, Sridhar and Murthy made my stay at Waterloo very memorable.

To my elder brother, Sunder, who has always been a source of encouragement throughout my life.

Finally, to my wife, Vijaya, my biggest thanks, although thanks is perhaps not the best word. I thank her for having endured my hectic schedule for the past couple of years. Your support and encouragement have meant a great deal to me. I could not have done this thesis without you.

To my mother and father

With love

Table of contents

PART-I Review

Chapter 1 – Power flow control

1.0 Introduction	1
1.1 General introduction to power flow controllers	4
1.2 Unified power flow controller concept	7
1.3 Unified power flow controller: Construction and operation	11
1.4 Motivation for this thesis	13
1.5 Summary	16

Chapter 2 – Literature review

2.0 Introduction	17
2.1 Review	18
2.1.1 Review on control strategy and control systems for UPFC	18
2.1.1.1 Static synchronous series compensator strategy (SSSC)	18
2.1.1.2 Phase shifter strategy	19
2.1.1.3 D-Q axis control strategy	20
2.1.2 Review on Load flow and dynamic models for UPFC	25
2.1.2.1 UPFC modeling	26
2.1.2.1.1 Load flow models	26
2.1.2.1.2 Dynamic models	33
2.2 Summary	36

Chapter 3 – Present study	38
Part- II stability analysis	
Chapter 4 – UPFC model for load flow	
4.0 Introduction	42
4.1 Model of UPFC	43
4.2 Norton’s equivalent circuit for UPFC	45
4.3 Real and reactive power equations for UPFC	46
4.4 Load flow procedure	47
4.5 Flowchart for load flow with UPFC	51
4.6 Summary	54
Chapter 5 – Does UPFC improve power system stability?	
5.0 Introduction	55
5.1 Small-signal stability analysis	56
5.1.1 State matrix formulation	56
5.1.1.1 UPFC modeling	58
5.2 Small-signal stability evaluation	62
5.2.1 Single machine infinite bus power system (SMIB)	62
a) Improvement in rotor angle mode damping	62
b) Effect of series inverter in-phase component (V_{sep}) on rotor angle mode damping	65
c) Effect of shunt inverter controlling the transmission line side bus voltage on rotor angle mode damping	66
5.2.2 Multi-machine power system (MMPS)	67

a) Improvement in inter-area damping	67
b) Effect of series inverter in-phase component (V_{sep}) on inter-area damping	70
c) Effect of shunt inverter controlling the transmission line side bus voltage on inter-area damping	71
5.3 Transient stability analysis	73
5.3.1 Single machine infinite bus power system	74
a) Improvement in rotor angle mode damping	74
5.3.2 Multi-machine power system	78
a) Improvement in inter-area damping	78
5.4 Summary	89

Chapter 6 –Improvement in power system stability using a fuzzy logic controller for

a UPFC – SMIB and MMPS	90
6.0 Introduction	90
6.1 Basics of fuzzy theory	92
6.2 Fuzzy logic controller	93
6.3 Knowledge base design for the series inverter of a UPFC	99
6.4 Simulation results	105
6.4.1 SMIB case	105
6.4.2 MMPS case	110
6.5 Summary	117

PART-III – Validation using PSCAD-EMTDC software

Chapter 7 – Shunt inverter construction, operation and control system design	118
7.0 Introduction	118
7.1 Shunt inverter transformer rating	119
7.2 Shunt inverter: construction and operation	120
7.2.1 Basic three-phase voltage source inverter	129
7.2.2 Construction of a 4-module voltage source inverter	121
7.2.3 Operation of a 4-module voltage source inverter	123
7.3 Shunt inverter: control system	125
7.3.1 Basics of de-coupled control system	126
7.3.2 De-coupled control system design for a 4-module voltage source inverter	131
7.4 Implementation of a 4-module voltage source inverter and its control system using PSCAD-EMTDC software	139
7.5 Performance studies on a 4-module voltage source inverter	142
7.5.1 Initialization	143
7.5.2 Step change in reactive power from 0 to –130 MVAR	143
7.5.3 Step change in reactive power from -130 MVAR to +130 MVAR	144
7.6 Summary	147
Chapter 8 – Series inverter construction, operation and control system design	149
8.0 Introduction	149

8.1 Series inverter transformer rating	150
8.2 Series inverter: construction and operation	152
8.2.1 Series inverter construction	152
8.2.2 Operation of a series inverter	154
8.3. UPFC DC link capacitor rating	158
8.4 Controller design for series inverter	160
8.5 Summary	168
Chapter 9– Performance of UPFC control system	170
9.0 Introduction	171
9.1 Shunt inverter control system with coordination controller	171
9.2 Performance of UPFC control system with series inverter controlling the real power flow in a transmission line using PI controller	176
9.2.1 Power system description	176
9.2.2 Step input response	178
9.3 Fuzzy logic controller design in PSCAD-EMTDC software	182
9.3.1 Performance of UPFC control system with series inverter controlling the real power flow in a transmission line using a fuzzy controller	185
9.3.1.1 Step input response with fuzzy controller	185
9.3.1.2 Power oscillation damping using fuzzy controller	188
9.4 Performance of coordination controller	194
9.5 Effect of in-phase series voltage injection on reactive power flow in a	

transmission line and shunt inverter reactive power	196
9.6 Summary	203
Chapter 10 – Reactive power coordination	206
10.0 Introduction	206
10.1 Need for reactive power coordination	207
10.2 Shunt and series inverter control system	209
10.2.1 Shunt inverter control system	209
10.2.2 Series inverter control system	211
10.3 Performance of the control system	213
10.3.1 Response to step change in transmission line reactive power reference	213
10.4 Reactive power coordination control design	218
10.5 Step response with reactive power coordination controller	220
10.6 Power oscillation damping	224
10.7 Summary	229
Chapter-11 A new control strategy for UPFC	231
11.0 Introduction	231
11.1 Proposed control strategy	232
11.2 Control system for the new control strategy	235
11.2.1 Shunt inverter control system	235
11.2.2 Series inverter control system	237

11.3 Performance of the new control strategy	238
11.3.1 Step input response	238
a) Response to step change in transmission line real power reference	239
b) Response to step change in receiving end voltage	242
11.4 Power oscillation damping	247
11.5 Summary	250
Chapter 12 – Conclusions and Future Work	252
12.0 Conclusions	252
12.1 Future Work	258
Appendix	
Appendix-1	
A1-1. Network data for SMIB	259
A1-2. Bus data for SMIB	259
A1-3. Generator data for SMIB	260
A1-4. Power system stabilizer data for SMIB	260
A1-5. UPFC parameters	261
A1-6. Small-signal stability analysis	261
Appendix-2	
A2-1. Network data for MMPS	273
A2-2. Bus data for MMPS	274
A2-3. Generator data for MMPS	275
A2-4. Power system stabilizer data for MMPS	276

A2-5. UPFC parameters	276
Appendix-3	
A 3-1. Complete list of eigen values without UPFC for MMPS	277
A 3-2. Complete list of eigen values with UPFC for MMPS	278
Appendix-4 PSCAD-EMTDC parameters	
A 4-1. Generator parameters	280
A 4-2. Power system stabilizer and exciter parameters	281
A 4-3 UPFC parameters	281
A 4-4 Synchronous motor parameters	282
References	283

List of Tables

Table 5.1	Eigen values with PSS (SMIB)	64
Table 5.2	Eigen values with PSS and UPFC (SMIB)	64
Table 5.3	Eigen values with UPFC for different values of in-phase component (V_{sep}) of series voltage (SMIB)	66
Table 5.4	Eigen values with shunt inverter of UPFC controlling the transmission line side bus voltage (SMIB)	66
Table 5.5	Eigen values with PSS (MMPS)	69
Table 5.6	Eigen values with PSS and UPFC (MMPS)	70
Table 5.7	Eigen values with UPFC for different values of in-phase component (V_{sep}) of series voltage (MMPS)	71
Table 5.8	Eigen values with shunt inverter of UPFC controlling the transmission line side bus voltage (MMPS)	71
Table 6.1	A Fuzzy knowledge base.	97
Table 6.2	Fuzzy knowledge base for series inverter of UPFC.	104

List of Figures

Fig.1.1 A power system with two machines connected by a transmission line with voltage sources V_{sh} and V_{sc} representing the UPFC.	7
Fig. 1.2 Phasor relationship between the voltage source V_{sc} and the line current I_{sc} for series compensation.	9
Fig. 1.3 Phasor relationship between the mid point voltage V_M and the series voltage source V_{sc} for phase shifter operation.	11
Fig.1.4 UPFC connection.	12
Fig.2.1 A UPFC connected to a Transmission line.	27
Fig.2.2 Coupled source model for UPFC.	27
Fig.2.3 Power system with UPFC.	30
Fig.3.1 Present Study	39
Fig.4.1 Unified power flow controller configuration.	43
Fig.4.2 UPFC model.	44
Fig.4.3 Norton equivalent circuit for UPFC.	45
Fig.4.4 Phasor diagram showing the two components of the series voltage source.	50
Fig.4.5 Flow chart for load flow study.	52
Fig.5.1 UPFC with its associated DC and AC side currents.	58
Fig.5.2 Single machine infinite bus power system.	63
Fig.5.3 Two area power system with UPFC.	68
Fig.5.4 Generator rotor speed ($\Delta\omega_r$) oscillation damping with and without UPFC.	75
Fig.5.5 Generator electrical power (P_e) oscillations with and without UPFC.	76

Fig.5.6 DC link capacitor voltage (V_{dc}) oscillations for three phase fault at the generator terminals.	77
Fig.5.7 Rotor angle oscillations of generator G2 with respect to generator G1 (δ_{21}) (with and without UPFC).	80
Fig.5.8 Rotor angle oscillations of generator G3 with respect to generator G1 (with and without UPFC).	81
Fig.5.9 Inter-area real power flow oscillations (with and without UPFC).	83
Fig.5.10 Real power flow oscillations in the double circuit line (with and without UPFC).	84
Fig.5.11 Rotor angle oscillations of generator G2 with respect to generator G1 (δ_{21}) (with and without UPFC).	85
Fig.5.12 Rotor angle oscillations of generator G3 with respect to generator G1 (δ_{31}) (with and without UPFC).	86
Fig.5.13 Inter-area real power flow oscillations ($P_{inter-area}$) (with and without UPFC).	87
Fig.5.14 Real power flow oscillations in the double circuit line (with and without UPFC).	88
Fig. 6.1 A sample fuzzy logic controller.	94
Fig.6.2 Five fuzzy sets.	95
Fig.6.3 Fuzzy sets with their respective support.	96
Fig.6.4 Consequent fuzzy sets.	99
Fig.6.5 Error in transmission line real power flow for a SMIB case.	101
Fig.6.6 Change in error in transmission line real power flow for SMIB case.	102
Fig.6.7. Change in control input V_{seq} for SMIB case.	103

Fig.6.8 Single machine infinite bus power system.	106
Fig.6.9 Generator rotor angle (δ) Oscillations.	106
Fig.6.10 Generator rotor speed ($\Delta\omega_r$) oscillation damping.	108
Fig.6.11 Generator electrical power (P_e) output.	109
Fig.6.12 Real power flow (P_{line}) in the UPFC line.	110
Fig.6.13 Two area power system with UPFC.	111
Fig.6.14 Rotor angle difference (δ_{21}) between generators G2 and G1. Fault at bus-5.	113
Fig.6.15 Rotor angle oscillations of generators G3 with respect to G1 (δ_{31}).	114
Fig.6.16 Inter-area real power flow ($P_{inter-area}$) oscillations.	115
Fig.6.17 Real power flow in the UPFC transmission line (P_{line}).	116
Fig.7.1 UPFC connected to a transmission line.	119
Fig.7.2 A basic three-phase voltage source inverter module.	121
Fig.7.3 4-Module voltage source inverter.	122
Fig.7.4 Phasor diagram for operation of a 4-module VSI.	124
Fig.7.5 Equivalent circuit of a 4-module VSI connected to a constant voltage source.	126
Fig.7.6 Phasor diagram for 4-module VSI connected to a constant voltage source.	127
Fig.7.7 De-coupled control system.	131
Fig.7.8 4-Module VSI performance	146
Fig.8.1 UPFC connected to a transmission line.	151
Fig.8.2 4-Module voltage source series inverter.	153
Fig.8.3 Phasor diagram for operation VSI-1 and VSI-2 of series inverter (V_{seQ}).	155
Fig.8.4 Phasor diagram for operation VSI-3 and VSI-4 of series inverter (V_{seD}).	157

Fig. 8.5 Power system for designing series inverter controller.	161
Fig.8.6 Series inverter real power flow controller.	165
Fig.9.1 UPFC connected to a transmission line.	172
Fig.9.2 UPFC shunt inverter control system with coordination controller.	175
Fig.9.3 Two machine power system with UPFC.	177
Fig.9.4 Series inverter real power flow controller (PI).	179
Fig.9.5 Response of the power system to step changes in real power reference of the UPFC (PI controller for series inverter)	181
Fig.9.6 Fuzzy logic controller implementation in PSCAD-EMTDC software.	184
Fig.9.7 Response of the power system to step changes in real power reference of the UPFC (Fuzzy controller for series inverter).	187
Fig 9.8 Two-machine power system with UPFC.	189
Fig.9.9 Response of the power system to three-phase fault without UPFC.	190
Fig.9.10 Response of the power system to three-phase fault with UPFC.	193
Fig.9.11 DC link capacitor voltage oscillations with and without coordination controller.	195
Fig.9.12 Equivalent circuit for a UPFC.	197
Fig.9.13. Effect of in-phase voltage injection on transmission line reactive power, shunt inverter reactive power and series inverter reactive power.	199

Fig.10.1 UPFC connected to a transmission line	208
Fig.10.2 Shunt inverter control system with real power coordination controller	210
Fig.10.3 Series inverter control system	212
Fig.10.4. Two machine Power system	213
Fig.10.5. Response to step change in reactive power reference	214
Fig.10.6. Shunt inverter control system with real and reactive power coordination controller	219
Fig.10.7. Step response with reactive power coordination controller	221
Fig.10.8. Real and reactive power oscillations without UPFC	226
Fig.10.9. Real and reactive power oscillations with UPFC	228
Fig.11.1 UPFC connected to a transmission line	233
Fig.11.2. Shunt inverter control system with real power coordination controller	235
Fig.11.3. Series inverter control system for the new control strategy	237
Fig.11.4. Two machine power system	238
Fig.11.5. Response of the power system to step changes in transmission line real power flow reference	239
Fig.11.6. Response to step changes in transmission line receiving end voltage from 0.925 p.u. to 1.03 p.u.	242
Fig.11.7. Response to step changes in transmission line receiving end voltage from 0.925 p.u. to 1.03 p.u. with UPFC	243
Fig.11.8. Response of the power system to pulse change in receiving end phase angle without UPFC	248

Fig.11.9. Response of the power system to pulse change in receiving end phase angle

with UPFC

249

Chapter 1

Power Flow Control

1.0 Introduction

Power systems in general are interconnected for economic, security and reliability reasons. Exchange of contracted amounts of real power has been in vogue for a long time for economic and security reasons. To control the power flow on tie lines connecting controls areas, power flow control equipment such as phase shifters are installed. They direct real power between control areas. The interchange of real power is usually done on an hourly basis. On the other hand, reactive power flow control on tie lines is also very important. Reactive power flow control on transmission lines connecting different areas is necessary to regulate remote end voltages. Though local control actions within an area are the most effective during contingencies, occasions may arise when adjacent control areas may be called upon to provide reactive power to avoid low voltages and improve system security. Document B-3 of Northeast Power Coordinating Council (NPCC) on

Guidelines for Inter-Area Voltage Control provides the general principles and guidance for effective inter-area voltage control. Section 3.1.2 of document B-3 states that

“Providing that it is feasible to regulate reactive power flows in its tie lines, each area may establish a mutually agreed upon normal schedule of reactive power flow with adjacent areas and with neighboring systems in other reliability councils. This schedule should conform to the provisions of the relevant interconnection agreements and may provide for:

- a) the minimum and maximum voltage at stations at or near terminals of inter-area tie lines
- b) the receipt of reactive power flow at one tie point in exchange for delivery at another
- c) the sharing of reactive requirements of tie lines and series regulating equipment (either equally or in proportion to line lengths)
- d) the transfer of reactive power from one area to another”

Section 3.2.2 of document B-3 states that

“ When an area anticipates or is experiencing an abnormal, but stable, or gradually changing bulk power system voltage condition, it shall implement steps to correct the situation. Recognizing that voltage control problems are most effectively corrected by control actions as close to the source as possible, the area shall use its own resources, but may request assistance from adjacent areas.”

The above statements clearly calls upon the power flow regulating equipment to not only be able to control real power but also simultaneously control reactive power

flow rapidly. Further, the voltage at stations at or near terminals of inter-area tie lines should be controlled within limits.

Power flow in a network is not easily controlled because line parameters that determine the flow of power in the system are difficult to control. Fortunately, the ability to control power flow at the transmission level has greatly been influenced by the advances made in the field of high power switching devices. Solid state devices provide transmission utilities the flexibility to control the system power flows. Today, with the availability of high power gate turn-off thyristors (GTO) it has become possible to look beyond the realm of conventional thyristors for power flow control. These devices are broadly referred to as Flexible AC Transmission Systems (FACTS) [1].

Power flow in a transmission line is a function of the sending (V_S) and receiving (V_R) end voltages, the phase angle difference (δ) between the voltages and the line impedance (X). Control of any of the above parameters can help to control the power flow and the process is known as compensation. FACTS devices could be placed either in series or in shunt with the transmission line with the intention of controlling the power flow in it. If the transmission line impedance is modified by the addition of FACTS, it is termed as series compensation. If the phase angle difference is modified, it is termed as phase angle compensation. Shunt compensation, in which the FACTS device is placed in parallel, is mainly used to improve the system voltage characteristics. Static var compensator (SVC) belongs to this family of FACTS devices.

1.1 General introduction to power flow controllers

Fixed series capacitors help in increasing stability limits in an interconnected power system. With transmission open access, each transmission system owning utility will increase their transmission capacity to attract more utilities to use its transmission facilities. Many existing power systems have already made the use of series compensation to increase their transmission capacity [56]. By series compensation, the amount of reactive power consumed by the line is reduced thereby increasing the amount of reactive power transferred to the receiving end and improving the voltage profile at the receiving end. This is one of the secondary benefits of using series compensation. Under system disturbance conditions like three phase faults or line tripping, controllable series compensation helps in damping power system oscillations.

Control of power flow by series compensation means that by changing the amount of impedance in the circuit, the current in individual transmission lines are varied thereby varying the power flow in it. In essence, it controls only the magnitude of the current in a transmission line. Hence the reactive power demand at the end points of the line is determined by the transmitted real power in the same way as if the line was uncompensated but had a lower line impedance [2]. The disadvantage associated with this is that with increasing series compensation the losses in the system increase which may be considerable. This is due to higher current flowing with reduced line impedance. Further, series compensation cannot control the reactive power flow in a transmission line. Economics dictates the use of fixed and variable compensation for increasing power transfer. Increasing the amount of fixed compensation leads to possible occurrence of sub-synchronous resonance (SSR). Thyristor controlled series compensation (TCSC)

under certain modes of operation (constant reactance control) cannot damp all the sub-synchronous resonance modes (SSR) [3]. From the impedance characteristics of a TCSC, the change from the capacitive to the inductive mode is discontinuous, and further, there is a region (resonant region) where the operation is restricted [4].

Phase angle compensation is a method of controlling power flow and has been used in many existing systems. Phase shifters by themselves do not cause SSR. Phase shifters have the advantage of mitigating SSR caused by series capacitors. A phase shifter can by no means increase the maximum amount of real power transfer, but can improve transient stability. The operation of a phase shifter is such that, it represents a small inductance in series with the line which leads to increased reactive power consumption in the line as compared with the uncompensated line [2]. Increase in reactive power consumption leads to increased system losses. A phase shifter could be more effective in helping to load circuits with poor loading (low angle across the line). Furthermore, phase shifters also cannot control the reactive power flow in a transmission line. It is seen that series compensation is more effective in some places and phase shifters in some other. But their operation increases system losses.

Power systems do operate with series, phase angle compensation and voltage control equipment. Co-ordination between them is an important aspect to be considered while operating a complex integrated power system. Utilities have encountered unwanted interactions between various FACTS devices which have lead them to reconsider their control strategies for satisfactory operation of the power system [5-7].

Advances made in the field of solid state devices has made it possible to combine the functionality of series, shunt and phase angle compensation into one device. Such a device has been named the unified power flow controller (UPFC). It has the ability to control real and reactive power flow in a transmission line, while simultaneously regulating the voltage of the bus to which it is connected. UPFC does not cause SSR. By using a UPFC, many distributed FACTS devices could be eliminated, thereby reducing capital costs. Also, the problem of unwanted interactions between the FACTS devices could be reduced to a little lesser extent, if not completely. As seen from the industry point of view, the unified approach of controlling power flow promises simplified design, reduction in equipment size and installation labor, and improvements in system performance [2].

1.2 Unified power flow controller concept

The UPFC concept was proposed by Gyugyi *et.al* [2]. To understand the unified power flow concept, consider a power system with two machines connected by a transmission line of reactance X_l (purely inductive) along with two voltage sources V_{sh} and V_{sc} representing the UPFC as shown in Fig.1.1. The voltage sources denoted by V_{sh} and V_{sc} in the Fig.1.1 are connected in shunt and series respectively at the mid- point of the transmission line.

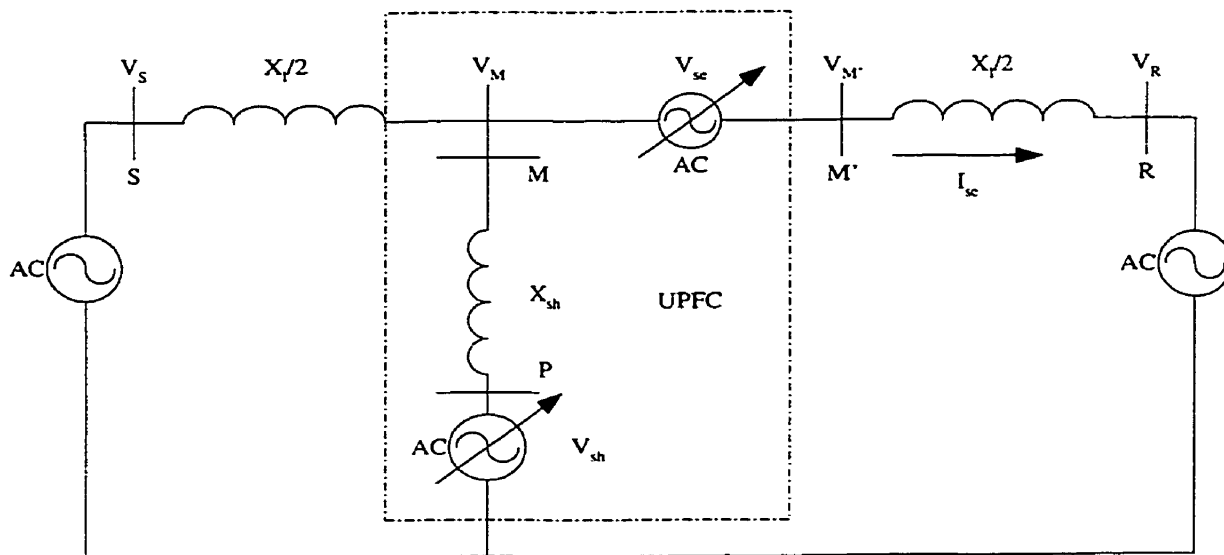


Fig.1.1 A power system with two machines connected by a transmission line with voltage sources V_{sh} and V_{sc} representing the UPFC.

Voltage source V_{sh} is connected to the transmission line through a transformer represented as a reactance X_{sh} . It is assumed that the voltage sources denoted by V_{sh} and V_{sc} , have the capabilities of varying their magnitude and their phase angle.

To understand the operation of the source V_{sh} , the source V_{se} is disconnected. Reactive power flows from the voltage source V_{sh} to bus M if the magnitude of the voltage source V_{sh} is greater than the mid-point voltage V_M and the phase of them are the same. If the phase angle of the voltage source V_{sh} leads the phase angle of mid-point voltage V_M and the magnitude of V_{sh} is greater than V_M , then real and reactive power will flow from the voltage source V_{sh} to the bus M . Conversely, if the magnitude of the shunt voltage V_{sh} is less than the mid point voltage V_M , but the phase angle difference between them is zero, then only reactive power will flow from the bus M to the bus P . In this process, the voltage source V_{sh} is consuming reactive power. If the phase angle of V_M leads the phase angle of V_{sh} , then both real and reactive power will flow from bus M to bus P and the voltage source is said to be consuming both real and reactive power. In summary, by controlling the magnitude and phase angle of the shunt voltage source V_{sh} , the direction of real and reactive power flow to the bus M can be controlled. Alternatively, the voltage source V_{sh} can be made to function as a load or as a generator for the power system. In the above operation, if the phase angle difference between the voltage at bus M and that of V_{sh} is maintained at zero, then by varying the magnitude of V_{sh} , reactive power can either be consumed or generated by V_{sh} . This operation can be compared with that of a thyristor controller reactor with fixed capacitor (shunt compensator) that generates or absorbs reactive power by altering its shunt reactive impedance. It should be noticed that the function of a shunt compensator is being duplicated by the voltage source V_{sh} .

Now consider only the operation of series voltage source V_{se} in Fig. 1.1 with the shunt voltage source V_{sh} inoperative. It is assumed that the magnitude and phase angle of the series voltage source V_{se} can be varied. The transmission line current I_{se} interacts with the series voltage source V_{se} causing real and reactive power to be exchanged between the series voltage source and the transmission line. If the voltage source V_{se} and the transmission line current I_{se} have a phase angle difference of 90 degrees and that the voltage phasor of V_{se} leads the line current, the voltage source V_{se} then generates only reactive power. The phasor diagram has been shown in Fig. 1.2.

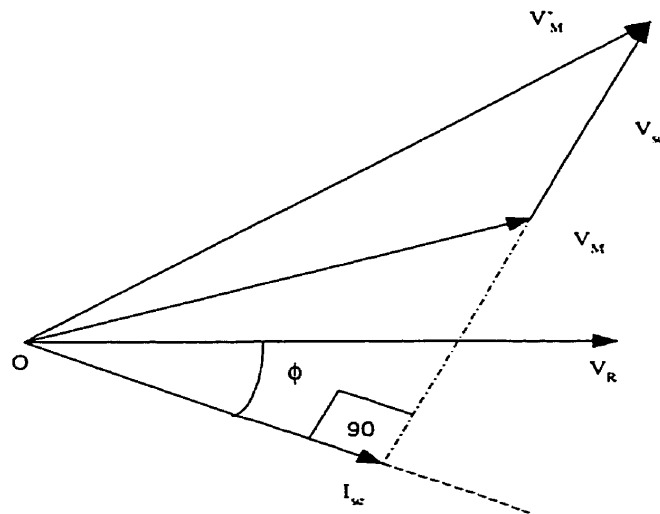


Fig. 1.2 Phasor relationship between the voltage source V_{se} and the line current I_{se} for series compensation.

Conversely, if the voltage source V_{se} phasor lags the transmission line current I_{se} phasor by 90 degrees, then the voltage source V_{se} will consume reactive power. The above operation should be compared with that of a series capacitor/series inductor in the

transmission line. When capacitors are placed in series with the transmission line, it generates reactive power. The amount of reactive power generated depends on the amount of series compensation and the line current. When inductors are placed in series with the transmission line, it consumes reactive power. In summary, the function of series capacitor could be performed by the series voltage source V_{se} by maintaining its phase to lead the transmission line current I_{se} phasor by 90 degrees. Conversely, the function of a series inductor could be performed by the series voltage source V_{se} by adjusting its phase angle to be lagging the line current I phasor by 90 degrees.

By properly adjusting the phase angle of the series voltage source V_{se} , the operation of a phase shifter could be obtained. In the case of a phase shifter, the phase angle of the series voltage source V_{se} leads or lags the voltage of the bus to which it is attached, by 90 degrees. This causes the voltage phasor to shift by an amount depending on the magnitude of the injected voltage. In this case, if the series voltage source V_{se} has a 90 degrees leading or lagging phase relationship with the bus voltage V_M , then a phase shift $\alpha = \tan^{-1}\left(\frac{V_{se}}{V_M}\right)$ could be obtained. Fig. 1.3 shows the phasor relationship of the series voltage source V_{se} leading the bus voltage V_M for phase shifter operation. In summary, by adjusting the phase angle of the series voltage source V_{se} to be either leading or lagging the bus voltage M by 90 degrees, a phase shifter operation could be obtained. In order to vary the magnitude of phase shift, the magnitude of the series voltage source V_{se} could be varied. The above illustration has shown all the possible functions of shunt compensation, series compensation and phase angle compensation that

could be obtained by manipulating the series and the shunt voltage sources magnitude and phase angle of a UPFC.

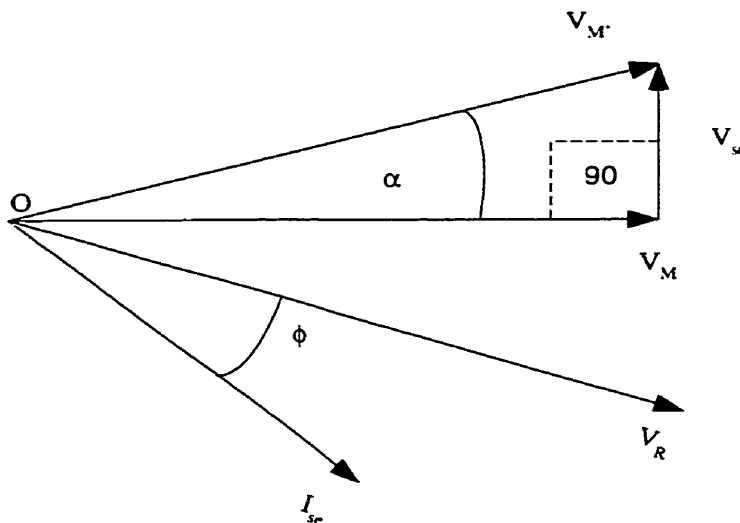


Fig. 1.3 Phasor relationship between the mid point voltage V_M and the series voltage source V_{sc} for phase shifter operation.

1.3 Unified power flow controller: Construction and Operation

The voltage sources V_{sh} and V_{sc} mentioned in section 1.2 are obtained by converting DC voltage to AC voltage. The conversion from DC voltage to AC voltage is obtained by using standard bridge circuits. These bridge circuits use GTO as their building blocks. Since these circuits convert DC voltage to AC voltage, they are termed as voltage source converters (VSC). The control system associated with VSC allows it to adjust its magnitude and phase angle. The term “inverter” has also been used to denote the VSC.

Consider now the connection of two VSC connected back to back with a common DC link capacitor 'C' as shown in Fig. 1.4. Such an arrangement allows for all the three functions namely series, shunt and phase angle compensation to be unified in one unit. Inverter 1 is connected to a shunt transformer and the inverter 2 is connected to a series transformer.

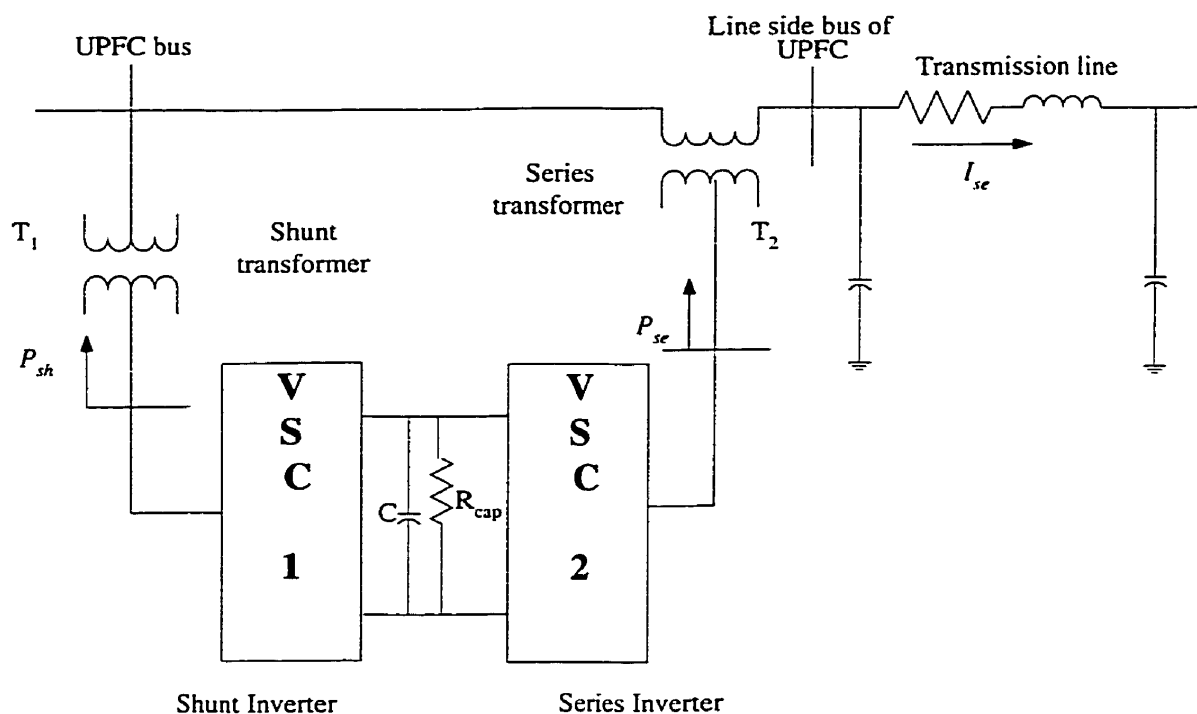


Fig.1.4 UPFC construction.

It is readily seen that the VSC connected to the shunt transformer can perform the function of a variable reactive power source similar to that of shunt compensator. In addition, the inverter 1 can charge the DC link capacitor. Inverter 2 can provide series or phase angle compensation by injecting a series voltage of proper phase relationship. In the case of series compensation, inverter 2 can function independent of the inverter 1, as inverter 2 supplies/consumes only reactive power and does not have any real power

exchange with inverter 1. In such a case, the DC link capacitor voltage will ideally be constant.

In the case of phase angle compensation, the series voltage source V_{se} has an arbitrary phase relationship with the transmission line current I_{se} and does have real and reactive power exchange with the transmission line. Under this mode of operation, the real power generated or consumed by inverter 2 (P_{se}) will lead to the discharging or charging of the DC link capacitor respectively. In the case of real power generation by inverter 2 (P_{se}), the DC link capacitor discharges, and the decrease in the voltage will reflect as a load on inverter 1. Under this circumstance, inverter 1 will provide the necessary real power (P_{sh}) and charge up the DC link capacitor. In the case when the inverter 2 consumes real power (P_{se}) leading to charging of the DC link capacitor and subsequent increase in its voltage, inverter 1 will supply the excess real power (P_{sh}) back to the line through the shunt transformer. In essence, the UPFC provides an alternate path for the real power i.e. from the bus to which the shunt transformer is connected, through inverter 1 to the capacitor, through inverter 2 and to the transmission line through the series transformer. Inverter 1 and inverter 2 can generate reactive power independently. In summary, the above arrangement of two VSC connected back to back coupled by a DC link capacitor can perform the job of all the three types of compensation.

1.4 Motivation for this thesis

a) Complexity in the design of a control system for UPFC

The control aspect of a UPFC is an important area of research. As seen from the operation of a UPFC, it is a multi-variable controller. The control system design should be such that the UPFC is able to function in a stable manner, provide power flow control

and power oscillation damping. The series inverter of a UPFC controls the power flow in a transmission line. The interaction between the series injected voltage and the transmission line current causes the series inverter to exchange real and reactive power with the transmission line. The real power exchange by the series inverter with the transmission line is supplied/absorbed by the DC link capacitor. This causes a decrease/increase in the DC capacitor voltage. For proper operation of the UPFC, the DC capacitor voltage should be regulated. The decrease/increase in the DC link capacitor voltage is sensed by the shunt inverter control system. The shunt inverter control system operates to meet the demand in decrease/increase in DC capacitor voltage by absorbing/supplying real power to the power system through the shunt inverter to maintain the DC capacitor voltage at a specified level. If the control system of the shunt and the series inverters is such that the shunt inverter is not able to meet the real power demand of the series inverter, then the DC capacitor voltage might collapse resulting in the removal of the UPFC from the power system. This is one problem that will be considered in this work during the design of the UPFC control system. This calls for coordination between the shunt and the series control system operation with respect to the real power flow through the DC link of the UPFC.

The next problem with the control system design for a UPFC is when the shunt inverter controls the voltage of the bus to which it is connected (UPFC bus), in addition to the DC link capacitor voltage. This is because the voltage of the bus to which the shunt inverter is connected (UPFC bus) does affect the real and reactive power flow through the transmission line. Since the shunt inverter controls the UPFC bus voltage and the DC capacitor voltage, it not only affects the real and reactive power flow through the

transmission line but also affects the real and reactive power flow through the shunt inverter. The real power flow through the shunt inverter affects the DC link capacitor voltage. If the control system is not designed properly, it could lead to growing oscillations in transmission line power flow and lead to system wide disturbances. This calls for proper design of the control system for UPFC.

The problem gets even more complicated when the series inverter of a UPFC controls the transmission line real and reactive power flow in the transmission line in addition to the control of the UPFC bus voltage and DC link capacitor voltage. This is because any change in the transmission line reactive power flow affects the UPFC bus voltage and this in turn affects all the other variables.

b) Complexity in the operation of a UPFC in an integrated power system

One of the problems that exist in an integrated power system environment is the presence of inter-area oscillations. These oscillations involve groups of generators in a control area swinging against another group of generators in a different control area. UPFC when placed on tie lines connecting two areas should be able to damp out these inter-area oscillations. Since UPFC is a multi-variable controller, it should be able to enhance power system stability under dynamic conditions.

Thus it is seen that though the concept of UPFC is elegant, the control system design for a UPFC is a very complicated one as it involves simultaneous control of multi-variables. Inappropriate design of the control system with respect to the four variables will definitely lead to instability. Thus extreme care has to be exercised during the design process of the control system for UPFC to provide fast control of power flow and effective power oscillation damping.

1.5 Summary

In this chapter, the importance of reactive power flow control on transmission lines has been briefly discussed. A brief review of various FACTS devices has also been made with respect to real and reactive power flow control. It has been concluded that none of the existing FACTS devices namely, static var compensator (SVC), TCSC or phase shifters can provide reactive power control on transmission lines. In this respect, UPFC has the advantage over SVC, TCSC and phase shifter that it can control not only real power but also reactive power flow on transmission lines simultaneously. The reactive power flow control capability of UPFC helps in regulating transmission line remote end voltages and improving system security.

This chapter has described the construction and operation of a UPFC. UPFC is the most versatile FACTS device as it combines the functionality of all existing FACTS devices. By combining the functionality of several devices, many distributed FACTS devices could be eliminated thereby reducing capital costs. Further, the interaction between various FACTS devices could be reduced to a little extent, if not completely.

The complexity of the control system design for UPFC has been discussed briefly. It must be understood here that the UPFC is a multi-variable controller and all the control variables interact with each other. This makes the control system design for UPFC very difficult. The next chapter explains the merits and demerits of different control strategies and their control systems used for power flow control and power oscillation damping.

Chapter 2

Literature Review

2.0 Introduction

Although a considerable amount of research has been done in the field of FACTS, very little literature exists with specific reference to UPFC. This is because UPFC is a relatively new FACTS device and power system problems associated with it have not been investigated thoroughly. The advantages of UPFC over other FACTS devices for real and reactive power flow control have been briefly discussed in chapter 1. Further, the need for reactive power flow control while simultaneously controlling real power flow on tie lines has also been described in chapter 1.

UPFC has the flexibility to incorporate any operation functionality. For example, as explained in chapter 1, UPFC can be made to operate as an Static synchronous series compensator (SSSC) or a phase shifter based on the strategy used. Different control strategies for UPFC and their control systems for power flow control have been discussed

in the literature. This chapter discusses the merits and demerits of various control strategies/control systems of UPFC for power flow control published in the literature.

2.1 Review

Given the integrated nature of the research, the relevant literature review has been divided into two sections. Accordingly, a section on review of control strategy and control systems for UPFC and a section on load flow and dynamic models for UPFC have been presented here.

2.1.1 Review on control strategy and control systems for UPFC

Very little work has been published in the area of UPFC control strategy for power flow control and control system design to achieve the control strategy. Three different types of strategies for real and reactive power flow control have been found in the literature and are described below.

2.1.1.1 Static Synchronous series compensator strategy (SSSC): This strategy is based on injecting the series voltage in quadrature with the transmission line current allowing it to function similar to that of a variable series capacitor. This fixes the phase angle of the series injected voltage to be in quadrature with the transmission line current. By varying the magnitude of the series injected voltage that is in quadrature with the transmission line current, the real power flow can be controlled [13,17,19,21,23,24]. The reactive power flow/transmission line side voltage is controlled by adjusting the phase angle of the series injected voltage. This has been achieved by introducing a component of the series injected voltage to be in-phase with the transmission line current [19,13,23].

Combining the quadrature component and the in-phase component, the magnitude and phase angle of the series injected voltage are obtained.

Concentrating on simultaneous control of real and reactive power flow/line side voltage using the above described strategy, control systems based on linear control techniques have been used [19,23]. The control system design based on this strategy requires a supplementary controller to damp out the real power flow oscillations when controlling the transmission line side voltage simultaneously using a high gain PI controller [23]. The design of coordination feedback between the series and the shunt inverter control systems has not been considered in the control system design [23]. The need for coordination controller comes from the fact that the real power demand of the series inverter has to be supplied by the shunt inverter. If there is no coordination between the series and the shunt inverter operation, the DC link capacitor voltage could collapse leading to the removal of the UPFC from the power system. The strategy also has the problem that if the in-phase injected voltage is out of action, the line side voltage could be very high causing reactive power flow problems. Further the problem of deterioration of the control system performance at operating points other than the one at which it is designed is a point to be considered.

2.1.1.2 Phase shifter strategy (PS): This strategy is based on injecting the series voltage in quadrature with the UPFC bus (the bus voltage to which the shunt inverter is connected) [15,18,20,25,26]. By doing so, the phase angle of the transmission line side bus can be adjusted for a specified real power flow. The reactive power flow is controlled by having a component of the series injected voltage to be in-phase with the UPFC bus [26]. This is similar to that of a tap-changer strategy. This allows the phase angle of the

series injected voltage to vary from its quadrature position, thereby changing the reactive power flow/line side voltage. Complete control system design for real and reactive power flow/line side voltage control that uses the above strategy has not been well documented.

Though the individual effect of quadrature series voltage injection, in-phase series voltage injection and shunt compensation on transient stability have been studied, the effect of combined operation has not been researched [15,18]. The effect of combined operation on transient stability has been later studied by Limiycheron *et.al* [20]. Here, three control inputs, namely the series quadrature injected voltage, in-phase series injected voltage and shunt compensation has been coordinated to improve transient stability. To achieve this coordination, fuzzy logic has been used. The model chosen for UPFC to show the effect of coordination on transient stability is not an accurate one. The shunt inverter has been modeled as a variable shunt capacitor in parallel with a current source. The variable shunt capacitor represents the shunt inverter compensation capability and the parallel current source representing the real power capability to charge/discharge the DC link capacitor. By doing so, they have neglected the model of the shunt inverter transformer and assumed that the real and reactive power flow through the shunt transformer are separated. Further, their coordination strategy has only been carried out on single machine infinite bus power system. Further, no coordination exists between the shunt and series inverter control system in terms of real power exchange between the series and shunt inverters thus casting serious doubts about the validity of such a coordination scheme.

2.1.1.3 D-Q axis control strategy: In this strategy, the D-Q axis current in the transmission line is individually controlled allowing for independent control of real and

reactive power flow [27-30]. The D-Q axis could be with respect to UPFC bus voltage or the remote end bus voltage. In this strategy, the series injected voltage is split into two components. One is in-phase with the D-axis and the other in-phase with the Q-axis. Similarly, the transmission line current is split into D and Q axis currents. The D-axis voltage controls the transmission line real power by varying the D-axis current in the transmission line and the Q-axis voltage controls the transmission line reactive power by varying the Q-axis current in the transmission line. Thus the in-phase series injected voltage component (D-axis) that controls the transmission line real power flow varies the line side voltage and the Q-axis component of the series injected voltage that controls the reactive power varies the phase angle of the UPFC bus. To achieve this type of strategy, the control system employs cascaded linear controllers. Proportional-Integral (PI) controllers have been used to implement the D-Q axis control strategy for the series inverter [27]. The coordination between the series and the shunt inverter control system has been considered [27]. The problem with this strategy for the series inverter is the complexity of the control system. Two control loops are required to regulate the real and reactive power flow. The outer loop to set the reference for the inner loop. The inner loop tracks the reference thus providing the control inputs to the series inverter. Further the problem of deterioration of the control system performance at operating points other than the one at which it is designed is a point to be considered. The shunt inverter control system is also based on the D-Q axis strategy and controls the shunt reactive power and the shunt inverter real power. The control of DC link capacitor voltage which is very essential for the proper operation of the UPFC, is done by another control loop that adjusts the shunt inverter real power reference. This further complicates the control

system. Further, they have neglected the dynamics of the DC link capacitor while designing their control system. By doing so, the control system design may not provide the best PI control gains.

A control system based on D-Q axis theory has been published in the literature by Round *et.al.*[30]. The strategy that has been used is that the D-axis voltage component controls the transmission line reactive power and the Q-axis voltage component of the series injected voltage controls the transmission line real power. This is in contrast with the strategy used by Papic *et.al.*[27] where the transmission line real power flow was controlled by the D-axis voltage and the transmission line reactive power flow was controlled by the Q-axis voltage. In this case, the UPFC is assumed to be located at the receiving end. Based on the receiving end real, reactive powers and receiving end D-Q axis voltages, current references of the series inverter are generated. Two PI controllers are used to generate the required D-Q axis control voltages for the series inverter to obtain desired real and reactive power flow in the transmission line. For the shunt inverter, based on the sending end real power, reactive power references and sending end D-Q axis voltages, the sending end D-Q axis current references are then generated. Knowledge of the sending and receiving end current references are used to generate the current references for the shunt inverter. By doing so, the shunt reactive power and the DC link capacitor voltage are controlled. Remote end signal measurement is required for this type of control system to operate. This would necessitate remote sensing units to be installed at the sending end. Further, coordination between the series and the shunt inverter control system has not been considered by the authors [30].

Other types of control systems have been designed based on the above control strategies which have neglected the DC capacitor voltage control systems [33-35]. Control systems for the shunt inverter have been designed based on Linear-Quadratic (L-Q) control, but have not shown as to how it can be applied to the series inverter control system [32]. The problem with LQ control is that it requires the measurement of all states used to design the controller [32].

In all the above strategies discussed for UPFC, the series inverter controls the real power flow in a transmission line by an output feedback control system. The problem in the design of an output feedback proportional-integral (PI) control system for UPFC is the presence of low margin of stability associated with the series inductance of the transmission line [23]. Intelligent controllers with specific reference to fuzzy controllers have been investigated in this thesis to overcome the problem. Further, the above control strategies suffer either in their complexity of the control system or non-inclusion of real power coordination controller between the series and the shunt inverter control systems or both.

A very fascinating capability of the UPFC has been reported in reference [42]. Any change in the transmission line reactive power flow is balanced by an equal and opposite change in the reactive power output of the shunt inverter of the UPFC when the shunt inverter is controlling the voltage of the bus to which it is connected. This means that any request for change in transmission line reactive power by the series inverter of a UPFC is actually supplied by the shunt inverter of the UPFC. Reference [42] states

“In essence, it can “manufacture” inductive and capacitive MVARs using the shunt inverter and “ export ” this reactive power into a particular transmission line (i.e.,

the one with the series insertion transformer) without changing the local bus voltage and without changing the reactive power on any of the other lines leaving the substation”.

In light of this fascinating capability of a UPFC, there is a need to investigate the mechanism by which changes in transmission line reactive power flow is related to the shunt inverter reactive power flow. Further, the effect of step changes in transmission line reactive power flow on UPFC bus voltage needs to be studied.

All the strategies published in literature have concentrated on the use of series inverter of a UPFC to control the transmission line reactive power flow. In view of the fascinating capability where the shunt inverter responds to a reactive power request from the series inverter control system, there is need to look into the possibility of a reactive power coordination controller in addition to a real power coordination controller.

The above fascinating capability leads to another point that is to be considered. As mentioned earlier, all the strategies published in the literature focuses on the use of series inverter for reactive power control. Changes in transmission line reactive power are reflected as an equivalent change in the shunt inverter reactive power flow. Thus the cause and the effect are on two portions of the UPFC. The cause being the series inverter control system and the effect seen on the shunt inverter reactive power flow. Thus all strategies discussed in the literature would fall under the category of indirect control with respect to reactive power flow. Thus there is a need to look into other strategies that provide direct control of transmission line reactive power flow / line side voltage and that which includes all the necessary coordination between the series and the shunt inverter for the proper operation of the UPFC. Further, the control system should utilize only local measurements for its control system. A new control strategy needs to be proposed that

utilizes the shunt inverter to directly control the transmission line reactive power flow. An advantage with such a strategy would be that it one can replace a part of the shunt inverter reactive power capability with switched shunt capacitors that are inexpensive. By doing so, a lower MVA rating of the shunt inverter and its transformer could be used thereby reducing the cost of the UPFC.

2.1.2 Review on Load flow and Dynamic models for UPFC

The purpose of reviewing the literature for load flow and dynamic models for UPFC are two fold. First, in all the above strategies discussed for UPFC in section 2.1.1, the real power flow in the transmission line is controlled by the series inverter of a UPFC by output feedback control system. The problem in the design of an output feedback control system for UPFC is the presence of low margin of stability associated with the series inductance of the transmission line [23]. Intelligent controllers with specific reference to fuzzy controllers have been investigated to overcome this problem. In order to obtain the necessary information to design the fuzzy controller, a suitable model for UPFC needs to be used in computer simulations. This includes both load flow and dynamic models. Load flow models are required as they form the backbone for any power system dynamic simulations. Dynamic models are required to capture the interaction between the series and the shunt inverter and provide information that would facilitate the design of the fuzzy controller. Literature survey has been conducted in the area of both load flow and dynamic modeling for UPFC.

Secondly, UPFC being a multi-variable controller, it is necessary to assess its impact on power system stability. Stability analysis of interconnected power systems with UPFC require proper load flow and dynamic models for UPFC. Frequency domain and

time domain analysis require model for UPFC that accurately model the interaction between the series and the shunt inverter. With a proper load flow and dynamic model for UPFC, one can thus analyze the impact of UPFC on power system stability.

2.1.2.1 UPFC Modeling

2.1.2.1.1 Load flow models: Different load flow models have been used to model the UPFC in varying degree of complexity and have been discussed here briefly. As mentioned in chapter-1, a UPFC consists of two inverters connected back to back with a DC link capacitor. One inverter is connected in shunt and the other in series with the transmission line as shown in Fig.2.1. The early modeling efforts for a UPFC were focussed on the series inverter modeling. The reason being that commercial software did not have series voltage source models. American Electric Power (AEP) and Westinghouse came up with a load flow model [8]. The requirement for the inclusion of the model was that the load flow should be a solved one. Basically, what was required was that the voltages and the angles of the power system buses had to be known in advance to include the UPFC model. The load flow model for UPFC consisted of two generators, one representing the shunt inverter and the other the series inverter. Different configurations of these generators were needed to model different operating conditions. Fig.2.2 shows the model that was used to include the UPFC into load flow studies [8]. Here the process of solving starts with the opening of the series line, and the generator

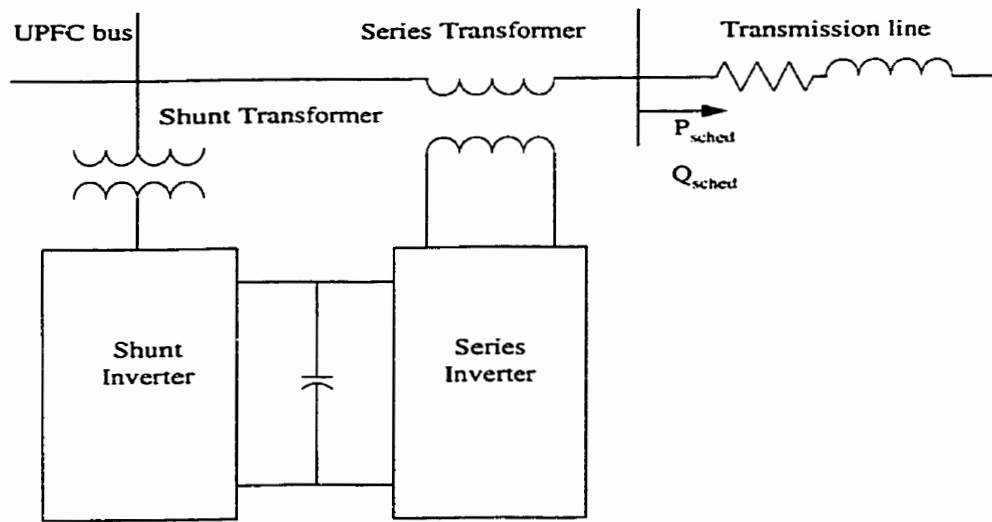


Fig.2.1 A UPFC connected to a Transmission line.

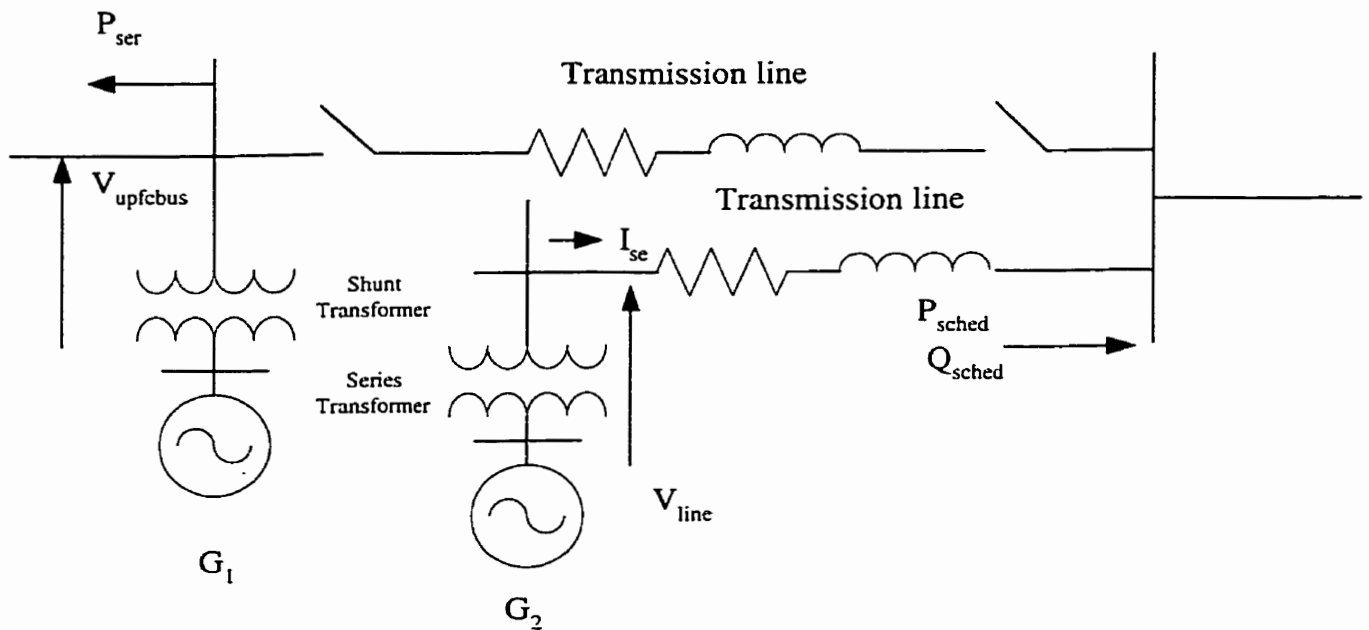


Fig.2.2 Coupled source model for UPFC.

G2 generates the scheduled real and reactive power. The scheduled power in the transmission line is converted into an equivalent load at the terminal where the generator

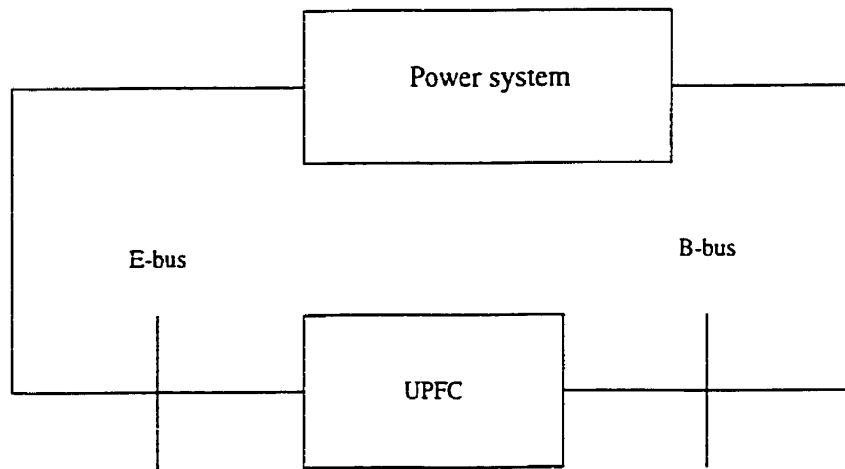
G1 is connected. The generator G1 generates the required reactive power to maintain scheduled bus voltage. Generator G2 also supplies the real power demand of the series inverter. The series injected voltage is the phasor difference between V_{line} and V_{upfcus} . The product of series injected voltage and the current I_{se} gives the amount of volt-ampere of the series inverter. The real part of the volt-ampere (P_{ser}) of the series inverter is added as a load at the shunt inverter bus. The algorithm to perform the addition of equivalent loads at the shunt inverter bus, to open the appropriate lines, have been included in their program. The problem is that it needs a solved load flow case. The idea of solving a load flow with an UPFC is to obtain the shunt and the series inverters' injected voltages for a given operating condition. This procedure is crude for solving a load flow with UPFC.

Another model for the UPFC where the shunt inverter is modeled as a current source and the series inverter is modeled as a voltage source in series with the transmission line has been used to solve power flow [9]. The model ensures the real power balance between the series and the shunt inverter. Though this model is good enough for doing parametric studies, they are not good for solving load flow. This is because, modeling of the shunt inverter by a current source does not reveal the voltage and the phase angle of the shunt inverter. Also, the model neglects the shunt inverter transformer in load flow studies.

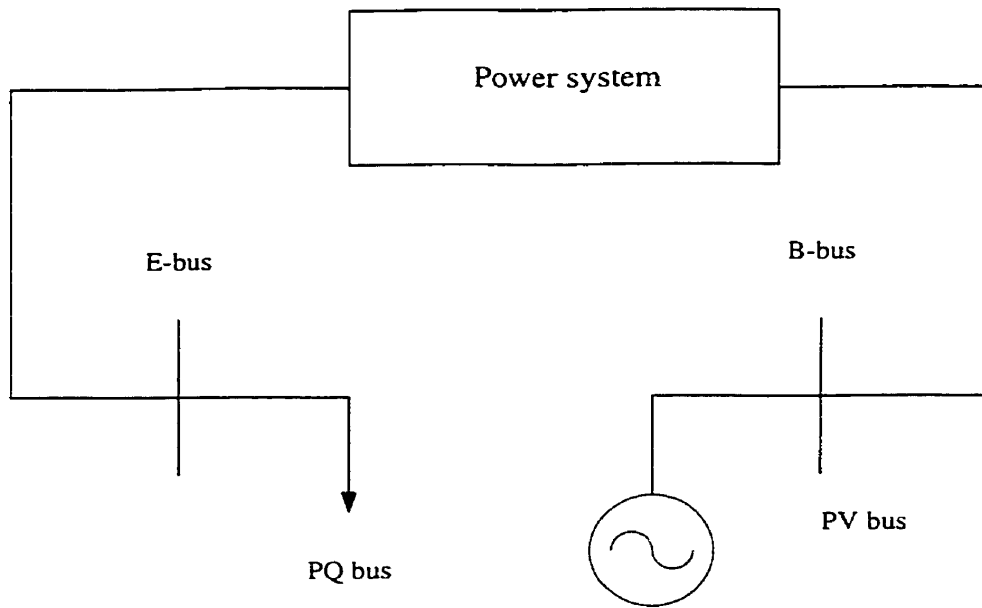
A model where the shunt and the series inverters have been modeled as real and reactive power injections have been used to solve load flows [10]. In this case, the series voltage has been converted into real and reactive power injections at both ends of the series inverter. The shunt inverter has also been converted into equivalent real and reactive power injections. The basic assumption that has been utilized here is that the real

power demand of the series inverter is provided by the DC capacitor. However, the real power demand of the series inverter should actually be supplied by the shunt inverter in steady state. This model neglects the interaction between the series and the shunt inverter.

A model where the bus to which the shunt inverter is connected is modeled as a PQ bus and the series inverter is modeled as a PV bus has also been used for load flow studies [11]. Fig.2.3 shows the model for power flow studies.



(a)



(b)

Fig.2.3 (a) Power system with UPFC.

(b) UPFC Power flow model.

Here the bus to which the shunt inverter is connected is modeled as a PQ bus (E-bus) and the other end of the UPFC is converted into a PV bus. The generator connected to the B-bus generates the scheduled real power and maintains a required voltage on the line side of the UPFC i.e the B-bus voltage. The power flow is solved and the voltages at the E-bus and the B-bus are used to solve another set of equations to derive the voltage and the phase angle of the shunt inverter and series inverter. The model neglects the interaction between the series and the shunt inverter during the first phase of load flow studies. Further, how the real power demand of the series inverter that is supplied by the shunt inverter is included during the load flow is unclear. The load flow solution process is basically a two step process and hence not an integrated method. This process could be used to perform load flow if all the variables are to be controlled, namely, the B-bus voltage, real power flow in the line and the reactive power by the shunt inverter. Further, if one wishes to control only the real power flow in the transmission line, it would be difficult to achieve using this model.

Another load flow model that has been used for the UPFC is that of modeling the shunt inverter as a separate voltage source and the series inverter as a set of complex power injections[12]. The shunt voltage source is modeled as PQ bus in the load flow. This model ensures that the real power demand of the series inverter is supplied by the shunt inverter. Also this load flow model is suitable for unified solution using the Newton-Raphson (N-R) method or a Gauss-Seidel (GS) method. The only problem using this model for the solution of a load flow using N-R method is that it needs a good initial estimate for the shunt and series voltage magnitude and angle. In this model, the shunt

reactive power is available as an additional variable that can be set to provide a scheduled voltage at the bus to which the shunt inverter is connected.

Of the load flow models described above, the last model [12] where the shunt inverter is modeled as a PQ bus and the series inverter is modeled as a set of complex power injections is the simplest and the most comprehensive of all the models available till now. The model provides for detailed interaction between the series and the shunt inverter. Also its unified solution process using the above model makes it attractive.

In this thesis, the above model [12] will be used to conduct power flow studies and obtain a steady state operating condition. The shunt inverter is modeled as a separate voltage source and the series inverter is modeled as a set of complex power injections. The program basically controls the real power flow in the line. It also takes into account the interaction between the shunt and the series voltage sources. In all the load flow solution procedures discussed in this section, the control strategy for real and reactive power control has not been included. This means that the load flow solution is obtained by defining the constraints on a UPFC bus or on the transmission line side bus voltage or on real power flow in a transmission line. It should be noted that, there is a possibility of multiple load flow solution with a UPFC [11,12]. It thus becomes imperative to include a strategy for the UPFC while solving load flows to obtain a reasonable operating condition. The program has been coded to include a phase shifter with a tap changer strategy. To achieve this, the series injected voltage is split into two components. One of the components is forced to be in quadrature with the UPFC bus voltage and the other component is forced to be in phase with the UPFC bus voltage. In the load flow program, the quadrature component that controls the real power flow is automatically adjusted

within the program. The in-phase component that controls the line side/reactive power is also adjusted automatically within the program. The advantage in doing so is that the real power flow control does not effect the reactive power flow and vice versa significantly. Thus the load flow solution procedure can be de-coupled. In this thesis, gauss-seidel method has been used to solve the load flow.

2.1.2.1.2 Dynamic model: The dynamic model for a UPFC is centered round the dynamics of the DC link capacitor. It is well known that the DC link capacitor dynamics is a function of the series and the shunt inverter control variables. The need for including the DC link capacitor dynamics while conducting dynamic studies arises from the fact that it provides the link between the series and the shunt inverter operation in terms of real power balance. Exchange of real power between the series injected voltage by the series inverter and the transmission line current causes the DC link capacitor voltage to either increase or decrease depending on the direction of real power exchange between them. The decrease/increase of the DC link capacitor voltage is sensed by the shunt inverter which absorbs/supplies the necessary real power through the shunt transformer to regulate the DC link capacitor voltage. The models present in the literature vary on the basis of the model used for the shunt and series inverter. The dynamic models for UPFC available in the literature have been divided into shunt inverter and series inverter modeling.

(i) Shunt inverter modeling: The modeling for the shunt inverter of a UPFC can be broadly divided into 4 different models.

- a) Current model [13,18,19,21,22] :- In this model the shunt inverter is assumed to be made of two current sources. One for the D-axis current and the other for the Q-axis current connected to the UPFC bus. The D-axis current in interaction with the bus voltage models the real power injection. By varying the Q-axis current, the amount of reactive power injected to the bus can be varied. This model neglects the interaction between the D and Q-axis currents as the real power flow into the VSI is a function of both currents. Further, the model neglects the DC link capacitor dynamics of the UPFC. The model also neglects the shunt transformer modeling. The model does not take into consideration the voltage generated by the shunt inverter in order to produce the D-Q axis current. It simply assumes that the shunt inverter is capable of producing a variable D-Q axis current and models it as two separate current sources.
- b) Real and reactive power injections [10,17]:- In this model, the shunt inverter is modeled as two separate power sources connected to the UPFC bus. One power source models the real power that is injected to the bus and the other power source models the reactive power injected to the UPFC bus. This model does not take into consideration the voltage generated by the shunt inverter. Further how the DC capacitor dynamics have been modeled is not clear.
- c) Current source in parallel with shunt susceptance [15,16,20]:- In this model the shunt inverter is modeled as variable shunt susceptance in parallel with a current source. The shunt susceptance models the reactive power that can be varied by changing the magnitude of the shunt susceptance. The real power flow through the shunt inverter is modeled as a current source. This model neglects the shunt transformer modeling. This model assumes that the reactive power is a function of the shunt susceptance and

thus dependant on the UPFC bus voltage magnitude. In reality, the shunt inverter can produce reactive power irrespective of the UPFC bus voltage magnitude. The real power flow through the shunt inverter should be a function of the D-Q axis currents. Again, the interaction between the real and reactive currents is neglected. Though the DC capacitor dynamics have been modeled, its dynamics is a function of only the UPFC bus voltage and the current source. On the contrary it should be a function of the real and reactive currents flowing through the shunt inverter.

d) Voltage source model [8,11,14,47,48]:- Here the shunt inverter is modeled as a separate voltage source in shunt with the UPFC bus. The transformer reactance has been included in this model. By modeling the shunt inverter as a separate voltage source in series with shunt transformer reactance, the interaction between the shunt real and reactive currents are modeled. This model for shunt inverter is appropriate for conducting dynamic studies.

(ii) Series inverter modeling [8,13-22,47,48]:- The series inverter is modeled as voltage source in series with the series inverter transformer impedance. This is the most appropriate model as the series inverter in reality injects a voltage in series with the transmission line and thus can be modeled as a voltage source in series with the line. Further, the series voltage source model can be converted into equivalent current injection for conducting dynamic studies [8].

Summarizing the review on modeling for UPFC, the model where the shunt inverter is modeled as a voltage source in series with its transformer reactance [8,11,14,47,48] and the series inverter modeled as a voltage source in series with its transformer

reactance [8,13-22,47,48] is the most appropriate model for conducting dynamic studies. This model includes the interaction between the series and shunt inverter operation. Further, the model includes the DC link capacitor dynamics.

2.2 Summary

A brief review on control strategy and control system design for UPFC has been conducted and summarized here.

1. The problem in the design of an output feedback control system for UPFC is the presence of low margin of stability associated with the series inductance of the transmission line. Intelligent controllers with specific reference to fuzzy controllers have been investigated to overcome this problem. To obtain information for the design of a fuzzy controller, review on various load flow and dynamic models for UPFC have been conducted.
2. All control strategies/control systems for UPFC discussed in the literature suffer either in their complexity of the control system or non-inclusion of real power coordination controller between the series and the shunt inverter control systems or both. Non-inclusion of real power coordination controller could lead to loss of DC link capacitor voltage and subsequent removal of UPFC from operation. A new real power coordination controller will be designed for the UPFC for improved coordination between the series and the shunt inverter operation.
3. Any change in the transmission line reactive power flow is balanced by an equal and opposite change in the reactive power output of the shunt inverter of the UPFC when the shunt inverter is controlling the voltage of the bus to which it is

connected. This means that any request for change in transmission line reactive power by the series inverter of a UPFC is actually supplied by the shunt inverter of the UPFC. This could lead to coordination problems with respect to transmission line reactive power flow control. A new reactive power coordination controller will be designed for this purpose.

4. All control strategies for UPFC discussed in the literature use the series inverter to control the transmission line real and reactive power flow. As mentioned earlier, it is the shunt inverter that actually supplies the reactive power that is requested by the series inverter. Thus the cause and the effect are on two portions of the UPFC. The cause being the series inverter and the effect seen on the shunt inverter. This type of strategy is termed as indirect with respect to transmission line reactive power flow control. A new control strategy for UPFC will be proposed where the shunt inverter directly controls the transmission line reactive power flow.

PSCAD-EMTDC software has been utilized to show the validity of the control system design and the control strategy.

Chapter 3

Present Study

This chapter provides an overall view of the thesis organization. The flow chart shown in Fig.3.1 describes the over all process in designing a control system for UPFC. The study has been bifurcated into two parts. One, using MATLAB simulations and the other using PSCAD-EMTDC simulations.

UPFC being a multi-variable controller, it is necessary to look into its overall effect on power system stability. Frequency domain (small-signal stability) and time domain analysis (transient stability) has been conducted to look into the stability improvement with UPFC. Small-signal stability analysis for power systems with UPFC controlling the real power, reactive power flow in the transmission line/line side bus voltage, DC link capacitor voltage and the UPFC bus voltage simultaneously has been conducted to look into its effect on interconnected power systems. In order to do so, an appropriate model for the UPFC has to be chosen. This includes both the load flow and the dynamic model. Chapter-2 has looked into the various load flow and dynamic models. An initial steady state operating condition is the basic requirement for

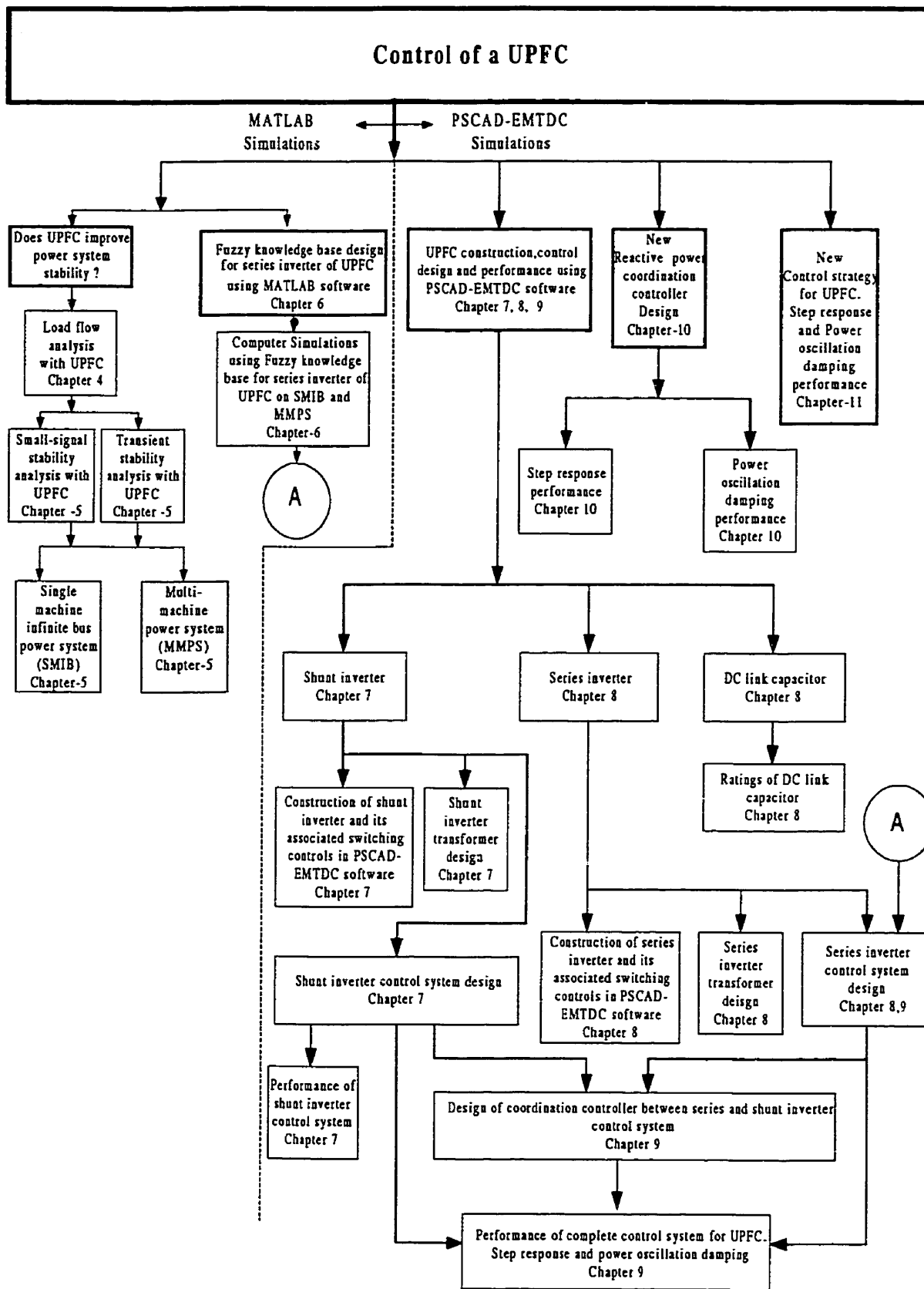


Fig.3.1 Present Study.

conducting frequency or time domain studies. The initial steady state operating condition is obtained by conducting load flow studies. Chapter 4 looks into the load flow analysis with UPFC. Chapter-5 provides the small-signal stability analysis with UPFC. As a corollary, by conducting small-signal stability analysis, the set of system equations needed for conducting time domain computer simulations are verified. Time domain analysis results with UPFC have also been presented in this chapter. Computer simulation has been carried out using the MATLAB software.

Computer simulation on power systems with UPFC included provides the necessary foundation for the design of the knowledge base for the series inverter of a UPFC. Information regarding the fuzzy knowledge base is obtained by conducting fault studies on power systems. The knowledge base designed in chapter-6 has been used in chapter-9 while conducting studies using the PSCAD-EMTDC power system simulation software. As a supplement, the improvement in power oscillation damping using the fuzzy knowledge base designed for the fuzzy controller for the series inverter of a UPFC has been brought in chapter-6.

The PSCAD-EMTDC software is a convenient tool to conduct real time power system studies. This tool has been used to build the UPFC that includes information up to the switching level of the gate-turn off switch (GTO). The shunt and the series inverter transformers, their control systems have been designed and tested using this software. The fuzzy knowledge base designed using the MATLAB software in chapter-6 has been used to build the fuzzy controller in PSCAD-EMTDC software and test it. Further, the coordination controller has been designed and included in the over all control system. The performance of the complete control system has been conducted and the advantage

of using a fuzzy controller for the series inverter has been brought out in this thesis. Chapter-7 deals with the construction of a shunt inverter of a UPFC, its control design and performance. The design of the DC link capacitor, series inverter transformer, fuzzy logic controller and coordination controller has been described in chapter-8 and chapter-9. The performance of the over all control system that includes the shunt, series and the coordination controller has been presented in chapter-9. The effect of series inverter voltage injection on shunt inverter operation has been described in chapter-9. Based on the effect analyzed in chapter-9, a new reactive power coordination controller has been designed. Its performance has been analyzed in chapter-10. Further, the improvement in power system stability has been shown through PSCAD-EMTDC computer simulations.

Based on the effect of series inverter voltage injection on shunt inverter operation. described in chapter-9, leads to another aspect of operation of UPFC. A new control strategy for UPFC has been proposed in chapter-11. Step response studies with the new control strategy for UPFC have been conducted to show the validity of the control strategy. Further, power oscillation damping studies have also been conducted to show the improvement in power system stability. Chapter-11 provides the details of the new control strategy and its performance. The conclusions and future work are presented in chapter-12.

Chapter 4

UPFC Model for Load Flow

4.0 Introduction

Steady state analysis of a power system in the presence of a unified power flow controller (UPFC) would necessitate a model for the UPFC to be included in load flow studies. It is well known that for solving load flows, real and reactive power at load buses, real power and voltage at generator buses, voltage and angle at slack bus have to be specified. An appropriate model for UPFC in terms of real and reactive power needs to be developed to incorporate it in to the load flow. This chapter provides the details of the load flow model used for UPFC. A flow chart depicting the procedure for conducting load flow studies with UPFC model has been presented. The results of load flow studies are important as it provides the initial conditions for conducting small-signal and transient stability studies. Further, the design of the fuzzy logic knowledge base for the series inverter of a UPFC is based on computer simulations which require accurate load flow solutions.

4.1 Model of UPFC

The construction and operation of a unified power controller have been discussed in chapter-1 section 1.3. In brief, a unified power flow controller consists of two voltage source inverters (VSI) connected back to back with a common DC coupling capacitor as shown in Fig.4.1. Such an arrangement allows for all the three functions namely series, shunt and phase angle compensation to be unified into one unit. Inverter-1 is connected to the power system through a transformer T_1 in shunt and the inverter-2 is connected to the power system through another transformer T_2 such that the secondary of the transformer T_2 is in series with the transmission line. The transformers T_1 and T_2 would be referred to as shunt and series transformers respectively for the purpose of clarity.

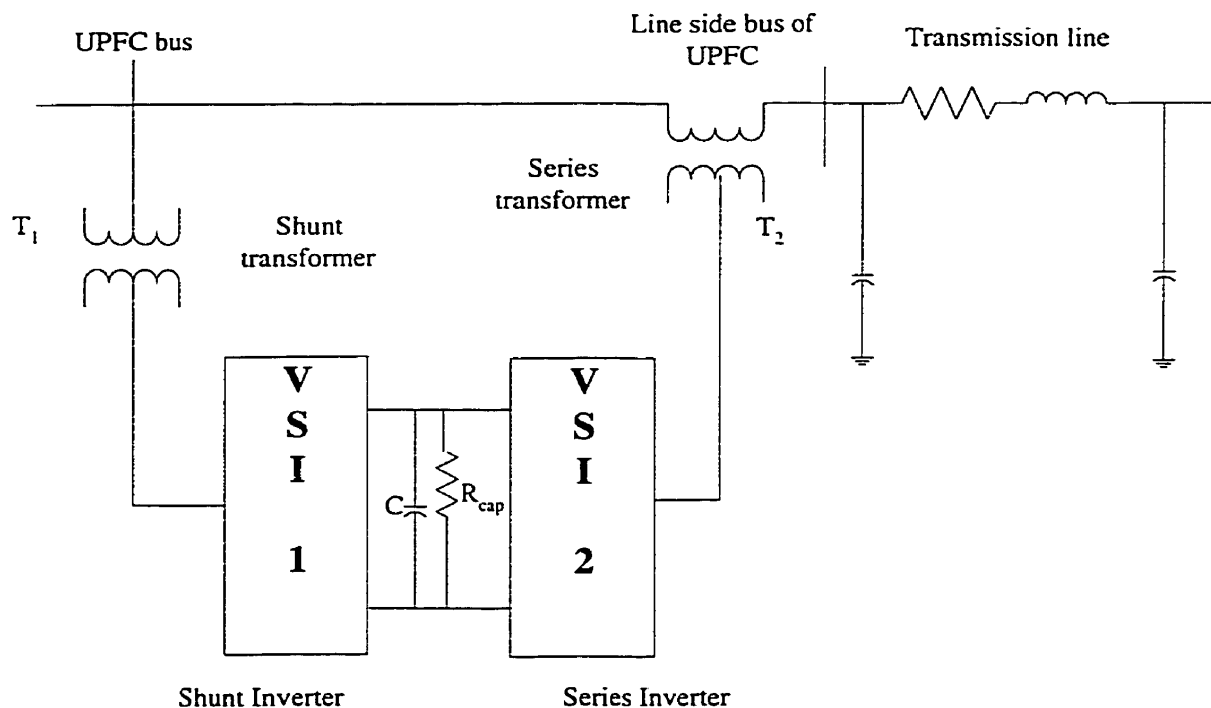


Fig.4.1 Unified power flow controller configuration.

Of the load flow models described in chapter-2, the model given in reference[12] where the shunt inverter and series inverter of a UPFC are modeled as a voltage source in series with their transformer reactance is the simplest of all the models. The model provides for detailed interaction between the series and the shunt inverter. Fig.4.2 shows the UPFC model. X_{sh} and X_{se} represent the reactance of transformers T_1 and T_2 respectively. V_{sh} and V_{se} represent the voltage generated by the shunt and the series inverter respectively. Bus-E and bus-F represent the UPFC bus and the transmission line side bus of UPFC respectively.

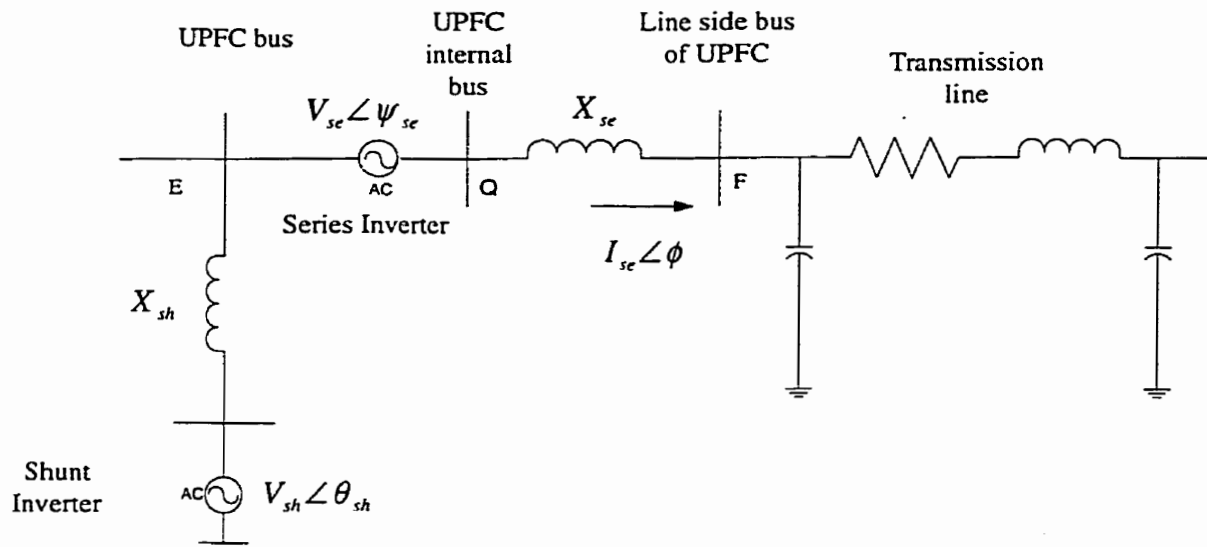


Fig.4.2 UPFC model.

For performing load flow studies with UPFC, the series and the shunt inverters are assumed to produce balanced 60 Hz voltages of variable magnitude and phase angle. The shunt and the series voltage sources phasors can be mathematically represented as

$$\begin{aligned}\bar{V}_{sh} &= V_{sh} (\cos \theta_{sh} + j \sin \theta_{sh}) \\ \bar{V}_{se} &= V_{se} (\cos \psi_{se} + j \sin \psi_{se})\end{aligned}\tag{4.1}$$

Where V_{sh} and V_{se} are the root mean squared magnitudes of the shunt and the series voltage sources. θ_{sh} and ψ_{se} are the shunt and the series voltage source angles with respect to a reference frame.

4.2 Norton's equivalent circuit for UPFC

The series voltage source along with its associated series transformer reactance X_{se} can be converted into equivalent current injections at bus-E and bus-F. Fig.4.3 shows the Norton's equivalent of the circuit shown in Fig.4.2.

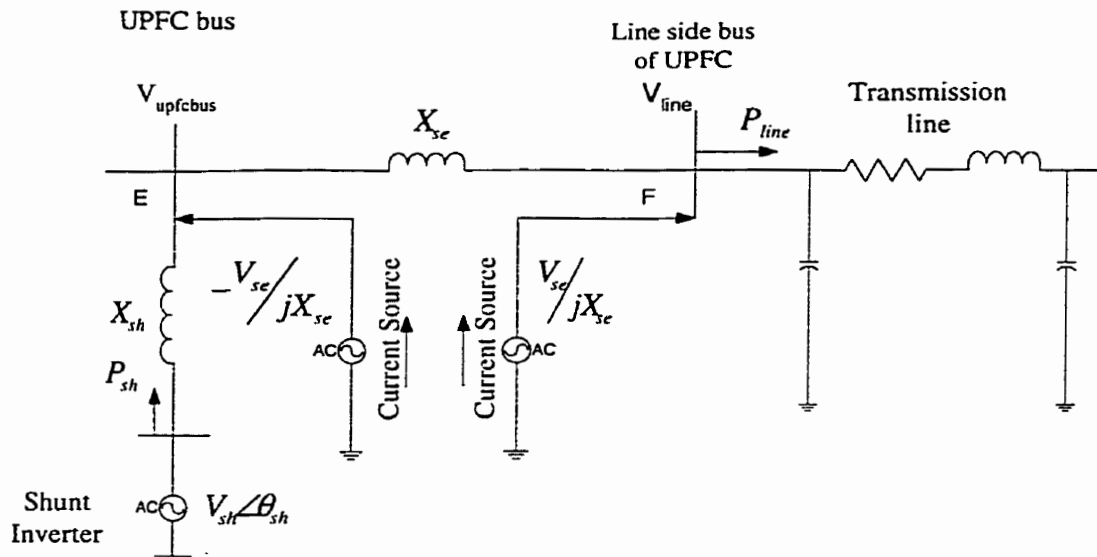


Fig.4.3 Norton equivalent circuit for UPFC.

4.3 Real and reactive power equations for UPFC

The current injections as shown in Fig.4.3 can be converted to appropriate real and reactive power injections at their respective buses. The real and reactive power injections at bus-E are

$$\begin{aligned} P_E &= -V_{se} Y_{EF} V_E \cos(\theta_E - \psi_{se} - \varphi_{EF}) \\ Q_E &= -V_{se} Y_{EF} V_E \sin(\theta_E - \psi_{se} - \varphi_{EF}) \end{aligned} \quad (4.2)$$

Similarly at the bus-F, the real and reactive power injections are

$$\begin{aligned} P_F &= V_{se} Y_{EF} V_F \cos(\theta_F - \psi_{se} - \varphi_{EF}) \\ Q_F &= V_{se} Y_{EF} V_F \sin(\theta_F - \psi_{se} - \varphi_{EF}) \end{aligned} \quad (4.3)$$

Where Y_{EF} is the admittance between the bus-E and bus-F and φ_{EF} is its phase angle. In this case Y_{EF} is the reciprocal of X_{se} . φ_{EF} is equal to -90 degrees as the series transformer is modeled as a pure reactance.

For constancy of DC link capacitor voltage, the following relation should be satisfied.

$$P_{sh} + P_{se} + P_{loss} = 0 \quad (4.4)$$

where P_{sh} and P_{se} are the real powers exchanged with the power system by the shunt and the series voltage sources respectively. P_{loss} represents the losses in the UPFC. Equation 4.4 means that the shunt voltage source compensates the real power demand of the series

voltage source. The above relation provides an equation for the real power demand by the shunt voltage source. The real power demand of the shunt voltage source would then be the negative of the real power exchanged by the series voltage source with the power system. The total real power demand of the shunt voltage source should include the loss due to R_{cap} . The real power demand P_{sh} by the shunt voltage source is given by

$$P_{sh} = -V_{se} V_K y_{km} \cos(\psi_{se} - \theta_K - \varphi_{km}) + V_{se} V_M y_{km} \cos(\psi_{se} - \theta_M - \varphi_{km}) - \frac{(V_{dc}^2)}{R_{cap}} \quad (4.5)$$

The shunt voltage source also provides variable reactive power whose magnitude can be independently adjusted to obtain a required voltage at bus-E. Equations 4.2, 4.3 and 4.5 are used to perform load flow studies for obtaining a steady state power flow conditions.

4.4 Load flow procedure

It is well known that load flow analysis is an iterative type of solution. UPFC has the capability of controlling the real power and transmission line side bus voltage/reactive power flow in a transmission line. Reference [9] provides a very simplistic method to solve load flow that is only applicable to small power systems. The method requires information regarding the short circuit impedance at the bus where the UPFC is to be installed. The algorithm provided to perform load flow study is applicable only to assess the impact of UPFC on power systems in a localized way. Niaki *et.al* [11] has provided a simpler method of performing load flow with UPFC. Here the bus to which the shunt inverter is connected is modeled as a PQ bus and the transmission line side bus is

modeled as a PV bus. This method works only when the variables namely, the UPFC bus voltage, real power flow in the transmission line, transmission line side bus voltage are controlled simultaneously. This method will fail if one wishes to control a subset of them. Further, the solution obtained is multi-valued, meaning that one could obtain a load flow solution that could not be feasible or the UPFC parameters could be out of acceptable limits. This requires that the variables be confined within acceptable limits to obtain feasible solutions. Arabi *et.al* [10] have modeled the shunt inverter and series inverter as a set of PQ injections at the appropriate buses. This model however neglects the interaction between the series and the shunt inverter. Esquivel *et.al* [12] have improved upon the limitations on the model by Niaki *et.al* [11] and provides a solution to the problem of UPFC parameters limitation by fixing the parameter that has violated the limits and freeing the regulated variable. In this case, the need for good initial conditions are emphasized.

To obtain a load flow solution with a specified real power flow in the transmission line and transmission line side voltage with UPFC, the series voltage source V_{se} is decomposed into two phasors. Fig.4.4 shows the phasor diagram with the two components of the series voltage source. The UPFC bus voltage phasor is denoted by V_E . One phasor denoted by V_{seq} is in quadrature with the UPFC bus voltage phasor (V_E) and the other phasor denoted by V_{sep} is in-phase with the UPFC bus phasor (V_E). The function of the quadrature component of the series voltage source V_{seq} is to vary the phase angle of bus V_E to achieve a specified real power flow in the transmission line. The function of the in-phase component of the series voltage source V_{sep} is to achieve a specified transmission line side voltage. The net voltage phasor V_{se} (the phasor sum of V_{sep} and V_{seq}) is denoted

by phasor AD in Fig.4.4. The D and the Q axes refer to the network axis. Since the series voltage phasor V_{se} is added to the UPFC bus voltage phasor V_E , the quadrature component of the series voltage that controls the real power has little effect on the reactive power. This is because the quadrature component of the series voltage changes the phase angle with little change in the magnitude of the bus voltage on the transmission line side (V_{line}). The in-phase component controls the voltage of the bus on the transmission line side (V_{line}) has greater effect on the reactive power than on the real power in the transmission line. This is because the in-phase component has little effect on the phase angle. Thus the interaction between the control of real and reactive power flow in a transmission line is to a great extent reduced. This allows the load flow solution process of achieving a specified real power flow in the transmission line and a line side voltage to be separated.

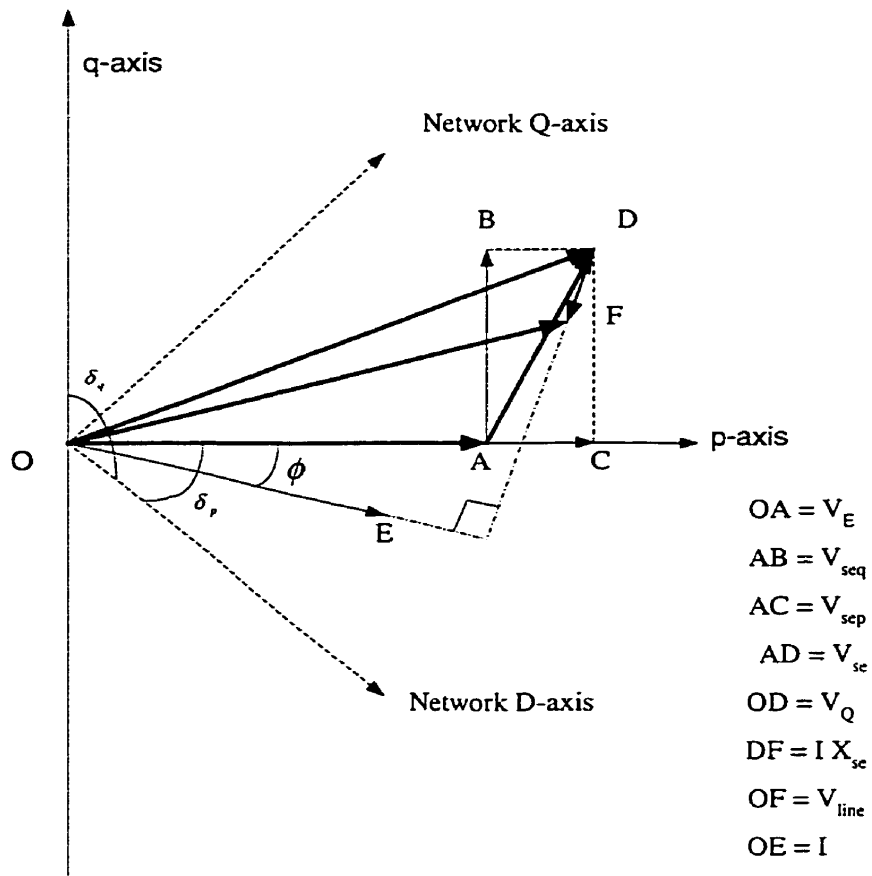


Fig.4.4 Phasor diagram showing the two components of the series voltage source.

4.5 Flowchart for load flow with UPFC

A flow chart for the load flow study is shown in Fig.4.5. As given in equations 4.2, 4.3 and 4.5, the two variables associated with the series voltage are V_{se} and ψ_{se} . The series voltage source magnitude and its phase angle are updated at the end of each iteration to meet the specified real power flow in the transmission line (P_{line}) and the transmission line side bus voltage (V_{line}). The updates for the quadrature and the in-phase component of the series voltage source are done as follows. Let P_{ref} and $V_{lineref}$ (bus-F) be the references for the real power flow in the transmission line and transmission line side bus voltage. From Fig.4.2 it is seen that the power flow through the series transformer reactance X_{se} is approximately given by the following equation.

$$P_{EF} \approx \frac{V_E V_F}{X_{se}} \sin(\theta_E + V_{seq} - \theta_F) \quad (4.6)$$

Let the difference between the P_{ref} and P_{line} be denoted ΔP_{EF} . Differentiating equation 4.6 with respect V_{seq} and introducing the iteration ' k^{th} ' as subscript, we get

$$\Delta P_{EF} \approx \frac{V_{E(k)} V_{F(k)}}{X_{se}} \cos(\theta_{E(k)} + V_{seq(k)} - \theta_{F(k)}) \Delta V_{seq(k)} \quad (4.7)$$

The update for V_{seq} is given by

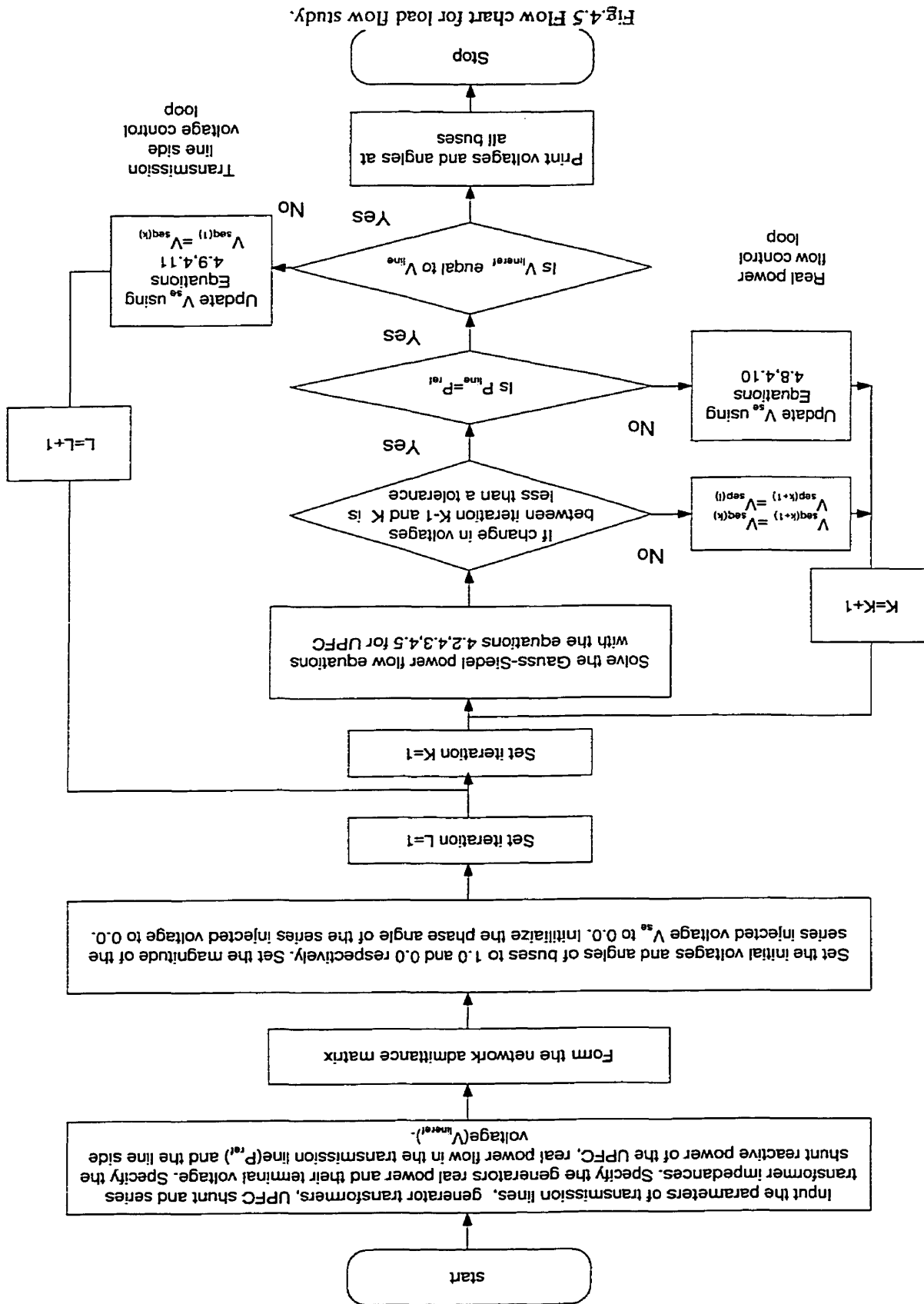


Fig.4.5 Flow chart for load flow study.

$$\Delta V_{seq(k)} \approx \frac{\Delta P_{EF} X_{se}}{V_{E(k)} V_{F(k)} \cos(\theta_{E(k)} + V_{seq(k)} - \theta_{F(k)})} \quad (4.8)$$

$$V_{seq(k+1)} = V_{seq(k)} + \Delta V_{seq(k)}$$

The update of the in-phase component in the ' l^{th} ' iteration that controls the transmission line side bus voltage V_F is given by

$$\Delta V_{sep(l)} = V_{lineref} - V_{F(l)}$$

$$V_{sep(l+1)} = V_{sep(l)} + af(\Delta V_{sep(l)}) \quad (4.9)$$

In equation 4.9, ' af ' represents the acceleration factor. The value chosen for ' af ' is 0.1. A larger value for ' af ' would cause the load flow to diverge. The updated values of V_{seq} and V_{sep} are used to find the magnitude and phase angle of the series voltage source using the following equation. For the real power flow control loop, the updates for the series voltage source are

$$\tilde{V}_{se} = V_{seq(k+1)} \left(\cos(\theta_E + \frac{\pi}{2}) + j \sin(\theta_E + \frac{\pi}{2}) \right) + V_{sep(l)} (\cos(\theta_E) + j \sin(\theta_E))$$

$$V_{se} = abs(\tilde{V}_{se}) \quad (4.10)$$

$$\psi_{se} = angle(\tilde{V}_{se})$$

For the transmission line side voltage control loop, the updates for the series voltage source are

$$\begin{aligned}\bar{V}_{se} &= V_{seq(k)} \left(\cos(\theta_E + \frac{\pi}{2}) + j \sin(\theta_E + \frac{\pi}{2}) \right) + V_{sep(l+1)} (\cos(\theta_E) + j \sin(\theta_E)) \\ V_{se} &= abs(\bar{V}_{se}) \\ \psi_{se} &= angle(\bar{V}_{se})\end{aligned}\tag{4.11}$$

4.6 Summary

Load flow studies are very important as it provides the necessary initial conditions for conducting small-signal and large-signal performance studies with UPFC. This chapter has discussed a load flow model for UPFC. The corresponding equations relating to integration of the UPFC model into load flow studies has been described. A flow chart for conducting load flow with UPFC has been provided that includes real power flow control in the transmission line and the transmission line side voltage control. The load flow procedure based on gauss-seidel method takes into consideration the effect of quadrature and in-phase component of series injected voltage on real and reactive power flow in the transmission line. The real power flow is adjusted automatically by the quadrature injected component of the series voltage and the transmission line side bus voltage is controlled by the in-phase component of the series voltage. This allows for least interaction between the control of real and reactive power in a transmission line. The logic for updating the series injected voltage in a load flow to meet the specified real power flow and line side voltage has been described.

Chapter 5

Does UPFC improve power system stability?

5.0 Introduction

UPFC being a multi-variable controller, it becomes necessary to assess its impact on power system stability. The steady state analysis with UPFC described in Chapter-4 provides the basic foundation for conducting dynamic stability studies with UPFC. Dynamic stability studies include frequency domain (small-signal stability) and time domain analysis that includes three-phase fault studies (Transient stability). The frequency domain analysis requires the formation of a state matrix that includes all the differential/algebraic equations associated with the power system. The differential/algebraic equations of the power system include that of generator, exciter, power system stabilizers (PSS) and power system network. In this context, it is important to include the DC link capacitor dynamics of the UPFC while analyzing power system stability. This is because the DC link capacitor forms a common link between the series and the shunt inverter. To accurately model the interaction between the series and the shunt inverter operation, inclusion of the DC link capacitor dynamics is necessary.

In order to conduct frequency and time domain analysis, an appropriate dynamic model for UPFC should include the DC link capacitor dynamics. This chapter provides a procedure leading to the formation of the state matrix that includes the UPFC DC link capacitor dynamics for analyzing small-signal stability.

The purpose of this chapter is to develop the necessary set of equations that includes the dynamics of the UPFC for conducting small-signal analysis and time domain computer simulations with UPFC to show the improvement in power system stability. Further, time domain simulations provide valuable information for the design of a fuzzy controller for the UPFC.

5.1 Small-Signal Stability Analysis

5.1.1 State matrix Formulation

Small-signal stability analysis provides information regarding the damping/frequency associated with the devices present in power system. For example, the range of frequencies over which electromechanical oscillations occur for generators a single machine infinite bus power system is between 0.7 and 2 Hz. In the case of multi-machine power system involving many areas, the range over which the inter-area oscillations between groups of generators occur is between 0.2 and 0.7 Hz.

Small-signal stability analysis with UPFC depends on the modeling of the UPFC. Small-signal stability analysis without modeling the DC link capacitor dynamics could lead to inaccurate result [13]. This is because any interaction between the series injected voltage and the transmission line current leads to real power exchange between the series inverter of the UPFC and the transmission line. The real power exchange leads to decrease/increase in the DC link capacitor voltage. Thus by neglecting the DC link

capacitor dynamics could lead to inaccurate results. DC link capacitor dynamics have been considered, but not all the variables have been utilized while studying stability [11, 14]. Independent research work were carried out by Huang *et.al* [26] and Kannan *et.al* [41] to model the interaction between the series and shunt inverter by including the DC link capacitor dynamics into small signal stability analysis. Though the DC link capacitor dynamics have been included into small-signal stability analysis, reference [26] has neglected the combined effect of power system stabilizers and UPFC on power system performance. The effect of combined operation of PSS and UPFC with the DC link capacitor dynamics included will be studied using small-signal stability analysis. Further, one needs to take note of the choice of input variables for conducting small-signal stability studies. In reference [26], the modulation index and the phase angle of the shunt and series inverters have been considered for conducting small-signal stability studies. On the contrary, the output of the control systems for the shunt and series inverters are the reference voltages that are to be generated by the shunt and series inverters. Based on these reference voltages the corresponding modulation index is calculated. Thus it would be appropriate to use the voltages and their phase angle as the input variables to correctly assess the impact of UPFC on power system stability.

Small-signal stability involves the formulation of a linear state equation that takes into consideration the dynamics of the power system components like generators, exciter, and power system stabilizers. In the presence of a UPFC, the equations governing its operation should be included in the linear state equation and the whole system should then be analyzed. In this context it would be necessary to develop a dynamic model for UPFC and include it with the models for generator, exciter and PSS in order to form the

state equation and analyze small-signal stability.

5.1.1.1 UPFC Modeling: In this section, a step by step procedure leading to the formulation of the dynamic equations associated with the UPFC for conducting small-signal stability studies and time domain analysis will be presented. The dynamics associated with the UPFC is that of the DC link capacitor. Fig.5.1 shows the UPFC with its associated DC and AC side current flows.

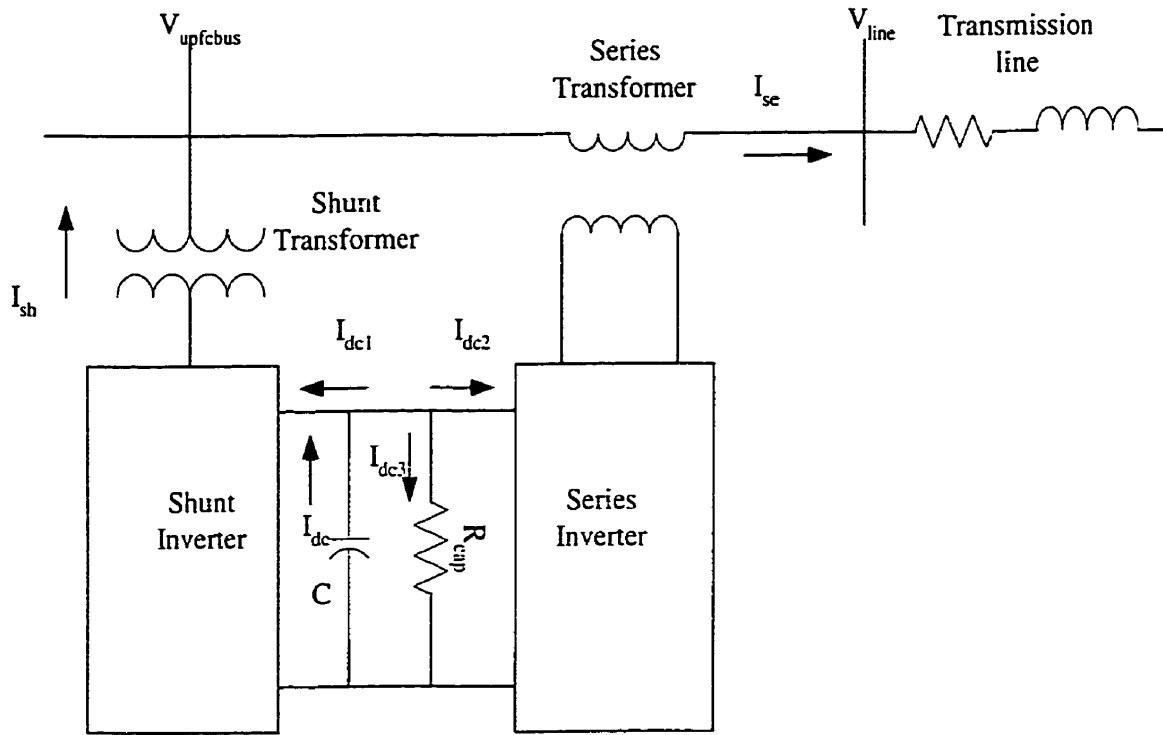


Fig.5.1 UPFC with its associated DC and AC side currents.

Let the voltage generated by the shunt inverter be denoted by $V_{sh} \angle \theta_{sh}$ and the series inverter voltage denoted by $V_{se} \angle \psi_{se}$. Let I_{sh} be the current flowing out of the shunt inverter through the shunt transformer and I_{se} be the transmission line current. Let the UPFC bus voltage be denoted by $V_{upfcbus}$ and the transmission line side bus voltage by V_{line} . Let I_{dc} be the dc current flowing out of the capacitor. Let I_{dc1} and I_{dc2} be the dc

currents flowing out of the shunt inverter and the series inverter respectively on the DC side. Let I_{dc3} represent the current through the shunt resistance connected in parallel across the DC link capacitor.

By kirchoff current law, we have,

$$\hat{I}_{dc} = \hat{I}_{dc1} + \hat{I}_{dc2} + \hat{I}_{dc3} \quad (5.1)$$

'^' represents the actual value. These will be converted to per unit representation later.

Consider now the real power flow on the AC side through the shunt transformer. The shunt transformer current I_{sh} and the shunt inverter voltage $V_{sh} \angle \theta_{sh}$ are split into their network D-Q axis components. Let I_{shD} and I_{shQ} be the network D-Q axis currents flowing through the shunt transformer and let V_{shD} and V_{shQ} be the network D-Q axis voltage of the shunt inverter. The three phase real power flowing out of the shunt inverter is given by

$$\hat{P}_{sh} = 3 \operatorname{Re} al \left[\left(\hat{V}_{shD} + j \hat{V}_{shQ} \right) \left(\hat{I}_{shD} + j \hat{I}_{shQ} \right)^* \right] \quad (5.2)$$

Where '*' denotes the conjugate. Representing the D-Q axis variables with their peak values, we get

$$\hat{P}_{sh} = \frac{3}{2} \left(\hat{V}_{shDpk} \hat{I}_{shDpk} + \hat{V}_{shQpk} \hat{I}_{shQpk} \right) \quad (5.3)$$

On the DC side the real power flowing out of the shunt inverter is given by

$$\hat{P}_{DCsh} = \hat{V}_{dc} \hat{I}_{dc1} \quad (5.4)$$

Assuming a loss-less operation for the shunt inverter we have

$$\hat{P}_{DCsh} = \hat{P}_{sh} \quad (5.5)$$

Thus, equating the two terms we get,

$$\hat{V}_{dc} \hat{I}_{dc1} = \frac{3}{2} \left(\hat{V}_{shDpk} \hat{I}_{shDpk} + \hat{V}_{shQpk} \hat{I}_{shQpk} \right) \quad (5.6)$$

In order to put equation 5.6 into per unit representation, assume the peak of the AC phase voltage as the base voltage and the peak of the AC current as the base current. The AC power base is given by

$$P_{ACbase} = \frac{3}{2} \hat{V}_{pk\phi} \hat{I}_{pk\phi} \quad (5.7)$$

Putting equation 5.6 in per unit we get,

$$I_{dc1} = \frac{3}{2V_{dc}} (V_{shD} I_{shD} + V_{shQ} I_{shQ}) \quad (5.8)$$

Assuming a loss-less operation for the series inverter, the power flow on the DC side through the series inverter is given by

$$\hat{P}_{DCse} = \hat{V}_{dc} \hat{I}_{dc2} \quad (5.9)$$

Let I_{seD} and I_{seQ} be the network D-Q axis currents flowing through the series transformer and V_{seD} and V_{seQ} be the network D-Q axis voltage of the series inverter. The three phase real power generated by the series inverter due to the interaction between the series injected voltage V_{se} and the transmission line current I_{se} is given by

$$\hat{P}_{se} = 3 \text{Re} al \left[\left(\hat{V}_{seD} + j \hat{V}_{seQ} \right) \left(\hat{I}_{seD} + j \hat{I}_{seQ} \right)^* \right] \quad (5.10)$$

Where '*' denotes the conjugate. Representing the D-Q axis variables by their peak values, we get

$$\hat{P}_{se} = \frac{3}{2} \left(\hat{V}_{seDpk} \hat{I}_{seDpk} + \hat{V}_{seQpk} \hat{I}_{seQpk} \right) \quad (5.11)$$

Assuming a loss-less operation for the series inverter and equating 5.9 and 5.11, we get,

$$\hat{V}_{dc} \hat{I}_{dc2} = \frac{3}{2} \left(\hat{V}_{seDpk} \hat{I}_{seDpk} + \hat{V}_{seQpk} \hat{I}_{seQpk} \right) \quad (5.12)$$

Representing equation 5.12 in per unit we get,

$$I_{dc2} = \frac{3}{2V_{dc}} \left(V_{seD} I_{seD} + V_{seQ} I_{seQ} \right) \quad (5.13)$$

The current through the resistance in parallel with the DC link capacitor is given by

$$\hat{I}_{dc3} = \frac{\hat{V}_{dc}}{\hat{R}_{cap}} \quad (5.14)$$

Representing equation 5.14 in per unit, we get

$$I_{dc3} = \frac{V_{dc}}{R_{cap}} \quad (5.15)$$

The dc link dynamics is given by the following equation

$$\frac{d\hat{V}_{dc}}{dt} = -\frac{\hat{I}_{dc}}{C} \quad (5.16)$$

where V_{dc} is the voltage on the DC link capacitor and 'C' is its capacitance in farads. The time 't' is in seconds. Putting equation 5.16 in per unit, we get

$$\frac{dV_{dc}}{dt} = -\omega_0 C' I_{dc} \quad (5.17)$$

Where C' is given by

$$C' = \frac{1}{\omega_0 Z_{base} C}$$

Expressing I_{dc} in terms of I_{dc1} , I_{dc2} and I_{dc3} using equation 5.8, 5.13 and 5.15 we get,

$$\frac{dV_{dc}}{dt} = -\omega_0 C \cdot \left[\frac{3}{2} \left(\frac{V_{shD} I_{shD} + V_{shQ} I_{shQ} + V_{seD} I_{seD} + V_{seQ} I_{seQ}}{V_{dc}} \right) + \frac{V_{dc}}{R_{cap}} \right] \quad (5.18)$$

Equation 5.18 represents the dynamic model for the UPFC.

5.2 Small-signal stability evaluation

5.2.1 Case-1: Single machine infinite bus power system (SMIB)

a) Improvement in rotor angle mode damping: Appendix-1 has detailed the formulation of the state matrix for studying the small-signal stability of a power system. In this section the procedure for the formulation of the state matrix as explained in the Appendix-1 will be applied to a single machine infinite bus power system. The improvement in the damping on the rotor angle mode in the case of SMIB will be shown based on eigen value analysis. Fig.5.2 shows a single machine infinite bus power system. The generator is rated at 900MVA and is connected to an infinite bus through a double circuit 230 kV line and a step up transformer. The total line length is 220 km. The series inverter of the UPFC is connected between bus-3 and bus-4. The shunt inverter is connected between bus-3 and bus-5 (not shown in Fig.5.2). The UPFC is used to control the transmission line real power flow (P_{line}) and provide power oscillation damping. Also the transmission line side bus voltage (V_{line}), i.e bus-4 voltage is controlled. The shunt inverter controls the DC link capacitor voltage (V_{dc}) and the UPFC bus voltage ($V_{upfcbus}$). In this case bus-3 represents the UPFC bus.

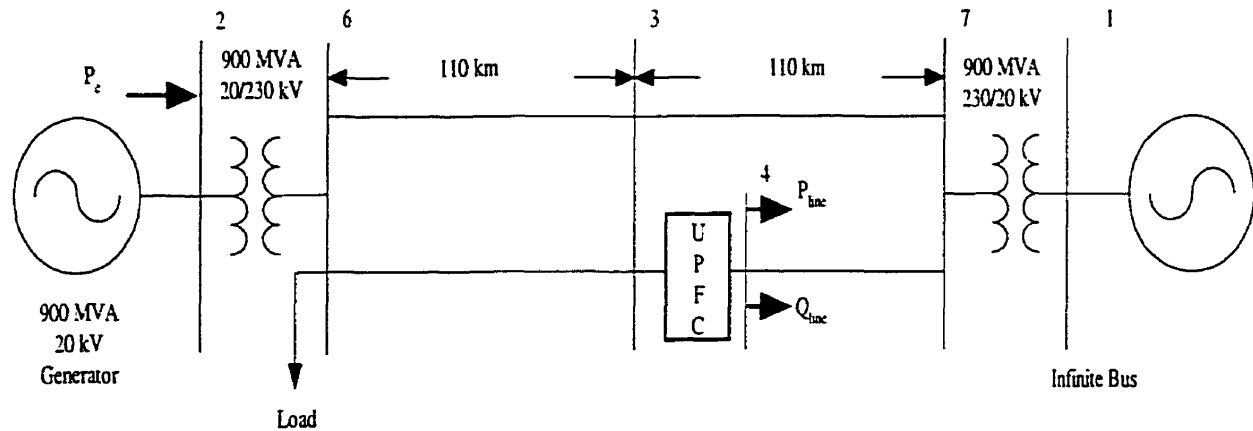


Fig.5.2 Single machine infinite bus power system.

The transmission line real power flow (P_{line}) is controlled by injecting a series voltage in quadrature (V_{seq}) and bus-4 voltage (V_{line}) is controlled by injecting a series voltage in-phase (V_{sep}). The phasor addition of the two voltages V_{sep} and V_{seq} provides the series inverter with the appropriate magnitude and phase angle for controlling P_{line} and V_{line} . The generator is equipped with a power system stabilizer (PSS) and a static exciter. The parameters of the generator, PSS, exciter UPFC and the network are given in Appendix-1. The matrices A, B, C and D of SMIB power system is formed as detailed in Appendix-1. The initial conditions for the UPFC are that the series inverter injects a voltage of 0.08 pu (V_{seq}). The in-phase voltage phasor (V_{sep}) is 0.01pu. The capacitor is rated at 1000 μ F. The real power flow in the transmission line (P_{line}) having the UPFC is 269 MW. The load at bus-3 is 200+j50 MVA. The shunt inverter is supplying 150 MVAR initially. The eigen values without the UPFC is given in Table 5.1. From Table 5.1 it is seen that all the eigen values are on the left half of the complex plane. Table 5.2 shows the eigen values of the SMIB power system with a UPFC. Comparing Table 5.1 and Table 5.2, the rotor angle mode damping has increased with the inclusion of UPFC. The damping factor of

the rotor mode oscillation has increased from 0.0736 (Table 5.1) to 0.140 (Table 5.2) with the addition of UPFC. The frequency of oscillations has increased from 0.97 Hz to 1.0 Hz. This study has shown that the UPFC helps in improving the damping of the generator rotor angle/speed oscillations.

Table 5.1 Eigen values with PSS (SMIB)

Eigen Number	Eigen Value
1	-54.6872
2	-50.0
3	-31.733
4	-14.85±j16.41
5	-0.4505±j6.1 ($\xi=0.073$ rotor angle mode)
6	-3.5484
7	-0.10
8	-0.1832

Table 5.2 Eigen values with PSS and UPFC (SMIB)

Eigen Number	Eigen Value
1	-54.4671
2	-50.0
3	-32.22
4	-15.455 ± j 14.156
5	-0.8963 ± j 6.33 ($\xi=0.14$ rotor angle mode)
6	-3.4316
7	-1.1316
8	-0.1011
9	-0.1827
10	-0.438
11	-104.28
12	-2.04
13	-0.7007

b) Effect of series inverter in-phase component (V_{sep}) on rotor angle mode damping:

In this section, the effect of in-phase component (V_{sep}) of series voltage control on rotor angle mode damping will be analyzed. The generator rotor angle mode eigen values of the power system with UPFC were analyzed for different operating conditions of reactive power flow in the transmission line. Table 5.3 shows the eigen values for different values of in-phase component of series voltage (V_{sep}). It is seen from Table 5.3 that the in-phase component of series voltage (V_{sep}) has insignificant effect on the rotor angle mode damping. This is due to the fact that the in-phase component of series voltage (V_{sep}) has more effect on the transmission line reactive power flow (Q_{line}) than on the transmission line real power flow (P_{line}). More detailed analysis on the effect in-phase component of series voltage (V_{sep}) on the transmission line reactive power flow (Q_{line}) and shunt inverter reactive power will be studied in chapter 9.

Table 5.3 Eigen values with UPFC for different values of in-phase component (V_{sep}) of series voltage (SMIB)

S.no	V_{seq}	V_{sep}	P_{line} (MW)	Q_{line} (MVAR)	Eigen value associated with rotor mode
1	0.08	-0.050	260	0	-0.8952 ± j 6.3302
2	0.08	-0.025	264	15	-0.8958 ± j 6.3315
3	0.08	-0.010	266	25	-0.8960 ± j 6.3322
4	0.08	0.010	270	38	-0.8963 ± j 6.3331
5	0.08	0.025	272	48	-0.8964 ± j 6.3337
6	0.08	0.050	275	65	-0.8964 ± j 6.3346

c) Effect of shunt inverter controlling the transmission line side bus voltage on rotor angle mode damping: The stability of the power system with the shunt inverter of a UPFC controlling the transmission line side bus voltage has been evaluated. In this analysis, the strategy used for UPFC is that the shunt inverter controls the DC link capacitor voltage and the transmission line side bus voltage. The series inverter controls the UPFC bus voltage and the transmission line real power flow. Table 5.4 shows the effect of shunt inverter controlling the transmission line side bus voltage.

Table 5.4 Eigen values with shunt inverter of UPFC controlling the transmission line side bus voltage (SMIB)

S.no	V_{seq}	V_{sep}	P_{line} (MW)	Q_{line} (MVAR)	Eigen value associated with rotor mode
1	0.08	-0.050	260	0	-0.8995 ± j 6.34
2	0.08	-0.025	264	15	-0.8986 ± j 6.34
3	0.08	-0.010	266	25	-0.8980 ± j 6.34
4	0.08	0.010	270	38	-0.8974 ± j 6.333
5	0.08	0.025	272	48	-0.8963 ± j 6.33
6	0.08	0.050	275	65	-0.8949 ± j 6.33

Table 5.4 shows that controlling the transmission line side bus voltage by the shunt inverter of a UPFC does not cause instability. In fact, it has improved the system stability as compared to without UPFC. Thus the strategy of controlling the transmission line side bus voltage by the shunt inverter of a UPFC is feasible and provides stable operation.

5.2.2 Case-2: Multi-machine power system (MMPS)

a) Improvement in inter-area oscillations: Low frequency oscillations are inherent to an interconnected power system. These oscillations can be spontaneous or caused due to sudden loss of transmission lines or due to load disturbances. Power system stabilizers (PSS) have been used on generators to damp these low frequency oscillations. UPFC placed in a network where power exchanges on tie lines take place, can be helpful in improving the damping of these power oscillations. In this study a multi-machine power system representing two areas have been considered for analyzing the inter-area oscillations. Fig.5.3 shows a multi-machine power system [36]. Generators 2 and 3 provide power to Area-1 loads and generators 1 and 4 provide power to Area-2 loads. The generation in Area-1 is 1400 MW and the load in Area-1 is $967+j100$ MVA. Area-2 has deficiency in generation of about 400 MW and hence imports real power from Area-1. Area-1 and Area-2 are connected by three transmission lines. The UPFC is located in Area-1. Area-1 is exporting around 400MW ($P_{inter-area}$) of power to Area-2. Area-2 has a load of $1767+j100$ MVA. A shunt capacitor of 350 MVAR is installed at bus-8. The UPFC is supplying 200 MVAR of shunt reactive power to support bus-5 voltage. The series inverter is injecting a voltage of 0.03 p.u in quadrature (V_{seq}) and 0.01 p.u in-phase

(V_{sep}). The real power flow in the UPFC line (P_{line}) is 229 MW. The generators, exciter/PSS, network and the UPFC parameters are given in Appendix-2.

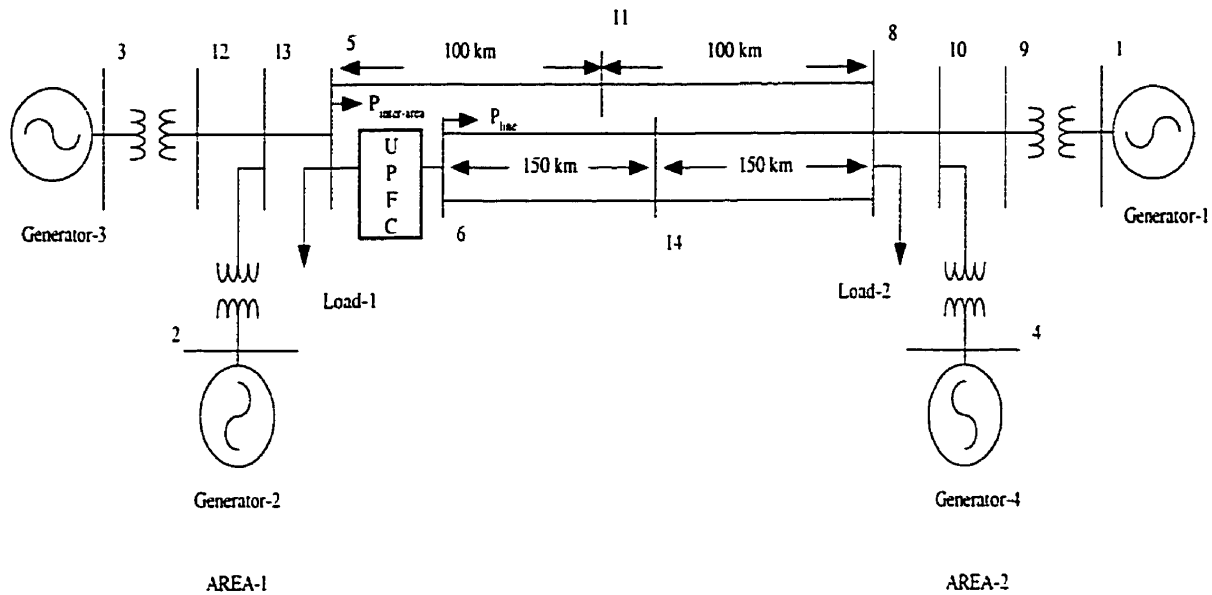


Fig.5.3 Two area power system with UPFC.

Each generator has been represented by 10 state variables. The UPFC is represented with one state variable. Generator-1 has been assumed as the reference generator. The rotor angle variables have been referenced to generator-1 rotor angle (δ_1). The state matrix is a square 41×41 matrix and is formed using the method described in Appendix-1. Since generator-1 is assumed as reference generator, the matrix is reduced by deleting the row and column corresponding to $\Delta\delta_1$ and expressing the other generator rotor angles with respect to generator-1. The matrix is modified by entering $-\omega_0$ in the column for $\Delta\omega_1$ in row corresponding to generators 2, 3 and 4 rotor angles. The loads have been modeled as constant impedance. The state matrix is a square 40×40 matrix. For the above two-area

power system, there are three swing modes. Two of them are local modes and one inter-area mode. Table-5.5 shows the swing modes of the two- area power system with PSS only. The complete list of eigen values with and without UPFC is given in Appendix-3. It would be observed from Appendix-3 that eigen number 29 in Table A3-1 and eigen number 32 in Table A3-2 are zero eigen value. This is due to the assumption that the generator torques are independent of speed deviation meaning that the damping due to governor action is zero.

Table 5.5 Eigen values with PSS (MMPS)

S.no	Eigen Value	Damping factor (ζ)	Frequeny Hz	Description
1	$-1.77 \pm j11.3$	0.154	1.79	Area-1 Local Mode
2	$-1.7066 \pm j10.872$	0.155	1.73	Area-2 Local Mode
3	$-0.5674 \pm j 6.009$	0.09	0.95	Inter-Area Mode

Table 5.6 shows the swing modes of the two-area power system with UPFC. Comparing Table 5.5 and Table 5.6, it is seen that with the addition of the UPFC, the local mode damping has remained almost the same but the inter area modes damping has increased. The frequency of oscillation of the local and inter-area has remained almost the same. This study has proved by small signal stability analysis that UPFC helps in damping the inter-area mode.

Table 5.6 Eigen values with PSS and UPFC (MMPS)

S.no	Eigen Value	Damping factor (ζ)	Frequency Hz	Description
1	$-1.808 \pm j11.4$	0.1566	1.814	Area-1 Local Mode
2	$-1.645 \pm j10.72$	0.1516	1.706	Area-2 Local Mode
3	$-0.8586 \pm j 5.8963$	0.144	0.938	Inter-Area Mode

b) Effect of series inverter in-phase component (V_{sep}) on inter-area mode damping:

The swing mode eigen values of the multi-machine power system with UPFC were analyzed for different operating conditions of in-phase component (V_{sep}) of series voltage. Table 5.7 shows the inter-area eigen values for different values of in-phase component (V_{sep}) of series voltage. It is seen from Table 5.7 that the in-phase component (V_{sep}) of series voltage has insignificant effect on the inter-area mode damping. This is due to the fact that the in-phase component (V_{sep}) of series voltage has more effect on the transmission line reactive power flow (Q_{line}) than on the transmission line real power flow (P_{line}).

Table 5.7 Eigen values with UPFC for different values of in-phase component (V_{sep}) of series voltage (MMPS)

S.no	V_{seq}	V_{sep}	P_{line} (MW)	Q_{line} (MVAR)	Eigen value associated with Inter-area mode
1	0.03	-0.050	222.10	-55.36	$-0.8505 \pm j 5.816$
2	0.03	-0.025	225.30	-46.60	$-0.8540 \pm j 5.850$
3	0.03	-0.010	227.15	-41.20	$-0.8560 \pm j 5.870$
4	0.03	0.010	229.50	-33.50	$-0.8586 \pm j 5.8963$
5	0.03	0.025	231.40	-27.65	$-0.8605 \pm j 5.9158$
6	0.03	0.050	234.35	-17.45	$-0.8634 \pm j 5.9479$

c) Effect of shunt inverter controlling the transmission line side bus voltage on inter-area mode damping: The stability of the multi-machine power system with the shunt inverter of a UPFC controlling the transmission line side bus voltage has been evaluated. In this analysis, the strategy used for UPFC is that the shunt inverter controls the DC link capacitor voltage and the transmission line side bus voltage. The series inverter controls the UPFC bus voltage and the transmission line real power flow. Table 5.8 shows the effect of shunt inverter controlling the transmission line side bus voltage.

Table 5.8 Eigen values with shunt inverter of UPFC controlling the transmission line side bus voltage (MMPS)

S.no	V_{seq}	V_{sep}	P_{line} (MW)	Q_{line} (MVAR)	Eigen value associated with inter-area mode
1	0.03	-0.050	222	-55	$-0.855 \pm j 5.81$
2	0.03	-0.025	225	-46	$-0.858 \pm j 5.85$
3	0.03	-0.010	227	-41	$-0.8606 \pm j 5.87$
4	0.03	0.010	229	-33	$-0.8631 \pm j 5.89$
5	0.03	0.025	231	-27	$-0.865 \pm j 5.91$
6	0.03	0.050	234	-17	$-0.8677 \pm j 5.95$

Table 5.8 shows that controlling the transmission line side bus voltage via the shunt inverter of a UPFC does not cause instability. Thus the strategy of controlling the

transmission line side bus voltage by the shunt inverter of a UPFC is feasible and provides stable operation.

5.3 Transient stability evaluation

Section 5.2 has shown by frequency domain analysis that the UPFC helps in damping local and inter-area mode oscillations. This section will confirm the improvement in local and inter-area mode damping with UPFC by time domain analysis. For the time domain analysis, the differential/algebraic equations associated with the generator, exciter, PSS and the UPFC are solved simultaneously using Runge-Kutta 4th order method.

DC link capacitor dynamics plays an important role when considering the simultaneous operation of the shunt and series inverter of a UPFC. The DC link capacitor dynamics have been neglected by most researchers while conducting computer simulations [16-19].

Since UPFC is a multi-variable controller, it is necessary that all the variables be included while conducting computer simulations. In reference [14], not all the variables have been included while conducting computer simulations.

In references [15,20], the model for UPFC used is not an accurate one. They model shunt inverter reactive power capability as a variable shunt capacitor and the real power capability as a parallel current source. They have excluded the shunt inverter transformer modeling while conducting computer simulations. By neglecting the shunt inverter transformer model, the interaction between the shunt real and reactive power is absent.

In all the computer simulations carried out here, the DC link capacitor dynamics have been included. Also variables namely P_{line} , V_{dc} and $V_{upfcbus}$ have been controlled simultaneously. As seen from Table 5.3 and Table 5.7, the effect of in-phase component

(V_{sep}) of series voltage on rotor angle mode/ inter-area mode damping is insignificant and hence disabling the line side voltage controller for all time domain simulations is justified. Further, the shunt inverter of the UPFC is modeled as a variable voltage source allowing for its magnitude and phase angle to be varied. The shunt inverter transformer has been included while conducting time domain computer simulations.

5.3.1 Single machine infinite bus power system (SMIB)

a) Improvement in generator rotor angle mode damping: The SMIB power system shown in Fig.5.2 is simulated using MATLAB software. The generators are represented by their differential/algebraic equations given in section 5.1.1.2. The exciter is modeled as a constant gain. The PSS consists of a washout circuit and two lead-lag blocks. The exciter/PSS block diagram is shown in Appendix-1. The UPFC dynamics is represented by equation 5.18.

Three-phase fault is applied at the generator terminals (bus-2) for 80 msec and removed without any change in the network configuration. Fig.5.4 shows the generator rotor speed ($\Delta\omega_r$) oscillations of the generator with and without UPFC. The addition of UPFC has improved the damping of the generator rotor speed ($\Delta\omega_r$) oscillations.

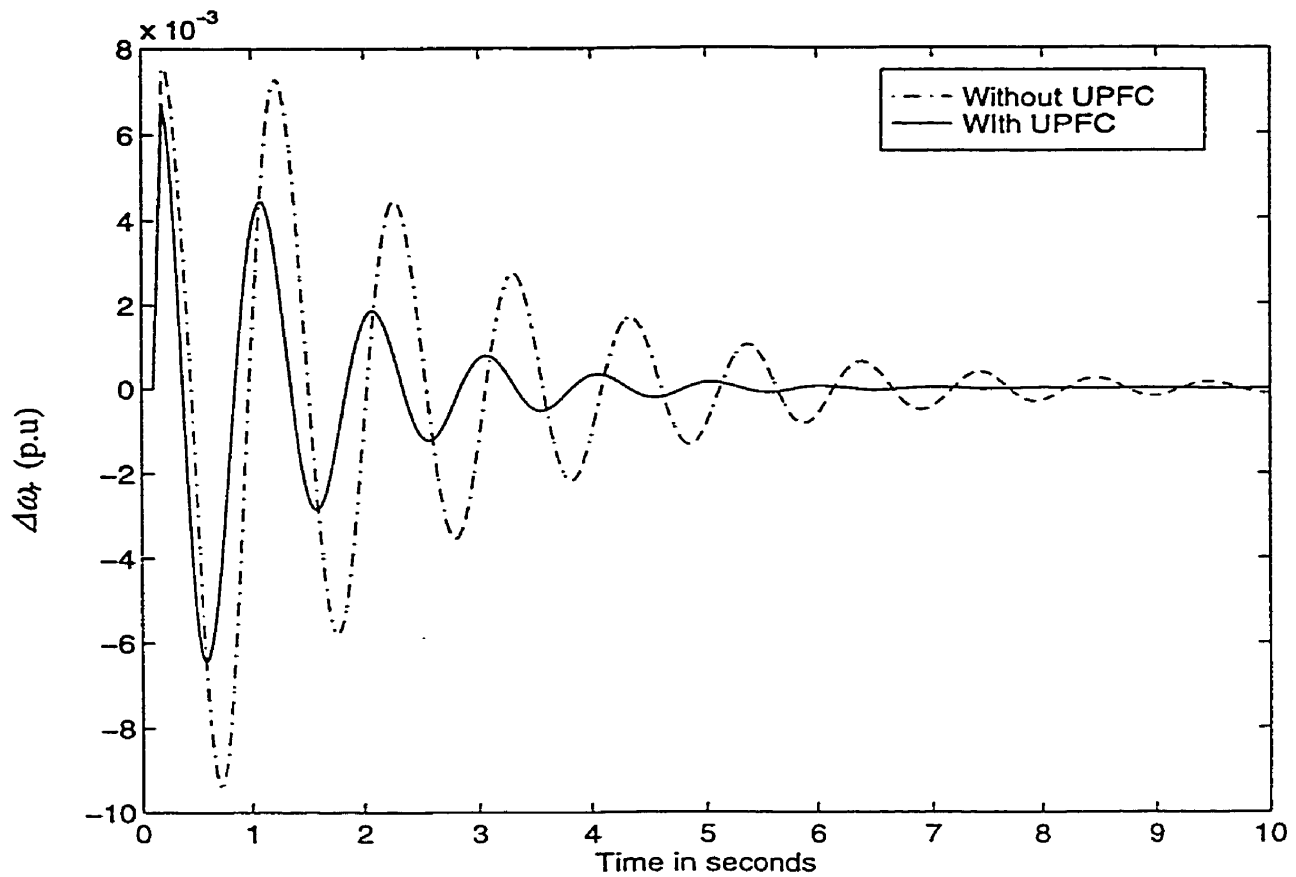


Fig.5.4 Generator rotor speed ($\Delta\omega_r$) oscillation damping with and without UPFC.

The generator rotor speed ($\Delta\omega_r$) oscillations of the generator without UPFC takes approximately 10 seconds to damp out, while with UPFC included, it takes around 5 seconds.

Fig.5.5 shows the generator electrical power (P_e) oscillations with and without UPFC.

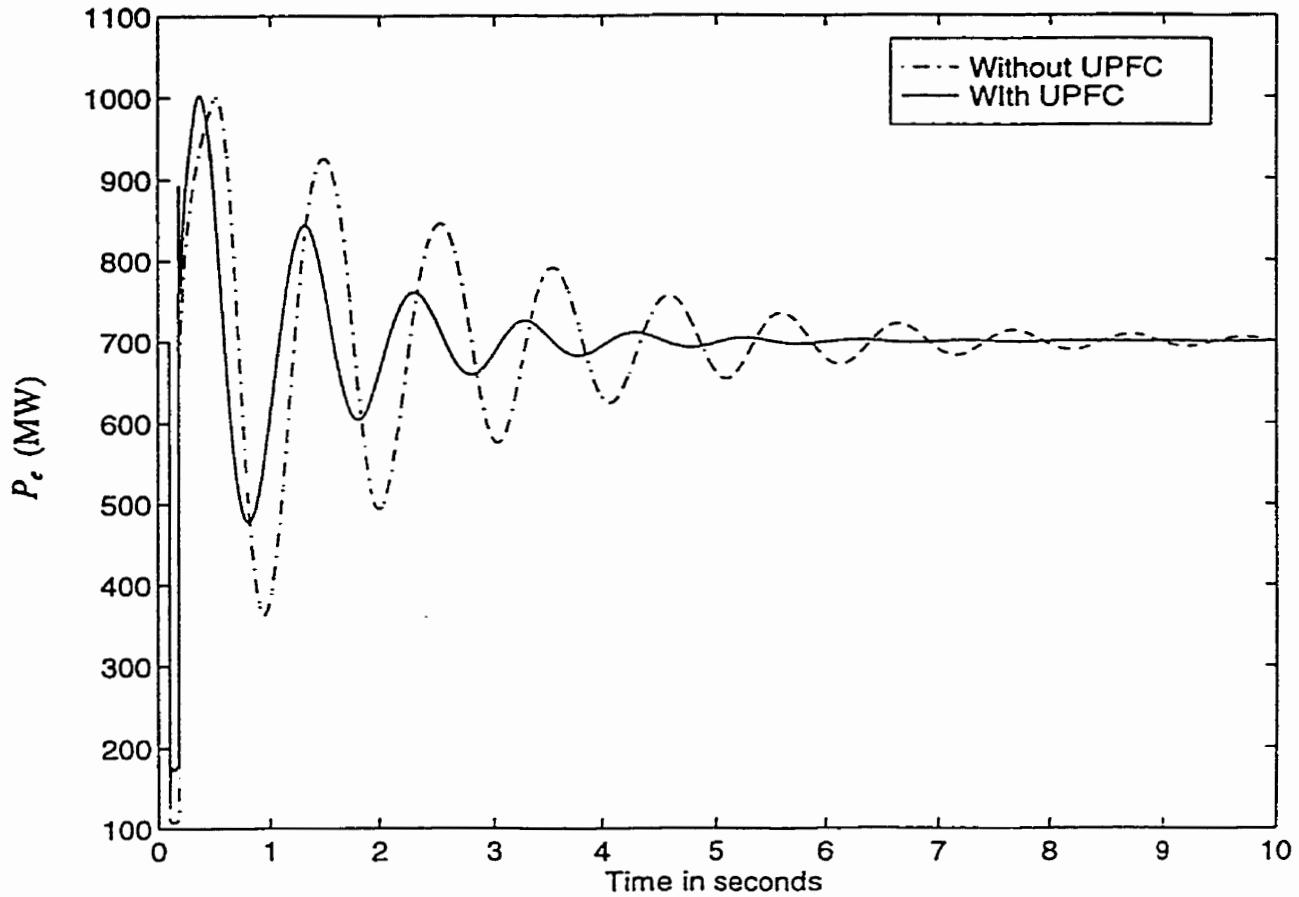


Fig.5.5 Generator electrical power (P_e) oscillations with and without UPFC.

The generator electrical power (P_e) oscillations show improved damping with UPFC. The generator electrical power (P_e) without UPFC takes about 10 seconds to damp out while with UPFC included, it takes about 5 seconds. The peak of the generator electrical power (P_e) is about 1000MW soon after the fault is removed. Further, subsequent generator electrical power oscillations (P_e) with UPFC included in the power system damp out quickly. Computer simulations on a SMIB power system have confirmed the results obtained from small-signal stability analysis. It has shown that with UPFC included in the power system, the damping of the generator rotor mode oscillation increases.

Fig.5.6 shows the DC link capacitor voltage (V_{dc}) oscillations due to three-phase fault at the terminals of the generator. The DC link capacitor voltage (V_{dc}) shows very little oscillations. This is because the shunt inverter has very effectively controlled the DC link capacitor voltage (V_{dc}). At the instant of fault occurrence, the DC link capacitor voltage (V_{dc}) drops as it supplies some of its stored energy to the fault. Subsequent to fault removal, the shunt inverter modulates its consumption of real power and controls the DC link capacitor voltage (V_{dc}) to its reference value.

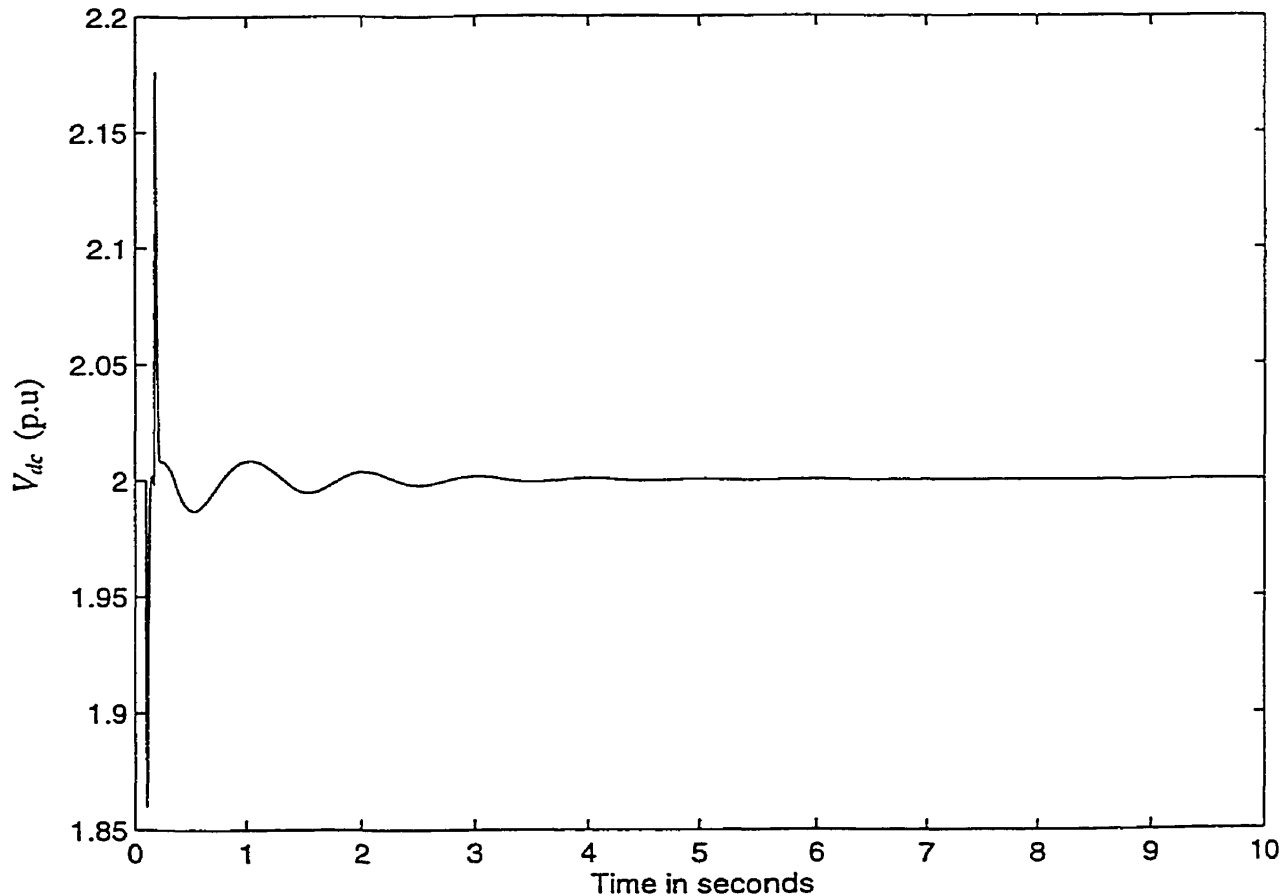


Fig.5.6 DC link capacitor voltage (V_{dc}) oscillations for three phase fault at the generator terminals.

5.3.2 Multi-machine power system (MMPS)

a) **Improvement in inter-area damping** : The power system shown in Fig.5.3 has been simulated using the MATLAB software. The load flow as explained in chapter-4 has been performed with the UPFC. The results of the load flow are used as initial conditions for performing transient simulations. The generators are equipped with PSS and static exciter. The generators are modeled in the d-q axis representation. Each of these generators is modeled with one d-axis damper and two q-axis damper windings. The differential/algebraic equations for the generator are in Appendix-1. For the multi-machine power system, generator G1 is assumed as the reference generator. For the UPFC, the shunt inverter controls the bus-5 voltage ($V_{upfcbus}$) and the DC link capacitor voltage (V_{dc}). Bus-5 voltage will also be referred to as UPFC bus voltage. The series inverter controls the transmission line real power flow (P_{line}) by injecting adjustable magnitude of voltage in quadrature (V_{seq}) with the UPFC bus voltage ($V_{upfcbus}$). The in-phase injection (V_{sep}) has been disabled as it has very little effect on the swing modes (Table-5.7). Two different fault location cases have been simulated to show the improvement of damping oscillations with UPFC. The conditions are

1. When Area-1 supplies Area-2 with 400MW of power and a three-phase fault occurs for 80msecs at the load bus in Area-1 (sending end) with no change in the network structure.
2. When Area-1 supplies Area-2 with 400MW of power and a three-phase fault occurs for 80msecs at the load bus in Area-2 (receiving end) with no change in the network structure.

i) Three-phase fault at bus-5 (Exporting area)

In this simulation a three-phase fault is assumed to occur in Area-1 for 80 msecs at bus-5 with no change in the structure of the power system. The three-phase fault condition was simulated by connecting an admittance of value $-j20$ in shunt with bus-5. In this simulation, it is assumed that the protection as a whole has failed to operate and hence no change in the power system structures. The real power flow in the double circuit line (P_{line}) (bus-6 to bus-14) without the UPFC is 228MW. The shunt inverter of the UPFC controls the bus-5 voltage ($V_{upfcbus}$) and the DC link capacitor voltage (V_{dc}). So to be able to compare the dynamic performance with the UPFC, the real power flow in the UPFC line (P_{line}) is adjusted to 228MW. This is achieved by injecting a series voltage of 0.03 p.u in quadrature (V_{seq}) with the UPFC bus voltage (bus-5). During and after the fault the shunt capacitors at the load buses are not disconnected. Also the UPFC is not disconnected during the fault period. The initial voltage on the DC link capacitor (V_{dc}) of the UPFC is 2.0 per unit. Fig.5.7 shows the rotor angle oscillations of generator G2 with respect to generator G1. As seen from Fig.5.7, the initial operating point for generator G2 with respect to generator G1 (δ_{21}) is around 10 degrees. With the three-phase fault at bus-5, the generator electrical powers (G3 and G2) in Area-1 go to a very low value causing the generators G3 and G2 rotor angle to increase in the first swing. For the assumed fault condition, in the first swing of the rotor angle oscillations of generator (G2) rotor angle (δ_{21}) with respect to generator (G1) without the UPFC is nearly 30degrees. The reason for the first swing to increase is that subsequent to fault occurrence and removal, the generator rotor angle of G3 (δ_3) and G2 (δ_2) increases much faster than that of G1 (δ_1). Since G1 is assumed as the reference generator, the difference in rotor angle between G2

and G1 (δ_{21}) increases. The simulation with PSS (without UPFC) shows very low damping of generator rotor angle (δ_{21}) oscillations. Further, the generator rotor angle G2 (δ_{21}) oscillations damp out after nearly 9 seconds without UPFC. With UPFC in service, the generator rotor angle oscillation (δ_{21}) damp out much faster with the first swing of nearly 25 degrees. Subsequent rotor angle oscillations are well damped with UPFC. It takes approximately 5 s to damp out the generator G2 rotor angle (δ_{21}) oscillations with UPFC.

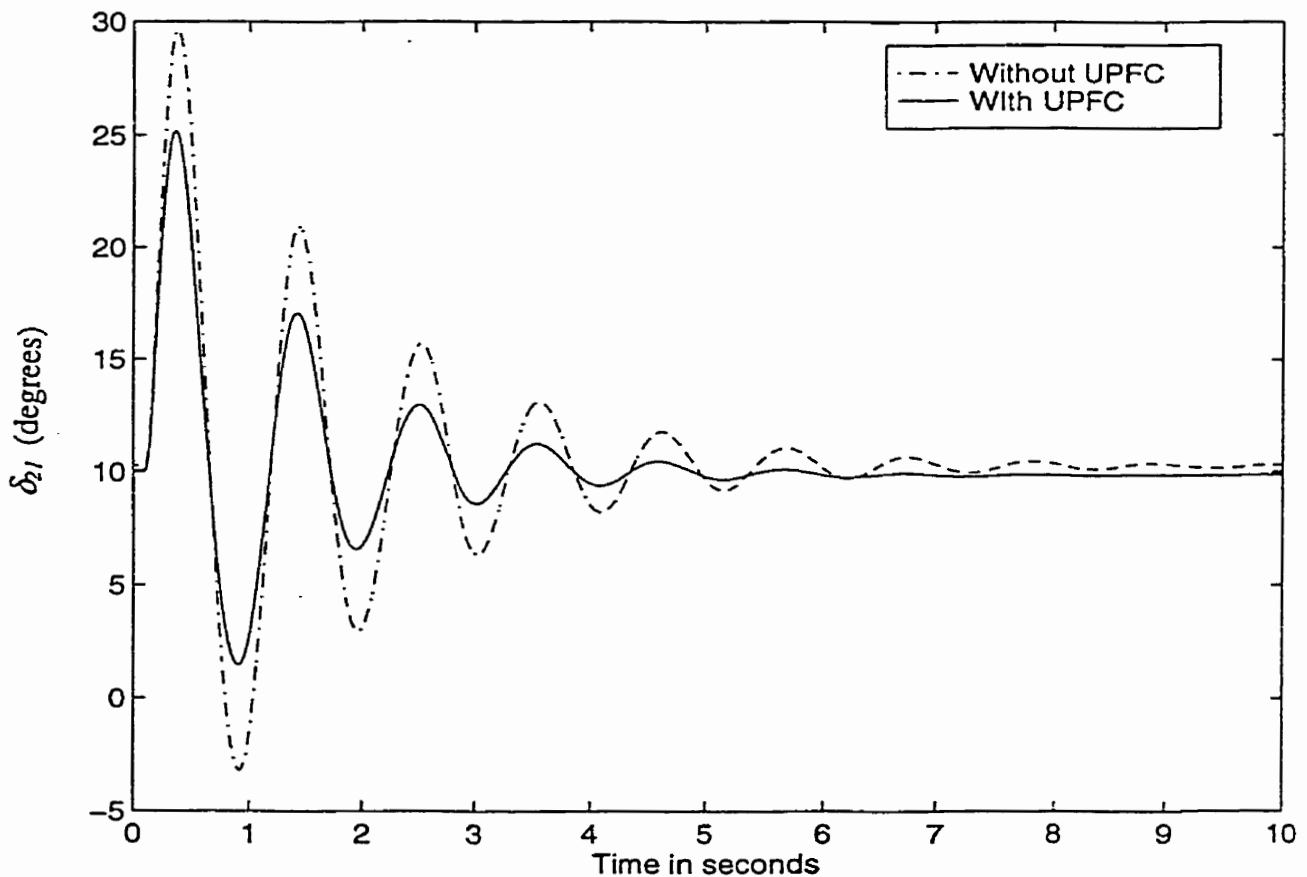


Fig.5.7 Rotor angle oscillations of generator G2 with respect to generator G1 (δ_{21}) (with and without UPFC).

Fig.5.8 shows the rotor angle oscillations of generator G3 with respect to generator G1 (δ_{31}). The initial angle difference between generator G3 and G1 is around 20 degrees. The first swing of generator G3 with respect to generator G1 with UPFC included is around 40degrees. As seen from the Fig.5.8, the damping of generator G3 rotor angle oscillations with respect to G1 (δ_{31}) is poor. It takes around nearly 9 seconds to damp out the oscillations. With the UPFC in service, the first swing is reduced significantly and it takes lesser time to damp out the oscillations.

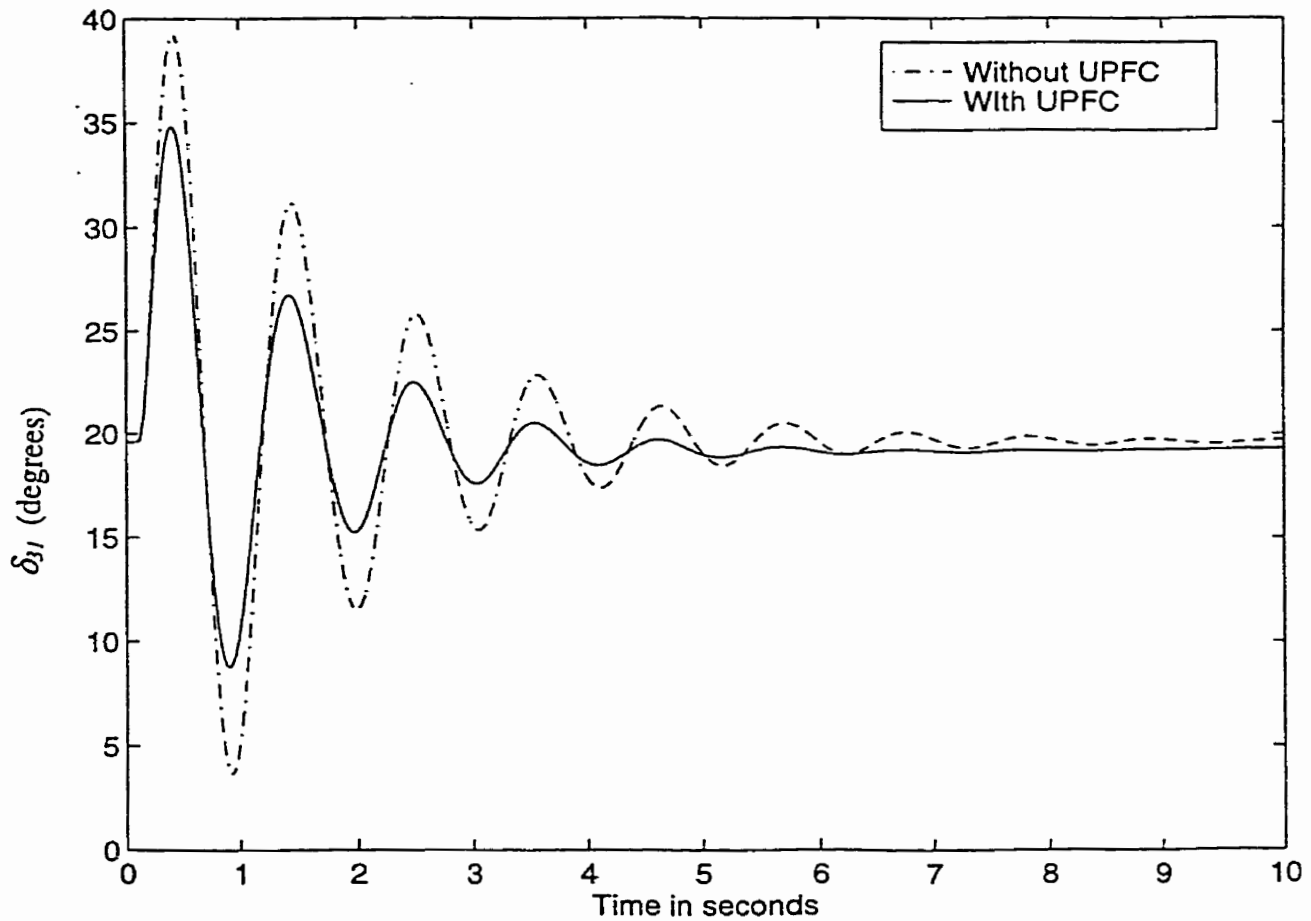


Fig.5.8 Rotor angle oscillations of generator G3 with respect to generator G1 (with and without UPFC).

Fig.5.9 shows the total inter-area real power flow ($P_{inter-area}$) oscillations for a three-phase fault at bus-5. The initial inter-area power flow ($P_{inter-area}$) is 400MW. This amount of real power is exported to Area-2 from Area-1 through a double circuit line of 300 km long and one single circuit line of 200 km long. The application of a three-phase fault causes the total generator electrical power of G3 and G2 (P_e) to drop to near zero. This causes the inter-area real power flow ($P_{inter-area}$) to drop to almost zero. After the fault removal with no change in the network structure, the inter-area real power flow ($P_{inter-area}$) shoots up to around 625MW without UPFC, while the over shoot with UPFC installed is around 575MW. The damping of the inter-area real power ($P_{inter-area}$) oscillations are improved with UPFC.

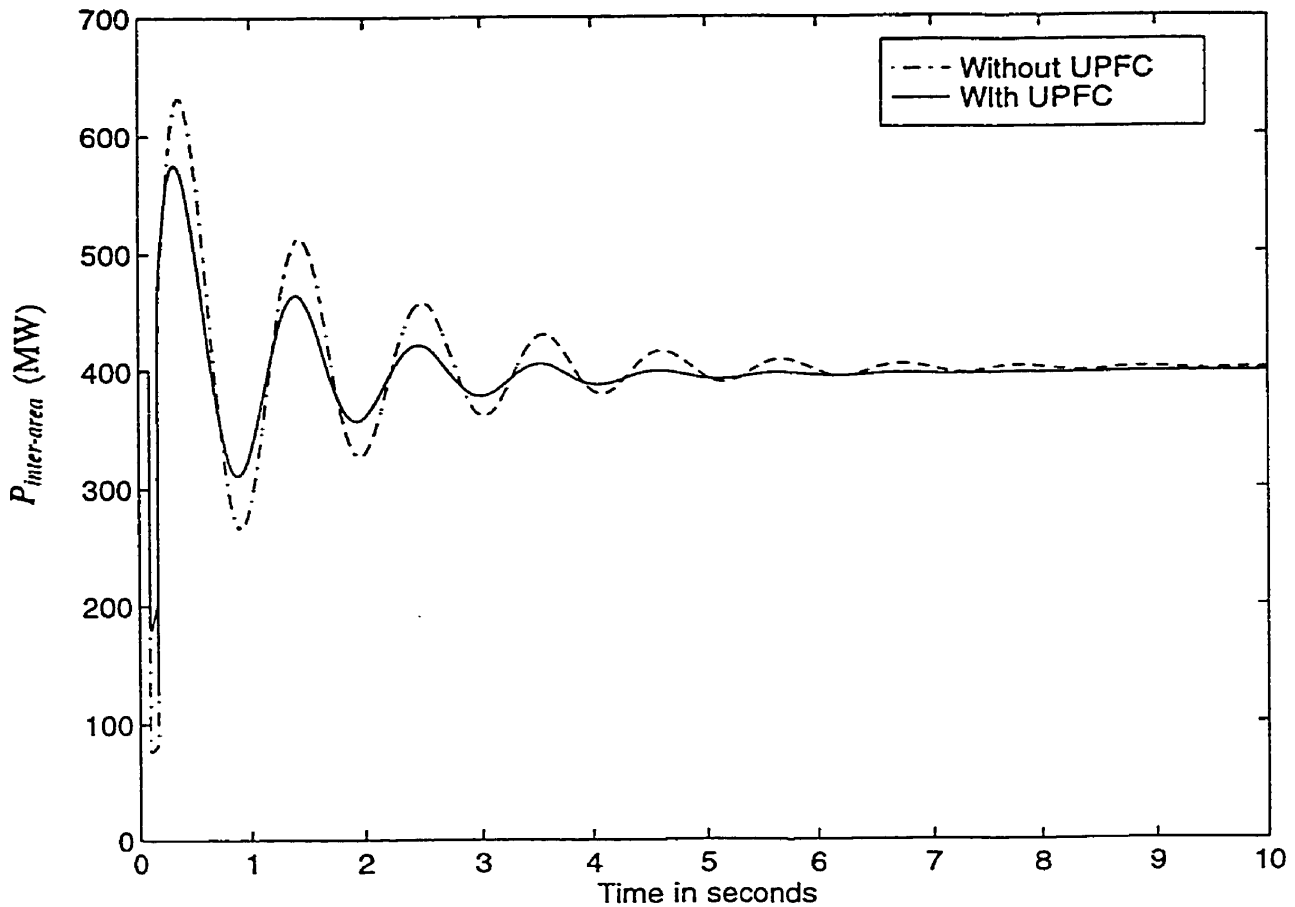


Fig.5.9 Inter-area real power flow oscillations (with and without UPFC).

Fig.5.10 shows the real power flow in the transmission line with UPFC (P_{line}). The initial power flow in the UPFC line (P_{line}) is around 228MW. The three phase fault causes the real power flow in the UPFC line (P_{line}) to drop to around 50MW during the fault period. Subsequent to fault removal the real power flow in the UPFC line (P_{line}) increases to about 350MW without UPFC. With UPFC the real power flow (P_{line}) in the first swing increases only up to 325 MW. Subsequent power swings of P_{line} are well damped.

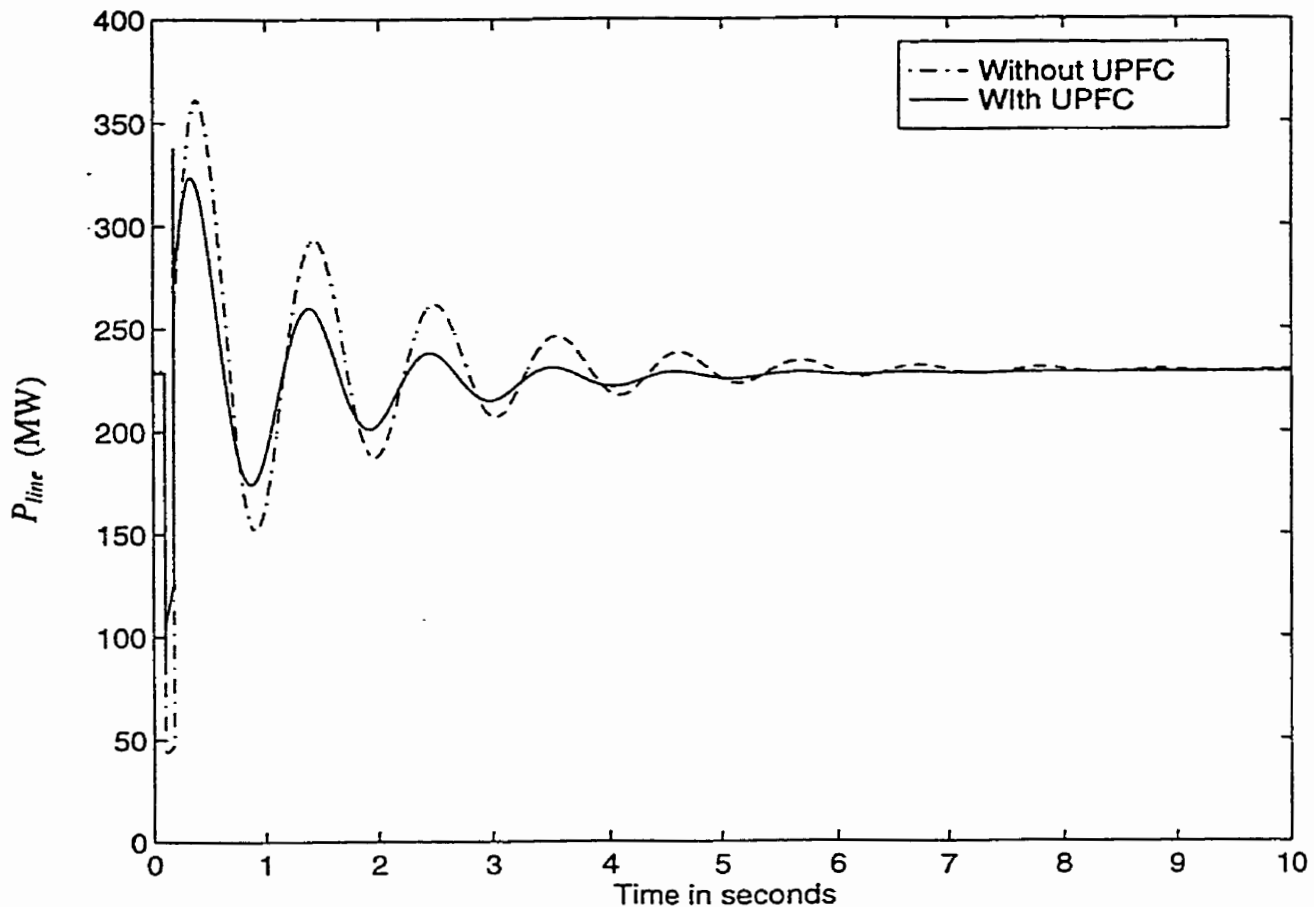


Fig.5.10 Real power flow oscillations in the double circuit line (with and without UPFC).

ii) Three-phase fault at bus-10 (Importing area):

In this simulation case, a three-phase fault is assumed to occur in Area-2. Subsequent to fault removal, no change is made in the structure of the power system. Also the shunt capacitors are assumed to be in service before and after the fault removal. The initial operating condition of the power system is such that Area-1 exports 400MW of real power to Area-2. Under this condition, the real power flow in the transmission line with UPFC (P_{line}) is 228MW. The series inverter of the UPFC injects 0.03pu (V_{seq}) in

quadrature with the UPFC bus voltage (bus-5). The shunt inverter controls the bus-5 voltage ($V_{upfcbus}$) and the DC link capacitor voltage (V_{dc}).

Fig.5.11 shows the rotor angle oscillations of generator G2 with respect to generator G1 (δ_{21}). The operating conditions are the same as that in the previous case. The three-phase fault is simulated by connecting a large admittance of value $-j20$ p.u in shunt at bus-10.

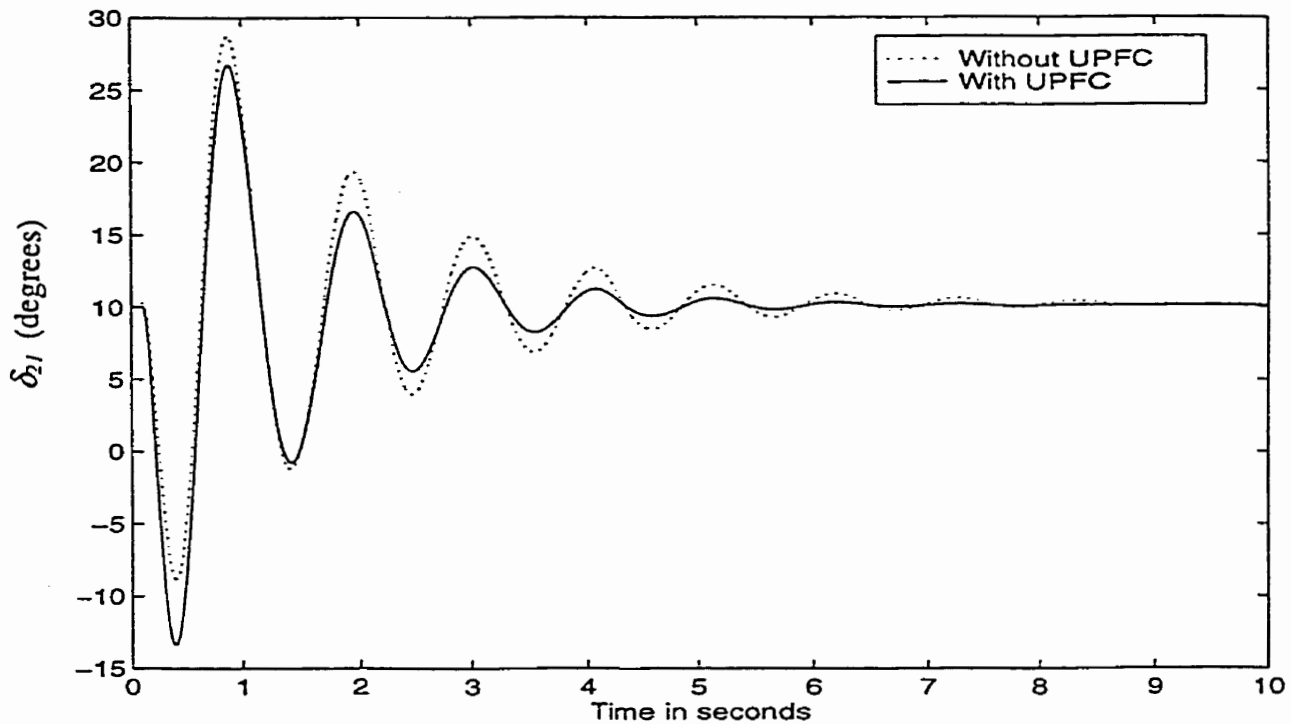


Fig.5.11 Rotor angle oscillations of generator G2 with respect to generator G1 (δ_{21}) (with and without UPFC).

A fault at bus-10 which is in the importing area causes the rotors of generators G1 and G4 to accelerate quickly thereby increasing the rotor angle difference between generator G2 and generator G1 (δ_{21}). It reaches a value of approximately -10 degrees in the first swing without UPFC. But the first swing with UPFC reaches a value of approximately $-$

15 degrees. The excursion of the rotor angle is nearly 25 degrees with UPFC. The reason that could be attributed to this is that since the fault is in Area-2 the excursion of the rotor angle of generator G2 is reduced due to the presence of UPFC (providing positive damping to Area-1 generators) and hence the difference between the rotor angles of generators G2 and G1 (δ_{21}) has increased. Subsequent oscillations of δ_{21} are well damped.

Fig.5.12 shows the generator rotor angle oscillations between G3 and G1 (δ_{31}). Here too, the excursion in the first swing is more with UPFC due to the reason mentioned above. Subsequent swings are well damped with UPFC.

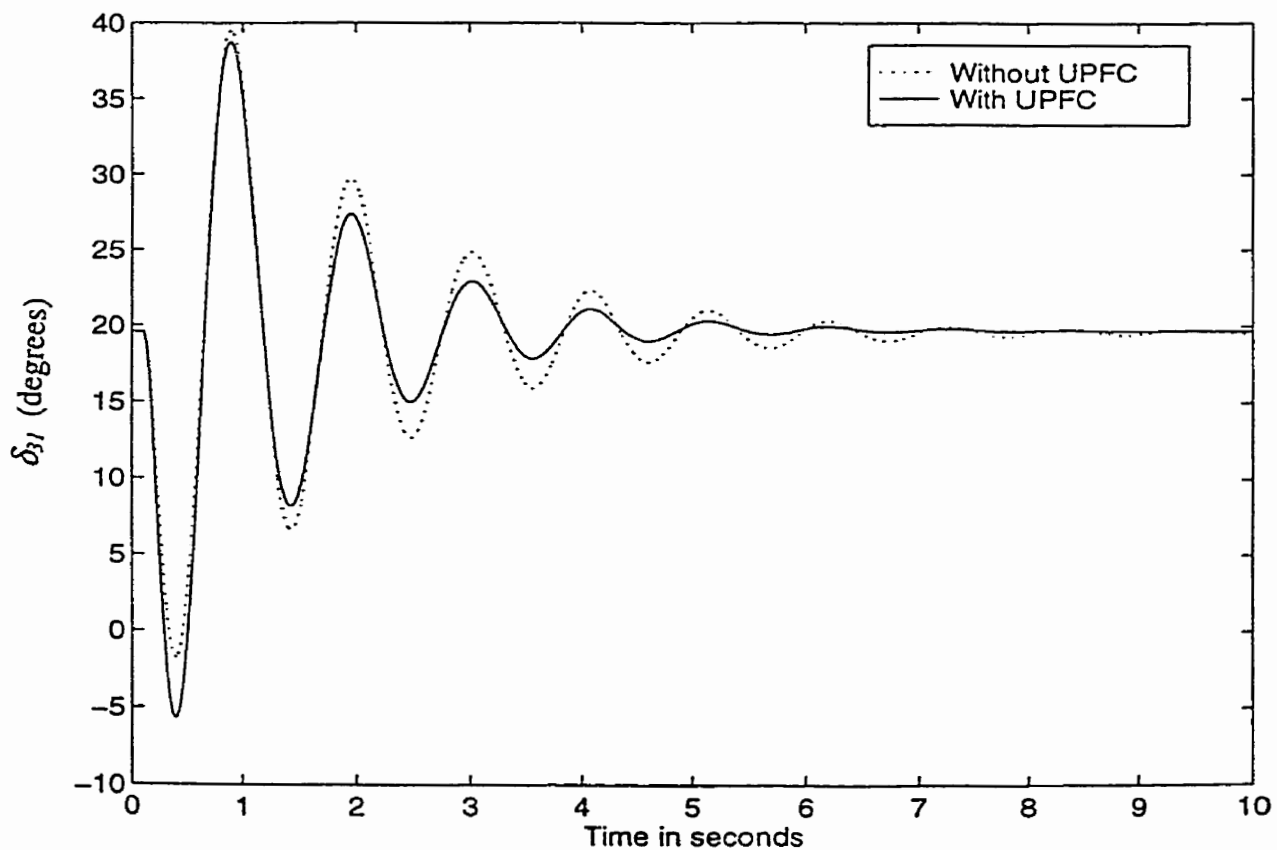


Fig.5.12 Rotor angle oscillations of generator G3 with respect to generator G1 (δ_{31}) (with and without UPFC).

Fig.5.13 shows the inter-area real power flow ($P_{inter-area}$) oscillations for a fault in Area-2. It is evident from Fig.5.13 that the damping of the inter-area power ($P_{inter-area}$) oscillations is improved with the UPFC. The first swing in the inter-area real power flow ($P_{inter-area}$) with and without UPFC is around 575MW. Subsequent swings of the inter-area real power flow ($P_{inter-area}$) show increased damping with UPFC. The UPFC thus provides increased damping to inter-area power flow as analyzed by small signal stability analysis.

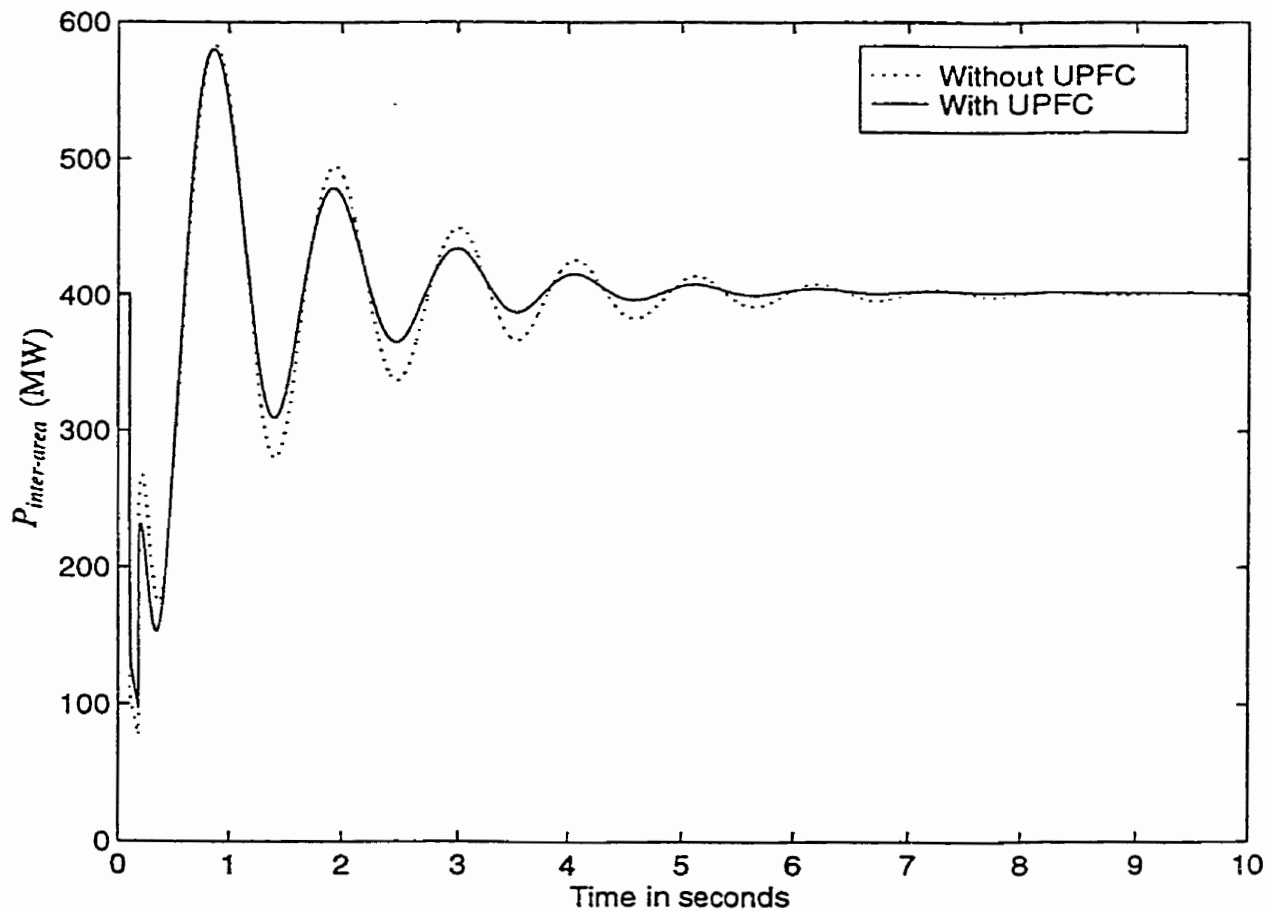


Fig.5.13 Inter-area real power flow oscillations ($P_{inter-area}$) (with and without UPFC).

Fig.5.14 shows the real power flow in the transmission line with UPFC (P_{line}). The initial real power flow (P_{line}) in the UPFC line is around 228MW. During the fault,

the real power flow (P_{line}) in the UPFC line drops down to around 50MW. The maximum excursion of the real power flow (P_{line}) is around 335MW without UPFC. The peak of the first swing of real power flow (P_{line}) with UPFC is almost the same as without UPFC. The improvement in damping of real power flow (P_{line}) with UPFC is evident in subsequent power swings. The real power flow (P_{line}) oscillations without UPFC shows low damping compared to power oscillations with UPFC.

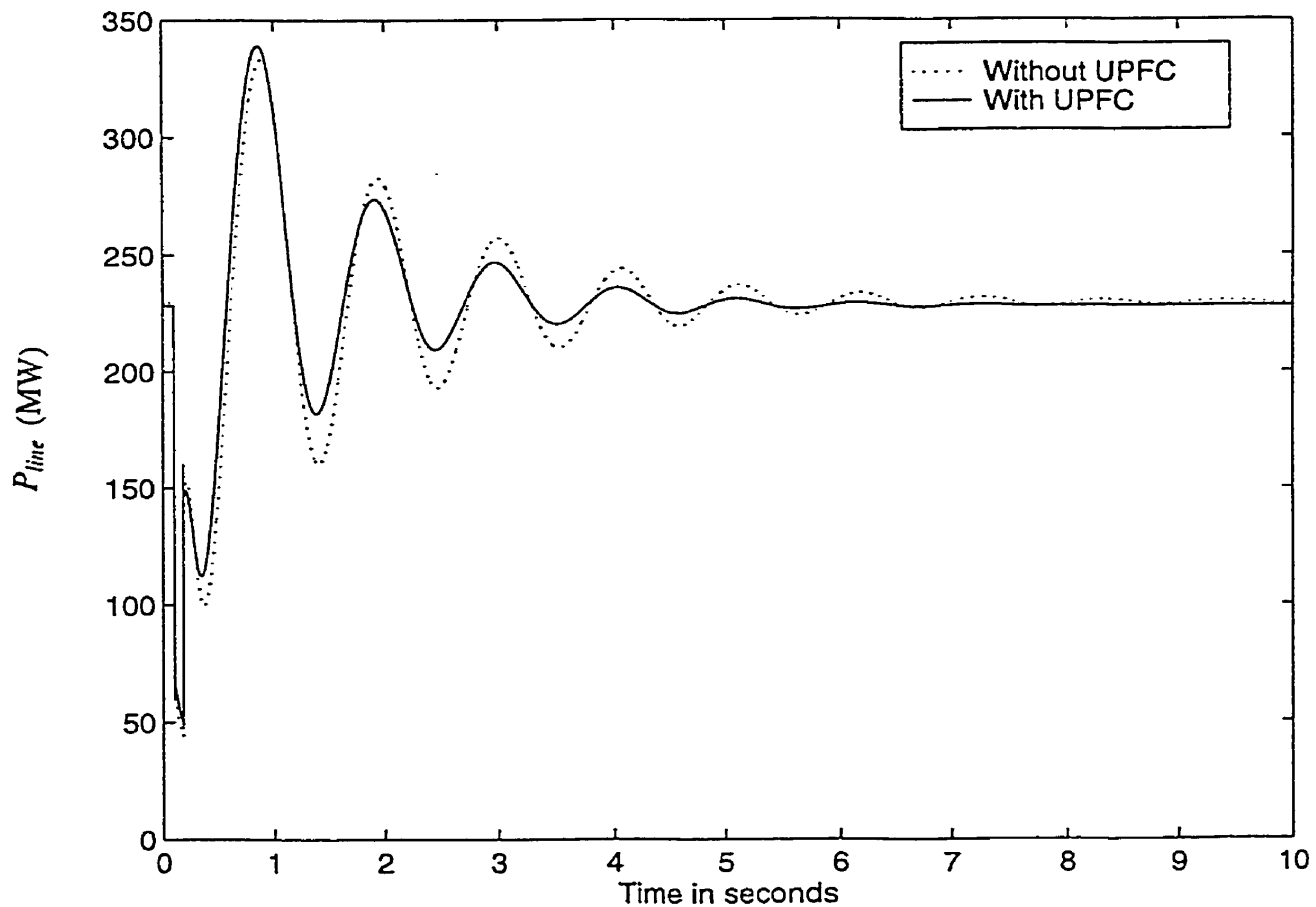


Fig.5.14 Real power flow oscillations in the double circuit line (with and without UPFC).

5.4 Summary

This chapter has presented a detailed procedure leading to the formulation of the state matrix with UPFC where the real power flow in the transmission line (P_{line}) is controlled by injecting a voltage in quadrature (V_{seq}) with the UPFC bus voltage and the line side bus voltage is controlled by injecting a voltage in-phase (V_{sep}) with the UPFC bus voltage. The shunt inverter controls the UPFC bus voltage ($V_{upfcbus}$) and the DC link capacitor voltage (V_{dc}). The DC link capacitor dynamics have been included while performing small-signal and transient stability analysis. The inclusion of DC link capacitor dynamics while performing small and transient stability accurately models the interaction between the series and the shunt inverter operation.

Small-signal and transient stability analysis has been carried out on SMIB and multi-machine power systems. The improvement in local mode and inter area mode damping has been brought forth with UPFC. The effect of combined operation of PSS and UPFC has been studied in this chapter through small-signal and transient stability analysis. Small-signal and transient stability analysis has shown that the UPFC contributes positively to local mode and inter-area mode damping. In the case of SMIB, the local mode damping increased from 0.073 to 0.14. In the case of multi-machine power system, the inter-area mode damping increased from 0.09 to 0.144.

The stability of the power system with the shunt inverter of UPFC controlling the transmission line side bus voltage (equivalent to controlling the transmission line reactive power flow), DC link capacitor voltage and the series inverter controlling the transmission line real power flow, UPFC bus has been evaluated. It has been found that this strategy is feasible and does not cause instability.

Chapter 6

Improvement in power system stability using a fuzzy logic controller for a UPFC – Single and Multi-machine power system

6.0 Introduction

The previous chapter has shown by small-signal stability analysis and time domain analysis that UPFC improves the over all stability of the power system. In doing so, PI controllers were used to control the transmission line real power flow (P_{line}), the UPFC bus voltage ($V_{upfcbus}$) and the DC link capacitor voltage (V_{dc}). Time domain simulation with UPFC provides valuable information for the design of fuzzy controller for a UPFC.

A vast amount of literature exists in the field of application of fuzzy logic to power system problems. Fuzzy logic based controllers have provided better solutions

than conventional controllers. Recently, fuzzy logic has been used to coordinate the control variables of a UPFC to achieve improvement in transient stability [20].

The purpose of this chapter is to two fold.

1. The series inverter of a UPFC plays a major role in providing power flow control and power oscillation damping. One purpose of this chapter is to design a fuzzy controller for the series inverter to control the transmission line real power and provide damping to them. The performance improvement by using a fuzzy controller over a PI controller will be brought out by computer simulations on a single machine infinite bus and multi-machine power systems. The complexity in the design of a fuzzy controller for the series inverter lies in the fact that the fuzzy controller should not only provide improvement in power oscillation damping but also see that it does not create instability. Instability could arise due to non-coordination of series and shunt inverter operation leading to possible collapse of the DC link capacitor voltage.
2. The analysis carried out by *Padiyar et.al* [23] show that the use of high gain PI controller for controlling the transmission line real power flow could lead to low damping. They state that
“ The main concern in the design of an output feedback controller is the stability of the oscillatory mode (in the D-Q axis frame of reference: near about ω_0 rad/s) associated with the series inductance”.

In this thesis, a fuzzy logic controller has been proposed to overcome the problem of low damping experienced when using a high PI gain output feedback to control the transmission line real power flow. The fuzzy knowledge base developed in this chapter provides the necessary foundation for solving the problem of low damping experienced

when using a high PI gain controller for controlling the transmission line real power flow. The developed knowledge base will be used in chapter-9 to show the improvement in step response with a fuzzy controller over PI controllers.

As a background, the basics of fuzzy logic and how it is implemented in a fuzzy logic controller has been reviewed briefly.

6.1 Basics of fuzzy theory

Fuzzy set: A fuzzy set 'F' having a universe of discourse 'U' is described by a membership value μ_F which can take values between 0 and 1. The fuzzy set 'F' is a set of pairs of elements 'u' in the set 'F' and its associated membership value μ_F .

Support of a fuzzy set: It is the fuzzy set of all elements 'u' in the universe of discourse 'U' for which $\mu_F(u) > 0$.

Linguistic variables: This is defined by the quintuple {x, T(x), U, G, S}, where 'x' is the name of the variable, T(x) is the term set of the variable i.e the set of names that characterize the variable 'x', 'U' the universe of discourse, 'G' the syntactic rule for generating the names of the values of 'x'. S is the semantic rule for associating with each value its meaning.

Union of two fuzzy sets: The membership function $\mu_{A \cup B}$ of the union of two fuzzy sets A and B defined for all elements 'u' is

$$\mu_{A \cup B} = \max [\mu_A(u), \mu_B(u)]$$

Intersection of two fuzzy sets: The membership function $\mu_{A \cap B}$ of the intersection of two fuzzy sets A and B defined for all elements 'u' is

$$\mu_{A \cap B} = \min [\mu_A(u), \mu_B(u)]$$

Complement of a fuzzy set: The membership value $\mu_{\bar{A}}$ of the complement of the fuzzy set A for any element 'u' is given by

$$\mu_{\bar{A}}(u) = 1 - \mu_A(u)$$

Cartesian product: If A_1, A_2, \dots, A_N are fuzzy sets in the universe of discourse U_1, U_2, \dots, U_N respectively, then the Cartesian product of A_1, A_2, \dots, A_N is a fuzzy set in the product space $U_1 \times U_2 \times \dots \times U_N$ with a membership function

$$\mu_{A_1 \times A_2 \times \dots \times A_N}(u_1, u_2, \dots, u_n) = \min (\mu_{A_1}(u_1), \mu_{A_2}(u_2), \dots, \mu_{A_N}(u_n))$$

6.2 Fuzzy Logic Controller

A fuzzy logic controller has four main components. They are

1. Fuzzification interface.
2. Knowledge base.
3. Decision making Logic
4. Defuzzification interface.

Each of the above will be explained with the help of an example.

Consider a fuzzy logic controller with inputs as error ' Δe ' and the rate of change of error ' $\Delta \dot{e}$ ' to it. Let A be the variable to be controlled and A_{ref} be its reference value as shown

in Fig. 6.1. Let the output of the controller be Δu . The fuzzy logic controller input signals are the error and the rate of change of error.

$$\Delta e = \frac{A_{ref} - A(k)}{\Delta T}$$

$$\Delta e' = \frac{\Delta e(k) - \Delta e(k-1)}{\Delta T}$$

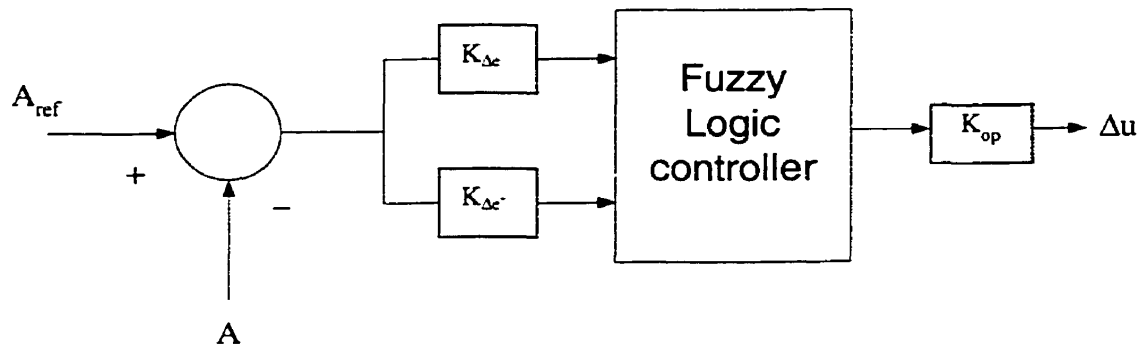


Fig. 6.1 A sample fuzzy logic controller.

Here the two input linguistic variables are the error and the rate of change of error. Each of the two linguistic variables is defined over a universe of discourse namely $U_{\Delta e}$ and $U_{\Delta e'}$ respectively. $K_{\Delta e}$ and $K_{\Delta e'}$ are constants used to massage the input signals to fit in within the universe of discourse. The output gain K_{op} is used to fine-tune the output signal. They have been chosen as unity for descriptive purpose. Let the universe of discourse for each of the input linguistic variable be divided into 5 fuzzy sets namely, Positive Big (PB), Positive Medium (PM), Zero (ZE), Negative Medium (NM), and Negative Big (NB). Each of the fuzzy set has a definite support. Each fuzzy set can be

triangular, or trapezoidal or sigmoidal. In this case, triangular fuzzy sets are used. Let the universe of discourse for the error be $\{-0.2 \text{ to } +0.2\}$. Let the universe of discourse for the rate of change of error be $\{-0.06 \text{ to } +0.06\}$. Each of the universe of discourse is divided among the five fuzzy sets with 50% overlap as shown in Fig.6.2. The five fuzzy sets named NB, NM, ZE, PM, PB can have variable support within the universe of discourse.

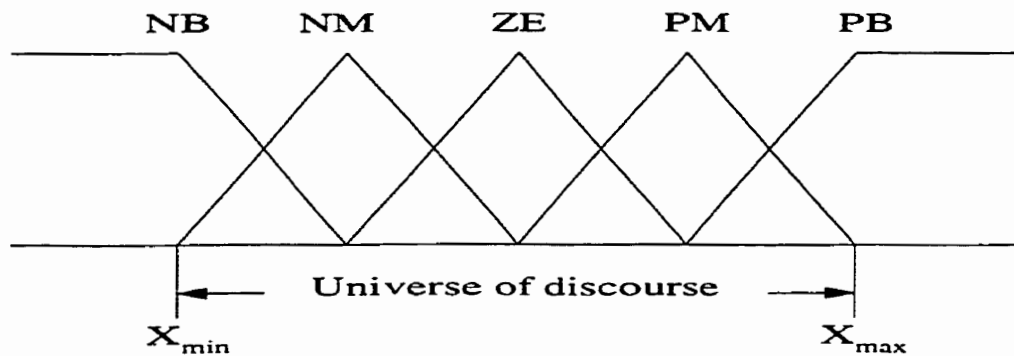


Fig.6.2 Five fuzzy sets.

Fuzzification Interface maps the crisp data input to a fuzzy set with a membership value. For example, the universe of discourse for the error is $\{-0.2 \text{ to } +0.2\}$. For convenience, they are equally divided between the five fuzzy sets as shown in Fig.6.3. Assume now that the error input is $+0.03$. So the error now appears in the fuzzy set ZE and the fuzzy set PM as shown in Fig.6.3.

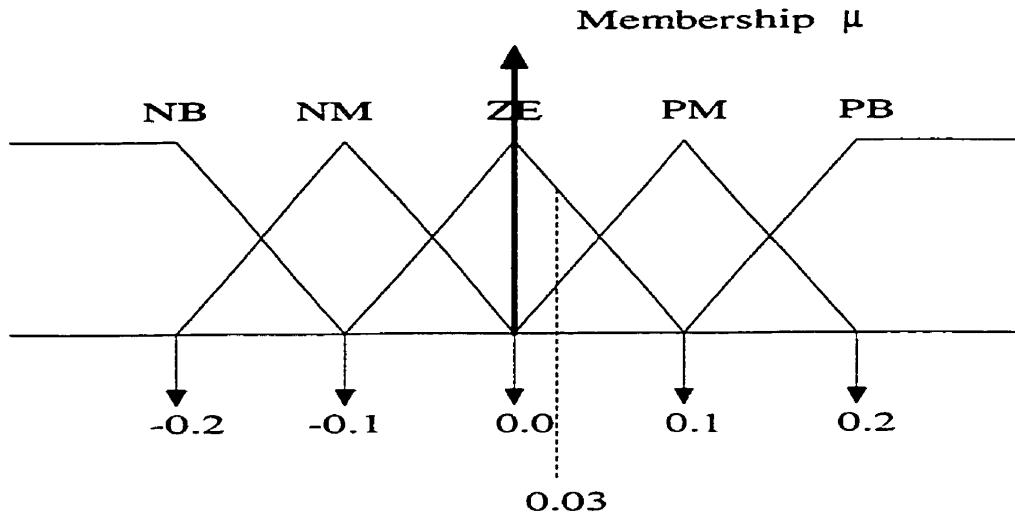


Fig.6.3 Fuzzy sets with their respective support.

The membership of the error in the fuzzy set ZE is

$$\mu_{ZE}(0.03) = (0.1 - 0.03) / 0.1 = 0.7$$

and in fuzzy set PM is

$$\mu_{PM}(0.03) = (0.03 / 0.1) = 0.3$$

Thus the function of the Fuzzification interface is to identify the fuzzy sets and their membership to which the input crisp value belongs.

Knowledge base comprises of the knowledge of the application domain and its control objectives. The expert knowledge is generally given in the following format.

“IF (a set of conditions) THEN (a set of consequent can be inferred)”.

These statements contain a set of conditions and a set of decisions to be inferred. The set of decisions could be fuzzy sets. For example:

IF (error is PM) and (rate of change of error is NM) THEN (change in output is PM)

The above statement means that IF the error is in the fuzzy set PM and the rate of change of error is in the fuzzy set NM, THEN the change in output value is PM. The knowledge base consists of many rules depending on the expert domain experience. For example, if there are 5 fuzzy sets, each for the error and the rate of change of error, then there are 25 rules. But in most cases not all the rules are used. An expert domain knowledge base can be put in a tabular form as shown in Table 6.1.

Table 6.1 A Fuzzy knowledge base

<i>Change of error</i> →	<i>PB</i>	<i>PM</i>	<i>ZE</i>	<i>NM</i>	<i>NB</i>
Error ↓					
PB		NM	PM	NM	
PM	NB	NM	ZE	PM	PB
ZE			NM		
NM			PB		
NB	NB	NS	NB	PS	PB

The decision-making logic is the process of simulating human like decision making based on fuzzy concepts. The idea behind this is to relate the input signals to the output signals. They are accomplished by the various operators available [38]. To explain the decision making process, consider the rules in Table 6.1.

“{IF (error is PB) AND (the rate of change of error is PB) THEN (change in output Δu is NB)} OR {IF (error is PM) AND (the rate of change of error is PM) THEN (change in output Δu is NM)}”

Consider the following statements.

Let the error be in the fuzzy sets PB and PM and have a membership value of 0.5 and 0.5 in their respective fuzzy sets. Let the change of error be in fuzzy sets PB and PM and have the membership values of 0.666 and 0.33 in their respective fuzzy sets. To relate the input signals to the output signal, consider the ‘min’ operator. This ‘min’ operator mimics the ‘AND’ function in the above rule. Using the min operator, the extent to which the fuzzy set NB is fired is $\min(0.5, 0.666)$ i.e 0.5. Similarly, using the min operator, the extent to which the fuzzy set NM is fired is $\min(0.5, 0.333)$ i.e 0.333. The above procedure has illustrated the process of decision making using the min operator. Other operators like product could also be used.

After having obtained the membership values of the consequent fuzzy sets, it is then required to defuzzify the control actions. This is done by the **Defuzzification interface**. The crisp control value is obtained by defuzzifying the information obtained from the decision making interface. This is generally done by the center of gravity method. To continue the example, the information obtained from the decision making interface is that, the membership value of the consequent fuzzy set NB is 0.5 and the membership value of the consequent fuzzy set NM is 0.333. Fig.6.4 shows the output or consequent fuzzy sets. Using the above information the crisp value for the control action is obtained by taking the center of gravity of the two inferred consequent sets namely NB and NM. The crisp control value is given by

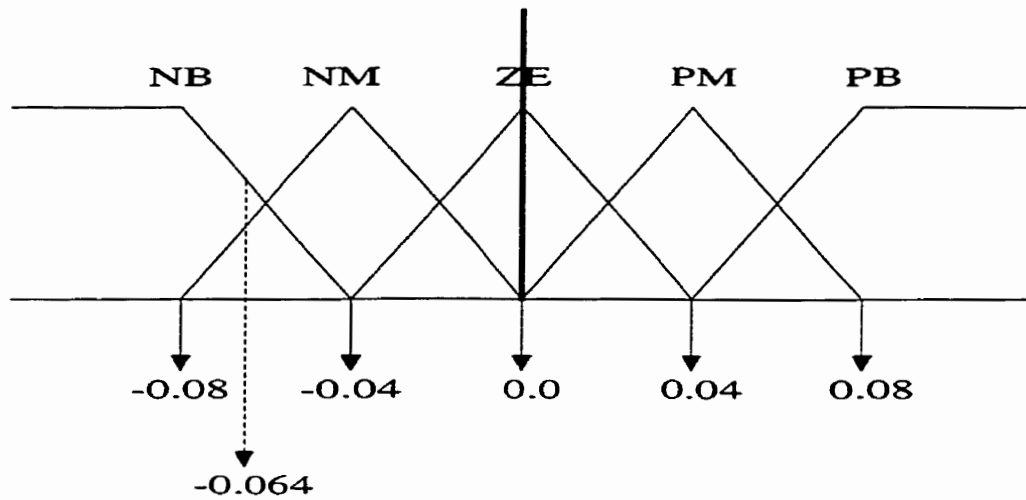


Fig.6.4 Consequent fuzzy sets.

$$\Delta u = \frac{(0.5 * \text{centroid of set NB}) + (0.33 * \text{centroid of set NM})}{(0.5 + 0.333)}$$

$$\Delta u = \frac{(0.5 * -0.08) + (0.333 * -0.04)}{0.8333} = -0.064.$$

Therefore the change of control output is -0.064.

6.3 Knowledge base design for the Series Inverter

In this section, a fuzzy knowledge base for a fuzzy logic controller has been developed for the series inverter of a UPFC that controls the real power flow in the transmission line. The most important part of a fuzzy controller is its knowledge base. These are basically linguistic rules that show the relation between the input quantities and

the output quantities. The input quantities chosen are the error in the transmission line real power flow (P_{line}) and the rate of change of real power flow in the transmission line where the UPFC is installed. The output variable of the knowledge base is the change in series injected voltage (ΔV_{seq}).

Seven fuzzy sets were used for error in real power flow, change of error in real power flow and the change in series injected voltage, namely Positive Big (PB), Positive Medium (PM), Positive Small (PS), Zero (ZE), Negative Small (NS), Negative Medium (NM) and Negative Big (NB). All membership functions have been assumed triangular in shape for the sake of simplicity. The product operator has been used for the decision making process. The center of gravity method has been used for Defuzzification.

While conducting computer simulations on a single machine infinite bus power system, the error in transmission line real power, change of error in transmission line real power and the change in control input (quadrature injected voltage ΔV_{seq}) were monitored and the range over which they varied were noted. Based on those findings the universe of discourse for the error, change in error and the change in control input are defined. Fig 6.5 shows the error in real power flow obtained from the simulations conducted in chapter 5 on a SMIB. As seen from Fig.6.5, the range over which they oscillate is ± 0.15 . Thus for the error in transmission line real power flow, the universe of discourse was chosen to be ± 0.2 . The input gain for error $K_{\Delta e}$ was chosen to be 1.0. The centroid of the fuzzy sets for error in real power flow are 0.2 (PB), 0.1 (PM), 0.03 (PS), 0.0 (ZE), -0.03 (NS), -0.1 (NM), -0.2 (NB).

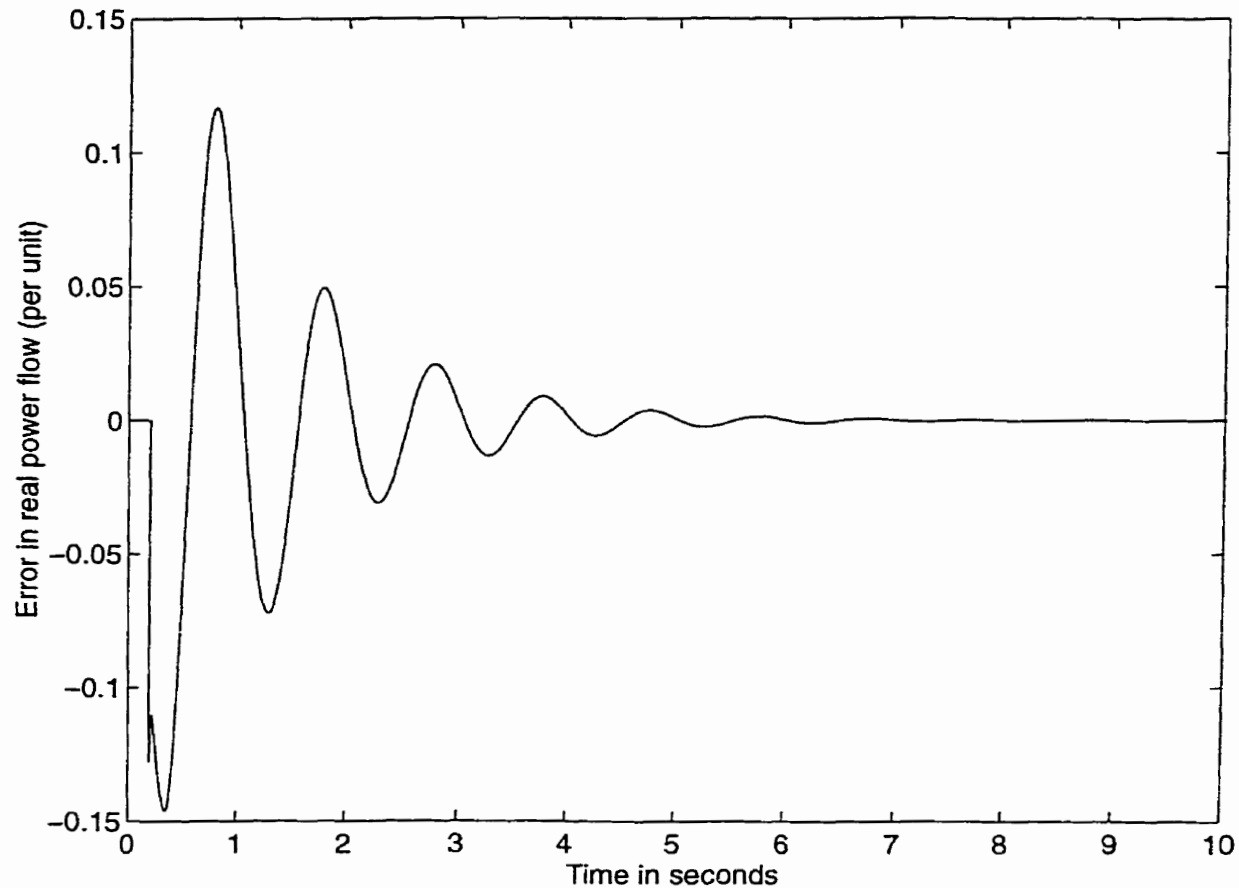


Fig.6.5 Error in transmission line real power flow for a SMIB case.

Fig.6.6 shows the change of error in transmission line real power flow for a SMIB case. It is seen that the change in error range from 1.0 to -0.6 . The universe of discourse for change of error in real power flow was chosen to be smaller than $+1.0$ and -0.6 . The universe of discourse was chosen to be ± 0.02 with an input gain $K_{\Delta e}$ of 0.1 . By doing so, the rules in the knowledge base on the outer periphery will be fired during the initial periods after the disturbance. This helps in providing more control effort (change in quadrature injected voltage ΔV_{seq}) during the initial periods to damp the power oscillations. The centroid of the fuzzy sets for change of error in transmission line real

power flow are 0.02 (PB), 0.01(PM), 0.003(PS), 0.0 (ZE), -0.003 (NS), -0.01 (NM), -0.02 (NB).

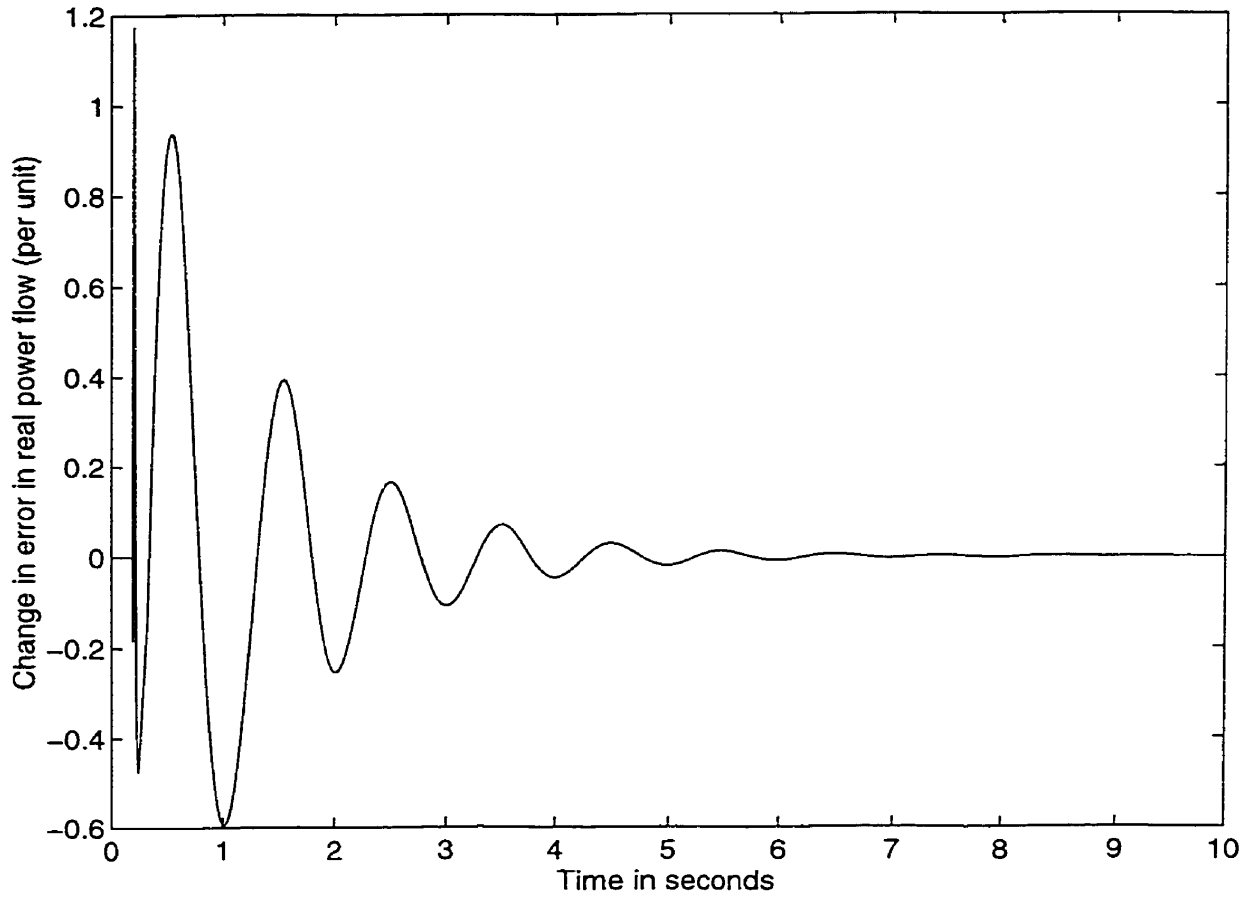


Fig.6.6 Change in error in transmission line real power flow for SMIB case.

Fig.6.7 shows the change in control input (ΔV_{seq}). The range over which they vary is about ± 0.00025 . The centroid of the fuzzy sets for change in series quadrature injected voltage are 0.00025 (PB), 0.0002(PM), 0.0001(PS), 0.0 (ZE), -0.0001 (NS), -0.0002 (NM), -0.00025 (NB). An output gain (K_{op}) of 4.0 was used for the SMIB case.

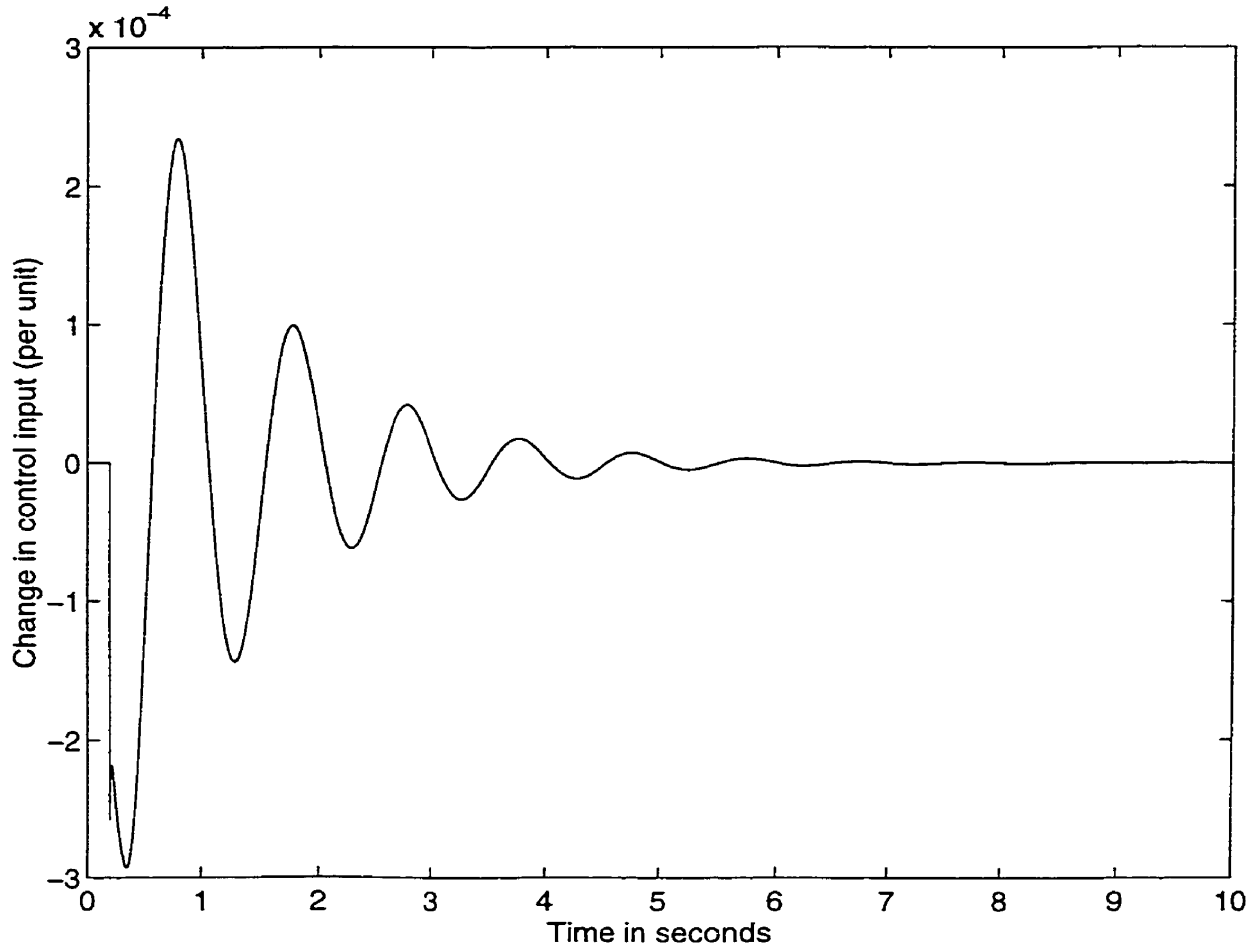


Fig.6.7. Change in control input V_{seq} for SMIB case.

Table.6.2 shows the knowledge base developed for control of real power flow. The rules in Table 6.2 have been generated by looking at the instances of the error, change of error in transmission line real power flow (P_{line}) and the change of control input (ΔV_{seq}) and relating them by fuzzy sets. For example, at approximately 1.0 sec, the error in transmission line real power flow is almost zero and the change of error in transmission line real power flow is very near to its negative maximum. At this instant the change in control input (ΔV_{seq}) is near zero and going to its negative maximum. From

this observation, the rule when error in transmission line real power flow is zero and change of error in transmission line real power flow is at its negative maximum, the change in output (ΔV_{seq}) is negative maximum has been developed. Based on such an analysis, the rest of rules have been developed. In Table-6.2, CE represents the change in error in transmission line real power flow and E represents the error in transmission line real power flow.

Table 6.2 Fuzzy knowledge base for series inverter of UPFC

$CE \blacktriangleright$	NB	NM	NS	ZE	PS	PM	PB
$E \blacktriangledown$							
PB	ZE	PS	PM	PB	PB	PB	PB
PM	NS	ZE	PS	PM	PM	PM	PB
PS	NM	NS	ZE	PS	PS	PM	PB
ZE	NB	NM	NS	ZE	PS	PM	PB
NS	NB	NM	NS	NS	ZE	PS	PM
NM	NB	NB	NM	NM	NS	ZE	PS
NB	NB	NB	NB	NB	NM	NS	ZE

The knowledge base developed in Table 6.2 comes from the fact that when the error in transmission line real power is positive, meaning that the transmission line real power flow is less than its reference value, the series quadrature injected voltage (V_{seq}) is increased to reduce the error. By doing so, the phase angle difference between the sending and receiving end increases causing the transmission line real power flow to increase and thereby reducing the error in it. Conversely and when the error in transmission line real power flow is negative, the series quadrature injected voltage (V_{seq}) is decreased to reduce the error.

Looking more carefully at the knowledge base, it is seen that the rules are separated into two regions along one of the diagonals. On one side of the diagonal are

positive changes to control input (V_{seq}) and on the other side negative changes to control input (V_{seq}). The rules that are closer to the diagonal are of smaller changes in control input (V_{seq}) and as one moves away from the diagonal, larger changes in control input are encountered. Thus there are not abrupt changes in rules. For example, a change from PM to NM between adjacent cells is not present. This helps in allowing for smooth transition of the control input (V_{seq}) from one region to the other. One of the outcomes is that the real power absorbed/generated by the series inverter due to interaction between the series injected voltage and the transmission line current makes a smooth transition from generating to absorbing and vice a versa and helps in allowing the shunt inverter to provide the necessary real power demand of the series inverter. By doing so, the voltage across the DC link capacitor is prevented from changing abruptly.

6.4 Simulation results

6.4.1 SMIB case: The single machine infinite bus power system shown in Fig.6.8 has been considered to show the improvement in damping of the generator rotor angle, generator rotor speed and transmission line real power flow oscillations using a fuzzy controller that uses the knowledge base developed in Table 6.2. The generator, exciter, PSS, UPFC and network data are given in Appendix-1. The generator is modeled in the d-q axis representation and is equipped with an exciter and a PSS. The generator differential/algebraic equations are given in section 5.1.1.2. The UPFC is represented with differential equation describing the DC link capacitor dynamics (equation 5.18). The exciter and PSS model are given in Appendix-1. The disturbance is a 80msec fault at the terminal of the generator with no change in the structure of the power system.Fig.6.9

shows the generator rotor angle oscillations with UPFC (PI controller) and with UPFC (Fuzzy controller).

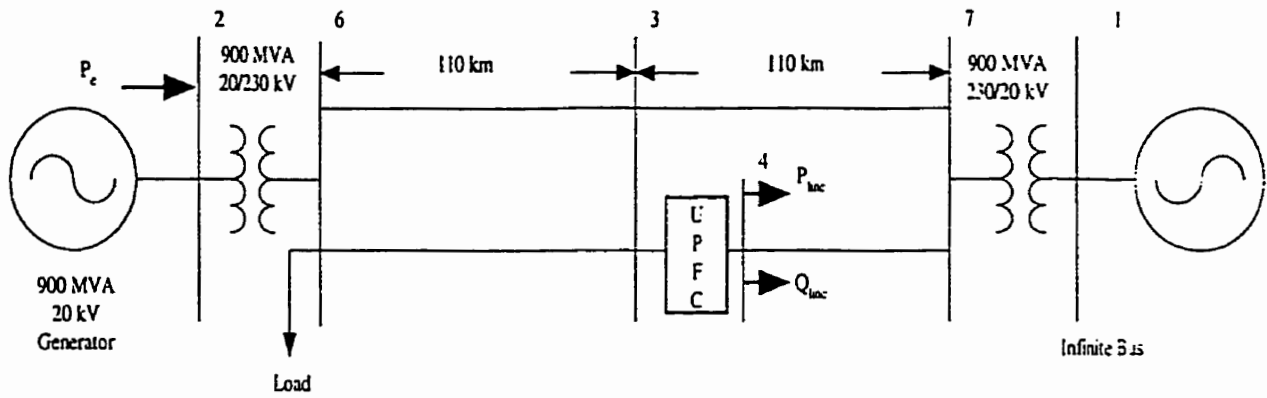


Fig.6.8 Single machine infinite bus power system.

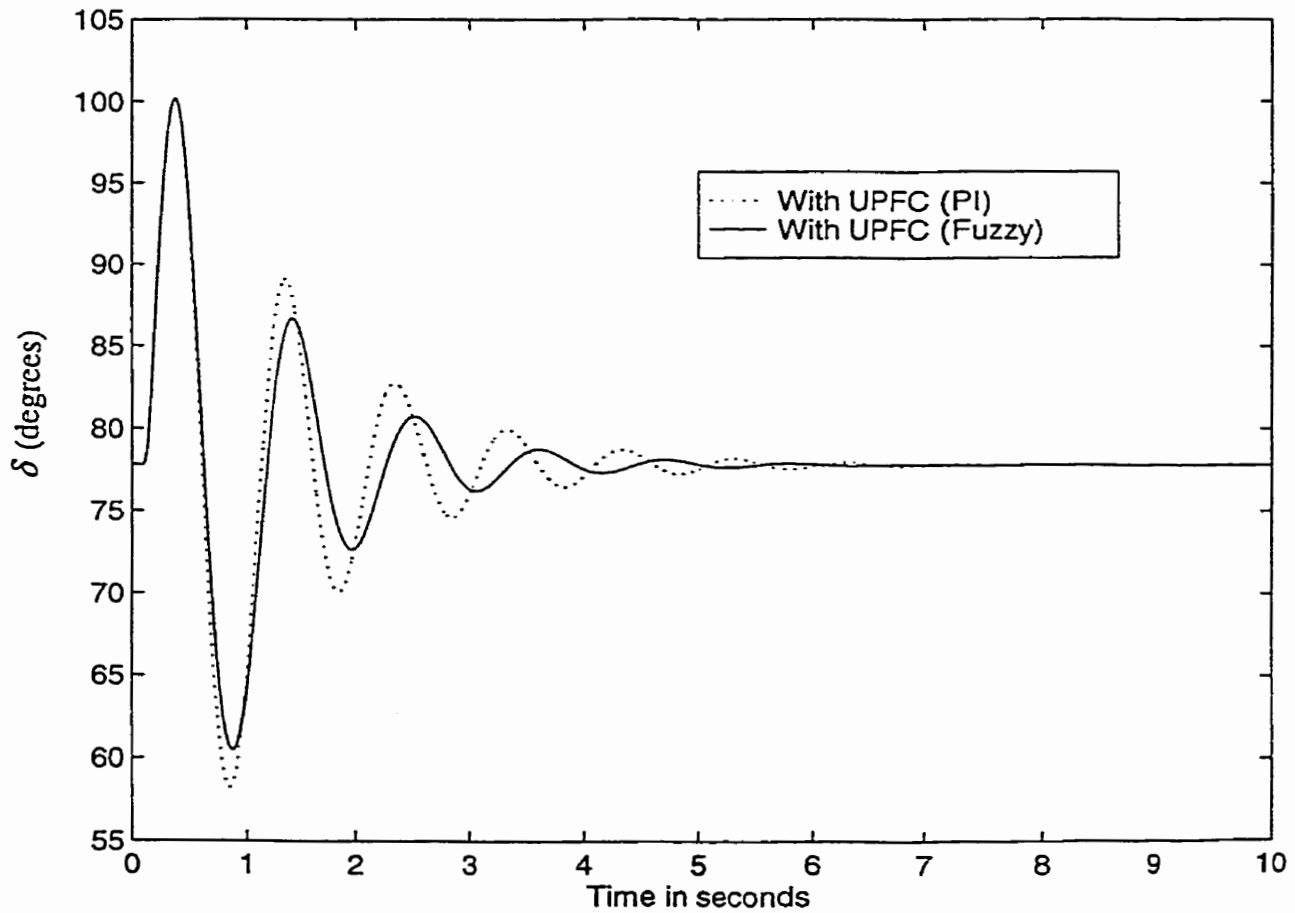


Fig.6.9 Generator rotor angle (δ) Oscillations.

The initial generator rotor angle (δ) is around 78 degrees. The three-phase fault is applied as a very high admittance at the generator terminals for 80msec and then removed. It is seen from Fig.6.6 that the first swing with the UPFC after the fault removal is the same with PI controller and with fuzzy controller. Subsequent oscillations with the fuzzy controller shows greater damping compared to the case when the UPFC is equipped with a PI controller. The simulation with UPFC equipped with a fuzzy controller for the series inverter has actually shown that the knowledge base used for the fuzzy controller is appropriate and does provide improved damping to generator rotor angle oscillations.

Fig.6.10 shows the generator rotor speed ($\Delta\omega_r$) oscillations for a three-phase fault at the terminals of the generator. The generator rotor speed ($\Delta\omega_r$) oscillations with UPFC equipped with a fuzzy controller shows increased damping as compared to when the UPFC is equipped with a PI controller. The difference in the damping is only evident in the subsequent oscillations.

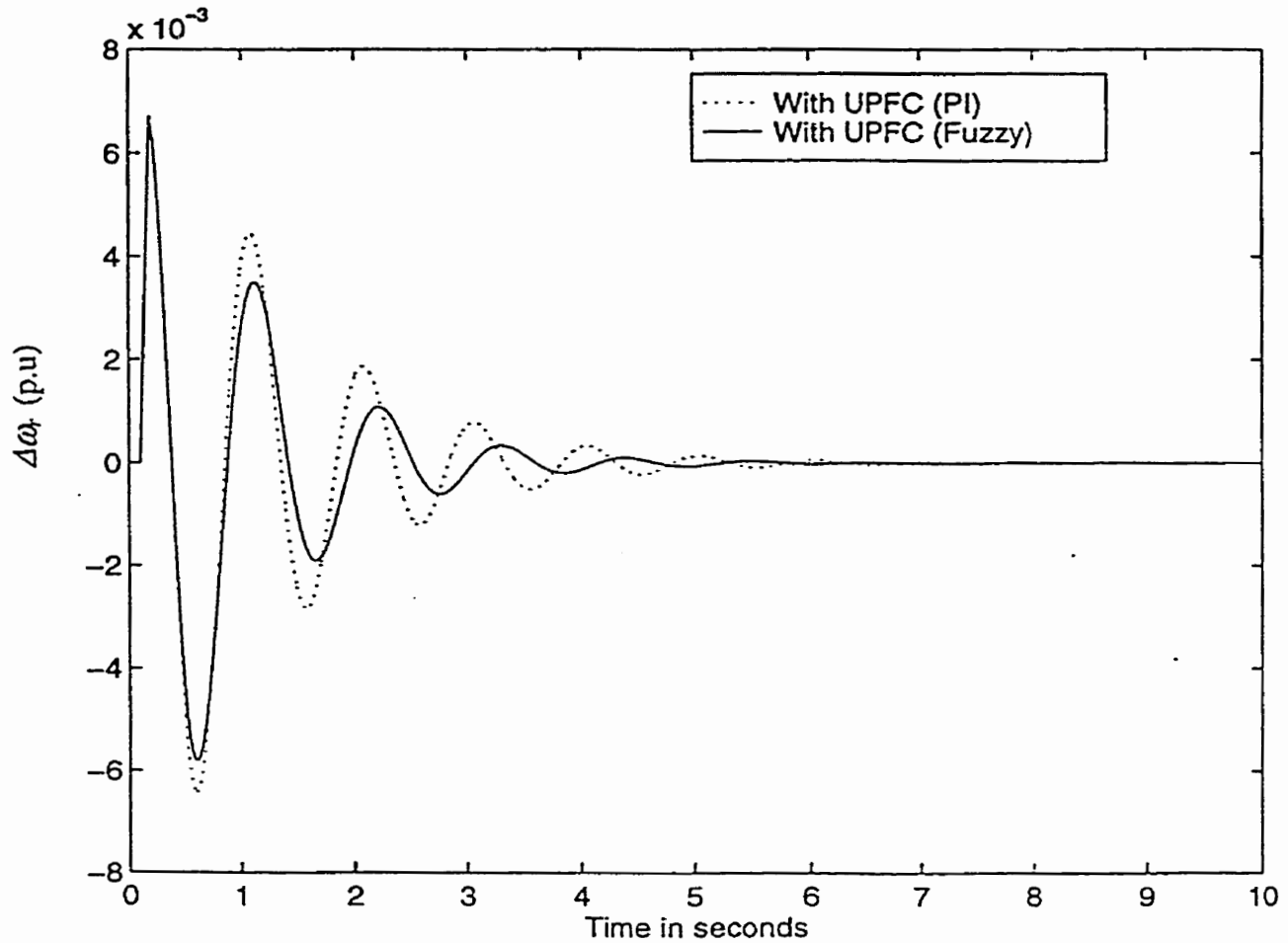


Fig.6.10 Generator rotor speed ($\Delta\omega$) oscillation damping.

Fig. 6.11 shows the generator electrical power (P_e) output for the three-phase fault at the generator terminals for 80 msec. The first swing of the generator electrical power reaches a peak of 1000 MW from the initial value of 700 MW. The damping of the generator electrical power is much more with the fuzzy controller than with PI controller. It takes approximately 4 seconds to damp the generator electrical power with the fuzzy controller for a UPFC compared to 5 seconds with PI controller.

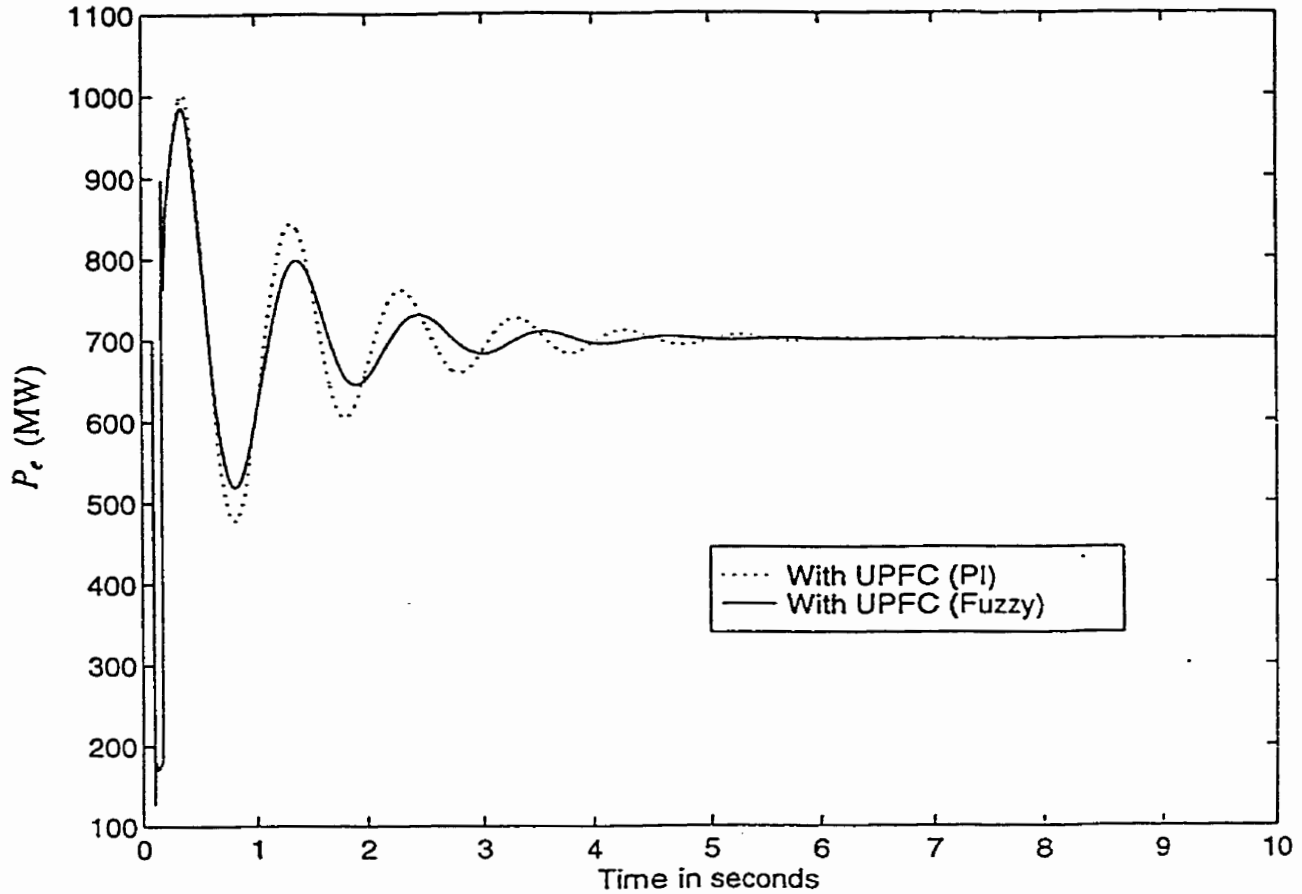


Fig.6.11 Generator electrical power (P_e) output.

Fig.6.12 shows the real power flow in the transmission line containing the UPFC (P_{line}). The initial power flow in the UPFC line (P_{line}) is about 250 MW. The first swing in real power in the UPFC line (P_{line}) reaches a value of 375 MW when the UPFC controls the real power flow with a PI controller. The first swing in transmission line real power flow is reduced to 360 MW when the UPFC is equipped with a fuzzy controller. Subsequent transmission line real power flow oscillations are better damped with fuzzy controller.

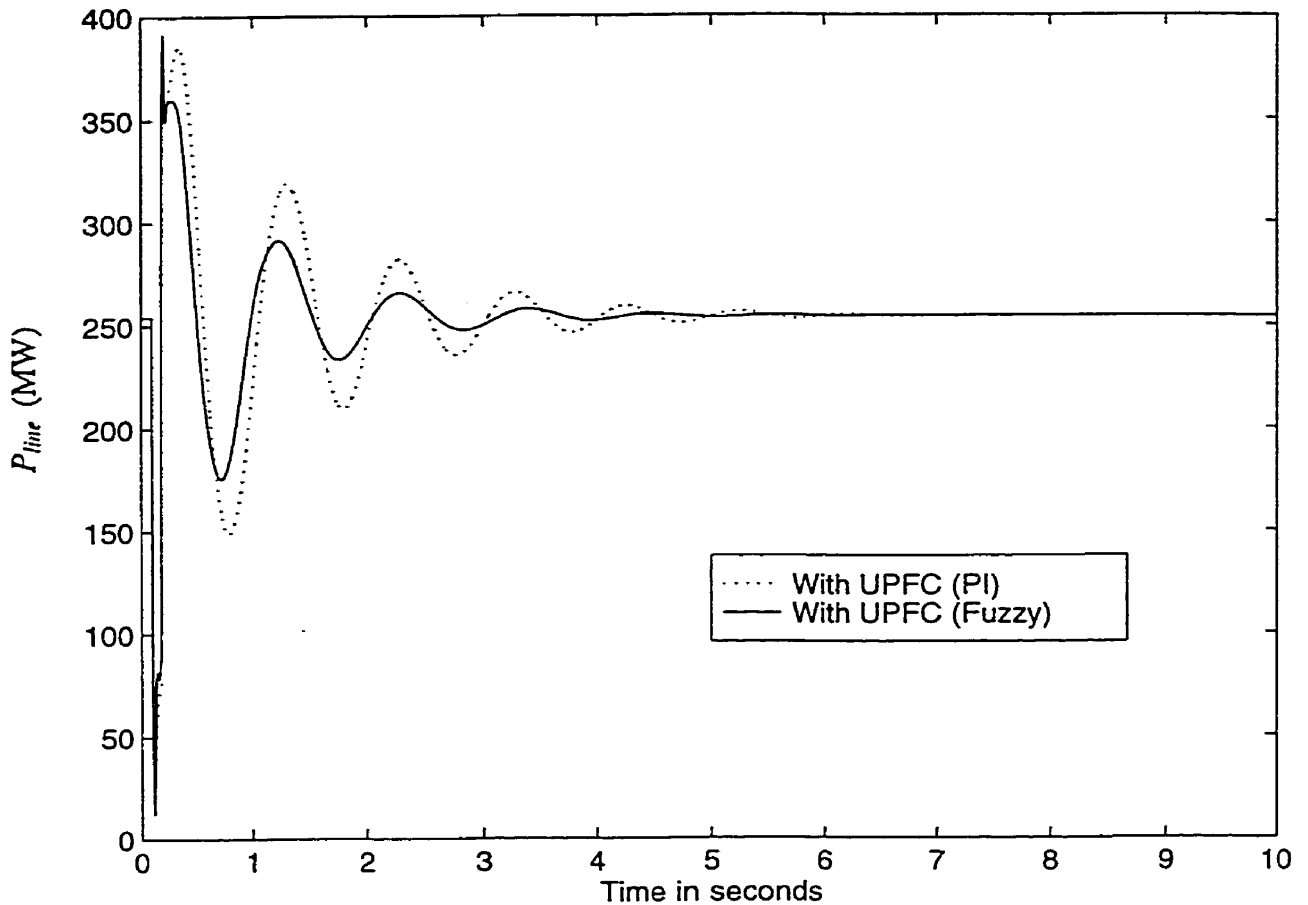


Fig.6.12 Real power flow (P_{line}) in the UPFC line.

6.4.2 Multi-machine power system (MMPS) case: Fig.6.13 shows a multi-machine power system. Generators 2 and 3 provide power to Area-1 loads and generators 1 and 4 provide power to Area-2 loads. The generation in Area-1 is 1400 MW and the load in Area-1 is $967+j100$ MVA. Area-2 has deficiency in generation of about 400 MW and hence imports real power from Area-1. Area-1 is exporting around 400MW of power to Area-2. Area-2 has a load of $1767+j100$ MVA. A shunt capacitor of 350 MVAR is installed at bus-8. The UPFC is supplying 200 MVAR of shunt reactive power to support bus-5 voltage. The series inverter is injecting a voltage of 0.03 p.u in quadrature with

bus-5 voltage. The real power flow in the UPFC line is 229 MW. The generators, exciter/PSS, network and the UPFC parameters are given in Appendix-2.

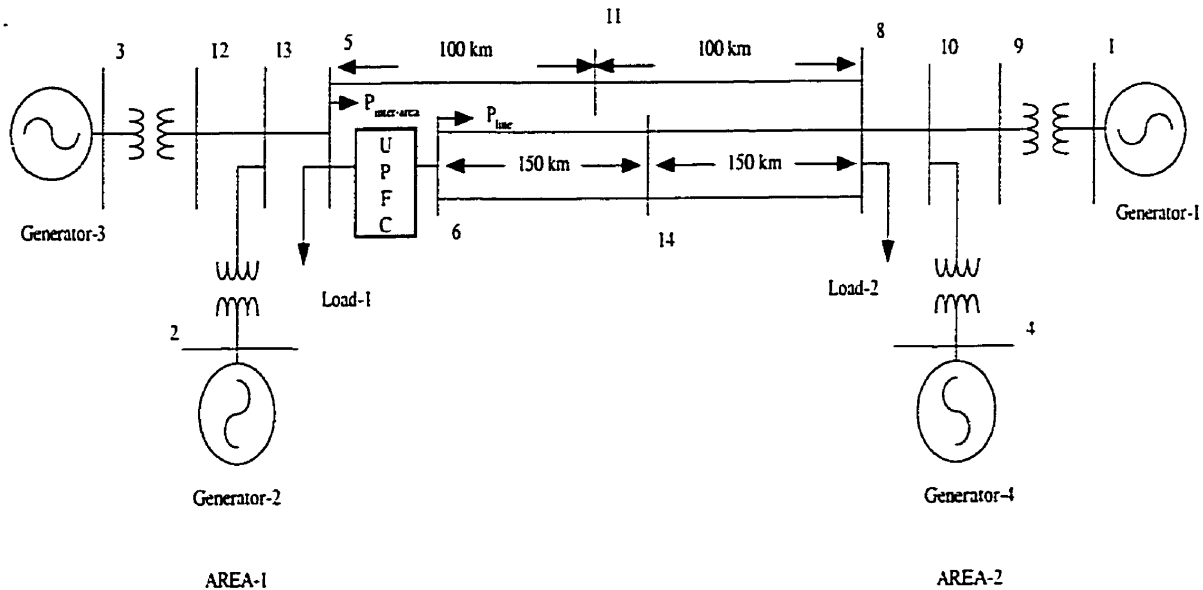


Fig.6.13 Two area power system with UPFC.

In this simulation a three-phase fault is assumed to occur in Area-1 for 80 msecs at bus-5 with no change in the structure of the power system. It is assumed that the protection as a whole has failed to operate and hence no change in the power system structures. The power flow in the double circuit transmission line (bus-6 to bus-14 in Fig.6.13) without the UPFC is 228MW. So to be able to compare the dynamic performance with the UPFC, the power flow in the UPFC line is adjusted to 228MW. This is achieved by injecting a voltage of 0.03 p.u in quadrature with the UPFC bus voltage (Bus-5). During and after the fault the shunt capacitors at the load buses are not disconnected. Also the UPFC is not disconnected during the fault period. The initial voltage on the DC link capacitor of the UPFC is 2.0 p.u.

For the MMPS case, seven fuzzy sets were used for the error in real power flow, change of error of real power flow and change in series quadrature injected voltage. Table 6.2 shows the fuzzy knowledge base used for the MMPS case. A universe of discourse of ± 0.2 was used for error in real power flow. The input gain that was used for the error was 2.0. For the change in real power flow, a universe of discourse of ± 0.2 was used. The input gain used for the change in real power flow was 0.01. The universe of discourse for the change in quadrature injected voltage was ± 0.0005 .

Fig.6.14 shows the rotor angle oscillations of generator G2 with respect to generator G1 for a 80 msec fault at bus-5. Generator G1 is assumed as the reference for all simulations.

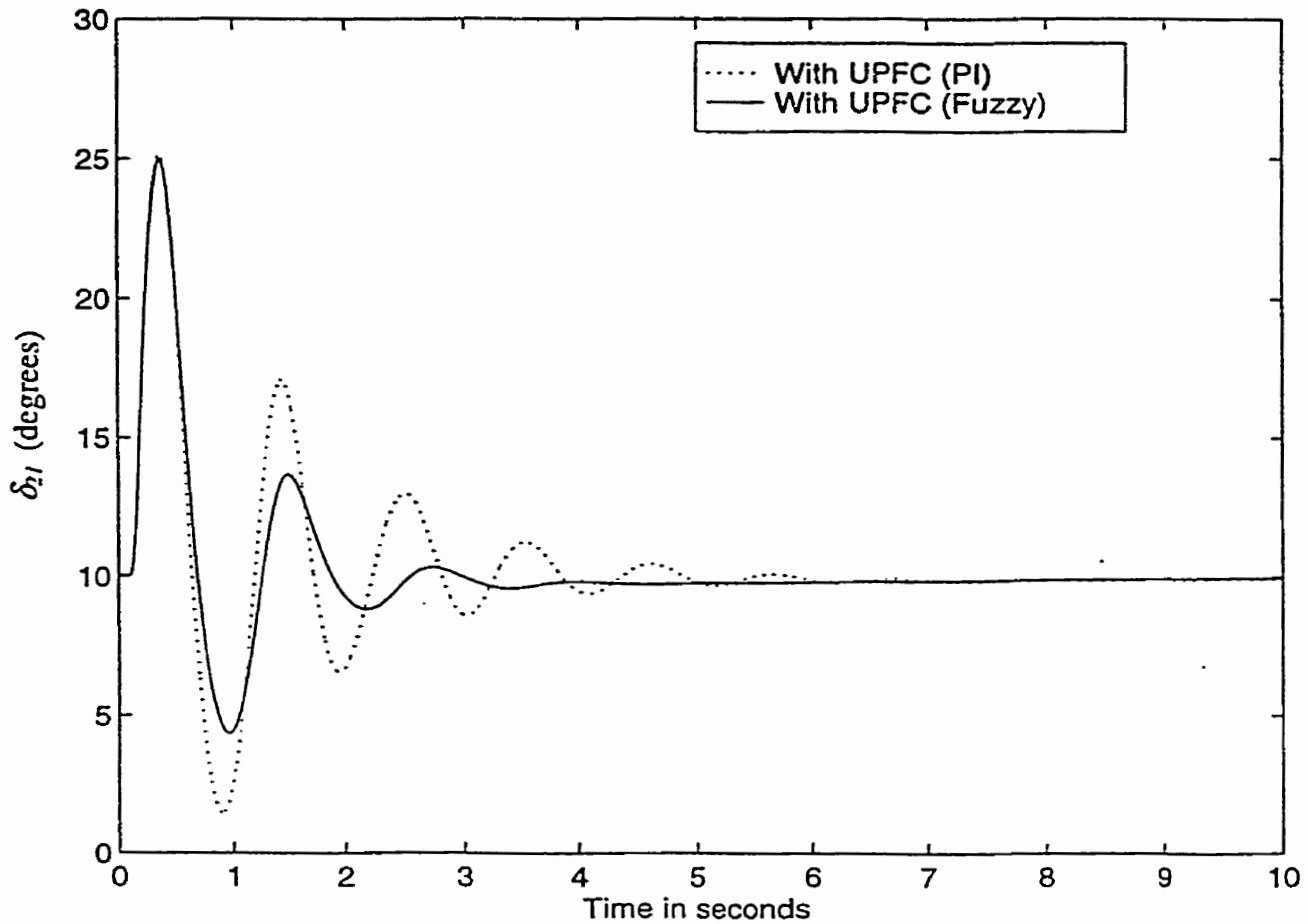


Fig.6.14 Rotor angle difference (δ_{21}) between generators G2 and G1. Fault at bus-5.

The initial operating point for generator G2 with respect to generator G1 (δ_{21}) is around 10 degrees as seen from Fig.6.14. With the three-phase fault at bus-5, the electrical power in Area-1 goes to a very low value causing the generators G3 and G2 rotor angle to increase in the first swing with respect to G1. The three-phase fault condition was simulated by connecting an admittance of value $-j20$ in shunt at location A. With the UPFC in service equipped with a PI controller, the generator G2 rotor angle oscillation (δ_{21}) damp out with the first swing of nearly 25 degrees. But with the UPFC in service

equipped with a fuzzy controller, the generator oscillations damp out very quickly within 3 seconds.

Fig.6.15 shows the rotor angle oscillations of generator G3 with respect to generator G1 (δ_{31}). The initial rotor angle difference between generator G3 and G1 is around 20 degrees. With the UPFC in service equipped with PI controller, the first swing reaches a value of 35 degrees and takes about 5 secs to damp out the oscillations. But with the UPFC equipped with a fuzzy controller, the generator G3 rotor angle (δ_{31}) oscillations damp out much faster within 3 seconds.

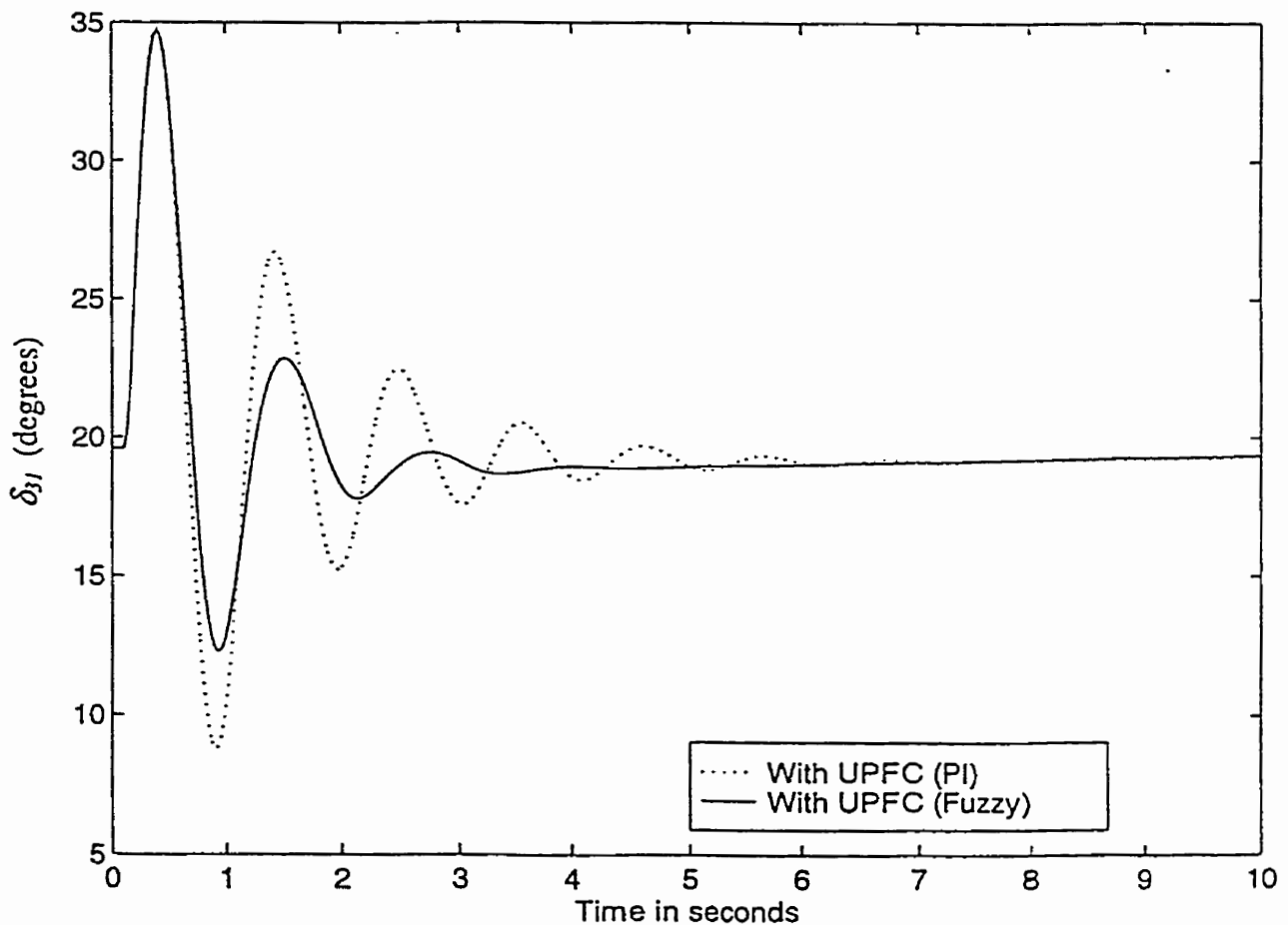


Fig.6.15 Rotor angle oscillations of generators G3 with respect to G1 (δ_{31}).

Fig.6.16 shows the total inter-area power flow ($P_{inter-area}$) oscillations for a three-phase fault at bus-5. The initial inter-area power flow ($P_{inter-area}$) is 400MW. 400 MW of real power is exported to Area-2 from Area-1 through the three transmission lines. The application of a three-phase fault causes the total inter-area real power ($P_{inter-area}$) to drop to near zero. After the fault removal and with no change in the network structure, the overshoot in inter-area real power flow ($P_{inter-area}$) with UPFC installed is around 575MW. UPFC when equipped with a fuzzy controller controlling the power flow in the double circuit line (bus-6 to bus-14 in Fig.6.13) provides increased damping to inter-area real power flow ($P_{inter-area}$) oscillations as compared to when equipped with PI controller.

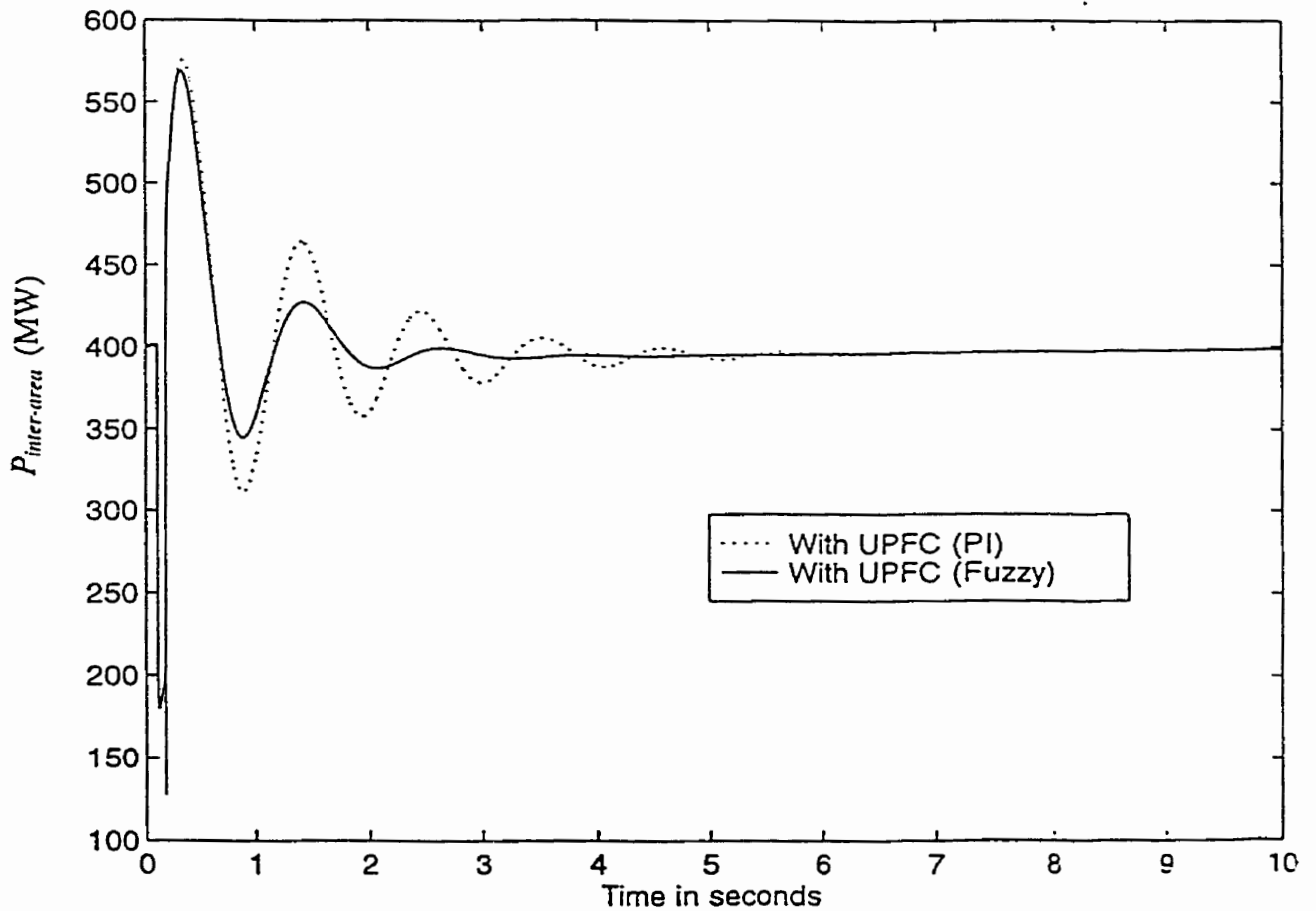


Fig.6.16 Inter-area real power flow ($P_{inter-area}$) oscillations.

Fig.6.17 shows the real power flow in the transmission line with UPFC (P_{line}). The initial power flow in the UPFC transmission line (P_{line}) is around 228MW. The three phase fault causes the real power flow in the UPFC transmission line (P_{line}) to drop to around 50MW during the fault period. With UPFC equipped with a PI controller, the real power flow in the UPFC transmission line (P_{line}) is damped in about 5 secs. But with UPFC is operated with a fuzzy controller, the UPFC effectively damps out the transmission line real power (P_{line}) oscillations within 2.5 seconds.

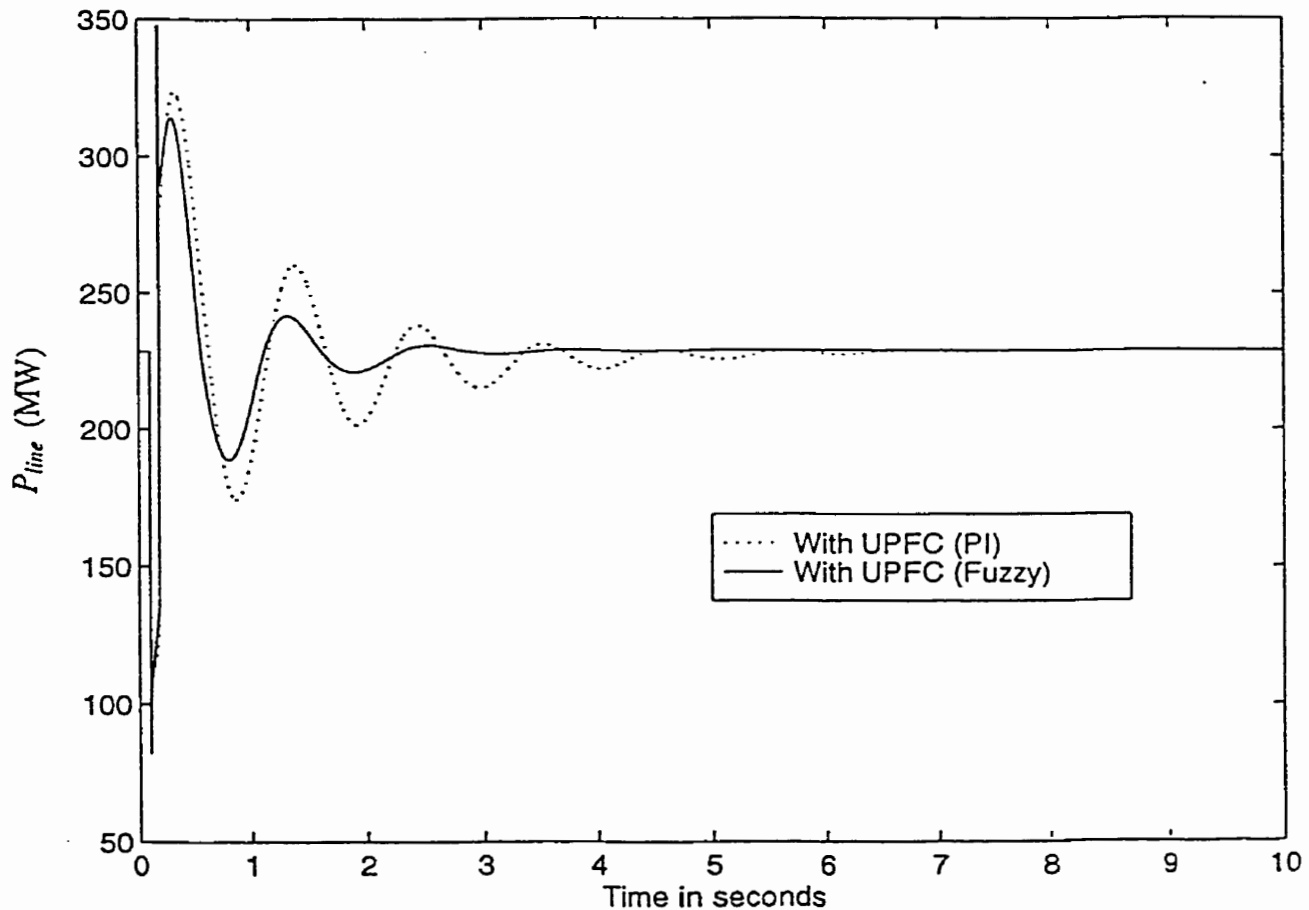


Fig.6.17 Real power flow in the UPFC transmission line (P_{line}).

6.5 Summary

A knowledge base for a fuzzy controller has been developed for the series inverter of a UPFC to improve on the damping of local and inter-area mode damping. The knowledge base developed includes information about the universe of discourse for the error in real power flow, change of error in real power flow and the change in quadrature injected voltage that has been obtained from simulations conducted in chapter-5.

Two important conclusions can be drawn from the simulations done on a SMIB and MMPS with UPFC equipped with a fuzzy controller.

1. UPFC equipped with a fuzzy controller for the series inverter can provide better performance compared to PI controlled UPFC.
2. These simulations have shown that the knowledge base developed for the fuzzy controller to be applied to the series inverter of a UPFC is justified.

The knowledge base developed together with the information regarding the universe of discourse for the error in real power flow and change of error in real power flow will be used in chapter 9 while designing the fuzzy controller for UPFC using the PSCAD-EMTDC software. Further, the same knowledge base will be used for the UPFC control system while operating it using the new control strategy.

Chapter 7

Shunt inverter construction, operation and control system design using PSCAD-EMTDC software

7.0 Introduction

UPFC as described in chapter 1 consists of two inverters connected back-to-back via a DC link capacitor with one inverter connected in shunt with the transmission line and the other inverter in series with the transmission line. The shunt inverter of a UPFC plays an important role by providing reactive power to support the voltage of the bus to which it is connected and maintaining a credible DC link capacitor voltage that is required for the proper operation of both the shunt and series inverters. Also, it supplies the necessary real power demand of the series inverter of a UPFC.

This chapter focuses on the construction, operation and control of a shunt inverter using PSCAD-EMTDC software. A control system design procedure for the shunt

inverter has also been explained. The performance studies will be carried out to validate the control system design.

7.1 Shunt inverter transformer rating

Fig.7.1 shows a UPFC connected to a transmission line. The shunt inverter is connected to the UPFC bus through a transformer T_1 .

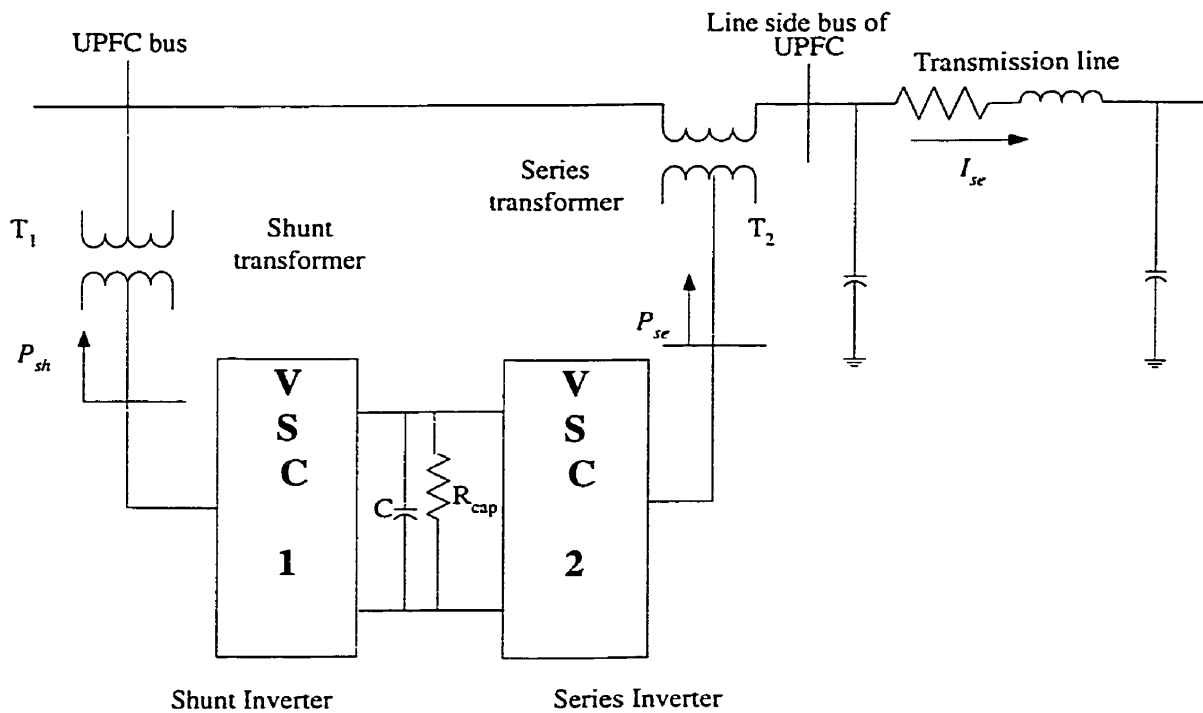


Fig.7.1 UPFC connected to a transmission line.

The design of the shunt transformer T_1 is a planning stage development. The rating of the shunt transformer would normally depend on the amount of reactive power needed to support the bus voltage. In the planning stage, the peak load conditions could

be used to come up with the ratings of the shunt transformer. In this thesis, a rating of 160 MVA has been assumed for the shunt transformer. A voltage rating of 345/66 kV and a per unit leakage reactance of 0.1 has been assumed for the shunt transformer.

7.2 Shunt inverter: Construction and Operation

7.2.1 Basic three-phase voltage source inverter (VSC): A basic three-phase VSC module consists of 6 GTOs (g1-g6) connected in a bridge fashion. To provide for the reverse current flow, diodes (d1-d6) are connected in anti-parallel to the GTO switch. Fig.7.2 shows a basic three-phase voltage source inverter module. The GTO block available in PSCAD-EMTDC software is modeled as a switch. In order to make it unidirectional, a diode is added in series with each GTO. The snubber circuit connected across each GTO is a series combination of a resistor and a capacitor. The values of the resistor is 5000 Ω and the capacitor is 0.05 μF . The on-state resistance of the GTO is 0.01 Ω and the off-state resistance of the GTO is 1.0E+06 Ω . The forward voltage drop is 1V. The parameters for the diode are the same as that of the GTO.

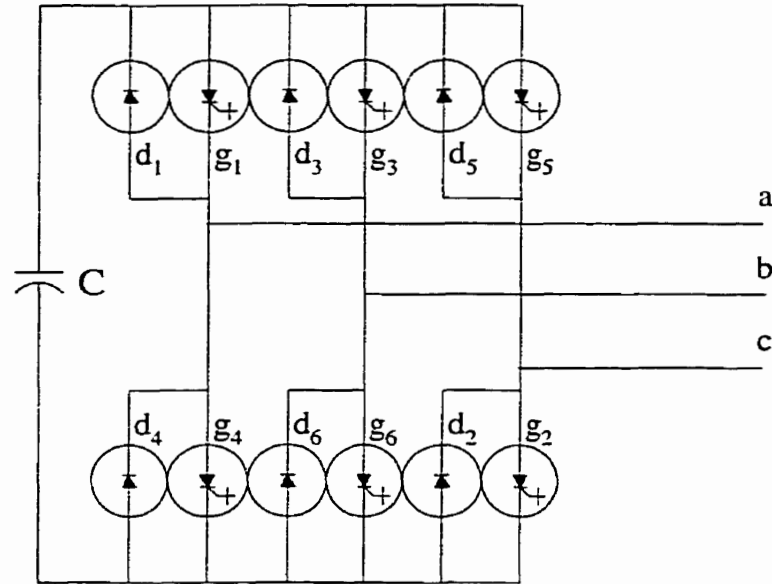


Fig.7.2 A basic three-phase voltage source converter module.

7.2.2 Construction of a 4-module voltage source inverter: In order to build a high power VSC module, a number of these basic three-phase voltage source converter modules have to be combined together. In this thesis, a 4-module voltage source inverter has been constructed. A 4-module VSC consists of 4 basic VSC inverter configuration connected in parallel across a common DC capacitor. Each of the basic VSC derives its DC voltage from the capacitor. Considering a sinusoidal pulse-width modulation (SPWM) for the operation of a VSC, each of these basic VSC modules generates a balanced three-phase voltage. Transformers are used to combine the voltage generated by each of these basic VSC. The primary of each of these transformers is connected either in Y or Δ configuration. The secondary of each of the transformer is connected in series. The arrangement is shown in Fig.7.3.

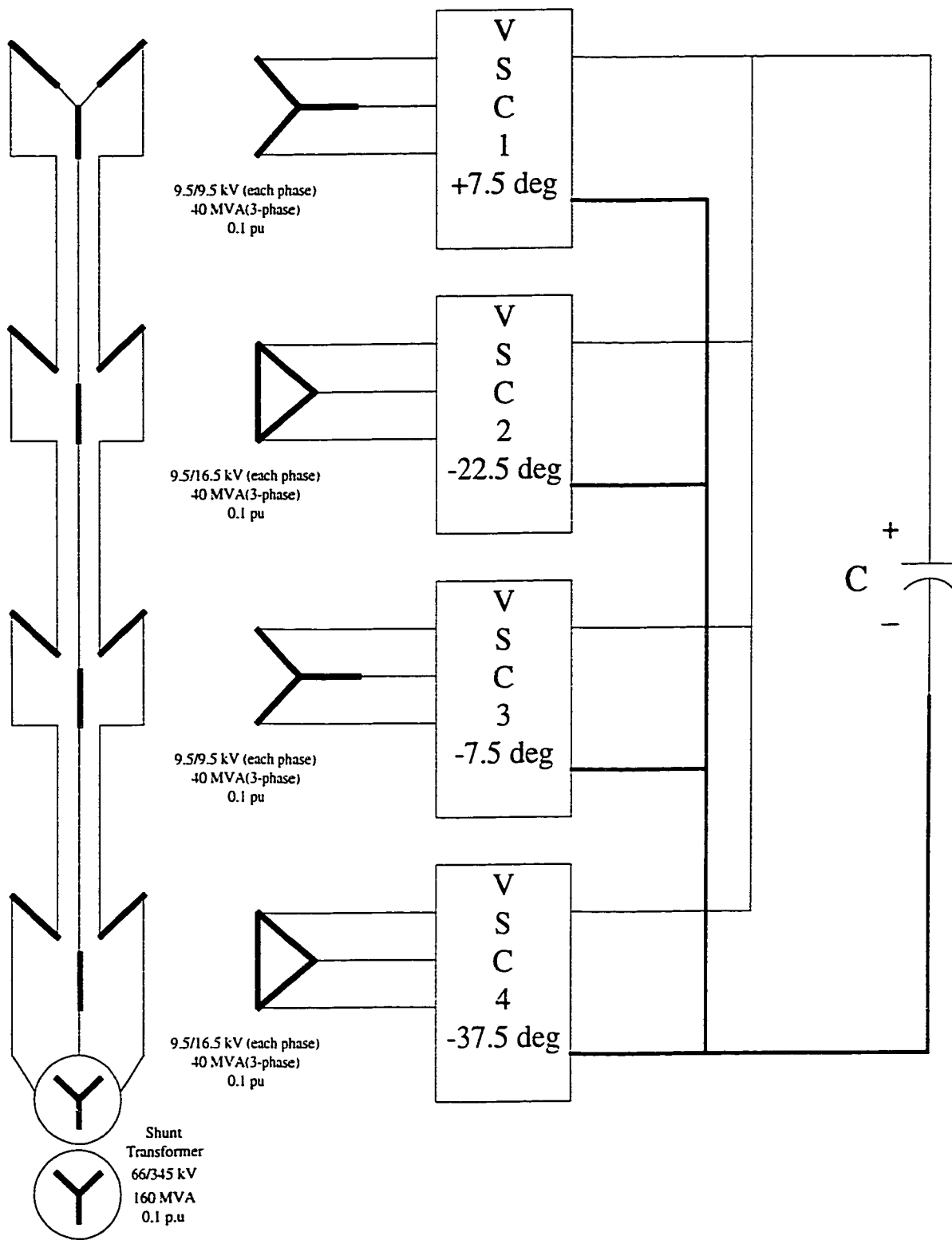


Fig.7.3 4-Module voltage source converter.

7.2.3 Operation of a 4-module voltage source converter: Each of the four VSC modules as shown in Fig.7.3 generate three-phase balanced voltages based on SPWM. In this type of modulation, a three-phase balanced sinusoidal signal is compared with a high frequency triangular waveform to produce the switching instants for the GTOs of the VSC. There is an inherent limitation on the maximum allowable switching frequency for the GTO device available so far. The maximum GTO switching frequency that can be allowed is about 1000 Hz. In this thesis, the switching frequency of the triangular waveform used is 9 times the fundamental so as to make the operation of the inverter as close as possible to reality. Further, the use of an odd multiple of the fundamental frequency allows for elimination of all even harmonics and the harmonic at the switching frequency (540 Hz) in the line-to-line voltages. Since a low switching frequency is being used, to eliminate the even harmonics in the line-to-line voltages a synchronized SPWM is used. In synchronized SPWM, the zero crossing of the three phase balanced sinusoidal signal is locked on to the zero crossing of the triangular waveform.

The three-phase voltage generated by each basic VSC module is added to obtain a high power, high voltage source inverter using the arrangement shown in Fig.7.3. In order to understand how the voltage generated by each of the 4 VSC modules are combined, consider the phasor diagram as shown in Fig.7.4. The letters A, B, and C represent the three phases and the numerals 1, 2, 3 and 4 represent the four basic VSC modules. The phasors of different phases with same numeral as their subscripts are phase shifted by 120 degrees. For example, the phasor 1A, 1B and 1C are phase shifted by 120 degrees. The phasors 2A, 2B and 2C are phase shifted from 1A, 1B and 1C by -

30 degrees. It should be observed that VSC-2 is connected to a delta connected transformer winding. Thus the secondary phase voltage is phase shifted by +30 degrees

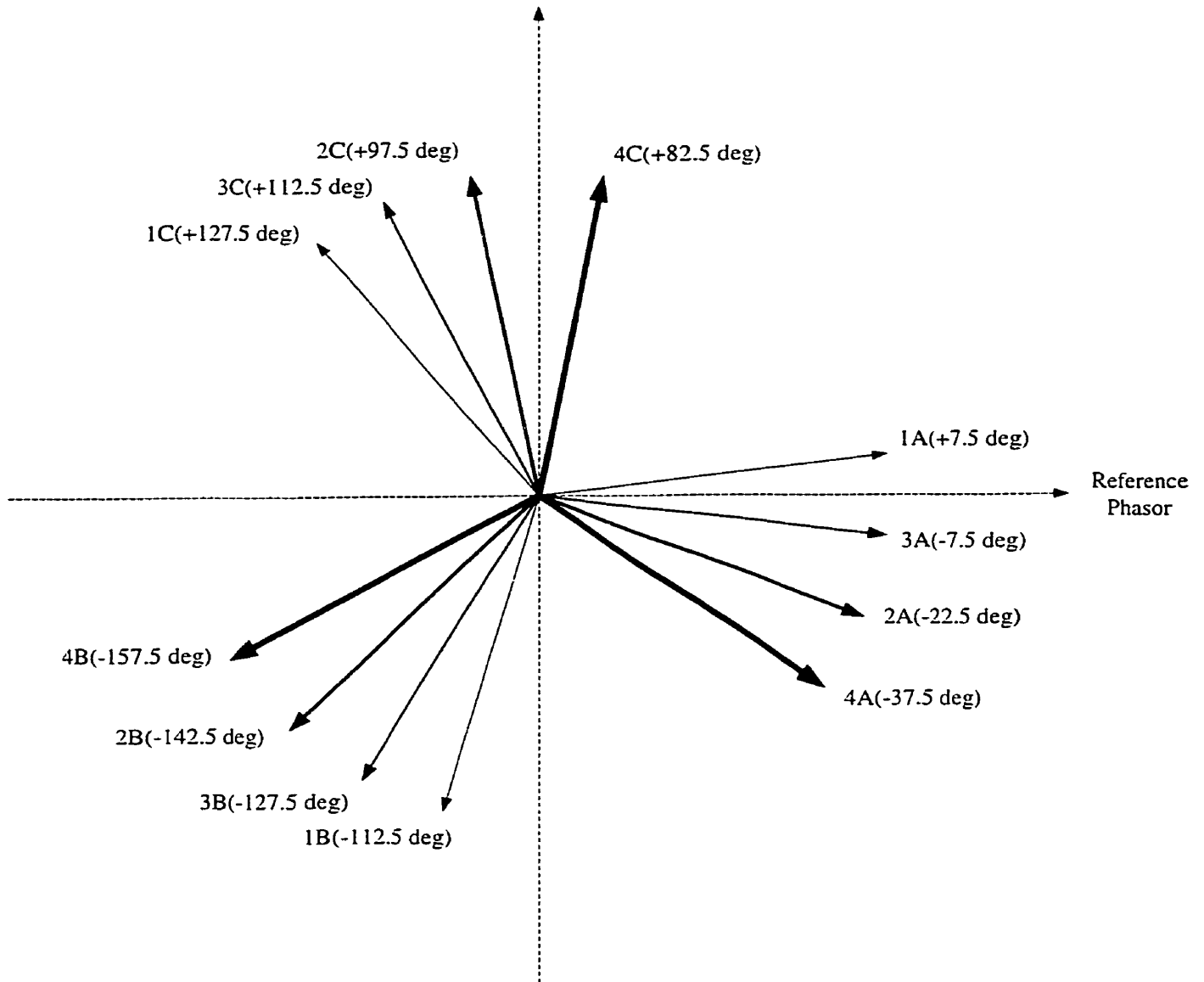


Fig.7.4 Phasor diagram for operation of a 4-module VSC.

and hence is in phase with the phasor 1A. Similarly, the phasor 3A is at an angle of -7.5 degrees. The phasor 4A is at an angle of -37.5 degrees. Since VSC-4 is connected to a

delta winding, the secondary phase voltage of 4A is in phase with 3A. This results in two phasors that are at +7.5 degrees and -7.5 degrees. The addition of the phasor at +7.5 degrees and -7.5 degrees results in a phasor that is in phase with the reference phasor. Further, in order for the voltage generated by each of the VSC to be the same on the secondary side, the transformer ratio of the delta winding is made $\sqrt{3}$ (primary : secondary) times that of the Y windings. Thus if the winding ratio of the transformer connected to VSC-1 is 9.5:9.5 kV for each phase, then the winding ratio for the VSC-2 delta transformer would be 16.5:9.5 kV for each phase. Thus when added by the series connection of the 4 transformers on the secondary side would result in each phase voltage to be approximately 38.1 kV ($9.5*4 \approx 38.1\text{kV}$). So the line to line voltage at the output of the 4 module VSC would be approximately 66kV.

The 4-module VSC described in this section will be operated as shunt inverter when considering the complete operation of a UPFC.

7.3 Shunt inverter: Control system

The objective of the shunt inverter is to provide fast control of reactive power (Q_{sh}) and maintain a constant DC link capacitor voltage (V_{dc}). The reactive power supplied/absorbed by the shunt inverter of a UPFC is controlled by adjusting the magnitude of its generated voltage. The DC link capacitor voltage (V_{dc}) is controlled by adjusting the phase angle of the generated voltage. By adjusting the phase angle of the shunt inverter generated voltage, real power is either consumed or generated thereby making it possible to control the DC link capacitor voltage (V_{dc}). The objective behind

maintaining a constant DC link capacitor voltage (V_{dc}) is to provide the series inverter of a UPFC with the necessary DC voltage for its operation and to supply its real power demand. In order to control both variables, namely the DC link capacitor voltage (V_{dc}) and reactive power output (Q_{sh}), the shunt inverter is operated using the de-coupled control system.

7.3.1 Basics of de-coupled control system design: The objective of the de-coupled control system is to control the real (P_{sh}) and the reactive power (Q_{sh}) simultaneously with the least interaction between them. By controlling the real power flow (P_{sh}) to/from the shunt inverter, the DC link capacitor voltage (V_{dc}) can be controlled.

To understand the de-coupled control system basics, consider a 4-module 160 MVA VSC as shown in Fig.7.3, connected to a constant 345 kV voltage source through a 66/345 kV step-up transformer. Fig.7.5 shows the equivalent circuit of the setup.

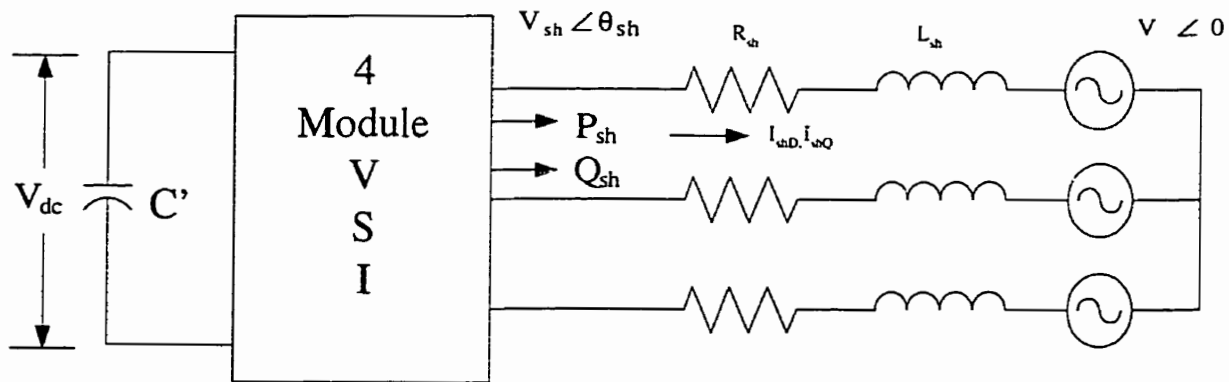


Fig.7.5 Equivalent circuit of a 4-module VSC connected to a constant voltage source.

Let V_{sh} be the per unit voltage generated by the 4-module VSC. Let θ_{sh} be the phase angle of the inverter voltage. Let V denote the per unit voltage of the constant voltage source. Let L_{sh} , R_{sh} represent the combined per unit reactance and resistance of the Y- Δ and the step-up transformers (Fig.7.3). Let C' represent the per unit capacitance of the DC link capacitor. The constant voltage source is assumed to be the reference.

Fig.7.6 shows the phasor diagram associated with the 4-module VSC. The D-axis coincides with the phase of the constant voltage source (V). The Q-axis leads the D-axis by 90 degrees. Let I_{shD} , I_{shQ} be the per unit D-Q axis currents with respect to the constant voltage source. V_{shD} and V_{shQ} represent the D-Q axis voltage of the 4-module VSC.

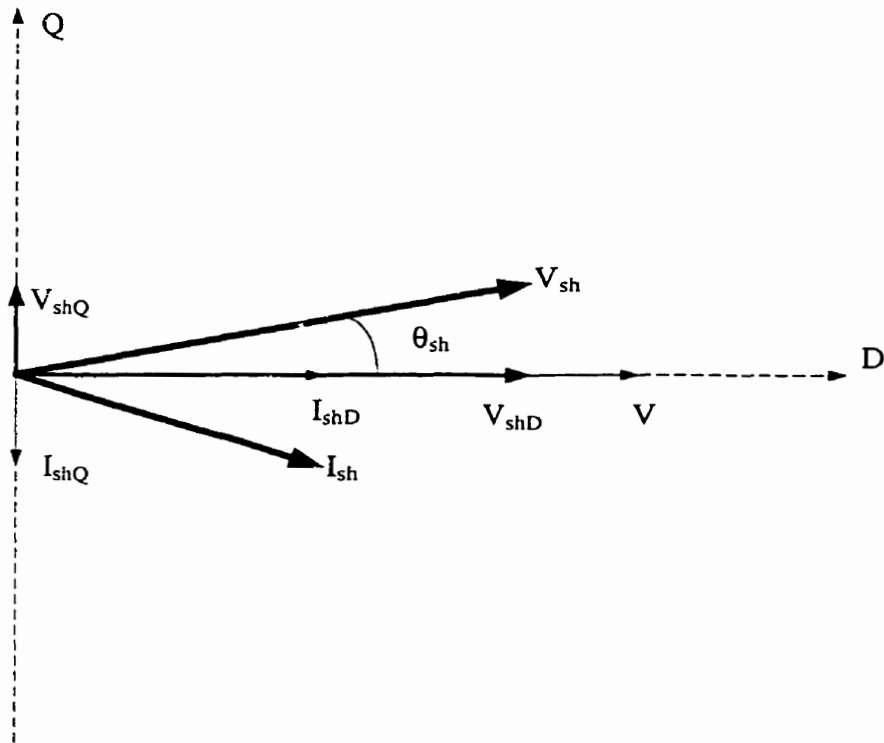


Fig.7.6 Phasor diagram for 4-module VSC connected to a constant voltage source.

Assuming the base voltage to be the peak of the phase voltage and the base current to be the peak of the phase current on the 345 kV side (Fig.7.3), the three-phase real and the reactive power in per unit is given by the equation 7.1.

$$\begin{aligned}
 P_{sh} &= \frac{3}{2} V I_{shD} \\
 Q_{sh} &= -\frac{3}{2} V I_{shQ}
 \end{aligned} \tag{7.1}$$

It is very evident from equation 7.1 that the real power (P_{sh}) is a function of I_{shD} and reactive power (Q_{sh}) is a function of I_{shQ} . Thus by regulating I_{shD} and I_{shQ} , real (P_{sh}) and reactive power (Q_{sh}) to/from the shunt inverter can be controlled independently. This forms the basis for designing the de-coupled control system [39].

The de-coupled control system allows for independent control of the D-Q axis currents. In order to achieve de-coupled control of real (P_{sh}) and reactive power (Q_{sh}), consider the equivalent circuit of the 4-module VSC connected to a constant voltage source as shown in Fig.7.5. Writing the system equations for the equivalent circuit shown in Fig.7.5 in terms of D-Q axis, we obtain equation 7.2.

$$\begin{aligned}
 \frac{dI_{shD}}{dt} &= -\frac{R_{sh}\omega_0 I_{shD}}{L_{sh}} + \omega\omega_0 I_{shQ} + \frac{\omega_0}{L_{sh}} (V_{shD} - V) \\
 \frac{dI_{shQ}}{dt} &= -\frac{R_{sh}\omega_0 I_{shQ}}{L_{sh}} - \omega\omega_0 I_{shD} + \frac{\omega_0}{L_{sh}} (V_{shQ})
 \end{aligned} \tag{7.2}$$

ω_0 represents the system frequency of 377 rads/sec. ω represents the system frequency of 1.0 in per unit. To achieve de-coupling of the D-Q axis currents, the control variable V_{shD} and V_{shQ} in equation 7.2 are modified as given in equation 7.3.

$$\begin{aligned} V_{shD} &= V + \frac{L_{sh}}{\omega_0} (u_1 - \omega \omega_0 I_{shQ}) \\ V_{shQ} &= \frac{L_{sh}}{\omega_0} (u_2 + \omega \omega_0 I_{shD}) \end{aligned} \quad (7.3)$$

where u_1 and u_2 are auxiliary control variables. Combining equation 7.2 and 7.3 together we get equation 7.4.

$$\begin{aligned} \frac{dI_{shD}}{dt} &= -\frac{R_{sh}\omega_0 I_{shD}}{L_{sh}} + u_1 \\ \frac{dI_{shQ}}{dt} &= -\frac{R_{sh}\omega_0 I_{shQ}}{L_{sh}} + u_2 \end{aligned} \quad (7.4)$$

Thus it is seen from equation 7.4 that by controlling u_1 and u_2 one can independently regulate I_{shD} and I_{shQ} thereby controlling the real (P_{sh}) and the reactive power flow (Q_{sh}) from the 4-module VSC. By controlling u_1 the real power flow (P_{sh}) and hence the DC link capacitor voltage (V_{dc}) can be regulated. By controlling u_2 the reactive power flow (Q_{sh}) can be regulated. To close the feedback loop, the auxiliary variables u_1 and u_2 are

controlled by proportional-integral (PI) controllers as given below in equation 7.5. The D-axis current I_{shD} is controlled by u_1 and the Q-axis current I_{shQ} is controlled by u_2 .

$$\begin{aligned} u_1 &= \left(K_{p1} + \frac{K_{i1}}{s} \right) (I_{shDref} - I_{shD}) \\ u_2 &= \left(K_{p2} + \frac{K_{i2}}{s} \right) (I_{shQref} - I_{shQ}) \end{aligned} \quad (7.5)$$

The variable 's' in equation 7.5 is the Laplace operator. Equation 7.5 forms the inner loop control system. The variable I_{shDref} can be controlled by an outer loop that controls the DC link capacitor voltage (V_{dc}). Similarly, if the 4-module VSC is used as a bus voltage controller, the variable I_{shQref} can be controlled by an outer loop that controls the voltage of the bus to which it is connected. PI controllers are used for the outer loop control. The outer loop control system is given by equation 7.6.

$$\begin{aligned} I_{shDref} &= \left(K_{p3} + \frac{K_{i3}}{s} \right) (V_{dcref} - V_{dc}) \\ I_{shQref} &= \left(K_{p4} + \frac{K_{i4}}{s} \right) (V_{ref} - V) \end{aligned} \quad (7.6)$$

Fig.7.7 shows the de-coupled control system for the 4-module VSC. The control system shown in Fig.7.7 will be used for the shunt inverter when considering the complete operation of a UPFC.

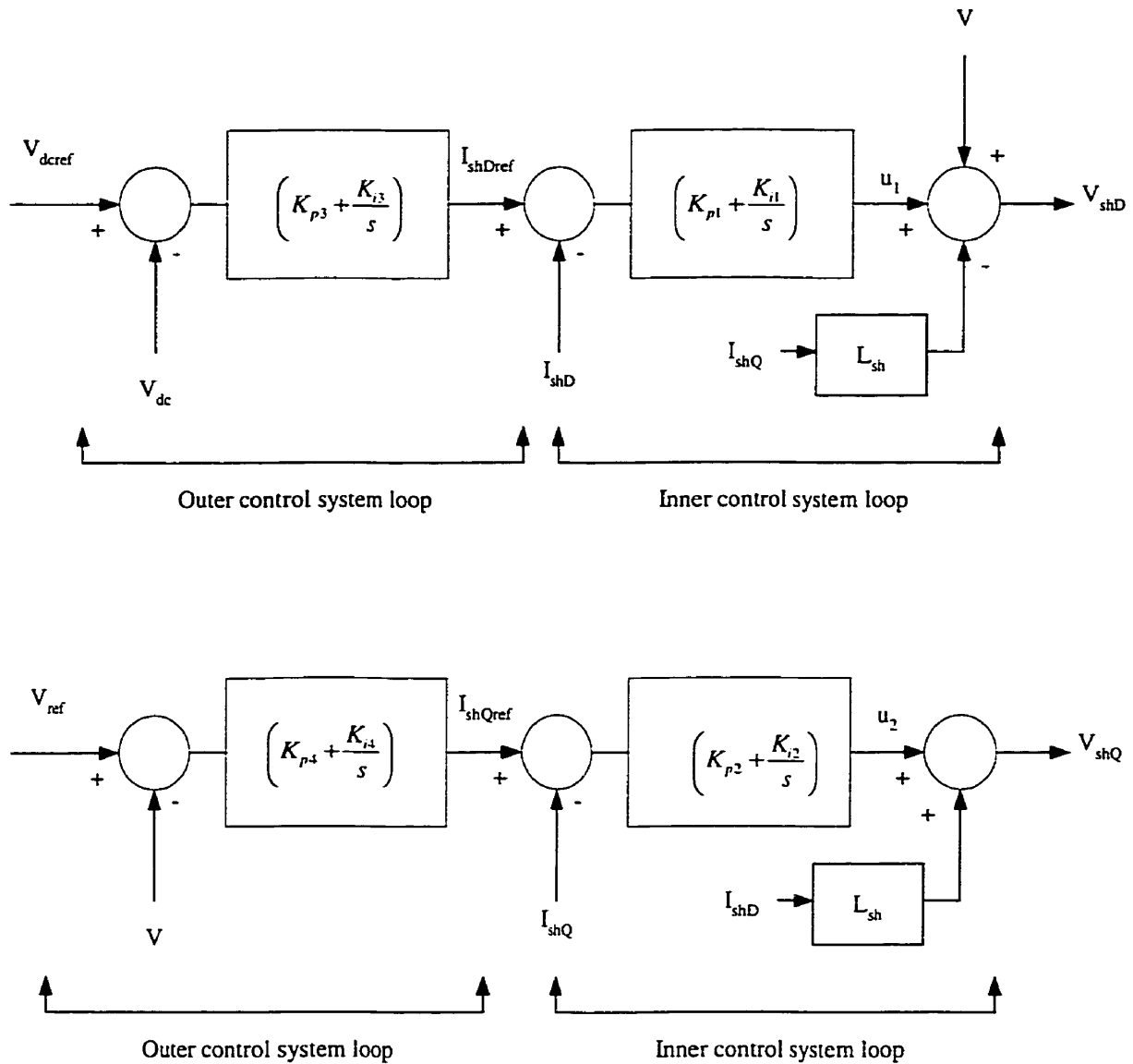


Fig.7.7 De-coupled control system.

7.3.2 De-coupled control system design for a 4-module VSC: The de-coupled control system design requires quantifying the PI controller gains. The de-coupled control system design is based on linear control techniques. For the 4-module VSC connected

to a constant voltage source (Fig.7.5), the differential equations associated with it are as given in equation 7.2 and have been reproduced here for convenience.

$$\begin{aligned}\frac{dI_{shD}}{dt} &= -\frac{R_{sh}\omega_0 I_{shD}}{L_{sh}} + \omega\omega_0 I_{shQ} + \frac{\omega_0}{L_{sh}}(V_{shD} - V) \\ \frac{dI_{shQ}}{dt} &= -\frac{R_{sh}\omega_0 I_{shQ}}{L_{sh}} - \omega\omega_0 I_{shD} + \frac{\omega_0}{L_{sh}}(V_{shQ})\end{aligned}\quad (7.12)$$

One of the important elements that effect the design of the de-coupled controller is the DC link capacitor (C). References [23,25,27] neglect the effect of DC link capacitor while designing the shunt inverter control system. This could lead to inaccurate PI controller gains and thereby an ineffective control system.

The DC link capacitor dynamics is given in chapter-5 equation 5.18 and has been reproduced as equation 7.13 for convenience.

$$\frac{dV_{dc}}{dt} = -\omega_0 C \left[\frac{3}{2} \left(\frac{V_{shD} I_{shD} + V_{shQ} I_{shQ} + V_{seD} I_{seD} + V_{seQ} I_{seQ}}{V_{dc}} \right) + \frac{V_{dc}}{R_{cup}} \right] \quad (7.13)$$

Since the focus of the control design here is on 4-module VSC operated as a shunt inverter, the two other control variables V_{seD} and V_{seQ} associated with the series inverter of a UPFC have been neglected. Equation 7.13 can now be written as equation 7.14.

$$\frac{dV_{dc}}{dt} = -\omega_0 C \left[\frac{3}{2} \left(\frac{V_{shD} I_{shD} + V_{shQ} I_{shQ}}{V_{dc}} \right) + \frac{V_{dc}}{R_{cup}} \right] \quad (7.14)$$

Thus the complete set of system equations corresponding to the 4-module VSC control design are equations 7.12 and 7.14.

To achieve de-coupling of the D-Q axis currents, the D-Q axis voltage of the shunt inverter V_{shD} and V_{shQ} given in equation 7.12 are substituted by equation 7.3. Equation 7.15 shows the system equations in terms of the auxiliary control variables u_1 and u_2 .

$$\begin{aligned}
 \frac{dI_{shD}}{dt} &= -\frac{R_{sh}\omega_0}{L_{sh}} I_{shD} + u_1 \\
 \frac{dI_{shQ}}{dt} &= -\frac{R_{sh}\omega_0}{L_{sh}} I_{shQ} + u_2 \\
 \frac{dV_{dc}}{dt} &= -\frac{3\omega_0 C}{2} \frac{[u_1 I_{shD} (L_{sh}/\omega_0) + |V| I_{shD} + u_2 I_{shQ} (L_{sh}/\omega_0)]}{V_{dc}} - \omega_0 C \frac{V_{dc}}{R_{cap}}
 \end{aligned}
 \tag{7.15}$$

Linearizing equation 7.15 around an operating point we get,

$$\begin{aligned}
 \frac{d\Delta I_{shD}}{dt} &= -\frac{R_{sh}\omega_0}{L_{sh}} \Delta I_{shD} + \Delta u_1 \\
 \frac{d\Delta I_{shQ}}{dt} &= -\frac{R_{sh}\omega_0}{L_{sh}} \Delta I_{shQ} + \Delta u_2 \\
 \frac{d\Delta V_{dc}}{dt} &= -\frac{3\omega_0 C}{2} \frac{\{V_{dc0} \{ [a_1 u_{10} \Delta I_{shD} + a_1 I_{shD0} \Delta u_1] + |V| \Delta I_{shD} + [a_1 u_{20} \Delta I_{shQ} + a_1 I_{shQ0} \Delta u_2] \} - \{u_{10} I_{shD0} a_1 + |V| I_{shD0} + u_{20} a_1 I_{shQ0}\} \Delta V_{dc}\}}{V_{dc0}^2} \\
 &\quad - \omega_0 C \frac{\Delta V_{dc}}{R_{cap}}
 \end{aligned}
 \tag{7.16}$$

where $a_l = L_{sh} / \omega_0$.

Putting equation 7.16 into state variable form we get,

$$\begin{bmatrix} \dot{\Delta I_{shD}} \\ \dot{\Delta I_{shQ}} \\ \dot{\Delta V_{dc}} \end{bmatrix} = \begin{bmatrix} -\frac{R\omega_0}{L_{sh}} & 0 & 0 \\ 0 & -\frac{R\omega_0}{L_{sh}} & 0 \\ a_{31} & a_{32} & a_{33} \end{bmatrix} \begin{bmatrix} \Delta I_{shD} \\ \Delta I_{shQ} \\ \Delta V_{dc} \end{bmatrix} + \begin{bmatrix} 1 & 0 \\ 0 & 1 \\ b_{31} & b_{32} \end{bmatrix} \begin{bmatrix} \Delta u_1 \\ \Delta u_2 \end{bmatrix} \quad (7.17)$$

where

$$a_{31} = -\frac{3\omega_0 C (a_1 u_{10} + |V|)}{2V_{dc0}}$$

$$a_{32} = -\frac{3\omega_0 C (a_1 u_{20})}{2V_{dc0}}$$

$$a_{33} = \frac{3\omega_0 C (u_{10} I_{shD0} a_1 + |V| I_{shD0} + u_{20} I_{shQ0} a_1)}{2V_{dc0}^2} - \frac{\omega_0 C}{R_{cap}}$$

$$b_{31} = -\frac{3\omega_0 C (a_1 I_{shD0})}{2V_{dc0}}$$

$$b_{32} = -\frac{3\omega_0 C (a_1 I_{shQ0})}{2V_{dc0}}$$

It is observed from equation 7.17 that the D-Q axis currents are de-coupled and hence it is possible to design PI controllers separately for regulating the D-Q axis currents. The design procedure starts with the design of the de-coupled controllers that uses only the D-Q axis equations (the first two in equation 7.16). Once the inner PI controllers (K_{p1} , K_{i1} , K_{p2} , K_{i2}) are designed, the DC capacitor equation is used to design the DC capacitor voltage PI controller (K_{p3} , K_{i3}) that forms the outer loop for the D-axis voltage control. For the Q-axis, since the 4-module VSC is connected to a constant voltage source

during design process, the outer loop controller (K_{pi}, K_{il}) that is generally used to control the voltage of the bus to which the VSC is connected has not been considered here for design. Nevertheless, it will be used in chapter 9 when operating the 4-module VSC as a shunt inverter.

To begin with the de-coupled control system design, consider the D-axis differential equation representation given in equation 7.16. Converting it into the Laplace domain and introducing the PI controller transfer function given in equation 7.5 into the D-axis equation, we get

$$s\Delta I_{shD}(s) = -\frac{R_{sh}\omega_0}{L_{sh}}\Delta I_{shD}(s) + \left[K_{pi} + \frac{K_{il}}{s} \right] \left[\Delta(I_{shDref} - I_{shD}) \right]$$

Solving the above equation we get,

$$\left(s^2 + \left[\frac{R_{sh}\omega_0}{L_{sh}} + K_{pi} \right] s + K_{il} \right) \Delta I_{shD}(s) = 0$$

Hence the characteristic equation for the D-axis is given by

$$\left(s^2 + \left[\frac{R_{sh}\omega_0}{L_{sh}} + K_{pi} \right] s + K_{il} \right) = 0$$

This is a second order equation. Placing the roots of the characteristic equation at specified locations, one can find the design values of the PI controller. Similar

procedure has been applied to the Q-axis. The operating conditions for the design are as given below. The operating conditions have been obtained from PSCAD-EMTDC simulations.

$$\begin{aligned}
 R &= 0.0014 \\
 L_{sh} &= 0.2 \\
 C &= 0.0324 \\
 I_{shD0} &= -0.042 \\
 I_{shQ0} &= 0.18 \\
 u_{10} &= -0.004 \\
 u_{20} &= 0.05 \\
 \omega_0 &= 377 \\
 V_{dc0} &= 2.22
 \end{aligned}$$

The poles for the D-axis PI controller (K_{p1} , K_{i1}) have been placed at $-3.9 \pm j2.5$. The corresponding PI controller gains are $K_{p1} = 5.0$ and $K_{i1} = 21.4$. The poles for the Q-axis PI controller (K_{p2} , K_{i2}) have been placed at $-1.5 \pm j 1.7$. The corresponding PI controller gains are $K_{p2} = 0.2$ and $K_{i2} = 5.0$. Having designed the inner loop controller for the D and Q axis current controllers, the DC link capacitor voltage PI controller (K_{p3} , K_{i3}) has to be designed. In order to design the DC link capacitor voltage PI controller (K_{p3} , K_{i3}), information regarding the inner loop PI controllers (K_{p1} , K_{i1} , K_{p2} , K_{i2}) have to be included into the complete system equations. Representing equation 7.17 in the state variable form, we get

$$\begin{aligned}\dot{X} &= AX + BU \\ Y &= CX + DU\end{aligned}\tag{7.18}$$

Where the matrices A and B are as given in equation 7.17. The matrices C and D are given below.

$$C = \begin{bmatrix} 1 & 0 & 0 \\ 0 & 1 & 0 \end{bmatrix}$$

$$D = \begin{bmatrix} 0 & 0 \\ 0 & 0 \end{bmatrix}$$

Equation 7.18 forms the input-output representation of the 4-module VSC connected to a constant voltage source. Using the procedure described in chapter 5 section 5.1.1.7, the PI controllers (K_{p1} , K_{i1} , K_{p2} , K_{i2}) can be included into the state matrix A to obtain a new set of input-output equation as given in equation 7.19.

$$\begin{aligned}\dot{X}_1 &= A_1 X_1 + B_1 U_1 \\ Y_1 &= C_1 X_1 + D_1 U_1\end{aligned}\tag{7.19}$$

Where

$$X_1 = [\Delta I_{shD}, \Delta I_{shQ}, \Delta V_{dc}, \Delta x_{c1}, \Delta x_{c2}]$$

$$A_1 = \begin{pmatrix} A - BK_{pr}C & -BK_{it} \\ MC & -DK_{it} \end{pmatrix}$$

$$B_1 = \begin{pmatrix} BK_{pr} \\ -M \end{pmatrix}$$

$$C_1 = (MC \quad -DK_{it})$$

$$D_1 = DK_{pt}$$

$$M = (I + DK_p)^{-1}$$

$$K_{pr} = (I + K_p D)^{-1} K_p$$

$$K_{it} = (I + K_p D)^{-1} K_i$$

$$U_1 = \begin{bmatrix} I_{shDref} \\ I_{shQref} \end{bmatrix}$$

x_{c1} and x_{c2} are the state variables associated with the D-Q axis current controllers. Since the inverter is connected to a constant voltage source, the Q-axis current reference is not regulated and hence ΔI_{shQref} is 0. Thus the U_1 matrix contains only ΔI_{shDref} . We can now design the outer loop for DC link capacitor voltage (V_{dc}) controller by using the above approach. Including the PI controller (K_{p3} , K_{i3}) for the DC link capacitor voltage (V_{dc}) in the state matrix we get the closed loop equation,

$$\dot{X}_2 = A_2 X_2 \tag{7.20}$$

Where

$$X_2 = [\Delta I_{shD}, \Delta I_{shQ}, \Delta V_{dc}, \Delta x_{c1}, \Delta x_{c2}, \Delta x_{c3}]$$

x_{c3} is the PI controller state variable for the DC link capacitor voltage controller (V_{dc}). Using a PI controller with values for the outer DC link capacitor voltage (V_{dc}) controller of $K_{p3} = -1.0$ and $K_{i3} = -2.0$, the eigen values of the system with all the controllers included are

$$-1.10 \pm j 6.46$$

$$-2.83 \pm j 0.42$$

$$-1.46 \pm j 1.7$$

The PI controller design values obtained above have been arrived at by iterating between design procedure and PSCAD-EMTDC simulation until satisfactory step response performance have been obtained. The de-coupled control system designed for a 4-module VSC will be used when operating it as a shunt inverter for the UPFC.

7.4 Implementation of 4-Module VSC and its control system using PSCAD-EMTDC software

The circuit of a 4-Module VSC shown in Fig.7.3 is set up using the PSCAD-EMTDC software. The 345 kV side is connected to a constant 345 kV constant voltage source. The main step-up transformer is rated at 160 MVA 66 kV/345 kV and is connected in Y-Y. The total inter-phase magnetics (the arrangement of the Y- Δ transformers) is also rated at 160 MVA. Each of the 4 transformers corresponding to each basic VSC module is rated at 40 MVA. The de-coupled control system designed in

section 7.3 is used to control the reactive power supplied by the 4-module VSC and its DC capacitor voltage. The DC link capacitor is rated at 3000 μ F. PI control blocks are available in the PSCAD-EMTDC software. They have been used to build the control system as shown in Fig.7.7. The D-Q axis control voltage signals namely V_{shD} and V_{shQ} generated by the control system shown in Fig.7.7 have to be converted into signals amenable to the operation of a 4-module VSC. The two variables associated with any VSC are its modulation index (mi) and phase angle (θ_{sh}). In the case of SPWM, a sinusoidal reference signal is compared with a triangular waveform to generate the proper instant of firing for the VSC. The ratio of the peak of the sinusoidal signal to the peak of the triangular waveform is called the modulation index mi . The phase angle θ_{sh} is the phase angle difference between the shunt inverter generated voltage and the reference voltage. With reference to Fig.7.5, the reference angle will be that of the constant voltage source. The value of the modulation index mi and the phase angle θ_{sh} depends on the number of modules of a VSC and the DC voltage magnitude. The line-to-line voltage generated by a SPWM based single VSC module as shown in Fig.7.2, is related to the DC capacitor voltage by the equation 7.21 [40].

$$\hat{V}_{sh(1-module)} = 0.612 mi \hat{V}_{dc} \quad (7.21)$$

The ‘ \wedge ’ represents the actual value. The shunt inverter in this case has been built up of 4 modules. Multiplying equation 7.21 by 4 gives the voltage generated by the 4-module

VSC. Equation 7.21 is modified to include the 4-module operation to obtain equation 7.22.

$$\hat{V}_{sh(4\text{-module})} = 2.448 \text{ } mi \hat{V}_{dc} \quad (7.22)$$

Rearranging equation 7.22 to obtain the modulation index, we get

$$mi = \frac{\hat{V}_{sh(4\text{-module})}}{2.448 \hat{V}_{dc}} \quad (7.23)$$

The D-Q axis control voltage signals namely V_{shD} and V_{shQ} generated by the control system shown in Fig.7.7 are in per unit. The magnitude of the voltage to be generated by the 4-module VSC in per unit is given by equation 7.24.

$$V_{sh} = \sqrt{V_{shD}^2 + V_{shQ}^2} \quad (7.24)$$

Since the 4-module is connected on the 66kV side of the step up transformer as shown in Fig.7.3, the per unit value of the voltage generated by 4-module VSC (V_{sh}) is multiplied by 66 to obtain its actual value in kV. Multiplying equation 7.24 by 66, the actual voltage that has to be generated by the 4-module VSC ($\hat{V}_{sh(4\text{-module})}$) is obtained.

Substituting for $\hat{V}_{sh(4\text{-module})}$ in equation 7.23 in terms of its per unit value we get,

$$m_i = \frac{66V_{sh}}{2.448 \hat{V}_{dc}} \quad (7.25)$$

The phase angle of the generated voltage is obtained from the ratio of the control signals as given in equation 7.26.

$$\theta_{sh} = \tan^{-1} \left(\frac{V_{shQ}}{V_{shD}} \right) \quad (7.26)$$

7.5 Performance studies on a 4-Module VSC

A 4-module VSC with its associated control system was set up in PSCAD-EMTDC software to study the performance of the control system design to step input changes. The 4-module VSC was connected to a constant voltage source as shown in Fig.7.5. Fig.7.8 shows the response of the shunt inverter to step changes in reactive power reference. Since the Q-axis controller input is I_{shQref} , the change in reactive power reference is translated into an equivalent Q-axis current reference I_{shQref} by dividing the reactive power reference (Q_{shref}) by the constant voltage source magnitude ($|V|$). Thus

$$I_{shQref} = \frac{Q_{shref}}{|V|} \quad (7.27)$$

7.5.1 Initialization: To start the simulation, the DC link capacitor voltage (V_{dc}) is initially uncharged. At around 0.75 sec, the VSC is switched to the constant 345 kV source and the DC link capacitor voltage (V_{dc}) controller is switched into service. The sudden switching of the 4-module VSC to the constant AC voltage source at 0.75 sec causes the DC link capacitor voltage (V_{dc}) to rise to 60 kV quickly as shown in plot-7 of Fig.7.8. The activation of the DC link capacitor voltage (V_{dc}) controller at 0.75 sec allows the 4-Module VSC to charge the DC capacitor to 60 kV by consuming real power (P_{sh}) from the constant AC voltage source to which the 4-Module VSC is connected. This is shown in plot-2 of Fig.7.8. The sudden switching of the VSC to the constant AC voltage source causes the real power (P_{sh}) consumed to dip to -80 MW allowing it to charge almost instantaneously. At around 1.0 sec, the 4-Module VSC starts to consume around 5MW of power to supply its losses and maintains the DC link capacitor voltage at 60 kV.

7.5.2 Step change of reactive power from 0 to -130 MVAR: At 3.0 sec, a step change in the reactive power reference (Q_{shref}) is made from 0.0 to -130 MVAR (4-Module VSC consuming reactive power). This step change in reactive power reference (Q_{shref}) causes the variable u_2 that controls I_{shQ} to change rapidly. This in turn causes the variable V_{shQ} to become positive as shown in Plot-6 of Fig.7.8 making θ_{sh} to become positive with respect to the constant voltage source reference. The positive phase angle of θ_{sh} causes the 4-Module VSC to release some of its real power causing the DC link capacitor voltage (V_{dc}) to drop. This is shown in plot-7 of Fig.7.8 at around 3.0 sec. This

drop in DC link capacitor voltage (V_{dc}) is sensed by the DC capacitor voltage controller and causes the variable V_{shD} to reduce as shown in plot-5 of Fig.7.8. This allows the VSC to consume more real power (P_{sh}) to maintain the DC link capacitor voltage at 60 kV and supply its switching losses. The real power (P_{sh}) consumed is about 25 MW.

Plot-1 of Fig.7.8 shows the fast response in reactive power (Q_{sh}) to the change in reactive power reference (Q_{shref}) from 0 to -130 MVAR. Plot-3 is the expanded version of plot-1 around 3.0 sec. It is seen from plot-3 that the VSC provides fast response times in the order of couple of cycles.

7.5.3 Step change of reactive power from -130 to +130 MVAR: At 6.5 sec, a step change in reactive power reference (Q_{shref}) is conducted from -130 MVAR to +130 MVAR. This step change in reactive power reference (Q_{shref}) causes the auxiliary variable u_2 that controls I_{shQ} to change rapidly and become negative causing V_{shQ} to become negative as shown in plot-6 at 6.5secs. The negative value of V_{shQ} means that the angle θ_{sh} between the constant voltage source and the VSC is negative causing the real power (P_{sh}) to flow from the constant AC voltage source to the VSC. This leads to an increase in the DC link capacitor voltage (V_{dc}). The increase in DC link capacitor voltage (V_{dc}) is sensed by the DC capacitor voltage controller making V_{shD} to be greater in magnitude than the constant AC voltage source as shown in Plot-5 of Fig.7.8 at around 6.5 sec. This causes the VSC to generate real power (P_{sh}) and brings back the DC link capacitor voltage (V_{dc}) to 60 kV. This is shown in plot-7 of Fig.7.8. Plot-4 shows the expanded version of plot-1 at around 6.5 sec. The VSC responds to the

sudden changes in reactive power reference (Q_{shref}) in a couple of cycles. It is observed from plot-2 that the real power flow (P_{sh}) from the constant voltage source to the VSC is a constant of magnitude 25MW. This due to the fact that irrespective of the direction of the current flow, the magnitude of the current remains the same when the VSC is either consuming -130MVAR of reactive power or generating +130 MVAR of reactive power.

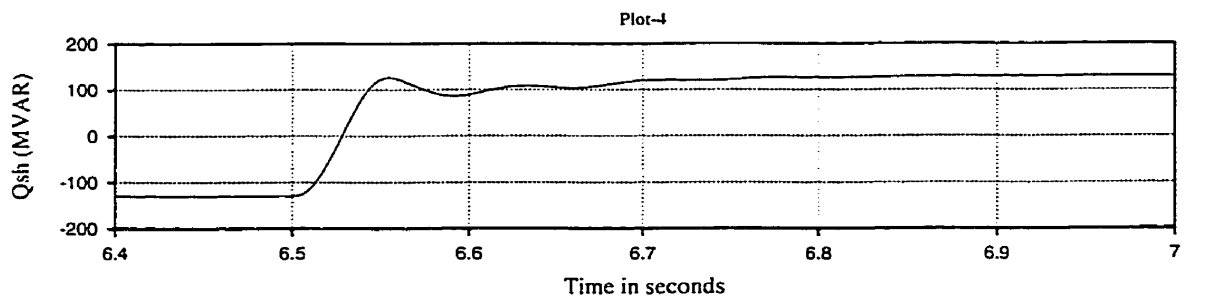
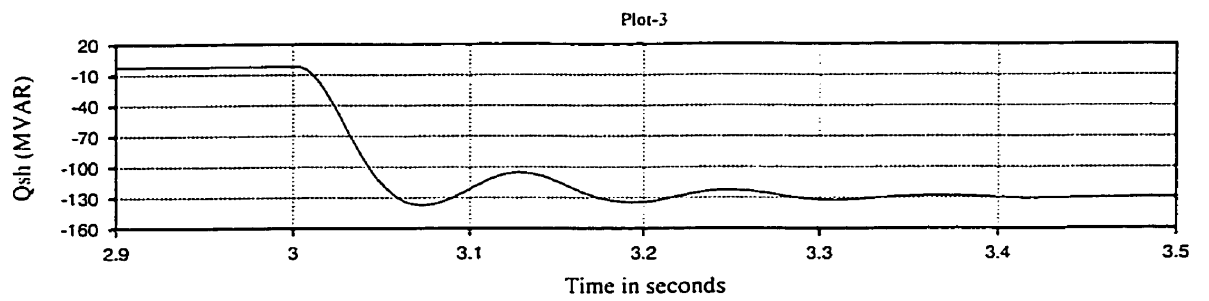
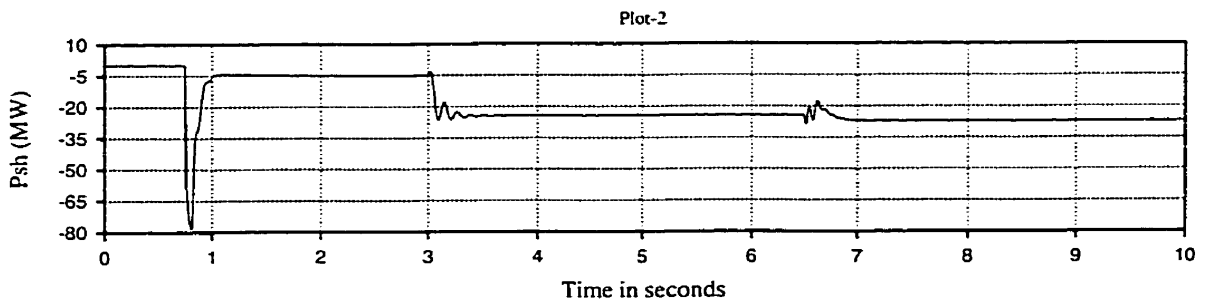
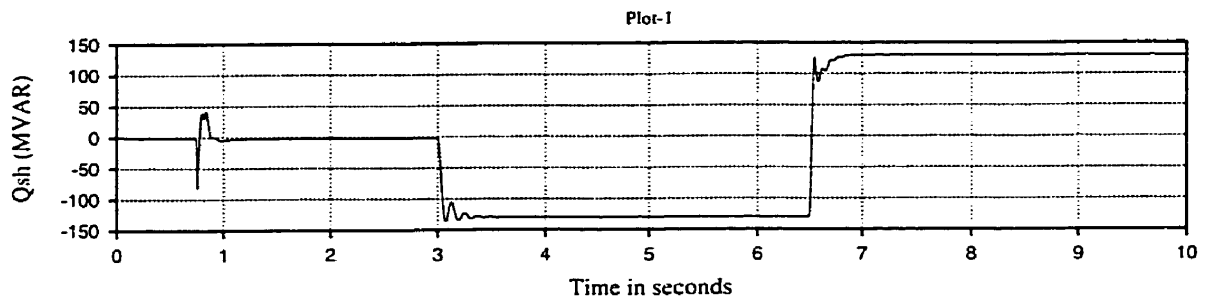


Fig.7.8 4-Module VSC performance (cont.).

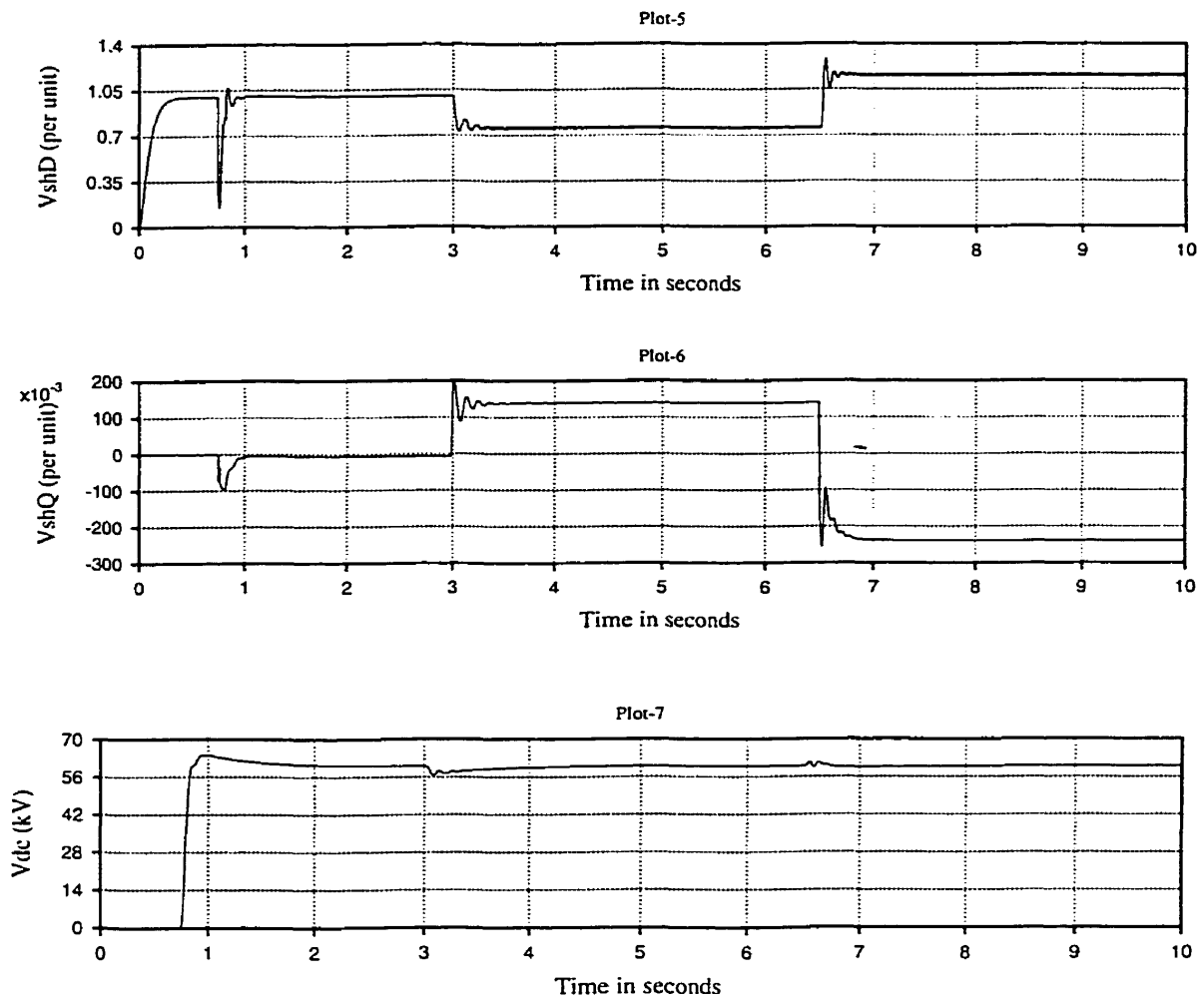


Fig.7.8 4-Module VSC performance.

7.6 Summary

The shunt inverter plays an important role in the operation of a UPFC. It maintains a required level of DC link capacitor voltage for the operation of the series and shunt inverter. It also supplies the necessary real power demand of the series

inverter. It can also provide necessary reactive power to the bus to which it is connected.

This chapter has described the construction and operation of a 4-module VSC using the PSCAD-EMTDC software. Three-phase voltages generated by each module of a VSC using SPWM are combined by Y- Δ transformers to obtain a high power VSC. The manner in which these transformers are connected have also been described.

The basics of de-coupled control system for regulating real and reactive power independently have been described in this chapter. The de-coupled control system has been designed based on linear control techniques that includes the DC capacitor dynamics. A step by step procedure has been presented to quantify the PI controller gains. The de-coupled control system consists of two loops. The inner loop tracks the D-Q axis currents and the outer loop sets the reference for the inner loop. The design procedure is loop based, in the sense that first the inner loop is designed and then the outer loop. The information regarding the inner loop PI gains are used while designing the outer loop PI controller.

The performance of the de-coupled control system design has been tested using the PSCAD-EMTDC software. Step response tests have been conducted to not only show the validity of the control system design, but also to bring out the ability of this scheme for fast response of the 4-module to reactive power demands while simultaneously regulating the DC link capacitor voltage.

Chapter 8

Series inverter construction, operation and control design using PSCAD-EMTDC software

8.0 Introduction

UPFC as described in chapter 1 consists of two inverters connected back-to-back via a DC link capacitor with one inverter connected in shunt with the transmission line through a shunt transformer and the other inverter in series with the transmission line through a series transformer. The series inverter of a UPFC plays an important role of controlling the power flow in the transmission line by injecting a voltage of adjustable magnitude and phase angle in series with the transmission line.

This chapter focuses on the construction, operation and control of a series inverter using PSCAD-EMTDC software. The DC link capacitor forms an integral part in the construction, operation and control of both the shunt and the series inverter of a UPFC. Under steady state conditions, the DC link capacitor provides the shunt and series inverter the necessary DC voltage for their operation. Under transient conditions, the DC

link capacitor supplies the real power demand of the series inverter. In this context, the rating of the DC link capacitor plays an important role in the proper operation of a UPFC. A design procedure for calculating the ratings of the DC link capacitor has also been described in this chapter. Further, a PI controller design for the series inverter for controlling the real power flow in a transmission line has been investigated.

8.1 Series inverter transformer rating

Fig.8.1 shows a UPFC connected to a transmission line. The series inverter is connected to the transmission line through a transformer T_2 . The design of the series transformer T_2 is a planning stage development. In this thesis, the series inverter is placed in series with a 345 kV transmission line. The rating for the series inverter and series transformer T_2 would depend on the product of maximum series voltage that could be injected on to the transmission line and the transmission line current. The maximum voltage that can be injected by the series inverter has been limited to 0.3 p.u. Exceeding this value would cause the line side voltage to be very high. For a 345kV system, the maximum allowable injected voltage would then be about 60kV per phase. Assuming a surge impedance loading (SIL) of 420 MW for a 345 kV system as reference, the ratings of the series inverter and series transformer T_2 works out to be 126 MVA. Since a 345 kV line can transfer more than its SIL power depending on the length of the transmission line, the series inverter and series transformer T_2 has been rated at 160 MVA to be on the conservative side.

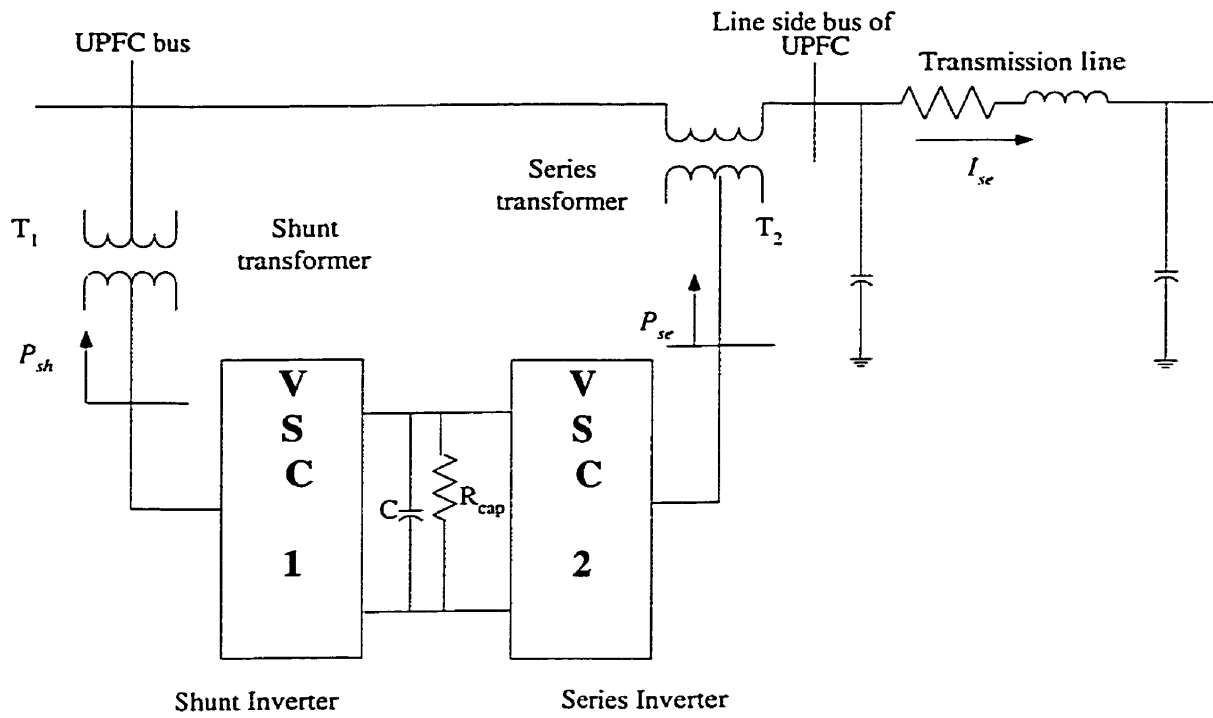


Fig.8.1 UPFC connected to a transmission line.

8.2 Series Inverter: Construction and Operation

8.2.1 Series inverter construction: In order to build a high power VSC module, a number of basic three-phase voltage source module shown in chapter 7 Fig.7.2 have to be combined together. In this thesis, a 4-module voltage source inverter has been constructed for the series inverter using PSCAD-EMTDC software. A 4-module VSC consists of 4 basic VSC inverter configuration connected in parallel across a common DC capacitor. Each of the basic VSC derives its DC voltage from the capacitor. Considering a sinusoidal pulse-width modulation (SPWM) for the operation of a VSC, each of these basic VSC modules generates a balanced three-phase voltage. Transformers are used to combine the voltage generated by each of these basic VSC. The primary of each of these transformers is connected either in Y or Δ configuration. The secondary of each of these transformers is connected in series. Fig.8.2 shows the 4-module voltage source series inverter.

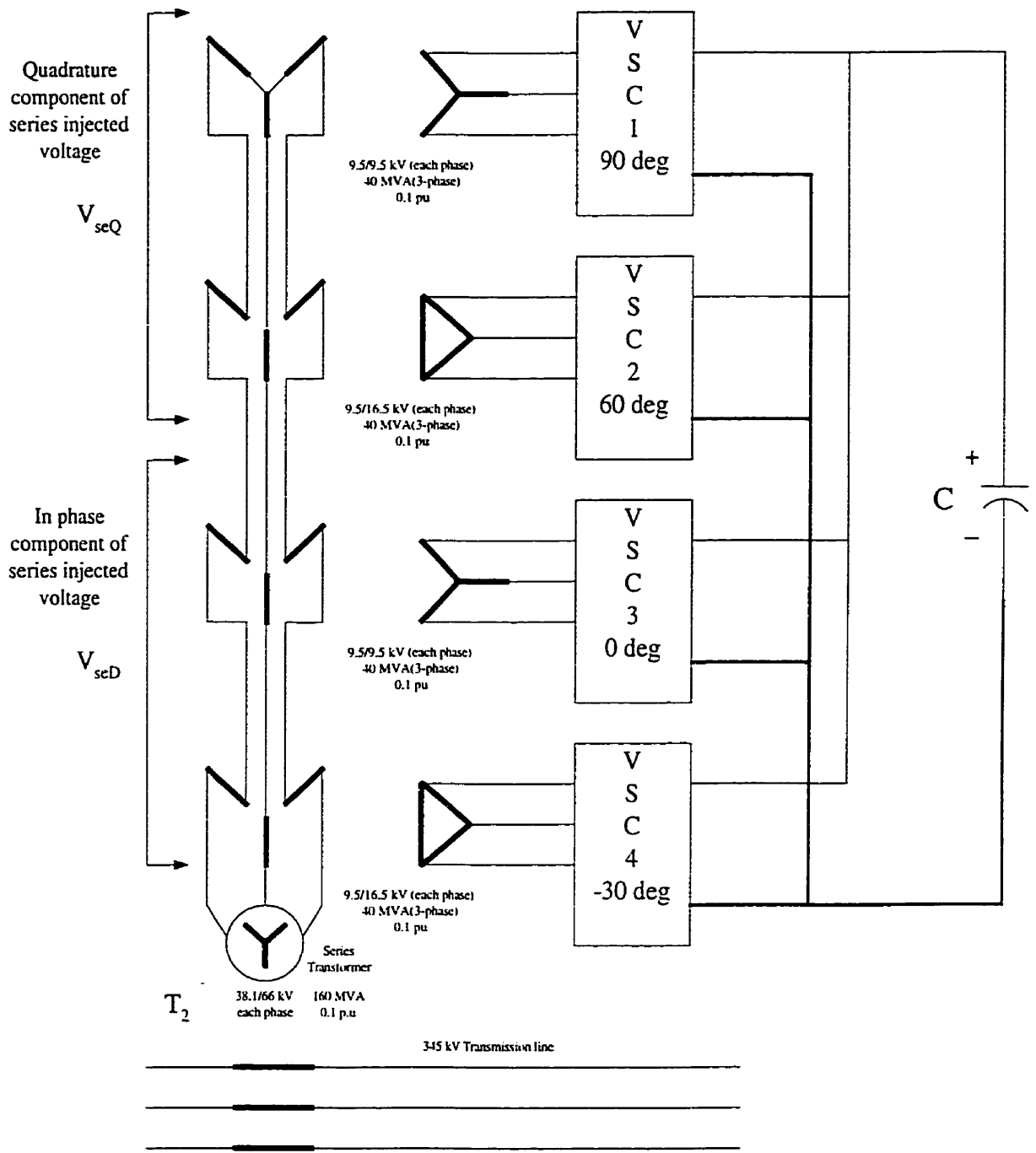


Fig.8.2 4-Module voltage source series inverter.

8.2.2 Operation of a series inverter: Each of the four VSC modules as shown in Fig.8.2 generate three-phase balanced voltages based on SPWM. In this thesis, the switching frequency of the triangular waveform of a SPWM is 9 times the fundamental. The use of an odd multiple of the fundamental frequency allows for elimination of all even harmonics and the harmonic at the switching frequency (540 Hz) in the line-to-line voltages. Since a low switching frequency is being used, to eliminate the even harmonics in the line-to-line voltages a synchronized SPWM is used.

The three-phase voltage generated by each basic VSC module is added to obtain a high power, high voltage source inverter using the arrangement shown in Fig.8.2. At this moment it should be emphasized that the series inverter has the ability to adjust the series injected voltage and phase angle. In order to be able to control both the series injected voltage magnitude and its phase angle, the series injected voltage is split into orthogonal components (V_{seD} , V_{seQ}). In order to understand how the voltage generated by each of the 4 VSC modules are combined for the series inverter to be able to control the series injected voltage magnitude and phase angle, consider the phasor diagram as shown in Fig.8.3 and Fig.8.4. Fig.8.3 shows the phasor diagram associated with the operation of VSC-1 and VSC-2 and Fig.8.4 shows the phasor diagram associated with the operation of VSC-3 and VSC-4. The letters A, B, and C represent the three phases and the numerals 1, 2, 3 and 4 represent the four basic VSC modules. The phasors of different phases with same numeral as their subscripts are phase shifted by 120 degrees. Consider the phasor diagram associated with the operation of VSC-1 and VSC-2 as shown in Fig.8.3. The phasor 1A, 1B and 1C are phase shifted by 120 degrees. The phasors 2A, 2B and 2C are phase shifted from 1A, 1B and 1C by -30 degrees. It should be observed that VSC-2 is

connected to a delta connected transformer winding. Thus the secondary phase voltage is phase shifted by +30 degrees and hence is in phase with phasor 1A. By doing so, the voltage generated by VSC-1 and VSC-2 are added together to obtain a component of the series injected voltage (V_{seQ}) that is 90 degrees leading the reference phasor.

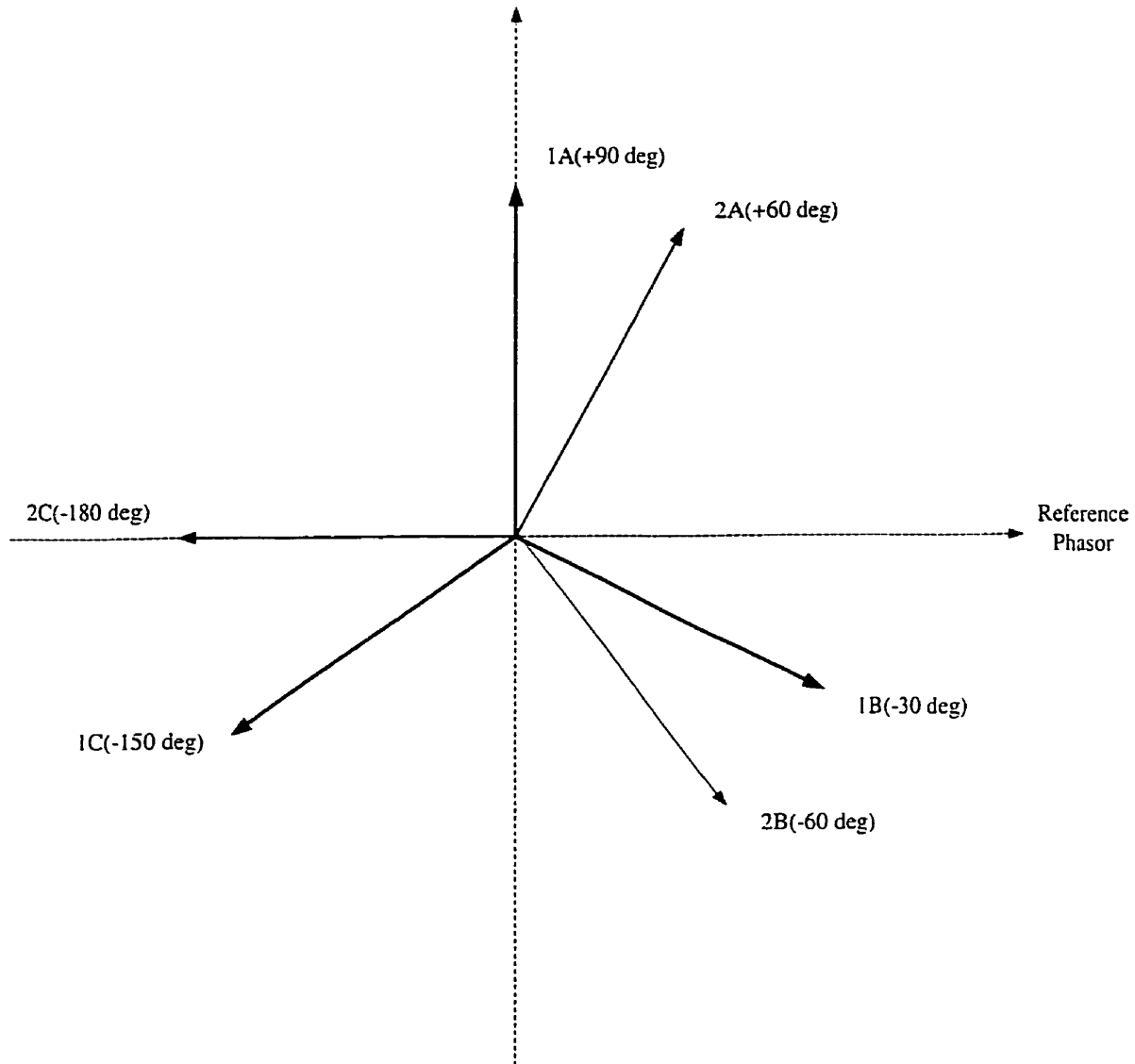


Fig.8.3 Phasor diagram for operation VSC-1 and VSC-2 of series inverter (V_{seQ}).

To understand the operation of VSC-3 and VSC-4, consider the phasor diagram associated with its operation as shown in Fig.8.4. The phasors 4A, 4B and 4C are phase

shifted from 3A, 3B and 3C by -30 degrees. It should be observed that VSC-4 is connected to a delta connected transformer winding. Thus the secondary phase voltage of VSC-4 is in phase with VSC-3. Thus one obtains a component of the series voltage that is in-phase (V_{seD}) with the reference phasor. The reference phasor is the same for inverters VSC-1 through VSC-4.

By splitting the injection of the series voltage into two components, one in-phase (V_{seD}) with and the other in quadrature (V_{seQ}) with the reference phasor, one can independently vary the magnitude of the orthogonal components and thereby control the magnitude and phase angle of the series injected voltage.

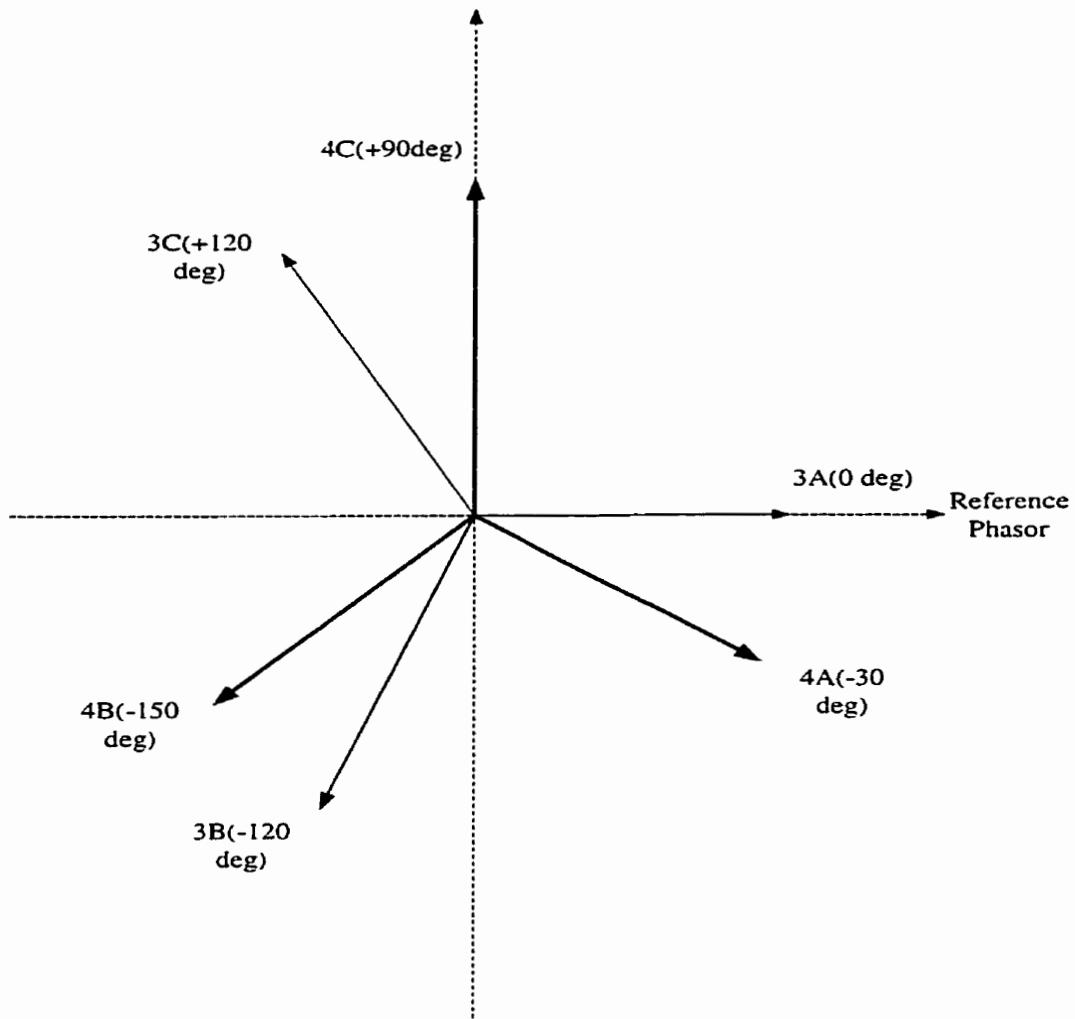


Fig.8.4 Phasor diagram for operation VSC-3 and VSC-4 of series inverter (V_{seD}).

8.3 UPFC DC link capacitor rating

The DC link capacitor plays an important role in providing the necessary DC voltage for the operation of the shunt and the series inverters. It also provides a path for the real power exchange between the series and the shunt inverters. Under steady state conditions, the real power demand of the series inverter is supplied by the shunt inverter. But during transient conditions, the shunt inverter does not respond very quickly and hence causes the DC capacitor to charge/discharge to meet the real power demand of the series inverter. This leads to an increase/decrease of DC capacitor voltage. Based on the amount of increase/decrease in DC capacitor voltage that could be permitted, the DC capacitor has been designed.

Under the assumption that the shunt inverter controls the voltage of the bus to which it is connected ($V_{upfcbus}$) at 1.0 per unit and that the voltage on the line side (V_{line}) is restricted to 1.05 p.u , the maximum value of the series injected voltage that would be in phase with the line current is about 0.05 p.u . At SIL (420 MW for 345 kV) level the line current is always in phase with voltage. The value of the current at SIL at 345 kV is 702 A. The three phase real power that the series inverter will supply under this condition is 20.97 MW ($P_{se} = 3 \times 0.05 \times \frac{345000}{\sqrt{3}} \times 702 = 20.97 MW$). Based on the assumption that a maximum of 20.97 MW will be exchanged between the series inverter and the transmission line within $\frac{1}{4}$ cycle of the AC voltage, the DC capacitor has been designed. A $\frac{1}{4}$ cycle time period has been chosen to quantify the fast operation of the series inverter. The following equations have been used in designing the DC capacitor. The energy stored in a capacitor W_c is given by equation 8.1.

$$W_C = \frac{1}{2} C V_{dc}^2 \quad (8.1)$$

where 'C' is the capacitance of the DC capacitor and V_{dc} is the DC voltage across the capacitor. Assuming 20.97 MW of power is released by the series inverter in $\frac{1}{4}$ cycle of the AC voltage, the associated energy is given by equation 8.2.

$$W_{se} = P_{se} \times t_r \quad (8.2)$$

Where W_{se} is the energy released by the series inverter, P_{se} is the real power generated by the series inverter and t_r is the time duration over which the P_{se} is released. The energy released by the series inverter is given by equation 8.3

$$W_{se} = 20.97 \times 0.004166 \times 10^6 = 87374.65 \text{ W sec} \quad (8.3)$$

The amount of energy released by the DC capacitor would cause the DC capacitor voltage to reduce. Assuming that the maximum value of decrease that could be allowed is 8 kV from its steady state value, the energy released by the capacitor is then given by equation 8.4.

$$W_C = \frac{1}{2} C (V_{dcref} - V_{dc})^2 = 0.5 \times C \times 8000^2 \quad (8.4)$$

Equating 8.3 and 8.4, we get $C = 2730 \mu\text{F}$. A value of $3000 \mu\text{F}$ has been chosen to be on the conservative side.

8.4 Controller design for series inverter

The series inverter of a UPFC has the ability to control real and reactive power flow in a transmission line. In this section, a PI controller will be designed for the control of real power flow in a transmission line (P_{line}).

The analysis carried out by Padiyar *et al* [23] and Papic *et al* [27] neglect the operation of shunt inverter and DC link capacitor dynamics while designing controllers for the series inverter. In this section, the design process for the series inverter controller takes into consideration the shunt inverter controllers and the DC link capacitor dynamics. The shunt inverter controls the shunt inverter reactive power (Q_{sh}) and the DC link capacitor voltage (V_{dc}). The series inverter controls the transmission line real power flow (P_{line}). The design of the PI controller for the series inverter is done by eigen value analysis. To design the PI controller for the series inverter, consider the power system as shown in Fig.8.5.

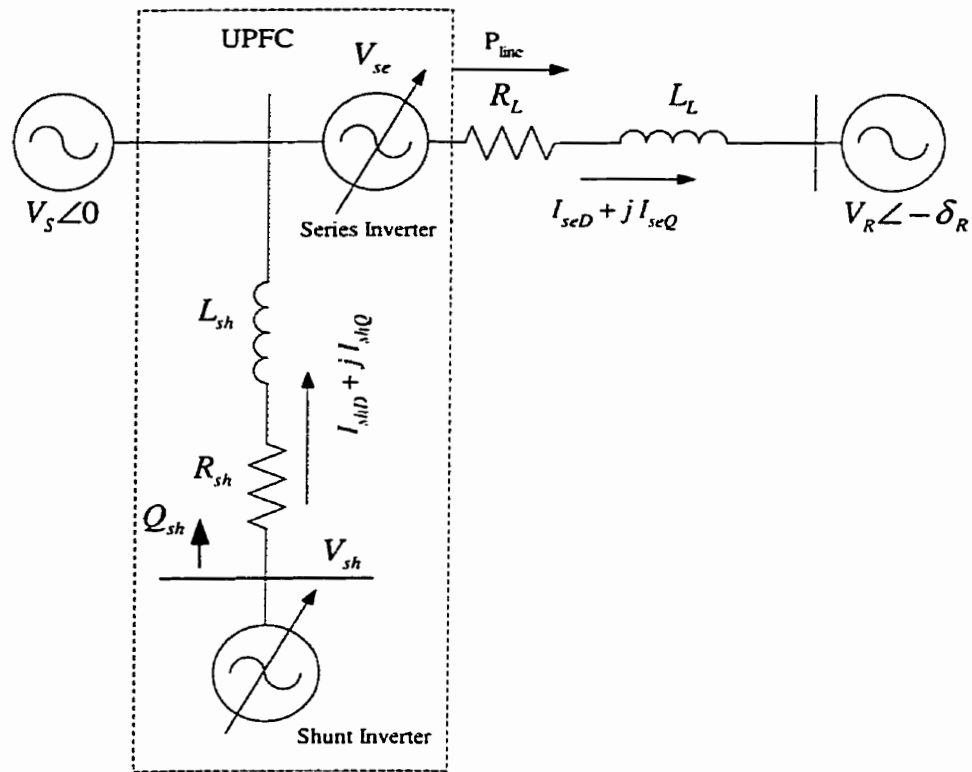


Fig. 8.5 Power system for designing series inverter controller.

The power system consists of two voltage sources V_S and V_R and connected through a transmission line. The line resistance is represented by R_L and line inductance by L_L . The shunt inverter modeled as a voltage source V_{sh} is connected to the transmission line by a resistance R_{sh} and an inductance L_{sh} representing the shunt transformer resistance and inductance. The series inverter is modeled as a series voltage source and is represented as V_{se} .

The power system shown in Fig.8.5 can be represented by two sets of equations. One set for the shunt inverter and the other for the series inverter. The equations for the shunt inverter in D-Q axis representation are

$$\begin{aligned}
\frac{dI_{shD}}{dt} &= -\frac{R_{sh}\omega_0 I_{shD}}{L_{sh}} + \omega\omega_0 I_{shQ} + \frac{\omega_0}{L_{sh}}(V_{shD} - V) \\
\frac{dI_{shQ}}{dt} &= -\frac{R_{sh}\omega_0 I_{shQ}}{L_{sh}} - \omega\omega_0 I_{shD} + \frac{\omega_0}{L_{sh}}(V_{shQ}) \\
\frac{dV_{dc}}{dt} &= -\omega_0 C \cdot \left[\frac{3}{2} \left(\frac{V_{shD}I_{shD} + V_{shQ}I_{shQ} + V_{seD}I_{seD} + V_{seQ}I_{seQ}}{V_{dc}} \right) + \frac{V_{dc}}{R_{cup}} \right] \quad (8.5)
\end{aligned}$$

where $\omega = 1.0$ and $\omega_0 = 377.0$ rads/s.

To achieve de-coupling of the D-Q axis currents, the control variable V_{shD} and V_{shQ} in equation 8.5 are modified as given in chapter 7 equation 7.3 and reproduced here as equation 8.6.

$$\begin{aligned}
V_{shD} &= V + \frac{L_{sh}}{\omega_0}(u_1 - \omega\omega_0 I_{shQ}) \\
V_{shQ} &= \frac{L_{sh}}{\omega_0}(u_2 + \omega\omega_0 I_{shD}) \quad (8.6)
\end{aligned}$$

where u_1 and u_2 are auxiliary control variables. Combining equation 8.5 and 8.6 together we get equation 8.7.

$$\begin{aligned}
\frac{dI_{shD}}{dt} &= -\frac{R_{sh}\omega_0}{L_{sh}} I_{shD} + u_1 \\
\frac{dI_{shQ}}{dt} &= -\frac{R_{sh}\omega_0}{L_{sh}} I_{shQ} + u_2 \\
\frac{dV_{dc}}{dt} &= -\frac{3\omega_0 C}{2} \cdot \frac{[u_1 I_{shD} (\frac{L_{sh}}{\omega_0}) + |V_s| I_{shD} + u_2 I_{shQ} (\frac{L_{sh}}{\omega_0}) + V_{seQ} I_{seQ} + V_{seD} I_{seD}]}{V_{dc}} - \omega_0 C \cdot \frac{V_{dc}}{R_{cup}} \quad (8.7)
\end{aligned}$$

The equations for the series inverter are as given in equation 8.8.

$$\begin{aligned}\frac{dI_{seD}}{dt} &= -\frac{R_L \omega_0 I_{seD}}{L_L} + \omega \omega_0 I_{seQ} + \frac{\omega_0}{L_L} (V_S + V_{seD} - V_{RD}) \\ \frac{dI_{seQ}}{dt} &= -\frac{R_L \omega_0 I_{seQ}}{L_L} - \omega \omega_0 I_{seD} + \frac{\omega_0}{L_L} (V_{seQ} - V_{RQ})\end{aligned}\quad (8.8)$$

Linearizing equations 8.7 and 8.8 we get equation 8.9.

$$\begin{aligned}\frac{d\Delta I_{shD}}{dt} &= -\frac{R_{sh} \omega_0}{L_{sh}} \Delta I_{shD} + \Delta u_1 \\ \frac{d\Delta I_{shQ}}{dt} &= -\frac{R_{sh} \omega_0}{L_{sh}} \Delta I_{shQ} + \Delta u_2 \\ \frac{d\Delta V_{dc}}{dt} &= -\frac{3\omega_0 C}{2} \left[\frac{\left\{ V_{dc0} \{ [a_1 u_{10} \Delta I_{shD} + a_1 I_{shD0} \Delta u_1] + |V_S| \Delta I_{shD} + [a_1 u_{20} \Delta I_{shQ} + a_1 I_{shQ0} \Delta u_2] + \right. \right. \\ &\quad \left. \left. V_{seD0} \Delta I_{seD} + I_{seD0} \Delta V_{seD} + V_{seQ0} \Delta I_{seQ} + I_{seQ0} \Delta V_{seQ} \right\} - \right. \\ &\quad \left. \left. \{ u_{10} I_{shD0} a_1 + |V_S| I_{shD0} + u_{20} a_1 I_{shQ0} + V_{seD0} I_{seD0} + V_{seQ0} I_{seQ0} \} \Delta V_{dc} \right]}{V_{dc0}^2} \right] \\ &\quad - \omega_0 C \cdot \frac{\Delta V_{dc}}{R_{cap}} \\ \frac{d\Delta I_{seD}}{dt} &= -\frac{R_L \omega_0}{L_L} \Delta I_{seD} + \Delta I_{seQ} \omega_0 \omega + \omega_0 \frac{\Delta V_{seD}}{L_L} \\ \frac{d\Delta I_{seQ}}{dt} &= -\frac{R_L \omega_0}{L_L} \Delta I_{seQ} - \Delta I_{seD} \omega_0 \omega + \omega_0 \frac{\Delta V_{seQ}}{L_L}\end{aligned}\quad (8.9)$$

where $a_1 = \frac{L_{sh}}{\omega_0}$.

Equation 8.9 can be put in the standard input-output format as given in equation 8.10.

$$\dot{X} = AX + BU \quad (8.10)$$

Where

$$\begin{aligned} X &= [\Delta I_{shD}, \Delta I_{shQ}, \Delta V_{dc}, \Delta I_{seD}, \Delta I_{seQ}] \\ U &= [\Delta I_{shDref}, \Delta I_{shQref}, \Delta V_{seQ}] \\ \Delta V_{sed} &= 0.0 \quad V_{sed0} = 0.0 \end{aligned}$$

The output variables are

$$Y = [\Delta I_{shD}, \Delta I_{shQ}, \Delta P_{line}]$$

The expression for the real power flow in the transmission line is given by equation 8.11

$$P_{line} = (|V_S| + V_{seD})I_{seD} + V_{seQ}I_{seQ} \quad (8.11)$$

Linearizing equation 8.11, we get equation 8.12

$$\Delta P_{line} = (|V_S| + V_{seD0})\Delta I_{seD} + I_{seD0}\Delta V_{seD} + V_{seQ0}\Delta I_{seQ} + I_{seQ0}\Delta V_{seQ} \quad (8.12)$$

The output matrix Y can be put in the following form

$$Y = CX + DU \quad (8.13)$$

The PI controller for the series inverter that controls the real power flow in the transmission line is as shown in Fig.8.6.

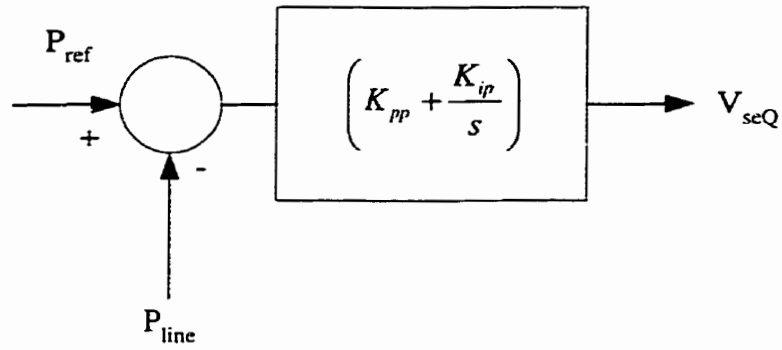


Fig.8.6 Series inverter real power flow controller.

Including the shunt inner loop PI controllers (refer chapter-7 Fig.7.7) and the series real power flow PI controller, the state equation is modified as given in equation 8.14.

$$\dot{X}_1 = A_1 X_1 + B_1 U_1 \quad (8.14)$$

Where

$$X_1 = \left[\Delta I_{shD}, \Delta I_{shQ}, \Delta V_{dc}, \Delta I_{seD}, \Delta I_{seQ}, \Delta x_{c1}, \Delta x_{c2}, \Delta x_{c3} \right]$$

x_{c1} and x_{c2} are the state variables associated with the D-Q axis PI current controllers. x_{c3} is the state variable associated with the series inverter PI controller. The state matrix is as given below.

$$A_1 = \begin{bmatrix} A - BK_{pr}C & -BK_{it} \\ MC & -DK_{it} \end{bmatrix}$$

$$B_1 = \begin{bmatrix} BK_{pr} \\ -M \end{bmatrix}$$

$$K_p = \begin{bmatrix} 5.0 & 0.0 & 0.0 \\ 0.0 & 0.2 & 0.0 \\ 0.0 & 0.0 & 0.2 \end{bmatrix} \quad K_i = \begin{bmatrix} 21.367 & 0 & 0.0 \\ 0 & 5.0 & 0.0 \\ 0.0 & 0.0 & 40.0 \end{bmatrix}$$

$$K_{pr} = [I + K_p D]^{-1} K_p$$

$$K_{it} = [I + K_p D]^{-1} K_i$$

$$M = [I + DK_p]^{-1}$$

The PI gains of the D and Q axis shunt inner loop current controllers are $K_{p1} = 5.0$, $K_{i1} = 21.367$ and $K_{p2} = 0.2$ and $K_{i2} = 5.0$ respectively. The gains of the series real power flow PI controller have been selected as $K_{pp} = 0.2$ and $K_{ip} = 40.0$ to provide for fast tracking to step changes in transmission line real power reference. To check the stability of system with the above PI control gains, it is necessary to evaluate the matrix A_1 which is a function of the operating condition. PSCAD-EMTDC simulations have been conducted to find the operating conditions. A voltage base of 345 kV and a power base of 160 MVA has been chosen to obtain the operating conditions in per unit. They are as given below.

$$\begin{aligned}
R_{sh} &= 0.0014 \\
L_{sh} &= 0.2 \\
C &= 0.0324 \\
I_{shD0} &= -0.11 \\
I_{shQ0} &= 0.1875 \\
u_{10} &= -0.02 \\
u_{20} &= 0.044 \\
\omega_0 &= 377 \\
V_{dc0} &= 2.22 \\
V_{seQ0} &= 0.144 \\
I_{seQ0} &= 0.198 \\
I_{seD0} &= 2.5 \\
R_L &= 0.01 \\
L_L &= 0.15
\end{aligned}$$

Incorporating the values for the variables given above with the PI controller gains in matrix A_I , the eigen values obtained are as given below

$$\begin{aligned}
&-0.3 \\
&-3.86 \pm j2.54 \\
&-1.46 \pm j1.69 \\
&-8.09 \pm j583.97 \\
&-112.08
\end{aligned}$$

Introducing the outer DC link voltage PI controller with gains of $K_{p3} = -1.0$ and $K_{i3} = -2.0$ and forming the state matrix, the eigen values are

$-1.18 \pm j6.48$
 $-2.83 \pm j0.32$
 $-1.46 \pm j1.69$
 $-8.09 \pm j583.97$
 -112.08

As evident from the list of eigen values, the PI controller values used for the shunt and series inverters provide for stable operation as all the eigen values have negative real parts. But it is clear from the eigen value ($-8.09 \pm j 583.97$) that the response will be oscillatory to step changes in real power reference inputs as the damping factor associated with it is 0.013. This is one problem of using a high gain PI controller. A fuzzy controller has been designed to overcome the problem of low damping associated with high gain PI controller and is described in chapter 9.

8.5 Summary

This chapter has provided the background for the construction, operation and control of a series inverter of a UPFC using PSCAD-EMTDC software. The series inverter has been split into two pairs of inverters. One for generating a voltage in quadrature (V_{seQ}) and the other for generating a voltage in-phase (V_{seD}) with the UPFC bus voltage ($V_{upfcbus}$). This allows for independent control of the quadrature (V_{seQ}) and in-phase (V_{seD}) injected component of the series voltage.

The ratings of the series inverter and series transformer have been calculated based on the SIL ratings of a 345 kV transmission line.

The DC capacitor which forms a common link between the series and the shunt inverter has been designed based on the maximum allowable voltage drop across it during transient operation of the UPFC.

Eigen value analysis have shown that use of high gain PI controller for the series inverter of a UPFC to control the real power flow in a transmission line (P_{line}) provides low damping. The analysis takes into consideration the shunt inverter operation, DC link capacitor dynamics and the transmission line dynamics. A fuzzy controller has been designed to overcome the problem of low damping associated with high gain PI controller and is described in chapter 9.

Chapter 9

Performance of UPFC control system

9.0 Introduction

Reliable operation of a UPFC involves coordinated operation of the shunt and series inverter control systems. This chapter focuses on the combined operation of the shunt and series inverter control system to control the real power flow in the transmission line (P_{line}), UPFC bus voltage ($V_{upfcbus}$) and the DC link capacitor voltage (V_{dc}) simultaneously.

Since UPFC is a multi-variable controller, simultaneous operation of the shunt and series inverter control system requires that they do not interact with each other in a destructive manner leading to instability. In order to provide for proper operation between the shunt and series inverter control system, a coordination controller has been designed. The performance of combined operation of the shunt, series and coordination controller will be studied in this chapter using the PSCAD-EMTDC software.

Combined operation of the UPFC control system requires that the controllers provide stable operation. Eigen value analysis conducted in chapter 8 has shown that the use of high gain PI controller for the series inverter for controlling the real power flow in a transmission line (P_{line}) by injecting a quadrature voltage (V_{seQ}) leads to low damping. A solution to the problem of low damping experienced when high gain PI controllers are used for series inverter of a UPFC to control the transmission line real power flow (P_{line}) has been proposed.

The in-phase component of the series inverter injected voltage has significant effect on transmission line reactive power flow and shunt inverter reactive power. The effect of in-phase component (V_{seD}) injection by the series inverter of a UPFC on transmission line reactive power flow (Q_{line}) and shunt inverter reactive power (Q_{sh}) has also been discussed. Further, the mechanism by which the shunt inverter reacts to changes in in-phase component has also been discussed.

9.1 Shunt inverter control system with coordination controller

To understand the design of a coordination controller for a UPFC, consider a UPFC connected to a transmission line as shown in Fig.9.1.

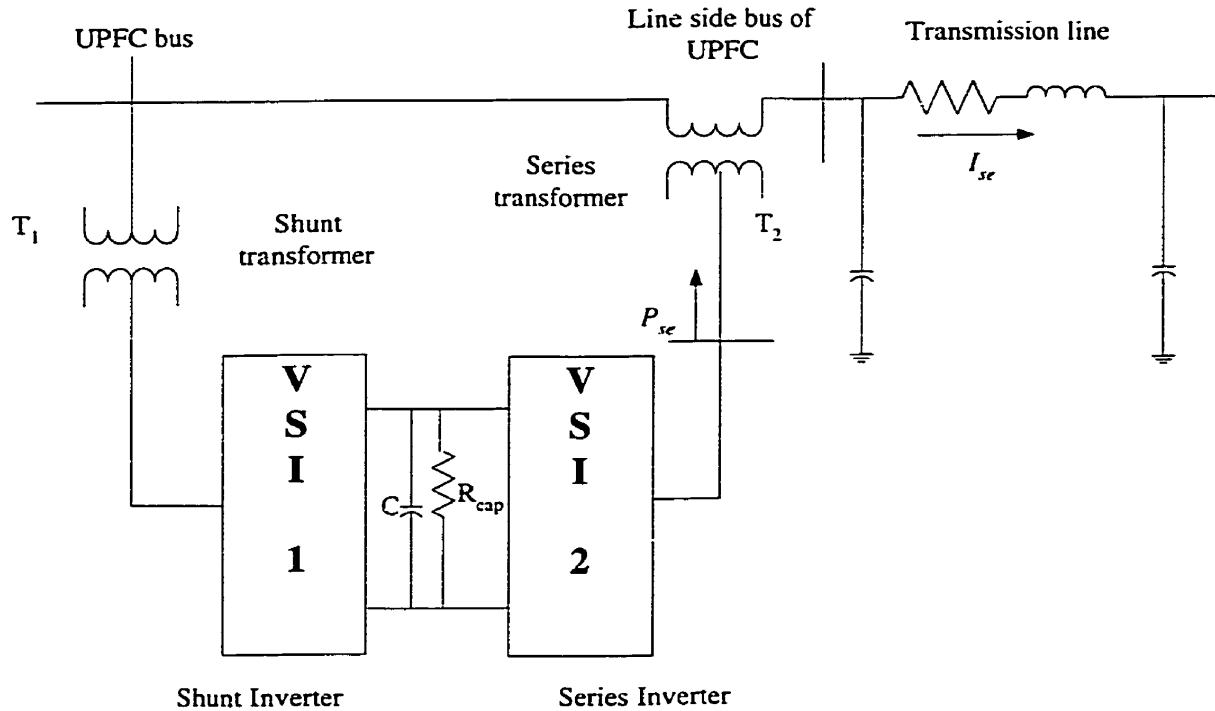


Fig.9.1 UPFC connected to a transmission line.

The series inverter of the UPFC injects a voltage in series with the transmission line thereby changing the power flow in it. The interaction between the series injected voltage and the transmission line current leads to exchange of real power between the series inverter and the transmission line. The real power demand of the series inverter (P_{se}) causes the DC link capacitor voltage (V_{dc}) to either increase or decrease depending on the direction of the real power flow from the series inverter. This decrease/increase in DC link capacitor voltage (V_{dc}) is sensed by the shunt inverter controller that controls the DC link capacitor voltage (V_{dc}) and acts to increase/decrease the shunt inverter real power flow to bring the DC link capacitor voltage (V_{dc}) back to its scheduled value. Stating it in another way, the real power demand of the series inverter is recognized by

the shunt inverter controller only by the decrease/increase of the DC link capacitor voltage (V_{dc}). Thus the shunt and the series inverter operation are in a way separated from each other. To provide for proper coordination between the shunt and the series inverter control system, a feedback from the series inverter is fed to the shunt inverter control system. This helps in faster response of the shunt inverter control system to real power demand of the series inverter. The feedback signal used is the real power demand of the series inverter (P_{se}).

References [10,11,13,14,16-18,23-26,30,42] have neglected the design of a coordination controller in the over all operation of a UPFC. In [19], Padiyar *et. al* have modeled the real power exchanged by the series inverter and the transmission line as an equivalent current flowing through the shunt inverter. Simulation results have neglected the effect of DC link capacitor dynamics under this method of modeling [19]. In [27], Papic *et. al* have modeled the feedback of the real power exchanged by the series inverter and transmission line as an additional real power that is to be absorbed/generated by the shunt inverter. The real power demand by the series inverter (P_{se}) is converted to an equivalent D - axis current reference for the shunt inverter. The D-axis current reference is fed through a predictive loop that includes additional PI controllers and thus reduces the effectiveness of the coordination controller.

An effective coordination controller for UPFC has been designed to coordinate the operation of the series and the shunt inverter and provide fast supply of the series inverter real power demand (P_{se}). In the coordination controller designed, the real power demand of the series inverter (P_{se}) is converted into an equivalent D-axis current for the shunt inverter (i_{Dse}). By doing so, the shunt inverter would immediately respond to such

a change in its D-axis current and provide the necessary real power to the series inverter. The equivalent D-axis current is an additional input to the D-axis shunt inverter control system as shown in Fig.9.2. Equation 9.1 shows the relationship between the series inverter real power demand (P_{se}) and the shunt inverter D-axis current (i_{Dse}).

$$i_{Dse} = \frac{P_{se}}{|V_{upfcbus}|} \quad (9.1)$$

In equation 9.1, P_{se} represents the real power demand of the series inverter. The real power demand of the series inverter P_{se} is the real part of product of the series inverter injected voltage V_{se} and the transmission line current I_{se} . $V_{upfcbus}$, i_{Dse} represent the voltage of the bus to which the shunt inverter is connected and the equivalent additional D-axis current that should flow through the shunt inverter to supply the real power demand of the series inverter. Fig.9.2 shows the UPFC shunt inverter control system including the coordination feedback between the series and the shunt inverters. In this case, the series inverter real power demand (P_{se}) is fed to the inner control system (Fig.9.2) thus increasing the effectiveness of the coordination controller. Further, the inner control system loop are fast acting PI controllers and ensures the fast supply of the series inverter real power demand (P_{se}) by the shunt inverter. The effectiveness of the coordination controller will be discussed in section 9.4.

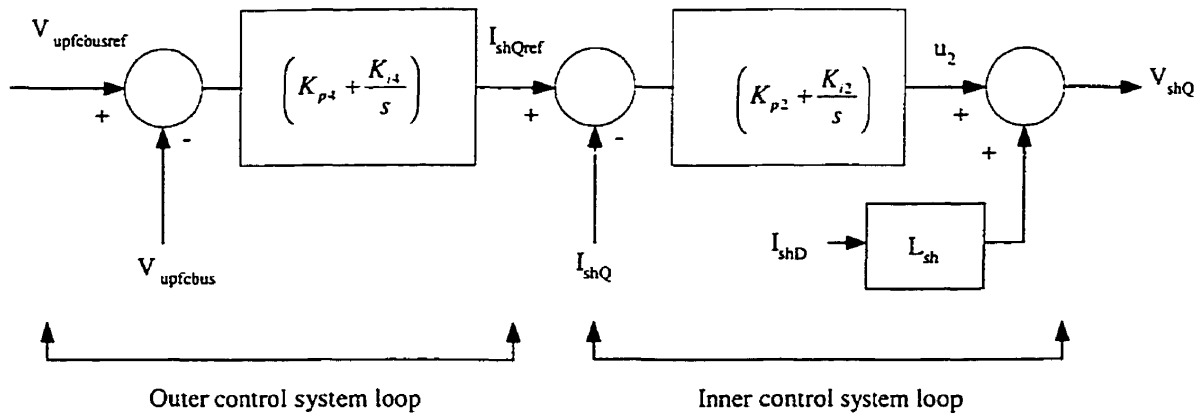
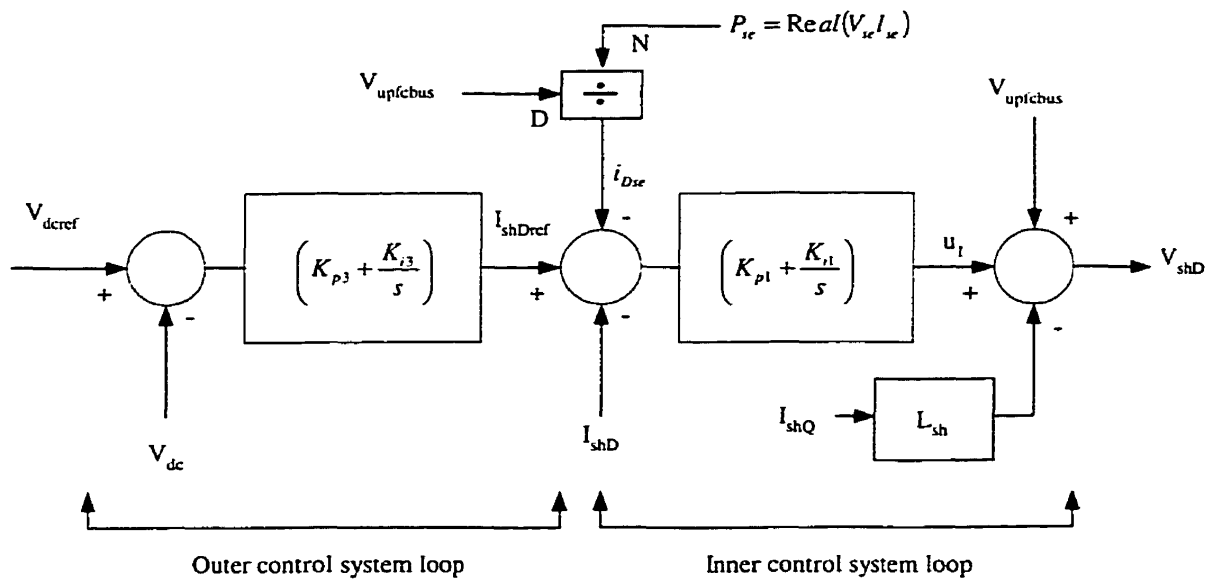


Fig.9.2 UPFC shunt inverter control system with coordination controller.

9.2 Performance of UPFC control system with series inverter controlling the real power flow in a transmission line with a PI controller

9.2.1 Power system description: A two machine power system with a UPFC located at the center of a 200 km 345 kV transmission line, shown in Fig.9.3, has been considered to study the performance of the UPFC to step input changes in real power reference. The power system along with the UPFC was constructed using the PSCAD-EMTDC software. The two machines have been modeled as constant voltage sources. The shunt inverter controls the UPFC bus voltage ($V_{upfcbus}$) at 1.0 p.u and the DC link capacitor voltage (V_{dc}) at 60 kV. The series inverter of the UPFC controls the real power flow in the transmission line (P_{line}) by injecting a voltage of adjustable magnitude in quadrature (V_{seQ}) with the UPFC bus voltage ($V_{upfcbus}$). The coordination controller has been included while studying the performance of the UPFC control system to step input changes. The initial power flow in the transmission line is 450 MW. The sending end voltage (V_S) is fixed at 1.03 p.u and the receiving end voltage (V_R) is fixed at 0.925 p.u. The phase angle difference between the two machines is 20 degrees.

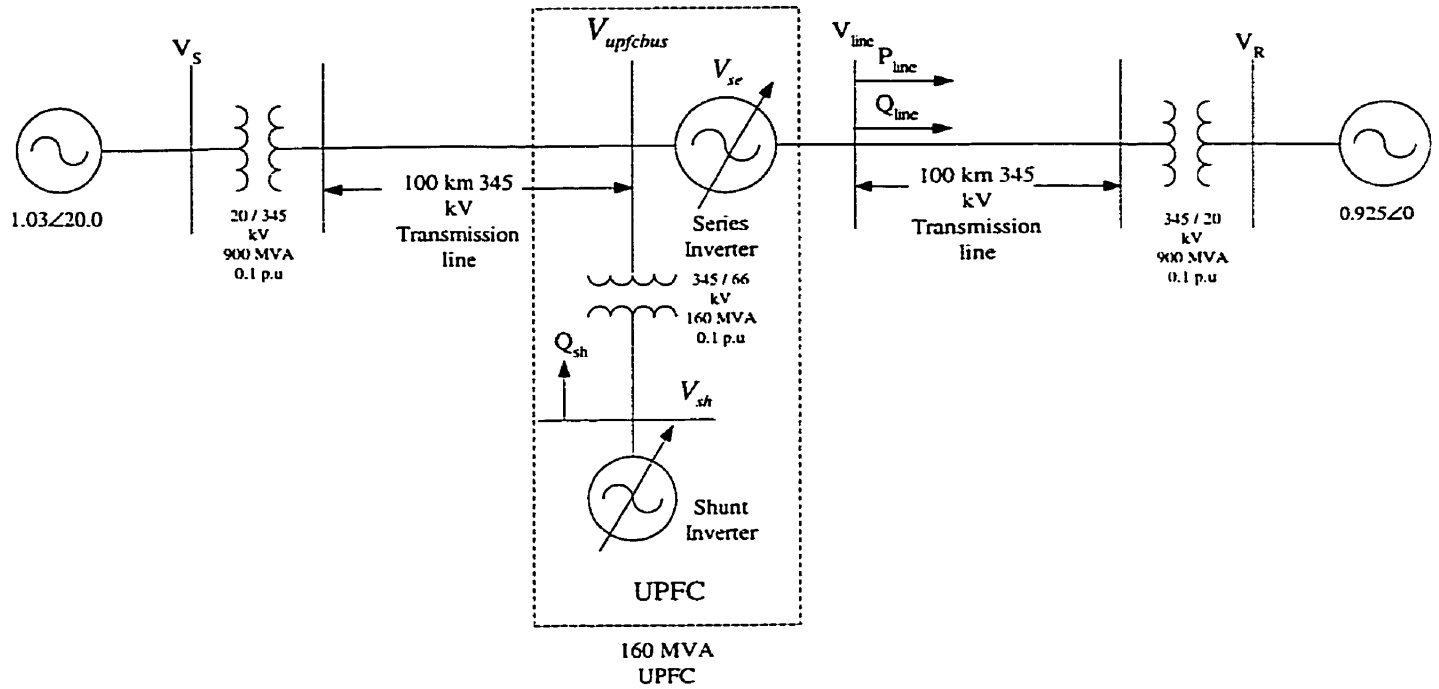


Fig.9.3 Two machine power system with UPFC.

The shunt inverter of the UPFC is a 4-module VSC connected to the 345 kV transmission line through a 160 MVA 66/345 kV transformer. The details of the 4-module VSC are given in section 7.2.2. The operation of the 4-module VSC is explained in section 7.2.3. The shunt inverter is operated using the de-coupled control system. The design of the de-coupled control system is given in section 7.3.2. In the design of the de-coupled control system carried out in chapter 7, the Q-axis outer control system loop denoted by the PI controller (K_{pd} , K_{id}) had not been designed. This is because the de-coupled control system design was carried out on a 4-module inverter connected to a constant voltage source. The Q-axis outer control system loop has been included here while conducting performance studies on a UPFC. The PI controller gains

for the Q-axis outer control system loop has been chosen to be $K_{p\omega} = -1.0$ and $K_{i\omega} = -133.0$ to provide fast tracking of the UPFC bus voltage reference ($V_{upfcbusref}$).

The construction and operation of a series inverter in PSCAD-EMTDC has been explained in section 8.2. The series inverter of the UPFC controls the real power flow in the transmission line (P_{line}) by injecting a voltage in quadrature (V_{seQ}) with the UPFC bus voltage ($V_{upfcbus}$). The in-phase component (V_{seD}) of the series injected voltage has been neglected to study the effect of PI controlled series inverter on real power flow control. The effect of in-phase component (V_{seD}) of the series injected voltage will be discussed in section 9.5.

9.2.2 Step input response: The analysis carried out in section 8.4 has shown that high gain PI controller for series inverter provides low damping to real power flow oscillations. The analysis neglects the effect of coordination controller on the damping of transmission line real power flow oscillations. In this section, the combined effect of all the controllers, namely, the shunt inverter controller, coordination controller and series inverter controller on the low damping in transmission line real power oscillations will be studied. The power system shown in Fig.9.3 has been considered for this study.

The PI controller block for the series inverter shown in chapter 8 Fig.8.6 has been shown here as Fig.9.4 for convenience. The PI controller gains for the series inverter are $K_{pp}=0.2$ and $K_{ip} = 40.0$.

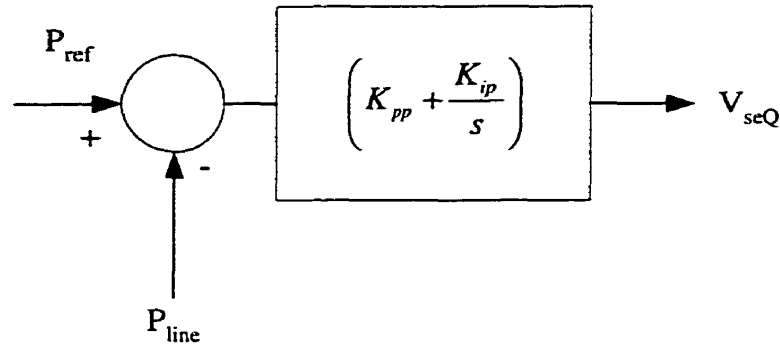


Fig.9.4 Series inverter real power flow controller (PI).

Plot-1 through plot-5 of Fig.9.5 shows the response of the power system to step changes in real power reference (P_{ref}) with high gain PI controllers for the series inverter. Step change in real power flow reference (P_{ref}) has been conducted at 10 s and 12 s. At 10 s, the real power flow reference (P_{ref}) was changed from 450 MW to 290 MW. Plot-1 shows the transmission line real power flow (P_{line}). It is observed from Plot-2 of Fig.9.5 that the transmission line real power flow (P_{line}) oscillates around 290 MW with low damping and finally reaches steady state after 11 s. At 12 s, the real power flow reference was changed from 290 MW to 450 MW. The enlarged version of Plot-1 of Fig.9.5 at around 12 s is shown in Plot-3. The real power flow in the transmission line (P_{line}) oscillates around 450 MW with low damping and reaches a steady state at around 13 s. Plot-4 of Fig.9.5 shows the UPFC bus voltage ($V_{upfcbus}$) profile. The shunt inverter controls the UPFC bus voltage ($V_{upfcbus}$) at 1.0 p.u. At 10 s and 12 s, the step change in real power reference (P_{ref}) has shown very little change in the UPFC bus voltage ($V_{upfcbus}$) as shunt inverter of the UPFC has very effectively controlled it by varying its reactive power output. Plot-5 of Fig.9.5 shows the DC link capacitor voltage (V_{dc})

variations due to step change in real power reference. The spikes seen in the DC link capacitor voltage (V_{dc}) plot at 10 s and 12 s is due to sudden change in the series inverter real power demand (P_{se}) due to the interaction between the series inverter injected voltage (V_{se}) and the transmission line current (I_{se}). The real power demand of the series inverter (P_{se}) is quickly conveyed to the shunt inverter control system through the coordination controller. The DC link capacitor voltage is rapidly regulated to 60 kV by the shunt inverter.

This simulation has validated the eigen analysis conducted in chapter 8 section 8.4 where it was shown that the use of high gain PI controller leads to low damping of the network mode. Linear supplementary controllers have been proposed to overcome the problem of low damping of the network mode [23]. But the response of the system may deteriorate at other operating conditions even with linear supplementary controllers.

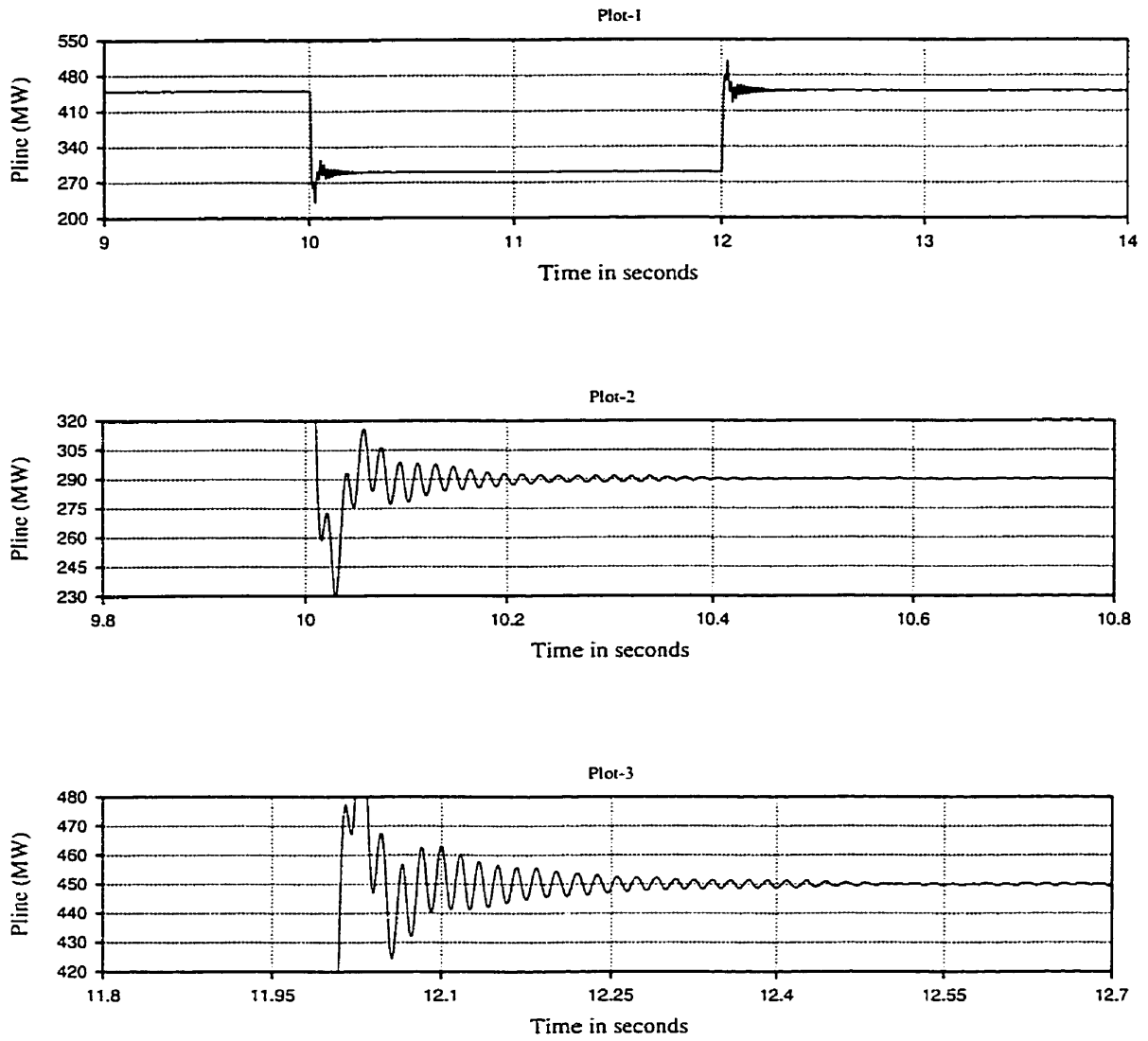


Fig.9.5 Response of the power system to step changes in real power reference of the UPFC (PI controller for series inverter) (contd.).

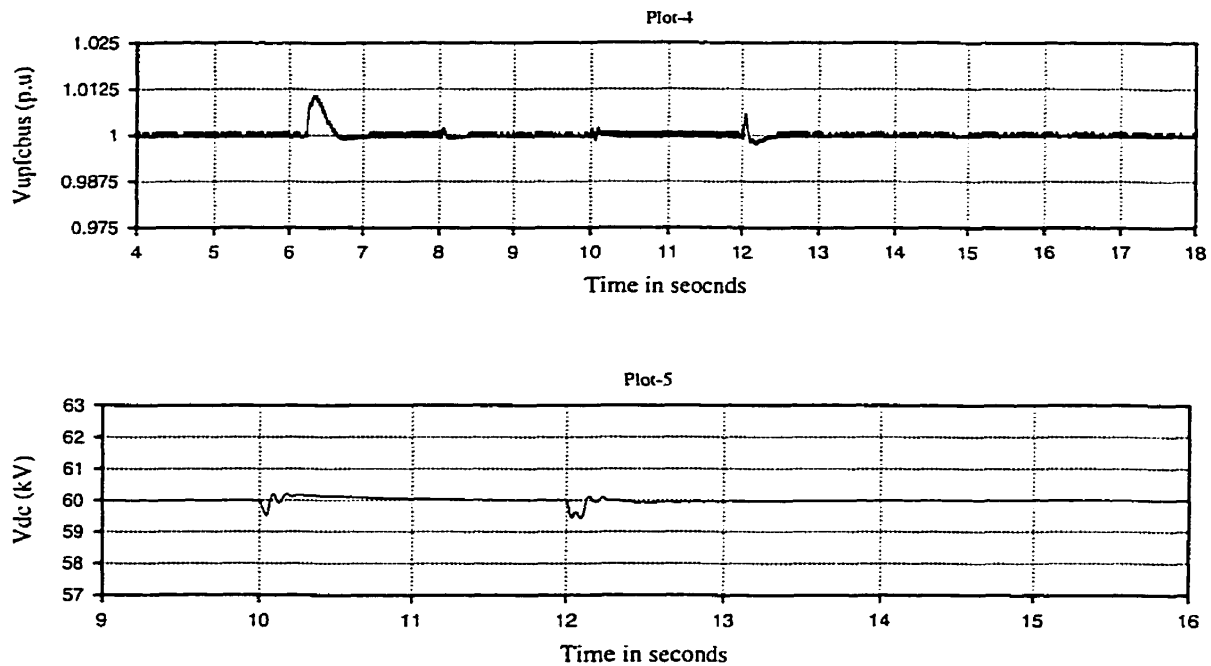


Fig.9.5 Response of the power system to step changes in real power reference of the UPFC (PI controller for series inverter).

9.3 Fuzzy Logic Controller Design in PSCAD-EMTDC Software

Knowledge based controllers (fuzzy logic controllers) for UPFC have been investigated for the control of real power flow in a transmission line to overcome the problem of low damping experienced by high gain PI controllers. The necessary background for the design of a fuzzy controller for the series inverter of a UPFC for controlling the real power flow in a transmission line (P_{line}) are given in chapters 4, 5 and 6. The fuzzy logic knowledge base designed in chapter 6 has been used for the control of real power flow in a transmission line (P_{line}).

The knowledge base for the fuzzy logic controller presented in chapter 6 has been implemented in PSCAD-EMTDC software. The software block developed in PSCAD-EMTDC software has two inputs and one output. The two inputs to the fuzzy logic software block are the error and the change of error in real power flow in the transmission line (P_{line}). The output of the fuzzy controller is the change in series quadrature injected voltage (ΔV_{seQ}). Fig.9.6 shows the fuzzy logic controller implementation in PSCAD-EMTDC software. Triangular membership functions have been used for both the error and the change of error inputs. The universe of discourse for the error was chosen to be ± 0.2 . The centroid of the fuzzy sets for error in real power flow are 0.2 (PB), 0.1 (PM), 0.03 (PS), 0.0 (ZE), -0.03 (NS), -0.1 (NM), -0.2 (NB). The universe of discourse for the change in error in real power flow was chosen to be ± 0.02 . The centroid of the fuzzy sets for change of error in real power flow are 0.02 (PB), 0.01 (PM), 0.003 (PS), 0.0 (ZE), -0.003 (NS), -0.01 (NM), -0.02 (NB). The universe of discourse for the error and change of error in real power are the same as that used in chapter 6. The universe of discourse for the change in series quadrature injected voltage is ± 0.1 . The centroid for the output fuzzy sets are PB (+0.1), PM (+0.066), PS (+0.033), ZE (0), NS (-0.033), NM (-0.066) and NB (-0.1).

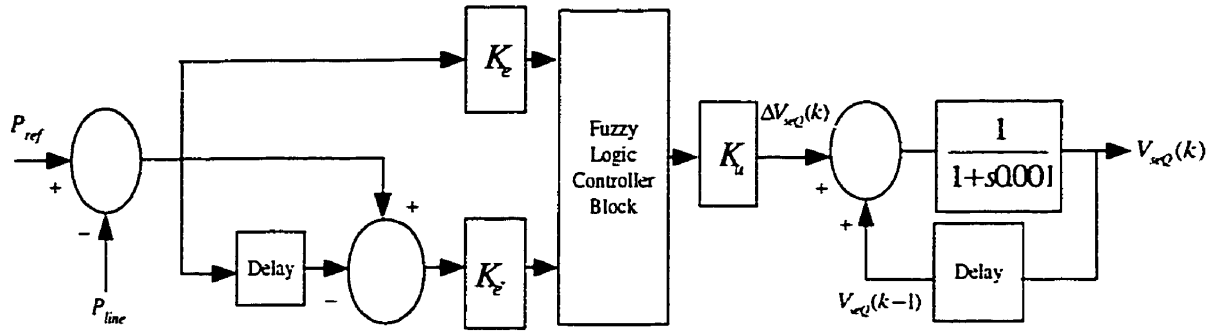


Fig.9.6 Fuzzy logic controller implementation in PSCAD-EMTDC software.

The error between the reference and the actual value is fed to one of the inputs of the fuzzy logic controller block through a gain block (K_e). The gain block (K_e) represents the input gain that can be tuned and is a flexible parameter. To obtain the change of error signal the following methodology has been implemented. The error is simultaneously fed to a delay block (Delay). The delay block shifts the error signal by a delay period as specified in the delay block. The delay that has been used is 0.01 s. The change of error signal is the difference between the present value of the signal and the value of the signal 0.01s earlier. The value of 10 ms is reasonable for a digital computer to acquire signal and process it. Thus a very conservative value of 10 ms has been chosen for the delay time. The present value of the error and the delayed error signal are subtracted to obtain the change in error signal. The change of error signal is fed to the second input of the fuzzy logic controller block through a gain block (K_e'). The gain (K_e') for the change of error can also be tuned. The output of the fuzzy controller is a crisp value that represents the change in the quadrature injected voltage ($\Delta V_{seQ}(k)$) at the

k^{th} instant. In order to obtain the output at the k^{th} instant, the signal $\Delta V_{seQ(k)}$ has to be integrated with the output at the $(k-1)^{\text{th}}$ instant. To obtain the present value of the output, the signal $\Delta V_{seQ(k)}$ is passed through a first order lag with a small time constant to remove the high frequency components. The output of the first order lag represents the output $V_{seQ(k)}$ at the instant k^{th} instant. The output $V_{seQ(k)}$ is fed back through a delay block of delay 0.01 secs to obtain $V_{seQ(k-1)}$. The signal $V_{seQ(k-1)}$ is added to $V_{seQ(k)}$ to obtain $V_{seQ(k)}$.

9.3.1 Performance of UPFC control system with series inverter controlling the real power flow in a transmission line with a fuzzy controller

9.3.1.1 Step input response with fuzzy controller: The power system with UPFC shown in Fig.9.3 has been considered to study the performance of the UPFC control system to step changes in transmission line real power reference (P_{ref}). The shunt inverter control system, coordination controller and the series inverter controller have been included in this simulation. The PI controller gains for the shunt inverter control system shown in Fig.9.2 are $K_{p1}=5.0$, $K_{i1}=21.367$, $K_{p2}=0.2$, $K_{i2}=5.0$, $K_{p3}=-1.0$, $K_{i3}=-2.0$, $K_{p4}=-1.0$ and $K_{i4}=-133.0$. The input gains for the error (K_e) and the change of error ($K_{e\cdot}$) of the fuzzy controller are 0.25 and 0.025 respectively. The output gain (K_u) has been selected as 0.5. These gains have been selected after obtaining a satisfactory response from a number of simulations.

The initial real power flow in the transmission line (P_{line}) is 450 MW. Step changes to real power flow reference (P_{ref}) have been conducted at 10 s and 12 s. Plot-1 of Fig.9.7 shows the real power flow in the transmission line (P_{line}) with a fuzzy controller. At 10 s, the real power reference (P_{ref}) is changed from 450 MW to 290 MW. Plot-2 of Fig.9.7 shows the transmission line real power flow (P_{line}) around 10 s. The real power flow in the transmission line (P_{line}) tracks the reference change within 100 ms. At 12 s the real power reference is changed from 290 MW to 450 MW. Plot-3 of Fig.9.7 shows the transmission line real power flow (P_{line}) around 12 s. The real power flow in the transmission line (P_{line}) tracks the step change in real power flow reference (P_{ref}) within 100ms.

The shunt inverter controls the DC link capacitor voltage (V_{dc}) and the UPFC bus voltage ($V_{upfcbus}$). Plot-4 and plot-5 of Fig.9.7 shows the UPFC bus voltage ($V_{upfcbus}$) variations and the DC link capacitor voltage (V_{dc}) variations due to step change in real power reference (P_{ref}) respectively. It is observed that the UPFC bus voltage ($V_{upfcbus}$) is controlled at 1.0 p.u by the shunt inverter. Also the DC link capacitor voltage (V_{dc}) has been controlled at 60 kV.

It is readily seen from plots-1 through plot-5 that the problem of low damping experienced by high gain PI controller has been overcome by using a fuzzy controller. This simulation has also validated the knowledge base designed for the fuzzy controller developed in chapter 6.

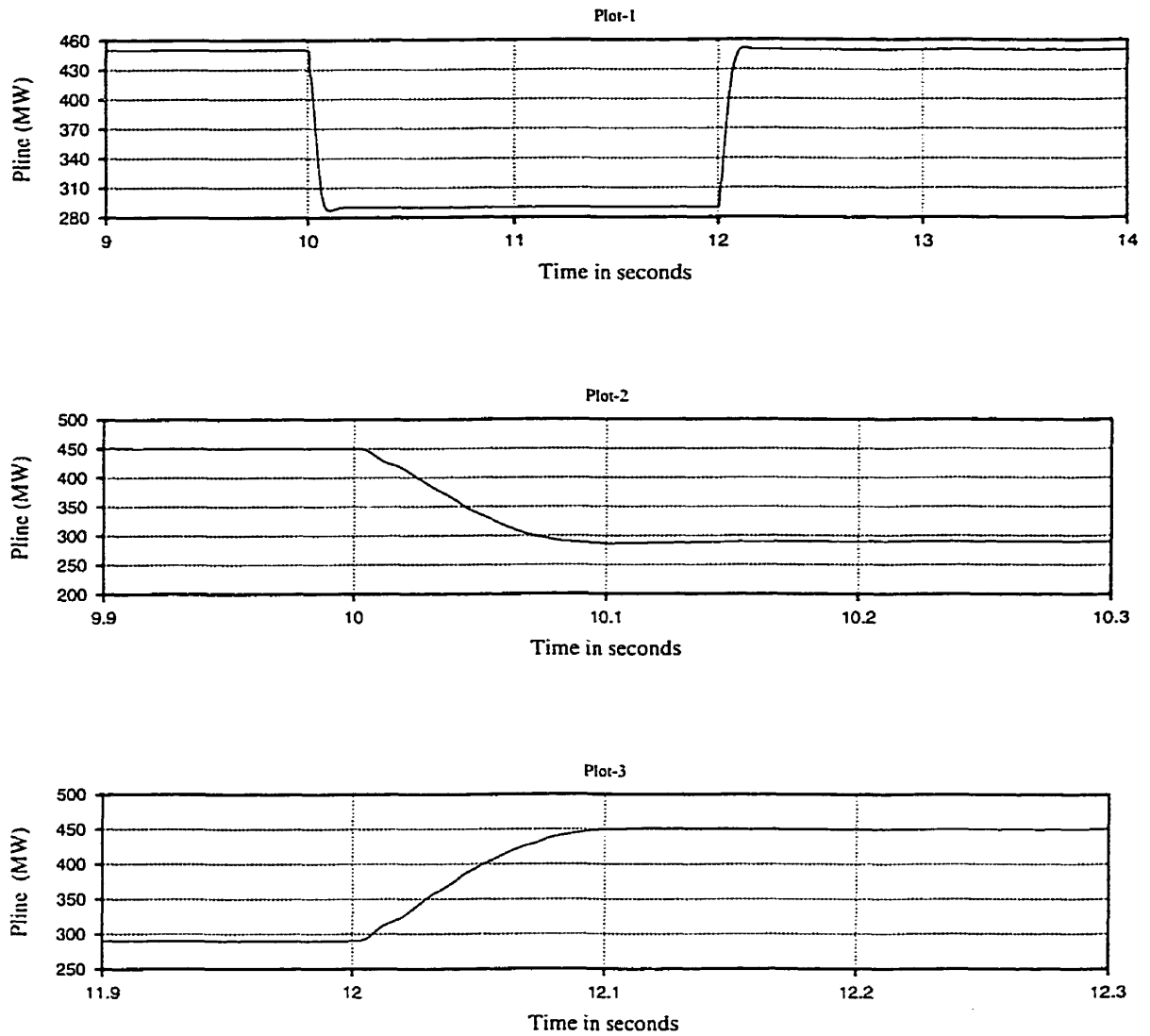


Fig.9.7 Response of the power system to step changes in real power reference of the UPFC (Fuzzy controller for series inverter) (contd.).

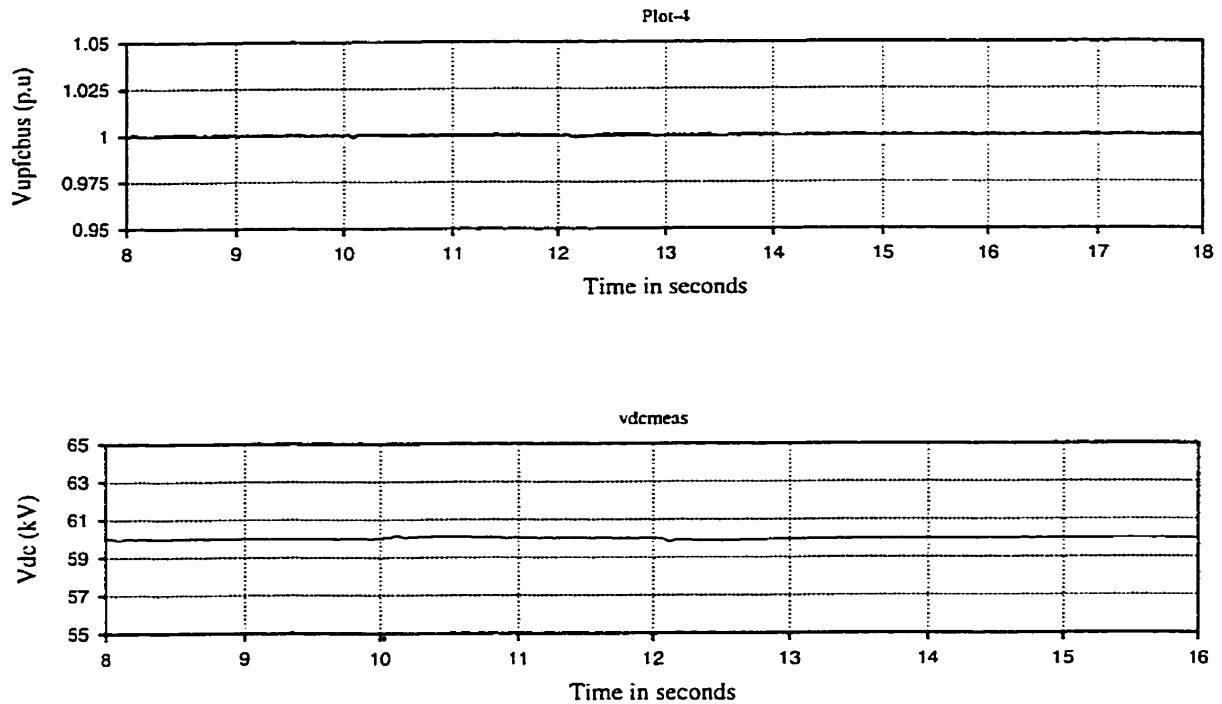


Fig.9.7 Response of the power system to step changes in real power reference of the UPFC (Fuzzy controller for series inverter).

9.3.1.2 Power oscillation damping with fuzzy controller: A two-machine power system has been modeled to study the improvement in power oscillation damping using a UPFC. Fig.9.8 shows a two-machine power system with UPFC. The two-machine (G1 and G2) power system with UPFC shown in Fig.9.8 has been modeled in PSCAD-EMTDC software. The machines are equipped with static exciters and PSS. The generator, exciter, PSS, synchronous motor load and UPFC parameters are given in Appendix-4 [36].

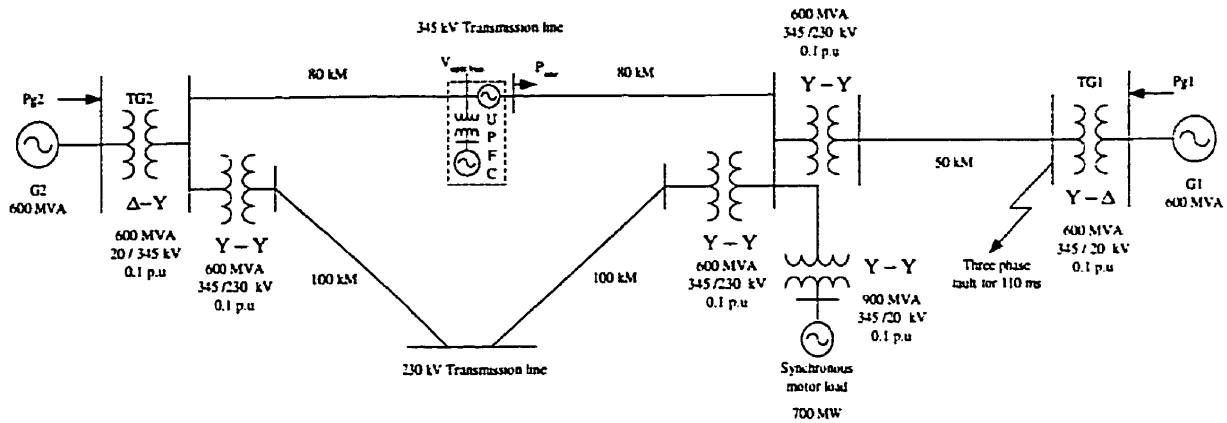


Fig 9.8 Two-machine power system with UPFC.

The total load in the power system is 700 MW. The load has been modeled as a synchronous motor. Generator G2 supplies 500 MW of power and the rest of the power is generated by G1. Generator G1 also supplies the system losses. Generator G2 transmits 500 MW of power through a 345 kV and 230 kV transmission line. The steady state power flow in the 345 kV transmission line is 400 MW. The 230 kV transmission line carries 100 MW of power. The UPFC is located at the center of the 160 km 345 kV transmission line. The shunt inverter and the series inverter of the UPFC are rated at 160 MVA. The shunt inverter of the UPFC controls the DC link capacitor voltage (V_{dc}) and the UPFC bus voltage ($V_{upfcbus}$). The series inverter of the UPFC controls the real power flow in the transmission line (P_{line}) at 400 MW. A three-phase fault is applied at the high voltage bus of generator G1 at 10 s for 110 ms and removed without any change in the network configuration. The response of the system was studied with and without the UPFC. Fig.9.9 shows the response of the system to three-phase fault without UPFC. Plot-1 of Fig.9.9 shows the electrical power (P_{g2})

oscillations of the generator G2 for a three-phase fault for 110 ms applied at the high voltage bus of generator G1. Plot-2 of Fig.9.9 shows the transmission line real power flow (P_{line}) oscillations in the 345 kV line without the UPFC for the three-phase fault. Following the three-phase fault on the high voltage bus of generator G1 for 110 ms, the real power generated by generator G1 drops to zero. The imbalance in generation and load causes generator G2 to vary its electrical power output. The peak of the electrical power of generator G2 (P_{g2}) is about 700 MW. The electrical power oscillations of generator G2 damp out in about 3 s. The peak of the real power flow in the 345 kV line (P_{line}) is about 550 MW. The real power oscillations in the 345 kV line (P_{line}) also damp out within 3 s.

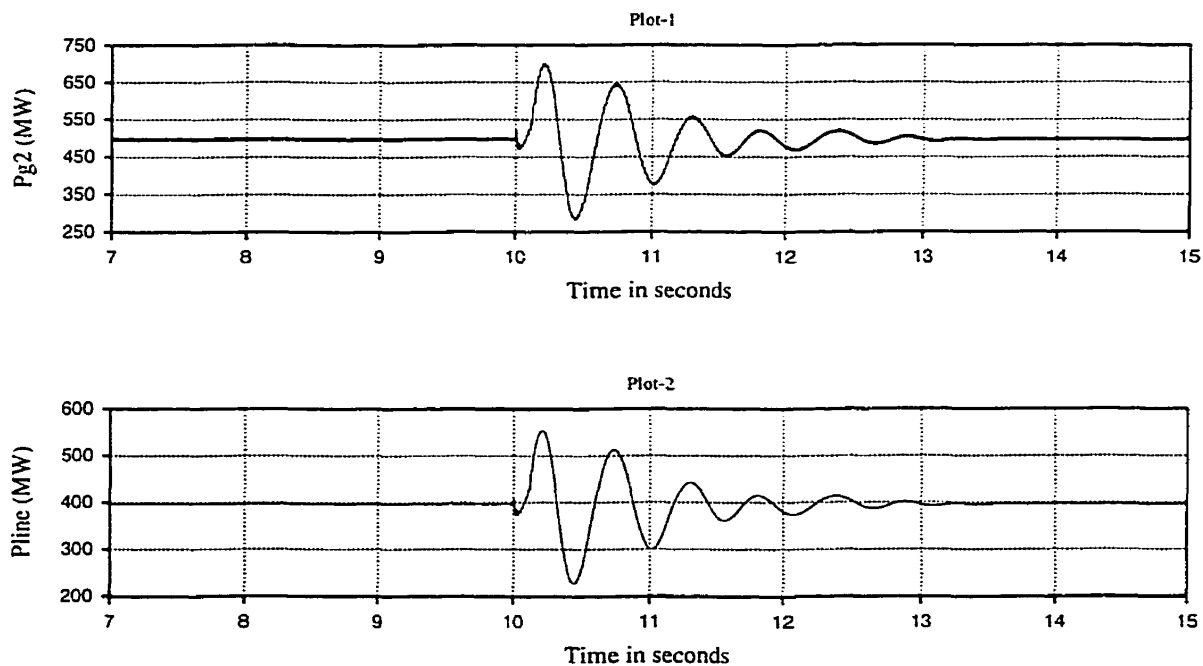


Fig.9.9 Response of the power system to three-phase fault without UPFC.

To study the improvement in the power oscillation damping with UPFC and also to validate its control system design under dynamic conditions, a UPFC was located in the middle of the 345 kV transmission line as shown in Fig.9.8. The real power flow in the 345 kV line (P_{line}) is controlled at 400 MW. The UPFC bus voltage ($V_{upfcbus}$) is regulated at 1.0 p.u. The DC link capacitor voltage (V_{dc}) is controlled at 60 kV. A three-phase fault is conducted at the high voltage side of generator G1 for 110 ms. Fig.9.10 shows the response of the power system to a three-phase fault on the high voltage side of generator bus G1. Plot-1 of Fig.9.10 shows the electrical power output of generator G2 (P_{g2}). Plot-2 of Fig.9.10 shows the real power flow in the 345 kV transmission line (P_{line}).

Comparing plot-1 of Fig.9.9 with plot-1 of Fig.9.10, it is seen that the UPFC has reduced the peak of the electrical power oscillation of generator G2 (P_{g2}). Without the UPFC, the peak of the electrical power (P_{g2}) generated by G2 was about 700 MW. With UPFC, the peak of generator G2 electrical power (P_{g2}) is about 600 MW. This simulation has shown that the UPFC has contributed to the damping of generator G2 electrical power oscillations.

Comparing plot-2 of Fig.9.9 with that of plot-2 of Fig.9.10, it is seen that the real power flow in the 345 kV line (P_{line}) has been controlled at 400 MW. The real power flow oscillations in the 345 kV line (P_{line}) without UPFC is about 550 MW. The real power flow in the 345 kV line (P_{line}) does not show any oscillations with UPFC. UPFC has thus effectively controlled the power flow oscillations in the 345 kV transmission line and improved generator G2 electrical power oscillation damping.

Plot-3 of Fig.9.10 shows the UPFC bus voltage ($V_{upfcbus}$) oscillation due to three-phase fault disturbance. The application of three-phase fault causes the UPFC bus voltage ($V_{upfcbus}$) to dip to about 0.84 p.u. This leads to the shunt inverter to provide reactive power to the UPFC bus and boost its voltage to 1.0 p.u. The shunt inverter control system regulates the UPFC bus voltage to 1.0 p.u.

Plot-4 of Fig.9.10 shows the DC link capacitor voltage (V_{dc}) oscillations for the three-phase fault disturbance. The application of a three-phase fault causes the UPFC to release some of its stored energy leading to decrease in the DC link capacitor voltage (V_{dc}). The decrease in DC link capacitor voltage (V_{dc}) is about 5 kV following the three-phase fault. This is seen from plot-4 of Fig.9.10 at around 10 s. The shunt inverter recognizes the drop in DC link capacitor voltage (V_{dc}) and regulates it to 60 kV.

This simulation has validated the fuzzy control system design and the UPFC control system as a whole. It has also shown that UPFC can provide effective power oscillation damping. Further, the ability to provide simultaneous and coordinated control of the variables namely (P_{line}), ($V_{upfcbus}$) and (V_{dc}) under dynamic conditions has been brought out through this simulation.

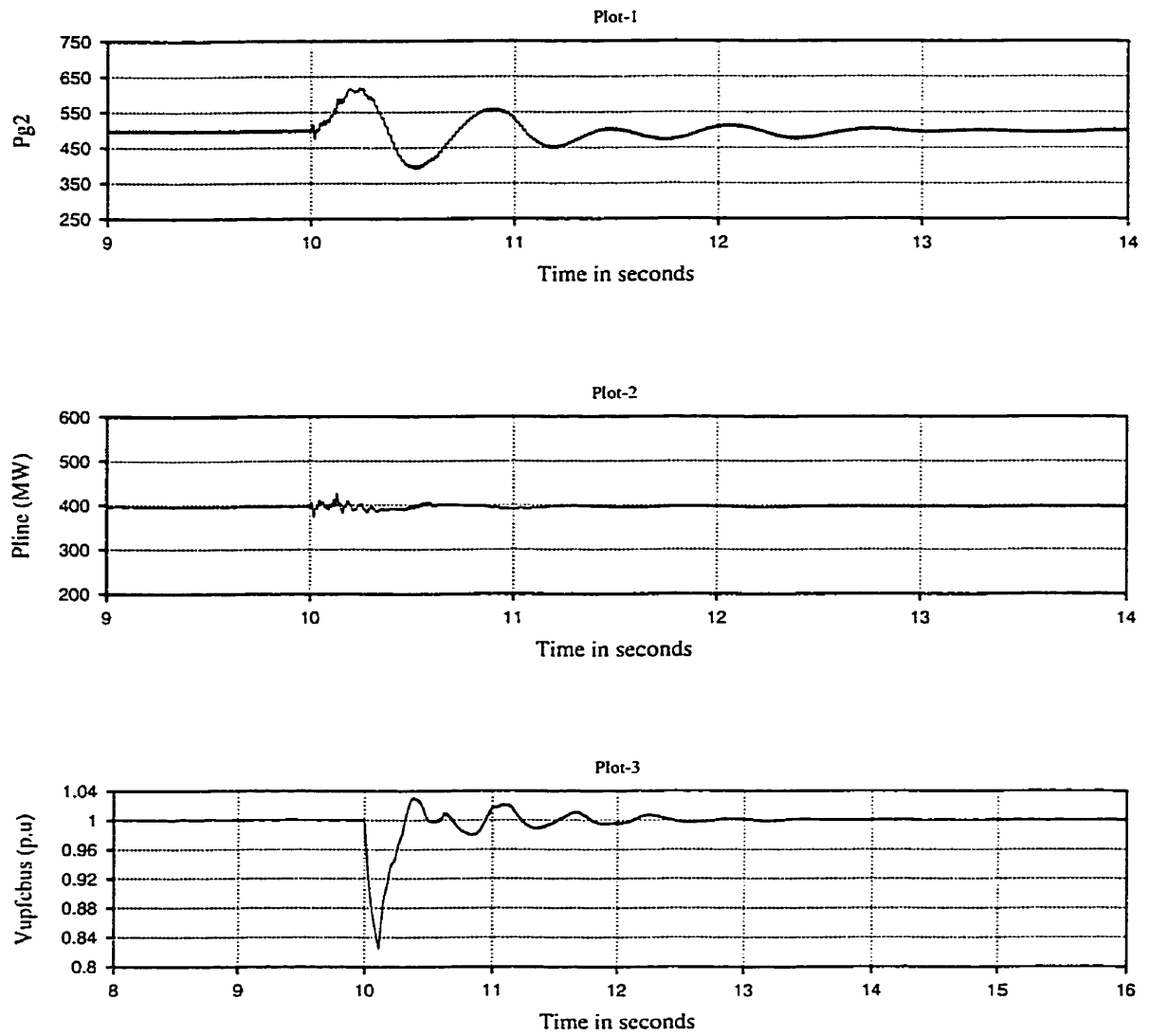


Fig.9.10 Response of the power system to three-phase fault with UPFC (contd.).

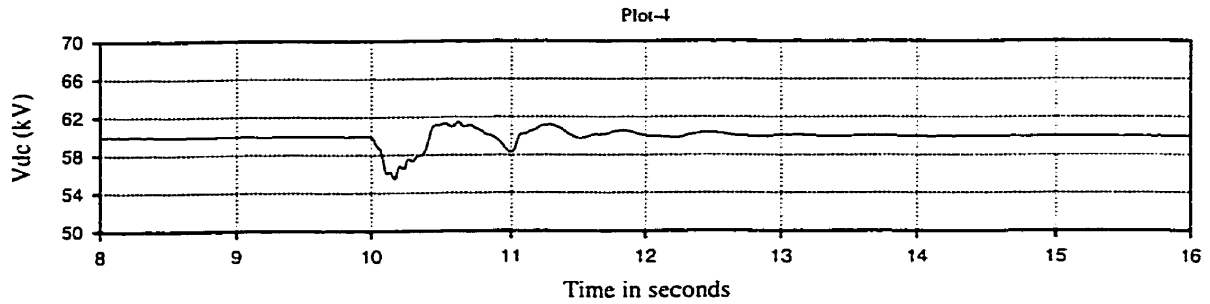
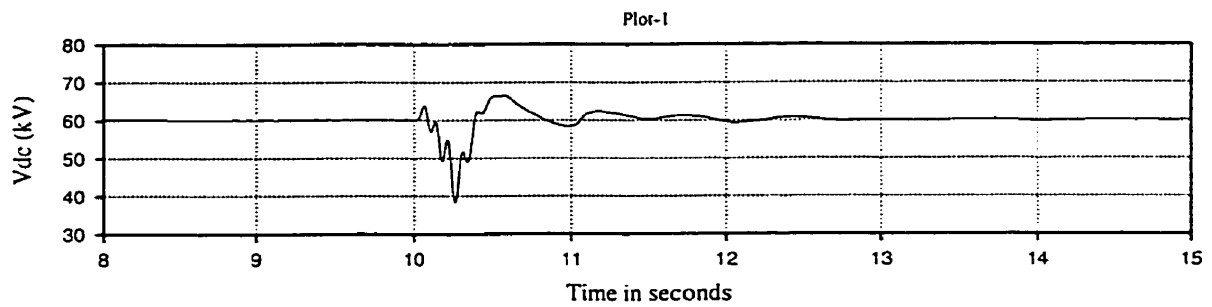


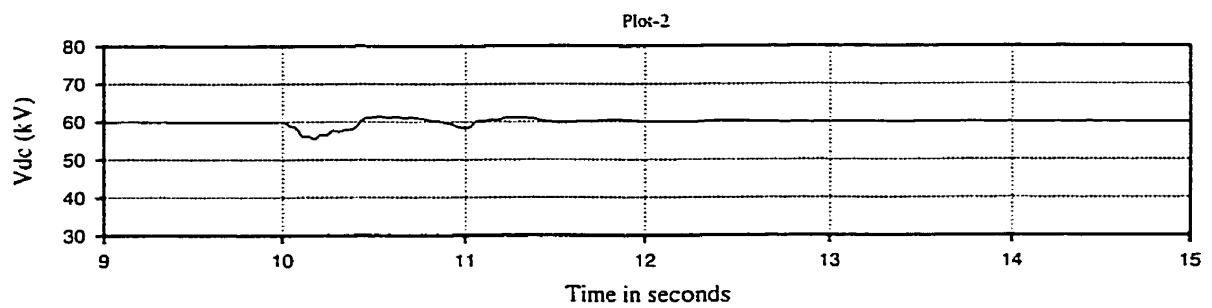
Fig.9.10 Response of the power system to three-phase fault with UPFC.

9.4 Performance of coordination controller

In order to study the performance of the coordination controller, the power system shown in Fig.9.8 was modeled in PSCAD-EMTDC software. A three-phase fault on the high voltage side bus of the generator G1 was considered to show the improvement in the damping of DC link capacitor voltage (V_{dc}) oscillations with coordination controller. Fig.9.11 shows the DC link capacitor voltage (V_{dc}) oscillations with and without the coordination controller for the UPFC. Plot-1 of Fig.9.11 shows the DC link capacitor voltage (V_{dc}) oscillations without the coordination controller. Plot-2 of Fig.9.11 shows the DC link capacitor voltage (V_{dc}) oscillations with the coordination controller.



(a)



(b)

Fig.9.11 DC link capacitor voltage oscillations with and without coordination controller.

- a). Without coordination controller.
- b). With coordination controller.

It is observed from plot-1 of Fig.9.11 that, without the coordination controller, the DC link capacitor voltage (V_{dc}) drops to about 40 kV immediately after the application of a three-phase fault on the high voltage side bus of generator G1. Further, the DC link capacitor voltage (V_{dc}) oscillations damp out in 3 s. In contrast, with the coordination controller in service, the DC link capacitor voltage (V_{dc}) drops to only 55 kV. Further, the DC link capacitor voltage (V_{dc}) oscillations damp out in less than 2 s. It is thus concluded that the coordination controller provides proper coordination between the series inverter and shunt inverter control system. With the coordination controller

included, the shunt inverter supplies the real power demand of the series inverter (P_{se}) very quickly allowing for smooth operation of the UPFC under transient conditions.

9.5 Effect of in-phase series voltage injection on reactive power flow in the transmission line and shunt inverter reactive power

PSCAD-EMTDC simulations carried out in section 9.2 and 9.3 have concentrated on the quadrature voltage component (V_{seQ}) of the series injected voltage for transmission line real power flow control (P_{line}) and neglected the in-phase component (V_{seD}) of the series injected voltage. In this section the effect of the in-phase component (V_{seD}) of the series injected voltage on transmission line reactive power flow (Q_{line}) and shunt inverter reactive power injection (Q_{sh}) at the UPFC bus will be studied.

Before studying the effect of the in-phase component on transmission line reactive power flow and shunt inverter reactive power, a few variables needs to be defined. Consider the equivalent circuit of UPFC as shown in Fig.9.12.

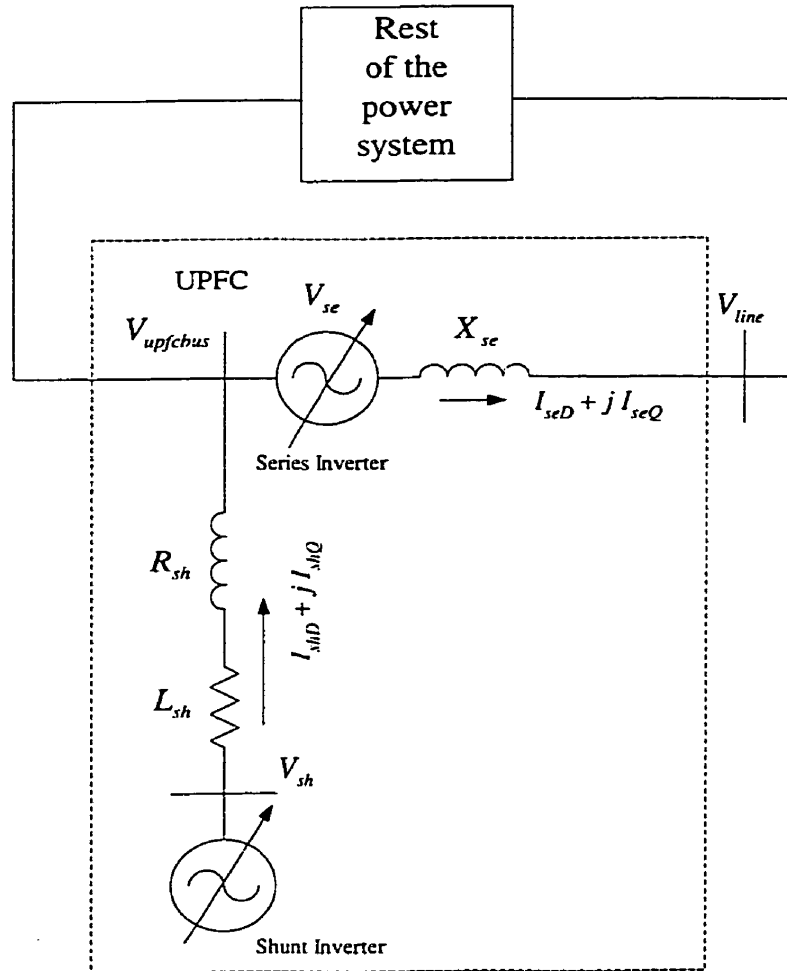


Fig.9.12 Equivalent circuit for a UPFC.

The transmission line side bus voltage is denoted by V_{line} . The UPFC bus voltage is denoted by V_{upfbus} . Let I_{seD} and I_{seQ} be the D and the Q axis components of the transmission line current. Writing the voltage equations for the series inverter we get,

$$V_{lineD} + jV_{lineQ} = V_{upfcbus} \angle 0 + I_{seQ} X_{se} - jI_{seD} X_{se} + V_{seD} + jV_{seQ} \quad (9.2)$$

where V_{lineD} , V_{lineQ} are the D and the Q axis components of the transmission line side voltage V_{line} . X_{se} represents the series transformer impedance. V_{seD} , V_{seQ} are the D and the Q axis components of the series injected voltage. Separating equation 9.2 into real and imaginary parts we get

$$\begin{aligned} V_{lineD} &= V_{upfcbus} \cos \theta + I_{seQ} X_{se} + V_{seD} \\ V_{lineQ} &= -I_{seD} X_{se} + V_{seQ} \end{aligned} \quad (9.3)$$

Let u_{seD} and u_{seQ} be two auxiliary inputs. The auxiliary variables u_{seD} and u_{seQ} are related to V_{seD} and V_{seQ} respectively by equation 9.4.

$$\begin{aligned} V_{seD} &= -I_{seQ} X_{se} + u_{seD} \\ V_{seQ} &= I_{seD} X_{se} + u_{seQ} \end{aligned} \quad (9.4)$$

Substituting for V_{seD} and V_{seQ} in equation 9.3 from equation 9.4 we get

$$\begin{aligned} V_{lineD} &= V_{upfcbus} + u_{seD} \\ V_{lineQ} &= u_{seQ} \end{aligned} \quad (9.5)$$

The power system with a UPFC shown in Fig.9.3 has been set up in PSCAD-EMTDC software to study the effect of in-phase component (V_{seD}) on the transmission line reactive power (Q_{line}) and shunt inverter reactive power (Q_{sh}) flow. It is seen from equation 9.4 that u_{seD} is directly related to V_{seD} . Thus step changes to u_{seD} have been conducted to study the effect of V_{seD} on transmission line reactive power flow (Q_{line}) and shunt inverter reactive power (Q_{sh}). The initial conditions are that the shunt inverter controls the UPFC bus voltage ($V_{upfcbus}$) at 1.0 p.u and the DC link capacitor voltage (V_{dc}) at 60 kV. The quadrature component of the series injected voltage (V_{seQ}) controls

the real power flow in the transmission line (P_{line}) at 290 MW. Fig.9.13 shows the effect of u_{seD} on transmission line reactive power (Q_{line}) and shunt inverter reactive power (Q_{sh}). Plots-1 through plot-6 of Fig.9.13 shows the series inverter auxiliary input (u_{seD}) voltage profile, transmission line side bus voltage (V_{line}) profile, UPFC bus voltage ($V_{upfcbus}$) profile, transmission line reactive power flow (Q_{line}), shunt inverter reactive power (Q_{sh}) and the series inverter reactive power (Q_{se}) respectively.

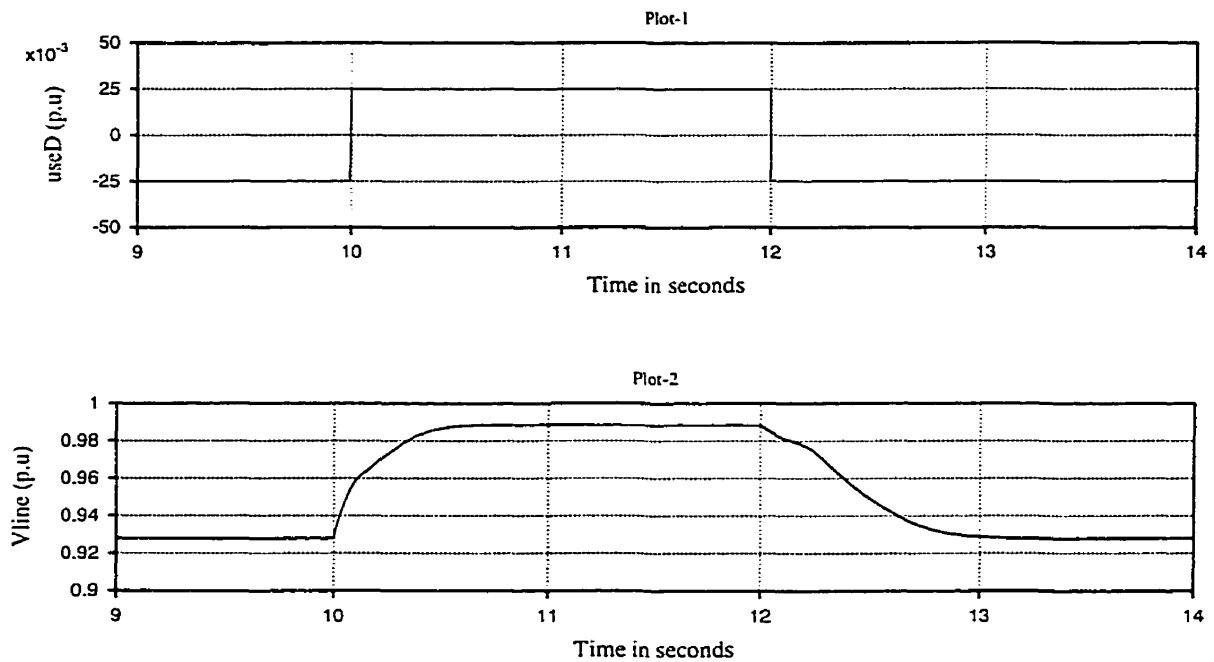


Fig.9.13. Effect of in-phase voltage injection on transmission line reactive power, shunt inverter reactive power and series inverter reactive power (contd.).

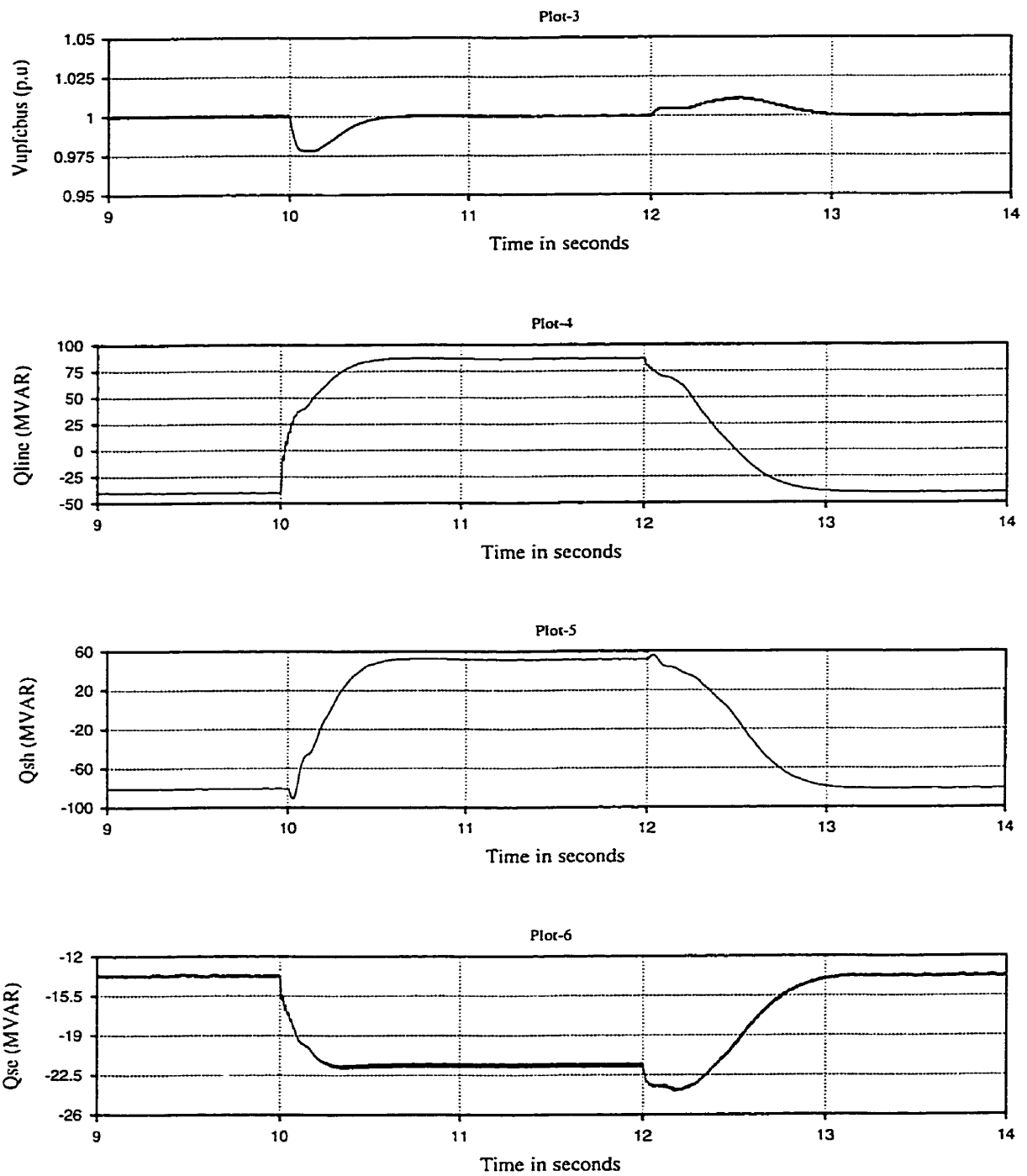


Fig.9.13. Effect of in-phase voltage injection on transmission line reactive power, shunt inverter reactive power and series inverter reactive power.

At 10 s, a step increase in u_{seD} was conducted from -0.025 p.u to 0.025 p.u. At 12s, u_{seD} was reduced from 0.025 p.u to -0.025 p.u. Plot-1 of Fig.9.13 shows the step changes to u_{seD} at 10 s and 12 s. The transmission line side bus voltage (V_{line}) changes from 0.93 p.u to 0.98 p.u for a change in u_{seD} from -0.025 to 0.025 p.u. It is observed from plot-3 that when u_{seD} increases from -0.025 to 0.025 p.u, the UPFC bus voltage ($V_{upfcbus}$) dips to 0.975 p.u momentarily. This decrease in UPFC bus voltage ($V_{upfcbus}$) causes the shunt inverter to increase its reactive power input to bring the UPFC bus voltage to 1.0 p.u. The initial shunt inverter reactive power (Q_{sh}) injection at the UPFC bus before the step change in u_{seD} was about -80 MVAR. The increase in shunt inverter reactive power (Q_{sh}) due to a step change in u_{seD} from -0.025 to 0.025 p.u is about 130 MVAR. Correspondingly, the increase in transmission line reactive power (Q_{line}) is also about 130 MVAR (plot-4 Fig.9.13). Thus the change in u_{seD} has increased the transmission line side voltage (V_{line}) from 0.93 to 0.98 p.u and has increased the transmission line reactive power (Q_{line}), shunt inverter reactive power (Q_{sh}) by 130 MVAR. Thus the increase in transmission line reactive power flow (Q_{line}) is supplied by the shunt inverter. The series inverter reactive power (Q_{se}) changes as shown in plot-6 of Fig.9.13 are insignificant compared to that of the shunt inverter reactive power (Q_{sh}) changes. At 12 s, u_{seD} is reduced from 0.025 to -0.025 . This leads to reduction in transmission line side bus voltage (V_{line}) and a corresponding decrease in transmission line reactive power flow (Q_{line}). The transmission line side bus voltage (V_{line}) drops from 0.98 to 0.93 p.u. The transmission line reactive power (Q_{line}) reduces from $+90$ MVAR to -40 MVAR. The UPFC bus voltage ($V_{upfcbus}$) momentarily changes from 1.0 p.u to 1.01 p.u due to the change in u_{seD} from 0.025 to -0.025 . Since the shunt inverter is controlling the

UPFC bus voltage, an equivalent amount of reactive power change takes place in the shunt inverter. The shunt inverter reactive power (Q_{sh}) reduces from +50 MVAR to -80 MVAR to bring the UPFC bus voltage back to 1.0 p.u.

This simulation has shown that u_{seD} has significant effect on the shunt inverter reactive power (Q_{sh}), transmission line reactive power (Q_{line}) and transmission line side bus voltage (V_{line}). Step changes in u_{seD} has shown that u_{seD} has indirect effect on shunt inverter reactive power (Q_{sh}) and hence on the transmission line reactive power flow (Q_{line}). This is because any change in u_{seD} directly effects the transmission line side bus voltage (V_{line}) and UPFC bus voltage ($V_{upfcbus}$). An increase in u_{seD} from -0.025 p.u to 0.025 p.u changes the transmission line side bus voltage (V_{line}) from 0.93 p.u to 0.98 p.u. The UPFC bus voltage ($V_{upfcbus}$) instantaneously dips from 1.0 p.u to 0.975 p.u for a step increase in u_{seD} from -0.025 p.u to 0.025 p.u. Since the shunt inverter is controlling the UPFC bus voltage ($V_{upfcbus}$), the decrease in UPFC bus voltage ($V_{upfcbus}$) causes the shunt inverter to increase its reactive power output (Q_{sh}) from -80 MVAR to 50 MVAR to bring the UPFC bus voltage to 1.0 p.u. This increase in shunt inverter reactive power (Q_{sh}) by 130 MVAR is transferred to the transmission line and is seen as an increase in transmission line reactive power flow (Q_{line}). It is seen that the cause and the effect are on two different parts of UPFC. The cause being the change in u_{seD} in the series inverter and the effect being the change in shunt inverter reactive power (Q_{sh}). One point more to be noted here is that the shunt inverter recognizes the need to increase/decrease its reactive power output only through the change observed due to decrease/increase in the UPFC bus voltage which ultimately gets transferred as an equal increase/decrease in transmission line reactive power flow. Thus controlling the transmission line reactive

power flow (Q_{line}) using in-phase voltage injection of the series inverter reduces the effectiveness of the control strategy. It suggests the need for reactive power coordination between the series and the shunt inverter control system for better overall performance. This also suggests that the transmission line reactive power (Q_{line}) could directly be controlled through the shunt inverter instead of by the series inverter.

9.6 Summary

The interaction between the series injected voltage (V_{se}) and the transmission line current (I_{se}) leads to real power exchange between the series inverter and the transmission line. The real power demand of the series inverter (P_{se}) is supplied by the shunt inverter. In order to coordinate between the operation of the shunt and the series inverter, a coordination controller has been designed. The coordination controller provides a D-axis current (i_{Dse}) feedback to the shunt inverter control system equivalent to the real power demand of the series inverter (P_{se}). It provides the link between the series and the shunt inverter control system allowing for proper operation of the combined UPFC control system. The effectiveness of the coordination controller has been brought out through PSCAD-EMTDC simulations. The DC link capacitor voltage excursion was reduced from 20 kV to less than 5 kV with coordination controller. The implementation of coordination controller could also help in using reduced ratings of the DC link capacitor and hence reduction in the overall cost of UPFC.

PSCAD-EMTDC simulations have shown that using a PI controller for the series inverter to control the real power flow in the transmission line (P_{line}) provides

oscillatory response to step input changes in real power flow references (P_{ref}). The problem of low damping has been overcome by using a fuzzy controller for the series inverter to control the real power flow in a transmission line (P_{line}). The improvement in the response to step input changes in real power references (P_{ref}) with fuzzy controllers as compared to PI controller for series inverter has been brought out in this chapter.

The improvement in power oscillation damping using UPFC with fuzzy controller has been brought out through PSCAD-EMTDC simulations. These simulations also validate the design of the shunt and series inverter control system. Further, power oscillation damping simulation has shown that the UPFC control system designed operates in a unified and stable manner. Under transient conditions, the UPFC control system has been able to control the transmission line real power flow (P_{line}), UPFC bus voltage ($V_{upfcbus}$) and DC link capacitor voltage (V_{dc}) simultaneously.

The effect of in-phase series voltage injection on transmission line reactive power (Q_{line}), series inverter reactive power (Q_{se}) and shunt inverter reactive power (Q_{sh}) has been discussed. Computer simulations using PSCAD-EMTDC software on a simple power system has shown that the in-phase series voltage injection which changes the transmission line side bus voltage (V_{line}) / reactive power flow (Q_{line}) has a significant effect on the shunt inverter reactive power (Q_{sh}). Any increase in transmission line side bus voltage (V_{line}) by injecting a positive in-phase component of series voltage causes the transmission line reactive power (Q_{line}) to increase by an amount equivalent to the increase in shunt inverter reactive power (Q_{sh}). Conversely, any decrease in transmission line side bus voltage (V_{line}) by injecting a negative in-phase component of series voltage causes the transmission line reactive power (Q_{line}) to decrease by an

amount equal to the decrease in shunt inverter reactive power (Q_{sh}). Thus the cause and the effect are on two portions of the UPFC. The cause being the in-phase injection component of the series inverter and the effect seen as an increase/decrease in shunt inverter reactive power. Thus controlling the transmission line reactive power flow (Q_{line}) using in-phase voltage injection of the series inverter reduces the effectiveness of the control strategy. Hence there is a need to provide for reactive power coordination between the series and the shunt inverter control systems for better overall performance. This also suggests the need to look at other control strategies whereby the transmission line reactive power could directly be controlled through the shunt inverter.

Chapter 10

Reactive power coordination

10.0 Introduction

The effect of in-phase component (V_{seD}) of the series injected voltage on shunt inverter reactive power (Q_{sh}), UPFC bus voltage ($V_{upfcbus}$), transmission line real (P_{line})/reactive power flow (Q_{line}) have been discussed in chapter 9. It has been shown that the in-phase component (V_{seD}) of the series injected voltage has considerable effect on the transmission line reactive power (Q_{line}) and the shunt inverter reactive power (Q_{sh}). In contrast, the in-phase component (V_{seD}) has insignificant effect on the series inverter reactive power (Q_{se}). Any increase/decrease in the transmission line reactive power (Q_{line}) due to in-phase component (V_{seD}) of the series injected voltage causes an equal increase/decrease in the shunt inverter reactive power (Q_{sh}) [42]. This suggests that the transmission line reactive power (Q_{line}) control system should be coordinated with the shunt inverter control system for better overall performance. Further the effect of controlling the transmission line reactive power (Q_{line}) through the series inverter on

UPFC bus voltage profile has been brought out in this chapter. A new reactive power coordination controller has been designed to overcome the problem arising from controlling the transmission line reactive power through the series inverter control system. Step response and power oscillation damping results with reactive power coordination controller have also been presented in this chapter.

10.1 Need for reactive power coordination

The first reason for requiring a reactive power coordination controller between the series and the shunt inverter has been discussed in chapter-9. In brief, it has been shown in chapter-9 that any request for change in transmission line reactive power flow (Q_{line}) which is achieved by increasing/decreasing the in-phase component (V_{seD}) of the series injected voltage is actually supplied by the shunt inverter. Thus the cause and the effect are on two portions of the UPFC. This calls for proper reactive power coordination between the series and the shunt inverter control system with respect to transmission line reactive power for better overall performance of the control system.

The second reason for including a reactive power coordination controller will be described in this section. PSCAD-EMTDC simulations have been conducted to show the need for reactive power coordination between the series and the shunt inverter control system. To do so, consider a UPFC connected to a transmission line as shown in Fig.10.1. In this case, the series inverter of a UPFC controls the real power (P_{line}) and reactive power (Q_{line}) flow in the transmission line. The shunt inverter controls the UPFC bus voltage ($V_{upfcbus}$) and the DC link capacitor voltage (V_{dc}). This mode of operation of a UPFC has been used widely in literature.

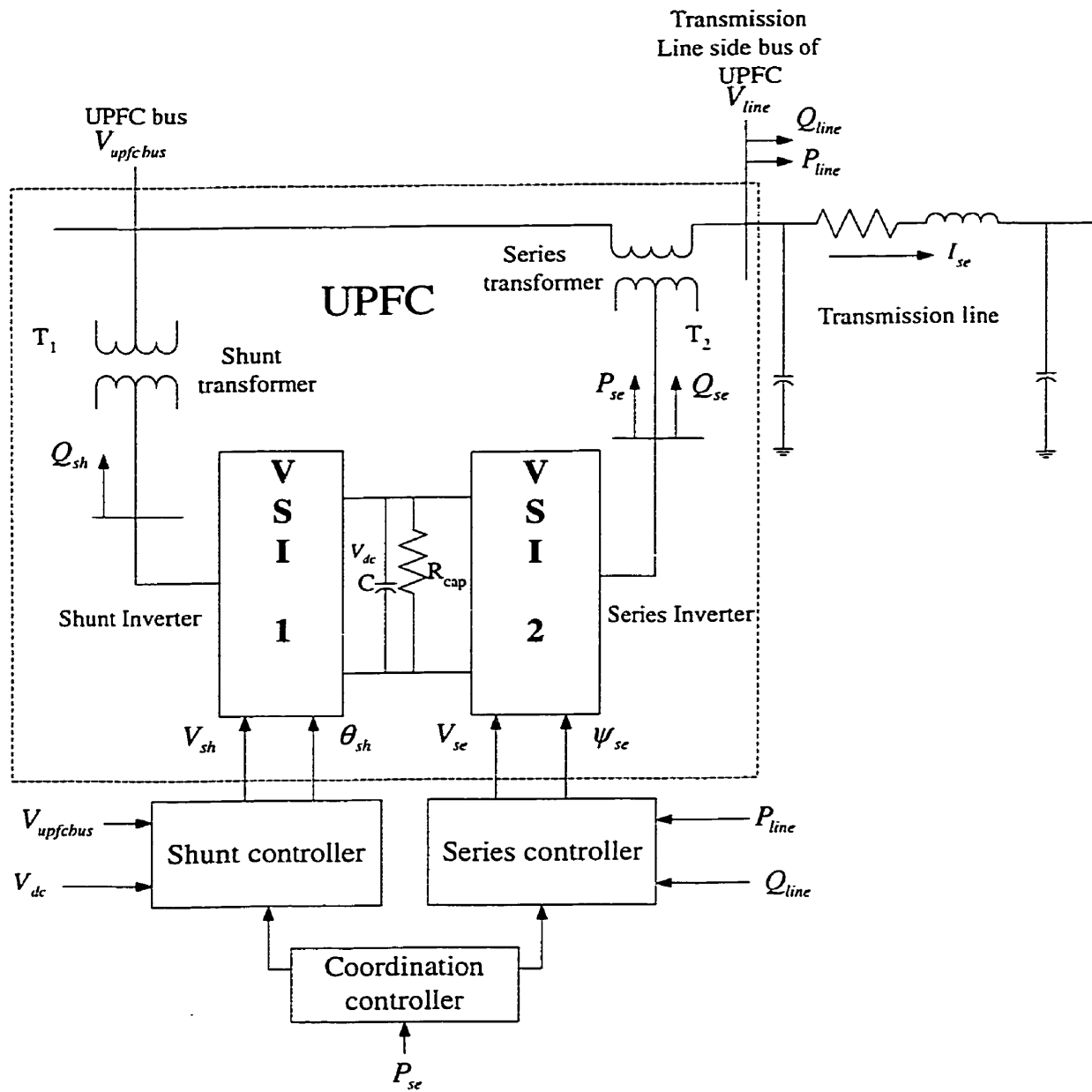


Fig.10.1 UPFC connected to a transmission line.

In this mode of control, the series inverter injected voltage is split into two components, one in-phase (V_{seD}) and the other in quadrature (V_{seQ}) with the UPFC bus voltage. The

quadrature component of the series injected voltage (V_{seQ}) controls the real power flow in the transmission line (P_{line}) and the in-phase component of the series injected voltage (V_{seD}) controls the transmission line reactive power flow (Q_{line})

10.2 Shunt and series inverter control system

10.2.1 Shunt inverter control system: The shunt inverter is controlled using the decoupled control system. Fig.10.2 shows the shunt inverter control system with the real power coordination controller. The shunt inverter controls the UPFC bus voltage ($V_{upfcbus}$) and the DC link capacitor voltage (V_{dc}).

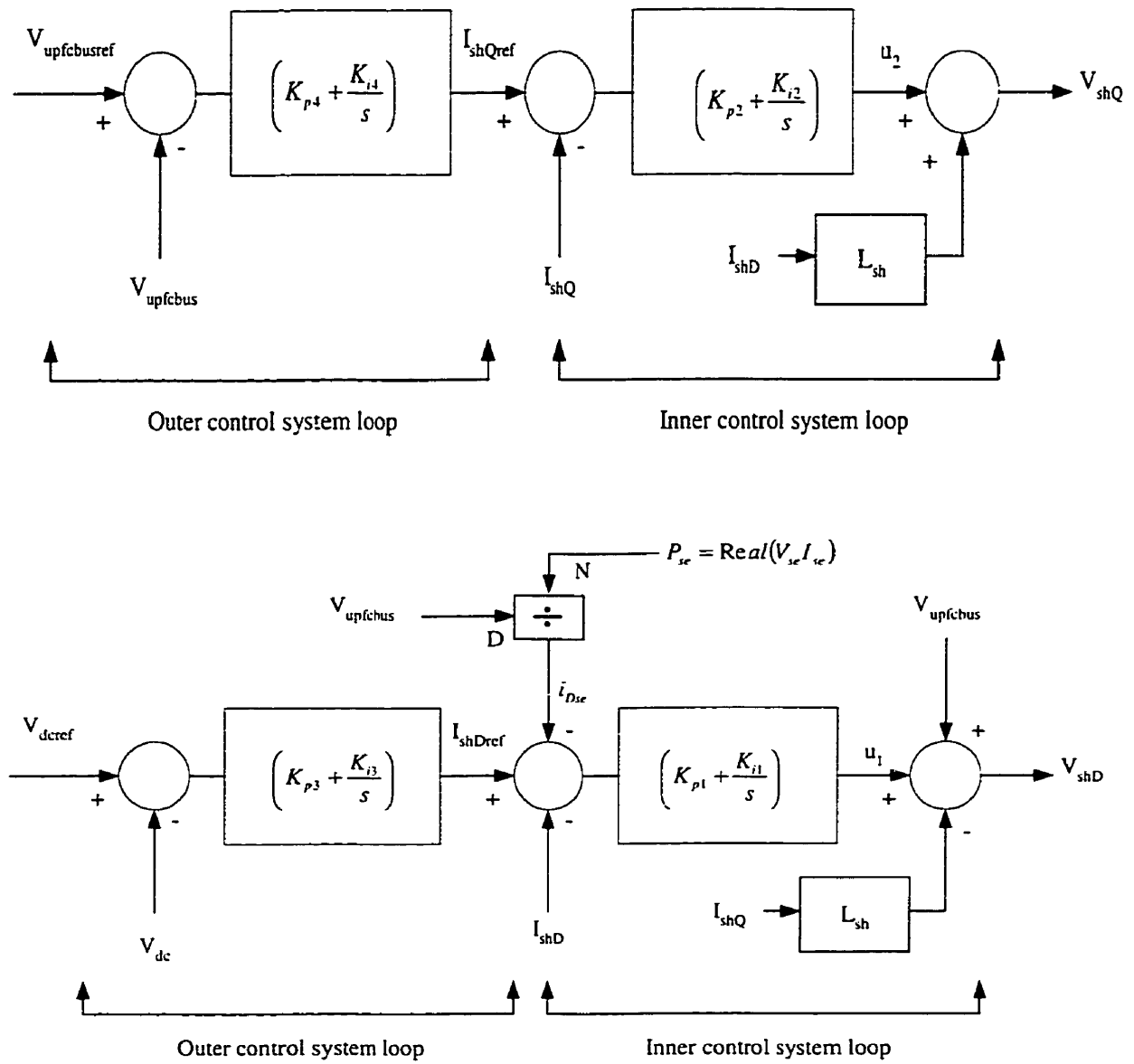
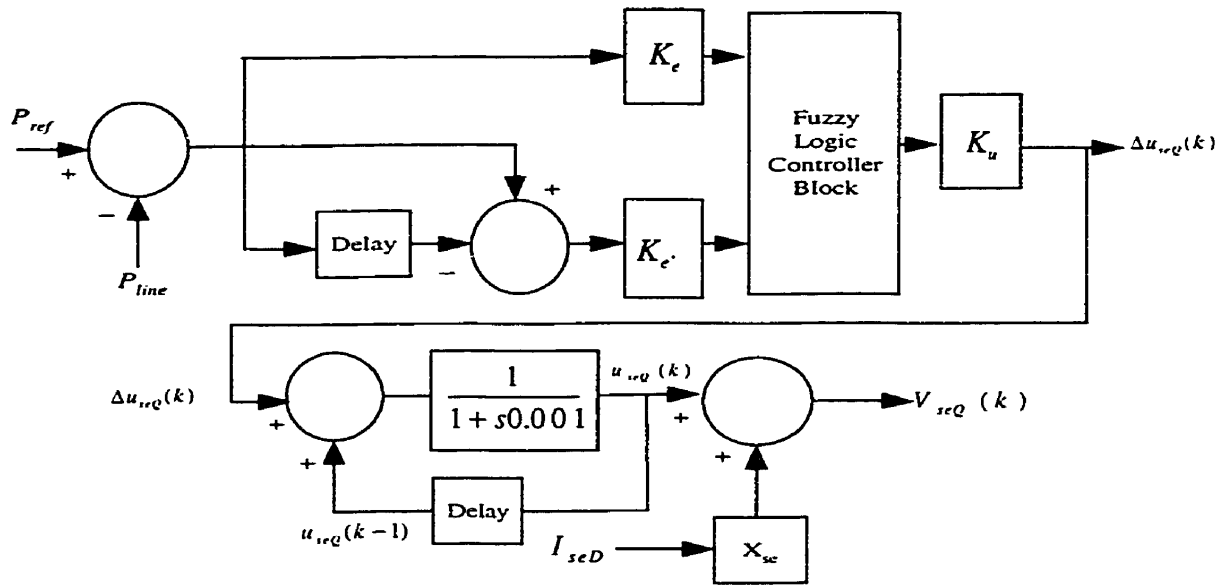


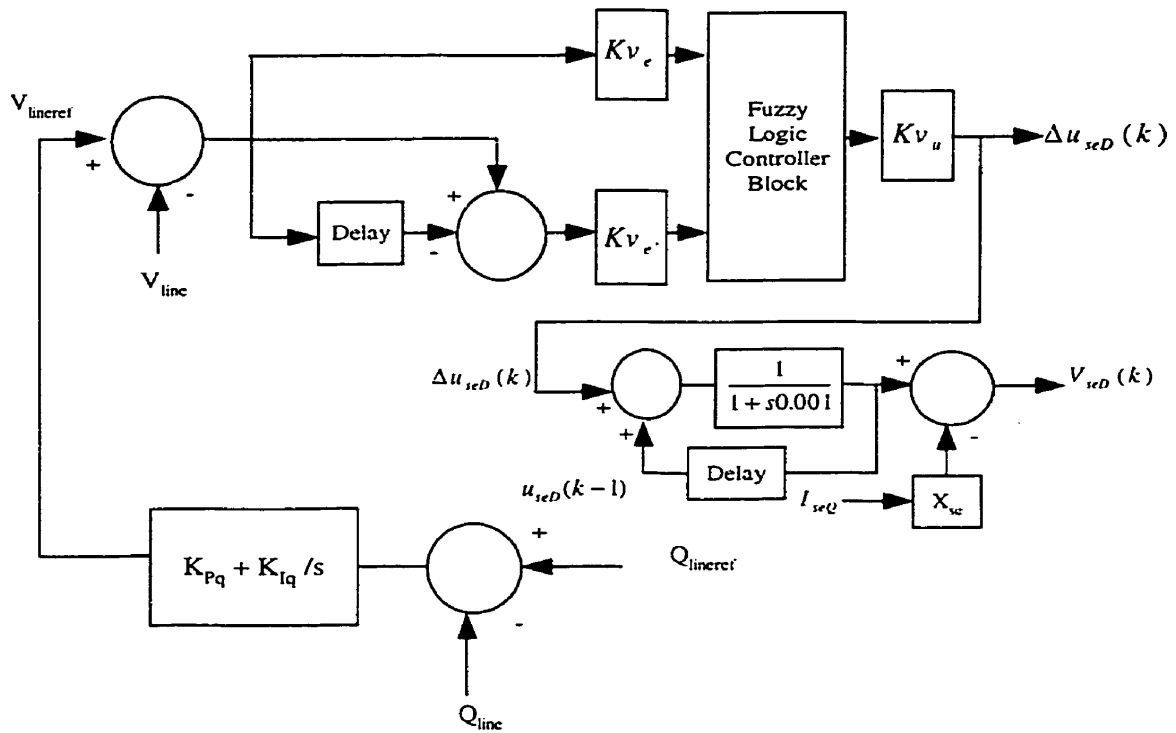
Fig.10.2. Shunt inverter control system with real power coordination controller.

It is seen from Fig.10.2 that the UPFC bus voltage ($V_{upfcbus}$) is controlled by the Q-axis shunt inverter voltage (V_{shQ}). The DC link capacitor voltage (V_{dc}) is controlled by the D-axis shunt inverter voltage (V_{shD}). The design of the shunt inverter control system has been carried out in Chapter-7. The PI controller gains used for the shunt inverter controller are $K_{p1} = 5.0$, $K_{i1} = 21.367$, $K_{p2} = 0.2$, $K_{i2} = 5.0$, $K_{p3} = -1.0$, $K_{i3} = -2.0$, $K_{p4} = -1.0$, $K_{i4} = -133.0$.

10.2.2 Series inverter control system: The series inverter injected voltage is split into two components, one in-phase (V_{seD}) and the other in quadrature (V_{seQ}) with the UPFC bus voltage. The series inverter controls the real power flow in the transmission line (P_{line}) by injecting a voltage in quadrature (V_{seQ}) with the UPFC bus voltage ($V_{upfcbus}$). The in-phase component (V_{seD}) of the series injected voltage controls the transmission line side bus voltage (V_{line}). By regulating the transmission line side bus voltage reference ($V_{lineref}$), transmission line reactive power flow (Q_{line}) can be controlled. The series inverter control system is as shown in Fig.10.3.



(a)



(b)

Fig.10.3 Series inverter control system.
 a) Transmission line real power flow controller.
 b) Transmission line reactive power controller.

transmission line (P_{line}), reactive power flow in the transmission line (Q_{line}), reactive power flow in the transmission line (Q_{line}) around 10 s, reactive power flow in the transmission line (Q_{line}) around 12 s, UPFC bus voltage profile ($V_{UPFCbus}$), DC link capacitor voltage profile (V_{dc}), shunt inverter reactive power (Q_{sh}) around 10 s and shunt inverter reactive power around 12 s respectively.

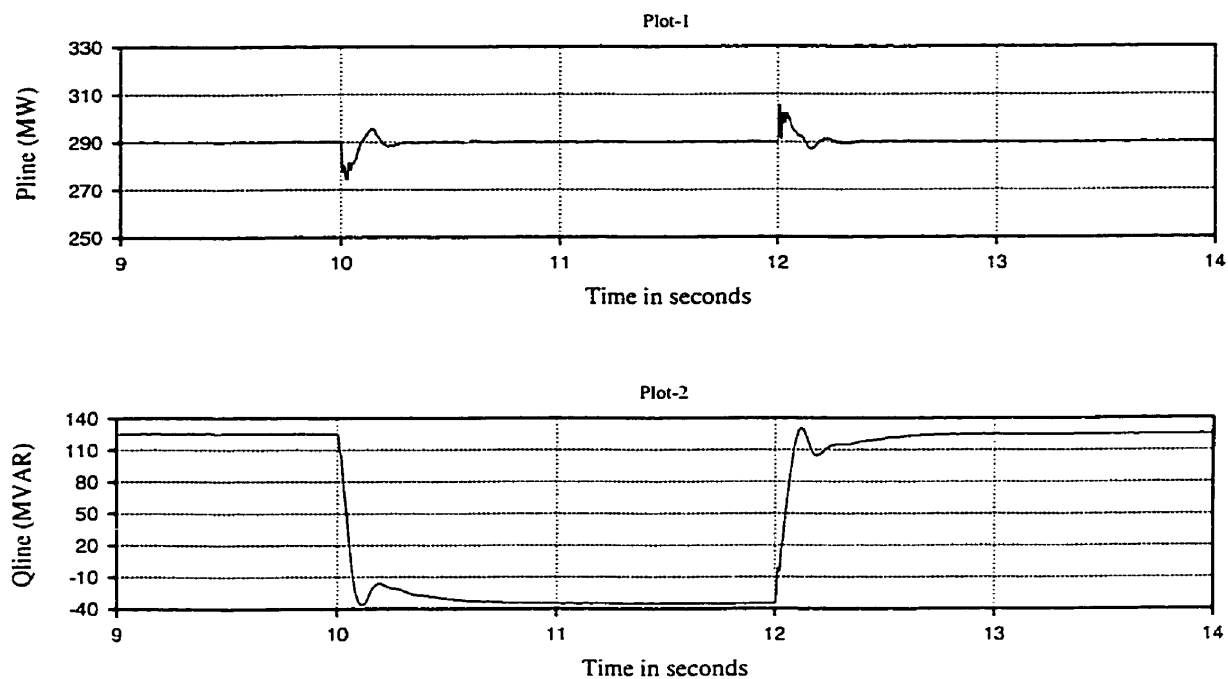


Fig.10.5. Response to step change in reactive power reference. (contd.)

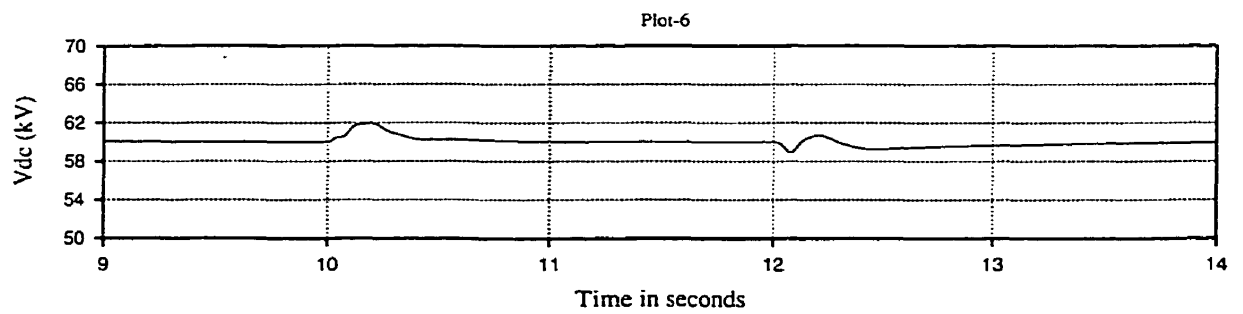
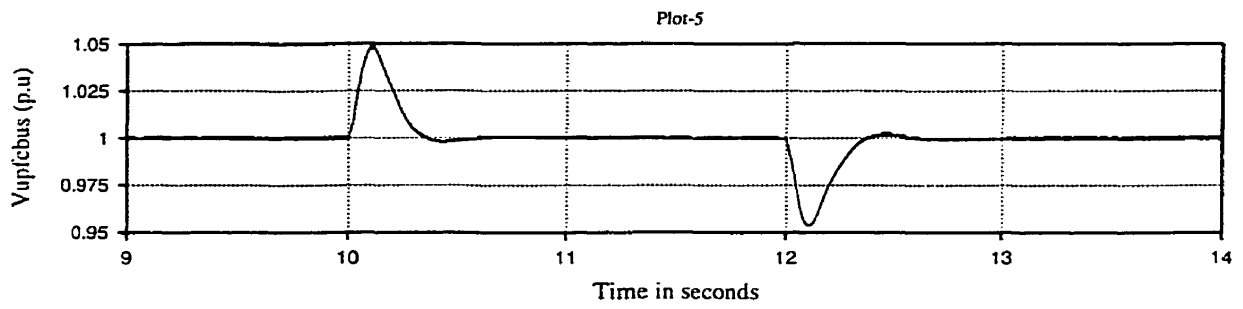
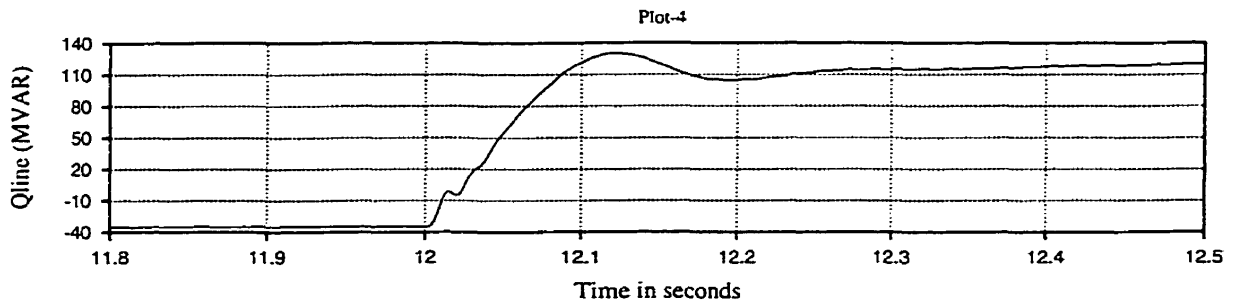
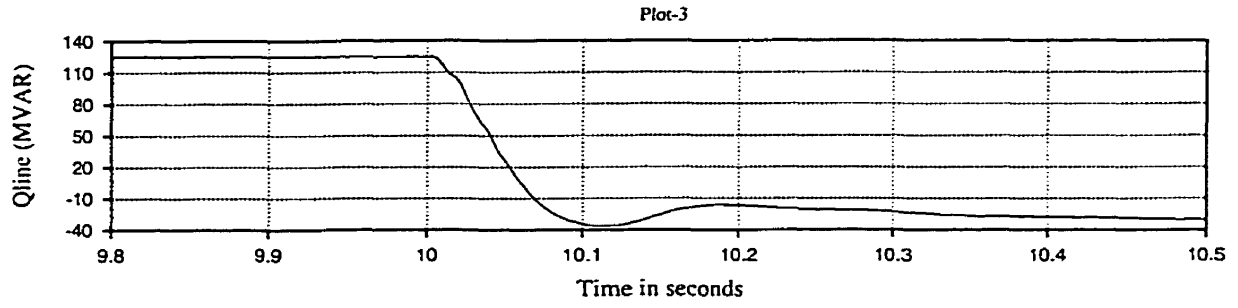


Fig. 10.5 Response to step change in reactive power reference. (contd.)

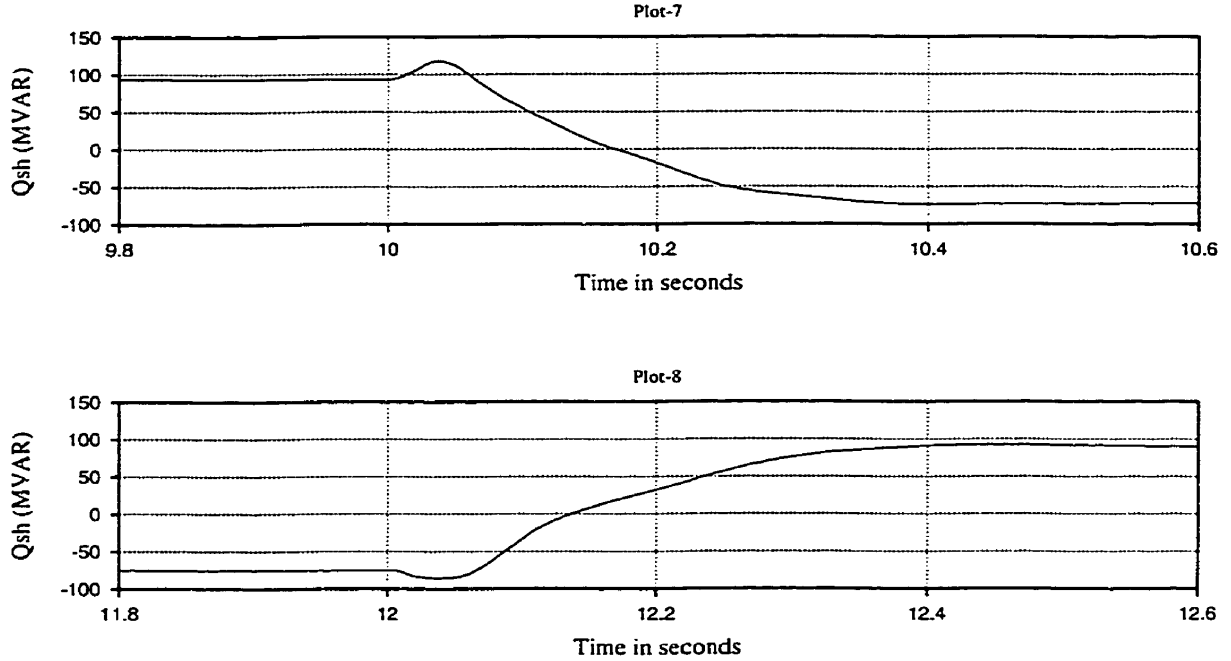


Fig.10.5 Response to step change in reactive power reference.

At 10 s, a step change is conducted in the transmission line reactive power reference from 125 MVAR to -35 MVAR. It is seen that the transmission line real power flow (P_{line}) (plot-1 of Fig.10.5) is not affected significantly during the step change in transmission line reactive power reference. The transmission line reactive power (Q_{line}) (plot-2 of Fig.10.5) changes from 125 MVAR to -35 MVAR in about 100 to 150 ms. Simultaneously the shunt inverter reactive power (Q_{sh}) reduces from about 80 MVAR to -80 MVAR (plot-7 of Fig.10.5). A step decrease in the transmission line reactive power reference from 125 MVAR to -35 MVAR causes a sudden increase in the UPFC bus voltage ($V_{upfcbus}$) (plot-5 of Fig.10.5) by about 0.05 p.u from 1.0 p.u momentarily. After about 200 ms the UPFC bus voltage ($V_{upfcbus}$) is brought back to 1.0 p.u by the shunt

inverter control system. At about 12 s, the transmission line reactive power (Q_{line}) is changed from -35 MVAR to 125 MVAR (plot-4 of Fig.10.5) by changing its reference value. Simultaneously, the shunt inverter reactive power changes (Q_{sh}) from about -80 MVAR to +80 MVAR (plot-8 of Fig 10.5). This time the UPFC bus voltage ($V_{upfcbus}$) changes from 1.0 p.u to 0.95 p.u momentarily. In this simulation the real power coordination controller has been included which helps in reducing the change in the DC link capacitor voltage (V_{dc}). This is seen from plot-6 of Fig.10.5. It is also observed that though the transmission line reactive (Q_{line}) reaches 90 % of its steady state value in about 100 to 120 ms, the shunt inverter reactive power (Q_{sh}) takes almost 300 to 400 ms to reach its steady state.

This simulation has shown that step changes in transmission line reactive power has a significant effect on the UPFC bus voltage ($V_{upfcbus}$) and shunt inverter reactive power (Q_{sh}). It is observed that the shunt inverter reactive power (Q_{sh}) takes about 300 to 400 ms to reach its steady state. This is because, the shunt inverter reacts only to the change in the UPFC bus voltage ($V_{upfcbus}$). A step decrease in transmission line reactive power reference at 10 s causes the UPFC bus voltage ($V_{upfcbus}$) to rise to 1.05 p.u. This increase is sensed by the shunt inverter control system which reduces its reactive power output bring the UPFC bus voltage ($V_{upfcbus}$) to 1.0 p.u. One reason that can be attributed to the sluggish response of the shunt inverter reactive power (Q_{sh}) is that the UPFC bus voltage controller forms the outer loop control thereby reducing the speed of response of the shunt inverter to rapid changes in UPFC bus voltage ($V_{upfcbus}$).

Another problem that is to be noted is that, if there are transmission lines emanating from the UPFC bus and connected to a load center, sudden changes in the

UPFC bus voltage ($V_{upfcbus}$) due to step changes in transmission line reactive power flow reference would cause power quality problems. The above two reasons amply demonstrate the need for a reactive power coordination controller to improve the overall performance of the UPFC control system.

10.4 Reactive power coordination control design

To design a reactive power coordination controller, one needs to look at the response of the shunt inverter reactive power (Q_{sh}) to step changes in transmission line reactive power reference. As seen from plot-7 and plot-8 of Fig.10.5, it is observed that for a change in transmission line reactive power of 160 MVAR (from 125 MVAR to -35 MVAR), the shunt inverter reactive power (Q_{sh}) changes from 80 MVAR to -80 MVAR. This change takes place in about 400 ms. The response seen in plot-7 and plot-8 of Fig.10.5 are very similar to that of the response of a first order system to step changes. The time constant of the response is in the range of 80 ms. This information is considered during the design of the reactive power coordination controller. Further, notice should also be taken that the change in shunt inverter reactive power (Q_{sh}) is equal to the change in transmission line reactive power (Q_{line}). Based on these two observations, the reactive power coordination controller is designed. Fig.10.6 shows the shunt inverter control system with reactive power coordination controller. The input signal to the reactive power coordination controller is the transmission line reactive power reference. The output of the reactive power coordination controller modulates the shunt inverter reactive current reference (I_{shQref}). Thus any change in the transmission line reactive power reference is directly transferred to the shunt inverter inner control system. It should be

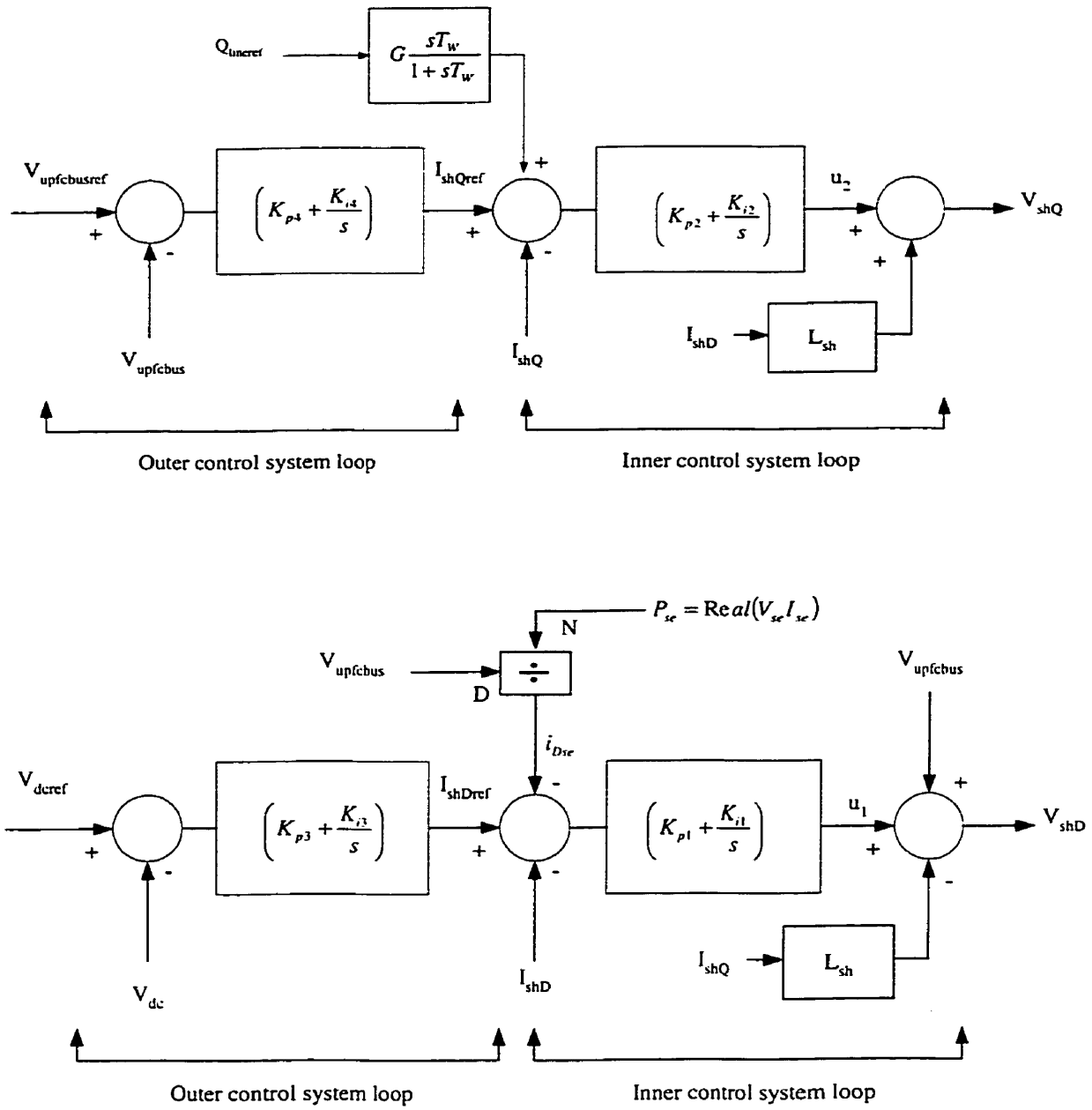


Fig.10.6. Shunt inverter control system with real and reactive power coordination controller.

noted that the output signal is fed to the inner loop control system. By doing so, the speed of response of the shunt inverter to changes in transmission line reactive power reference is increased. The gain (G) of the reactive power coordination block is chosen to be 1.0 as

the change in transmission line reactive power is to be transmitted in its entirety to the shunt inverter control system. The time constant T_W has been chosen to be greater than 80 ms. The time constant T_W is chosen to be 0.5 s. By doing so, the change in shunt inverter reactive current reference (I_{shQref}) would take a longer time to decay to zero allowing for sufficient time for the outer loop UPFC bus voltage controller to react.

10.5 Step response with reactive power coordination controller

The power system shown in Fig.10.4 has been considered to show the effect of the including the reactive power coordination controller on the transmission line reactive power flow (Q_{line}) and the UPFC bus voltage profile ($V_{upfcbus}$). The shunt inverter control system shown in Fig.10.6 includes the real and reactive power coordination controller. The series inverter control system is as shown in Fig.10.3.

A step change in transmission line reactive power reference is conducted at 10 s and 12 s. Plot-1 through plot-9 of Fig.10.7 shows the response of the system to step change in transmission line reactive power reference. At 10 s, the transmission line reactive power reference ($Q_{lineref}$) is changed from 125 MVAR to -35 MVAR. At 12 s, the transmission line reactive power reference ($Q_{lineref}$) is changed from -35 MVAR to

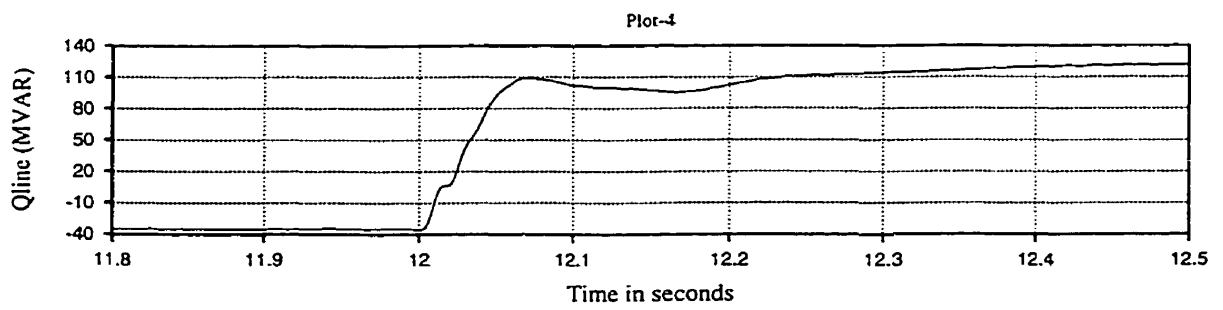
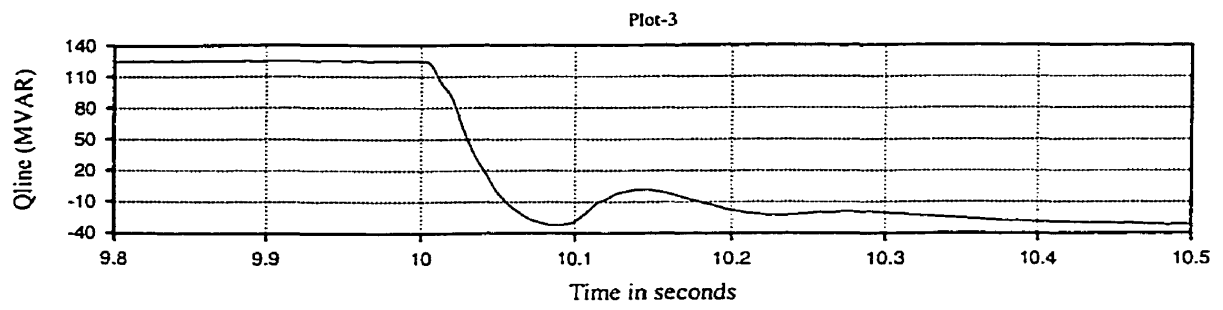
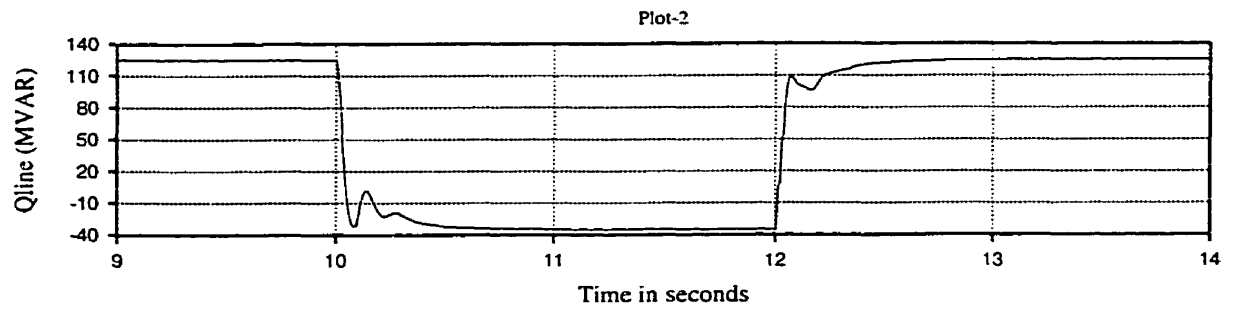
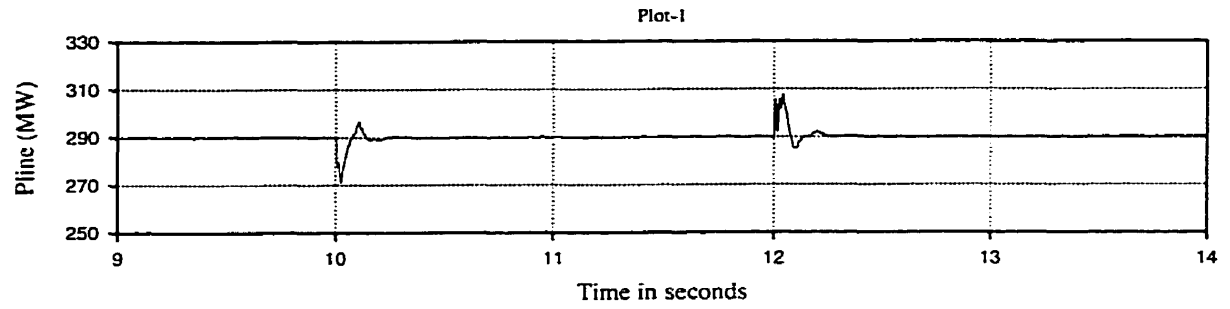


Fig.10.7 Step response with reactive power coordination controller. (contd).

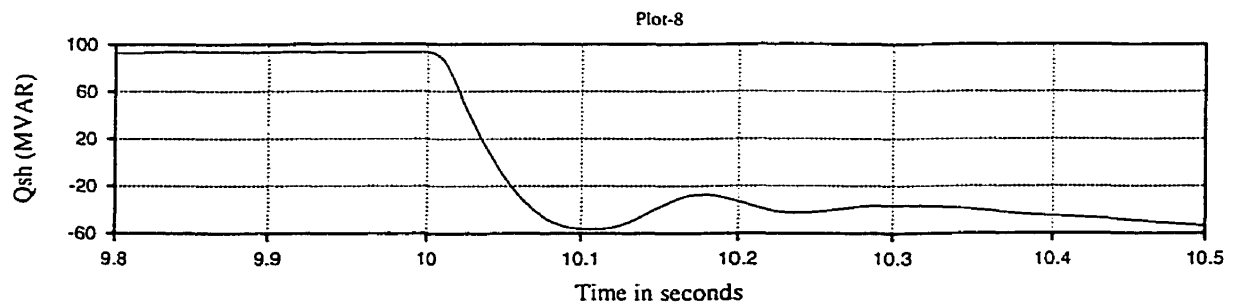
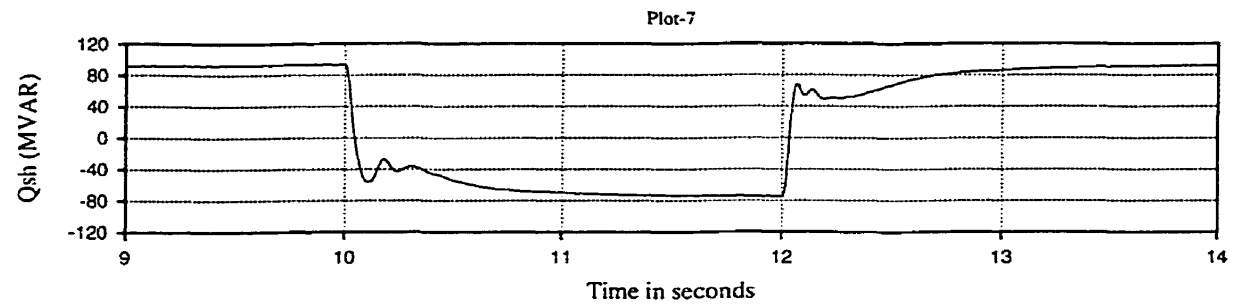
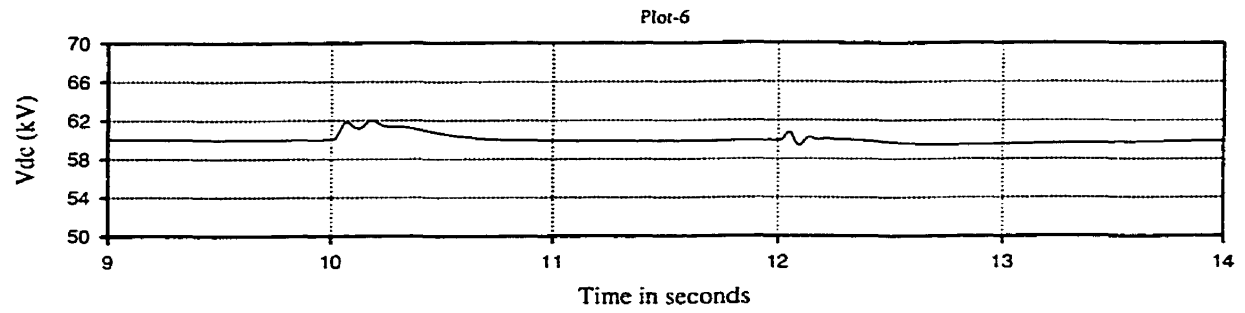
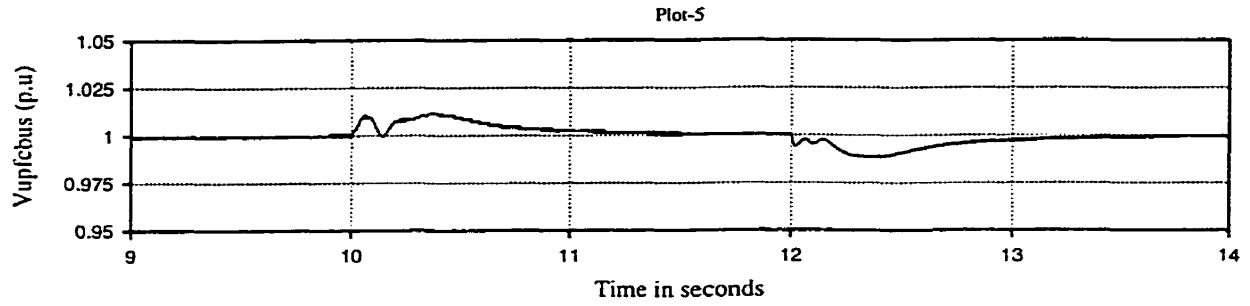


Fig.10.7 Step response with reactive power coordination controller. (contd.)

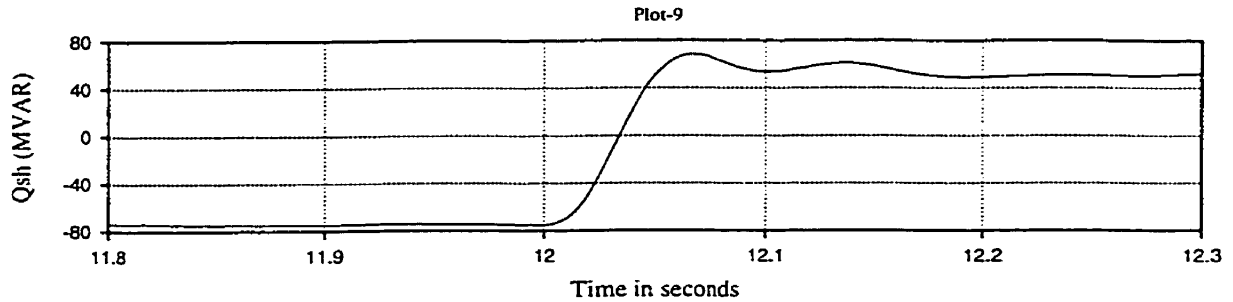


Fig.10.7 Step response with reactive power coordination controller.

125 MVAR. It is seen from plot-1 of Fig.10.7 that the real power flow is not affected much due to step changes in transmission line reactive power flow reference. It is seen from plot-3 and plot-4 of Fig.10.7 that the transmission line reactive power response has been slightly affected though not significantly due to the inclusion of the reactive power coordination controller. Comparing plot-3 and plot-4 of Fig.10.5 and plot-3 and plot-4 of Fig.10.7 between the time 10 s, 10.1 s and 12 s, 12.1 s, it is seen that the transmission line reactive power rises much faster with reactive power coordination controller than without it. It should also be observed that the transmission line reactive power reaches 90% of its steady state value within 100 ms (-20 MVAR for step change from 125 MVAR to -35 MVAR and 110 MVAR for step change from -35 MVAR to 125 MVAR) with reactive power coordination controller as compared to 150 ms without reactive power coordination controller. Plot-5 of Fig.10.7 shows the UPFC bus voltage profile ($V_{upfcbus}$). It is seen that at 10 s, the UPFC bus voltage ($V_{upfcbus}$) changes by only 0.01 p.u. from 1.0 p.u. for a change in transmission line reactive power change of 160 MVAR as compared to 0.05 p.u. without reactive power coordination controller (see plot-5 of Fig.10.5). Thus the reactive power coordination controller has reduced the peak of the UPFC bus voltage

profile ($V_{upfcbus}$) and made it to gradually reach its steady state. It should be observed from plot-8 and plot-9 of Fig.10.7 that the shunt inverter reactive power (Q_{sh}) responds much faster as compared to without the coordination controller. The response of the shunt inverter reactive power (Q_{sh}) with coordination controller is about 100 ms (plot-8 and plot-9 of Fig.10.7) as compared to about 400 ms (plot-7 and plot-8 of Fig.10.5) without reactive power coordination controller.

At 12 s, the transmission line reactive power reference is changed from -35 MVAR to $+125$ MVAR. The UPFC bus voltage profile ($V_{upfcbus}$) is shown in plot-5 of Fig.10.7. At 12 s UPFC bus voltage drops to about 0.98 p.u. for a change in transmission line reactive power of 160 MVAR as compared to 0.95 p.u (plot-5 of Fig.10.5) without the reactive power coordination controller.

This simulation has shown that the inclusion of reactive power coordination controller helps in improving the UPFC bus voltage profile and reduce power quality problems (voltage sag / voltage rise). Further it helps in improving the response time of the shunt inverter to changes in transmission line reactive power reference, thereby improving the over all performance of the UPFC control system.

10.6 Power oscillation damping

A two-machine power system with UPFC shown in Fig.10.4 has been considered to study the performance of the UPFC control strategy and its control system under dynamic conditions. This power system was chosen over that in Fig.9.8 for the following reason. Inclusion of the reactive power controller for the UPFC for the power system in Fig.9.8 caused switching problems for the GTO's.

The voltage sources shown in Fig.10.4 have been converted into a second order system to model them as generators. This power system model has been chosen to depict a two-area power system. The sending and receiving end voltage source has been modeled as a second order transfer function as given below.

$$\frac{Output}{Input} = \frac{\omega_n^2}{1 + 2\zeta\omega_n s + \omega_n^2} \quad (10.1)$$

The sending end voltage source parameters are $\omega_h = 1.5$ Hz and $\zeta = 0.1$. For the receiving end voltage source, the parameters are $\omega_h = 1.3$ Hz and $\zeta = 0.05$. The input and output are phase angle of the sending end voltage source. This is because the second order function only tracks the input signal. For example, a step change of 1.0 p.u causes the output to reach 1.0 p.u based on the parameters ω_h and ζ . As seen the second order function with the above parameters represents an under damped system.

Fig.10.8 shows the response of the power system to a pulse change in the receiving end voltage source phase angle without UPFC. Plot-1 of Fig.10.8 shows the real power flow oscillations (P_{line}) in the transmission line without UPFC. The reactive power oscillations (Q_{line}) without UPFC is shown in plot-2 of Fig.10.8. The real power flow in the transmission line (P_{line}) before the disturbance is 400 MW. The peak of the real power flow in the transmission line (P_{line}) after the disturbance is about 550 MW. The initial reactive power flow in the transmission line (Q_{line}) is 80 MVAR. The positive peak of the reactive power flow (Q_{line}) in the transmission line after the disturbance is about 95 MVAR. The transmission line real and reactive power flows (P_{line}, Q_{line}) exhibit low damping.

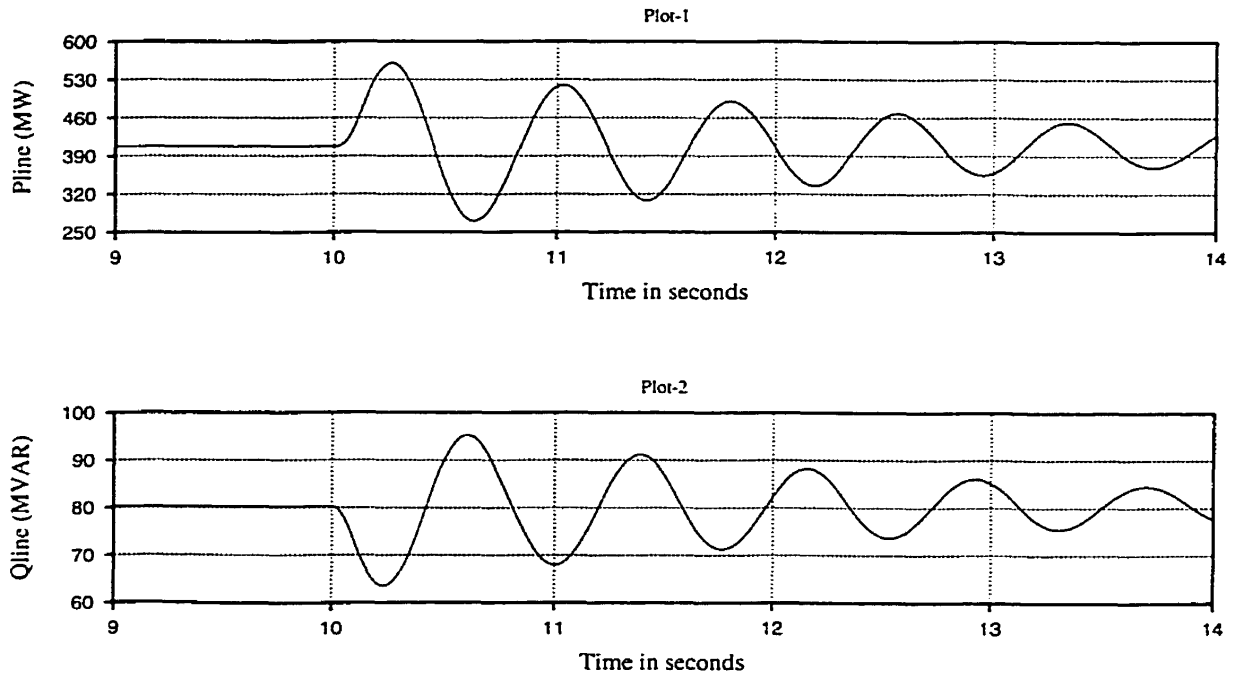


Fig.10.8 Real and reactive power oscillations without UPFC.

To study the performance of the UPFC control system under dynamic conditions, a pulse change in the phase angle of the receiving end voltage source is conducted to simulate a power oscillation arising from a control area. The control strategy used for UPFC is such that the shunt inverter of the UPFC controls the UPFC bus voltage ($V_{upfcbus}$), DC link capacitor voltage (V_{dc}) and the series inverter of the UPFC controls the real power flow in the transmission line (P_{line}), transmission line reactive power flow (Q_{line}). It should be noticed that the reactive power coordination controller does not take part in the damping of real and reactive power oscillations. This is because the input to the reactive power coordination controller is the transmission line reactive power reference. As long as the transmission line reactive power reference is fixed, the output of

the reactive power coordination controller is zero. The coordination controller is only active during transient changes in transmission line reactive power reference. Thus the reactive power coordination controller plays no role in damping reactive power oscillations in the transmission line.

Plot-1 through plot-4 of Fig.10.9 shows the real power (P_{line}), reactive power flow in the transmission line (Q_{line}), UPFC bus voltage ($V_{upfcbus}$) and the DC link capacitor voltage profile (V_{dc}) for the simulated disturbance. The disturbance is a pulse change in the receiving end voltage phase angle conducted at 10 s. The initial power flow in the 345 kV transmission line where the UPFC is installed is 450 MW. The shunt inverter of the UPFC controls the transmission line side bus voltage ($V_{upfcbus}$) at 1.0 p.u and the DC link capacitor voltage (V_{dc}) at 60 kV. The series inverter controls the real power flow in the transmission line (P_{line}) at 450 MW and the transmission line reactive power flow (Q_{line}) at 125 MVAR. Comparing plot-1 and plot-2 of Fig.10.8, and plot-1 and plot-2 of Fig.10.9, it is readily seen that the real and reactive power oscillations are well damped with UPFC. The real power and reactive flow in the transmission line takes about 2 s to damp as compared to more than 4 s without UPFC. Further, the UPFC bus voltage ($V_{upfcbus}$) as shown in plot-3 of Fig.10.9 is controlled to 1.0 p.u. The DC link capacitor voltage (V_{dc}) oscillations shown in plot-4 of Fig.10.9 are also well damped as the real power coordination controller has been included during this simulation. The DC link capacitor voltage oscillations also damp out in 2 s.

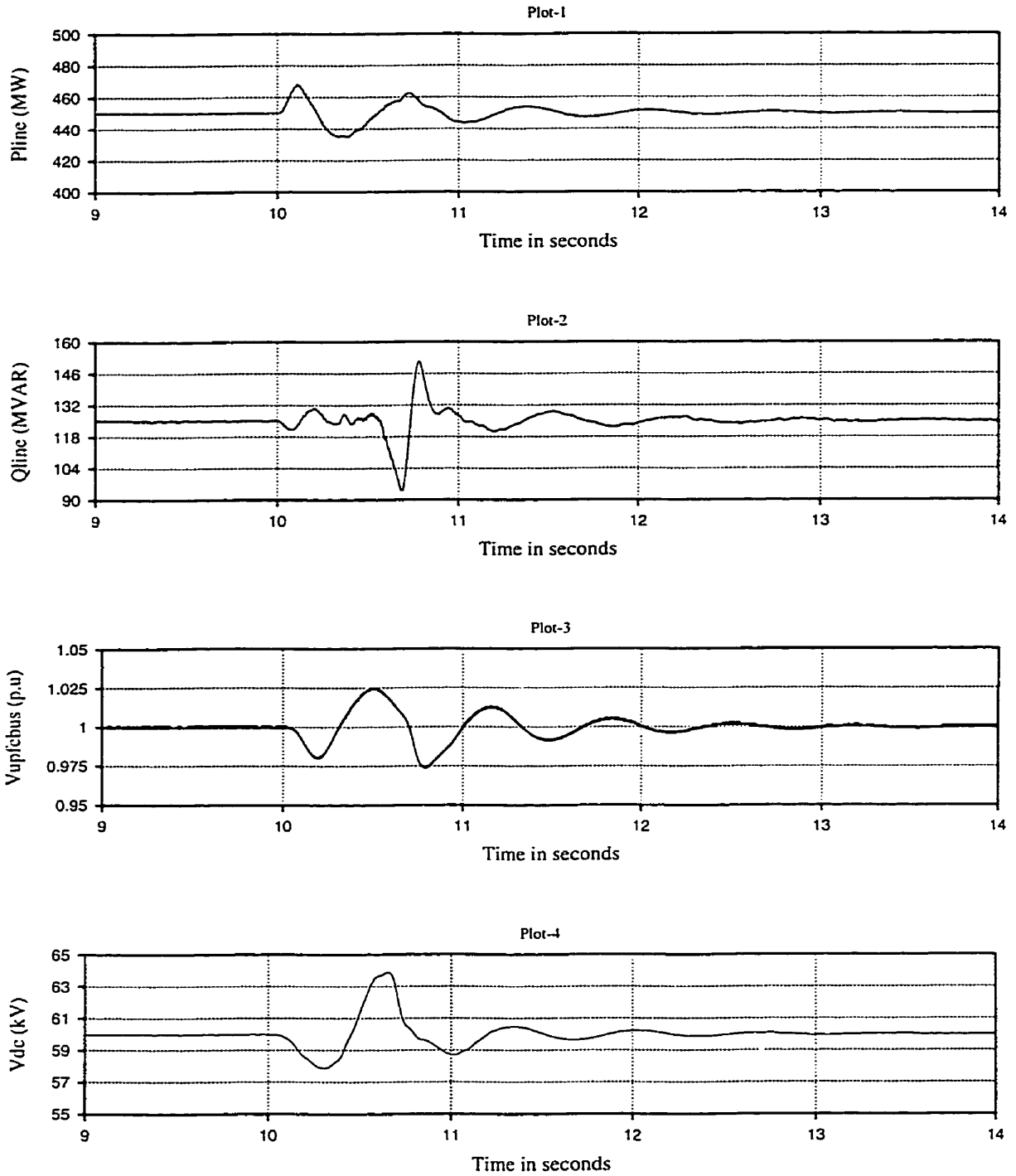


Fig.11.9. Real and reactive power oscillations with UPFC.

The improvement in power oscillation damping obtained in chapter–9 excluded the reactive power flow controller. This simulation has brought out the improvement in power oscillation damping when the UPFC is controlling the transmission line real power flow, reactive power flow, UPFC bus voltage and the DC link capacitor voltage simultaneously. Further, it should be noted that the real power coordination controller has been included in this simulation.

10.7 Summary

The need for reactive power coordination controller has been discussed. The first reason being that any request for transmission line reactive power change is actually supplied by the shunt inverter. The mechanism by which it works is that any change in transmission line reactive power reference is seen by the shunt inverter as a change in the UPFC bus voltage profile. Since the shunt inverter controls the UPFC bus voltage, an equal amount of reactive power change is observed in the shunt inverter reactive power to bring the UPFC bus voltage back to reference value. Thus the cause and the effect are on two portions of the UPFC. Hence there is a need to coordinate between the series and the shunt inverter controller with respect to transmission reactive power flow for better overall performance of the UPFC control system.

The second reason for requiring a reactive power coordination controller for a UPFC is related to power quality problems (voltage sag/voltage rise). Any change in transmission line reactive power reference causes the UPFC bus voltage to change significantly. If there are customers located close to or connected to the UPFC bus, they could experience voltage related problems.

A reactive power coordination controller has been proposed to reduce power quality problem and improve the over all performance of the UPFC control system. The input to the reactive power coordination controller is the transmission line reactive power reference. Any change in transmission line reactive power reference is translated into an equivalent reactive power reference for the shunt inverter thereby improving the response of the shunt inverter to transmission line reactive power requests. The reactive power coordination controller has been designed and tested on a two-machine power system. For a change in transmission line reactive power flow from 125 MVAR to -35 MVAR, the UPFC bus voltage excursion has been reduced from 0.05 p.u without the reactive power coordination controller to 0.01 p.u with reactive power coordination controller. Similarly, when the transmission line reactive power reactive is changed form -35 MVAR to 125 MVAR, the UPFC bus voltage excursion is reduced from 0.05 p.u to 0.02 p.u.

Power oscillations damping simulation have been conducted to show the improvement in damping while controlling the transmission line real power, transmission line reactive power, UPFC bus voltage and DC link capacitor voltage simultaneously. It should be noted that the reactive power coordination controller does not take part in power oscillation damping.

Chapter 11

A new control strategy for UPFC

11.0 Introduction

Chapter 9 has shown that the control system designed for the UPFC is able to control the transmission line real power flow (P_{line}), the UPFC bus voltage ($V_{upfcbus}$), and the DC capacitor voltage (V_{dc}) simultaneously. Further, the effect of in-phase component (V_{seD}) of the series injected voltage on shunt inverter reactive power (Q_{sh}) and transmission line real (P_{line})/reactive power flow (Q_{line}) have also been discussed in chapter 9. It has been shown that the in-phase component (V_{seD}) of the series injected voltage has considerable effect on the transmission line reactive power (Q_{line}) and the shunt inverter reactive power (Q_{sh}). In contrast, the in-phase component (V_{seD}) has insignificant effect on the series inverter reactive power (Q_{se}). Any increase/decrease in the transmission line reactive power (Q_{line}) due to in-phase component (V_{seD}) of the series injected voltage causes an equivalent increase/decrease in the shunt inverter reactive power (Q_{sh}). This suggests that the transmission line reactive power (Q_{line}) could directly

be controlled by the shunt inverter and eliminating the need for reactive power coordination controller.

A new control strategy has been proposed to achieve simultaneous control of four variables namely, transmission line real power flow (P_{line}), transmission line reactive power (Q_{line}), UPFC bus voltage ($V_{upfcbus}$) and the DC link capacitor voltage (V_{dc}). The associated control systems have been described. The performance of the new control strategy for UPFC will be studied based on its ability to track step input changes and provide power oscillation damping.

11.1 Proposed control strategy

To understand the proposed control strategy, consider a UPFC connected to a transmission line as shown in Fig.11.1. In the proposed strategy, the series inverter of a UPFC controls the real power flow in the transmission line (P_{line}) and the UPFC bus voltage ($V_{upfcbus}$). The shunt inverter of the UPFC controls the transmission line reactive power (Q_{line}) and the DC link capacitor voltage (V_{dc}).

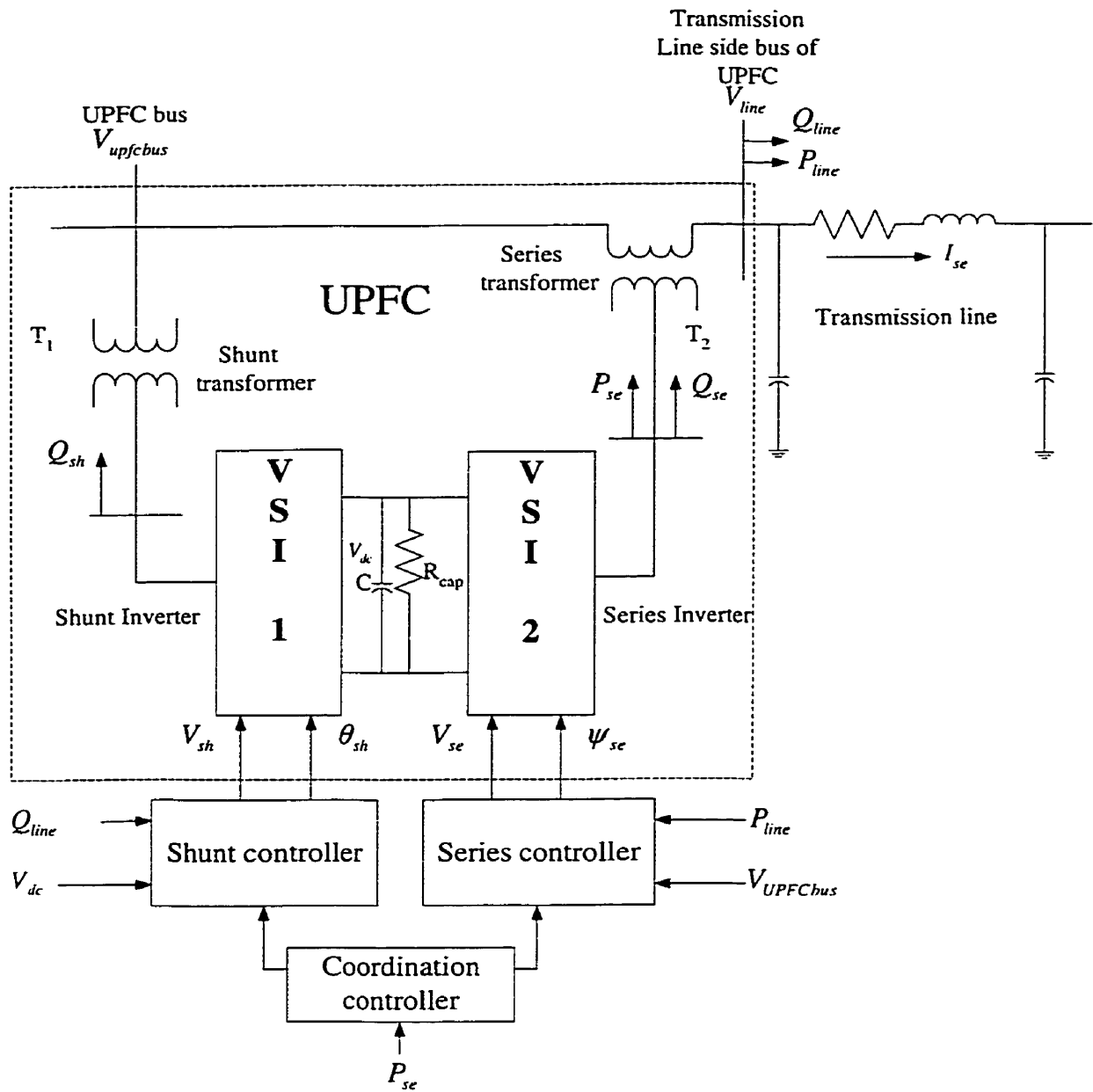


Fig.11.1 UPFC connected to a transmission line.

To achieve this type of control strategy for UPFC, the series inverter injected voltage is split into two components, one in-phase and the other in quadrature with the UPFC bus voltage. The quadrature component of the series injected voltage (V_{seQ}) controls the real power flow in the transmission line (P_{line}) and the in-phase component of the series injected voltage (V_{seD}) controls the UPFC bus voltage (V_{upfbus}).

The advantage with this strategy is that by controlling the transmission line reactive power flow directly by the shunt inverter, the need for reactive power coordination controller as designed in chapter-10 is eliminated. Looking from a different perspective, the burden of controlling the real and reactive power flow in a transmission line is split between the series and the shunt inverter respectively. By doing so, the shunt inverter can be used to manufacture and export required quantity of reactive power to the transmission line. The second advantage is that one could replace part of the shunt inverter reactive power capability by inexpensive shunt capacitors and help in reducing the cost of UPFC.

11.2 Control system for the new control strategy

11.2.1 Shunt inverter control system: The shunt inverter is controlled using the decoupled control system. Fig.11.2 shows the shunt inverter control system with the real power coordination controller. In the proposed strategy, the shunt inverter controls the transmission line reactive power flow (Q_{line}) and the DC link voltage (V_{dc}).

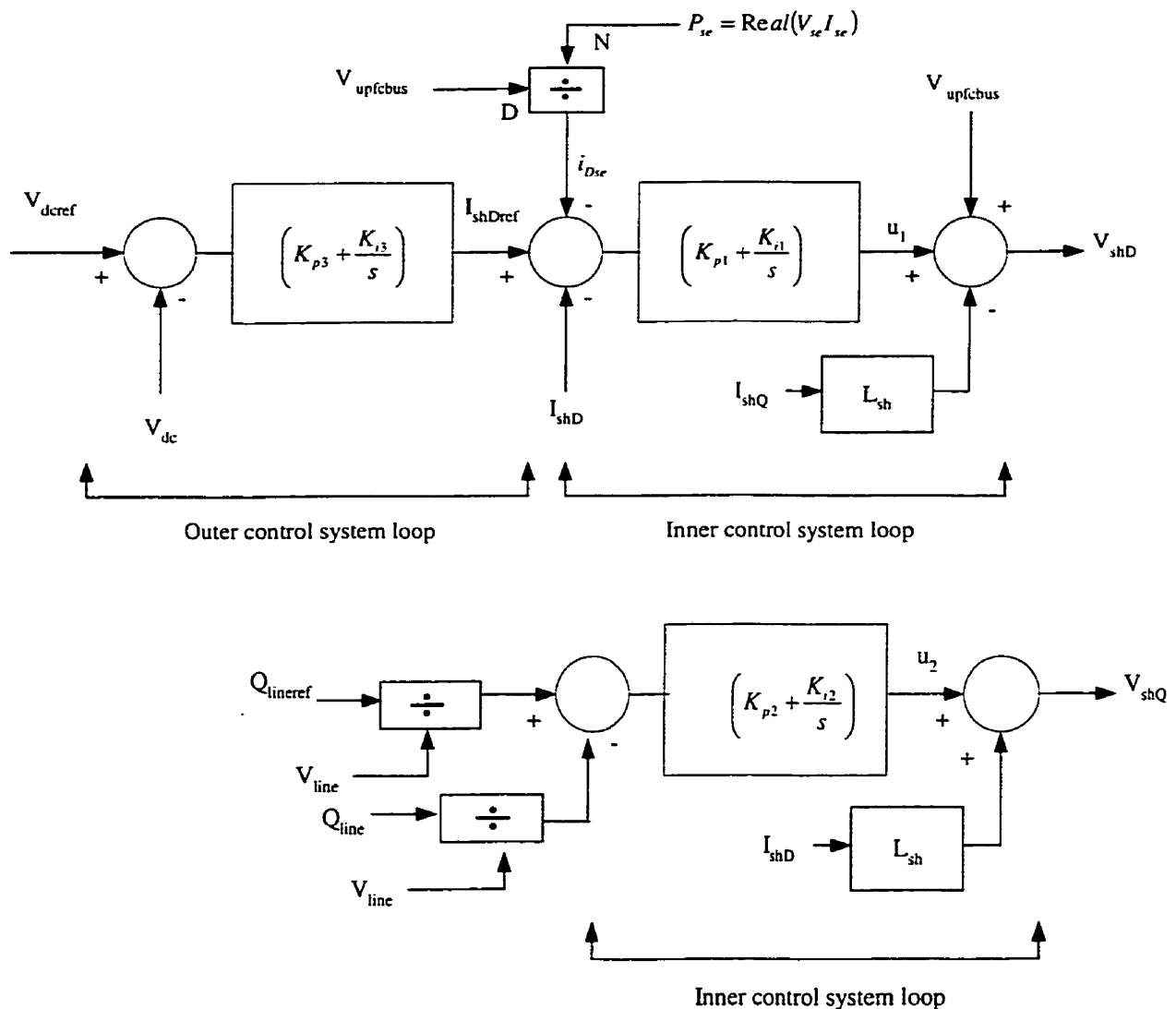


Fig.11.2. Shunt inverter control system with real power coordination controller.

It is seen from Fig.11.2 that the transmission line reactive power (Q_{line}) is controlled by the Q-axis shunt inverter voltage (V_{shQ}). The DC link capacitor voltage (V_{dc}) is controlled by the D-axis shunt inverter voltage (V_{shD}). The PI controller gains used for the shunt inverter controller are $K_{p1} = 5.0$, $K_{i1} = 21.367$, $K_{p2} = 0.2$, $K_{i2} = 5.0$, $K_{p3} = -1.0$, $K_{i3} = -2.0$.

11.2.2 Series inverter control system: The series inverter injected voltage is split into two components, one in-phase (V_{seD}) and the other in quadrature (V_{seQ}) with the UPFC bus voltage. The series inverter controls the real power flow in the transmission line (P_{line}) by injecting a voltage in quadrature (V_{seQ}) with the UPFC bus voltage ($V_{upfcbus}$). The in-phase component (V_{seD}) of the series injected voltage controls the UPFC bus voltage ($V_{upfcbus}$). Two fuzzy controllers have been implemented to control the real power flow in the transmission line (P_{line}) and the UPFC bus voltage ($V_{upfcbus}$). The knowledge base used for controlling the UPFC bus voltage is the same as that used for the real power flow control. Thus two variables have been controlled using the same knowledge base. On the other hand, a conventional PI controller could be used for controlling the UPFC bus voltage. But, conventional PI controller performance could deteriorate at operating conditions other than that at which it is designed. Fig.11.3 shows the two fuzzy controllers used for the series inverter. The gains for K_{v_e} , K_{v_e} and K_{v_u} are 1.0, 0.1 and -0.5 respectively. The gains for the real power flow control are given in section 8.5.

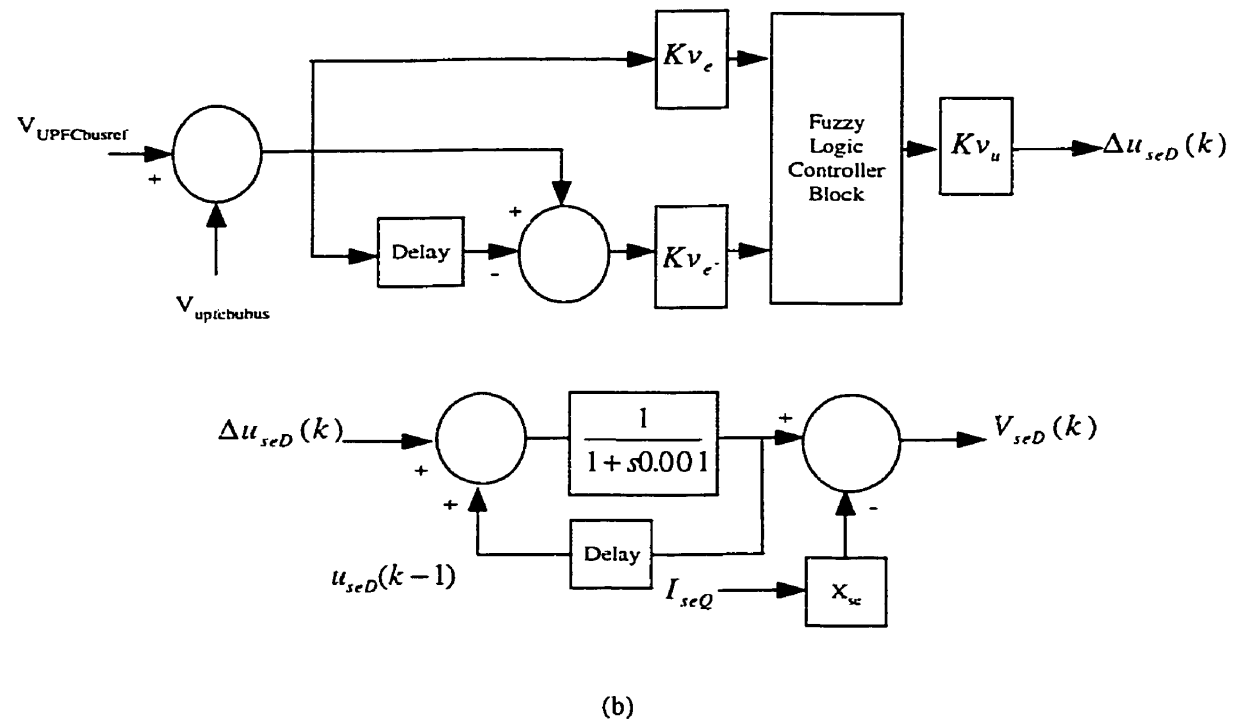
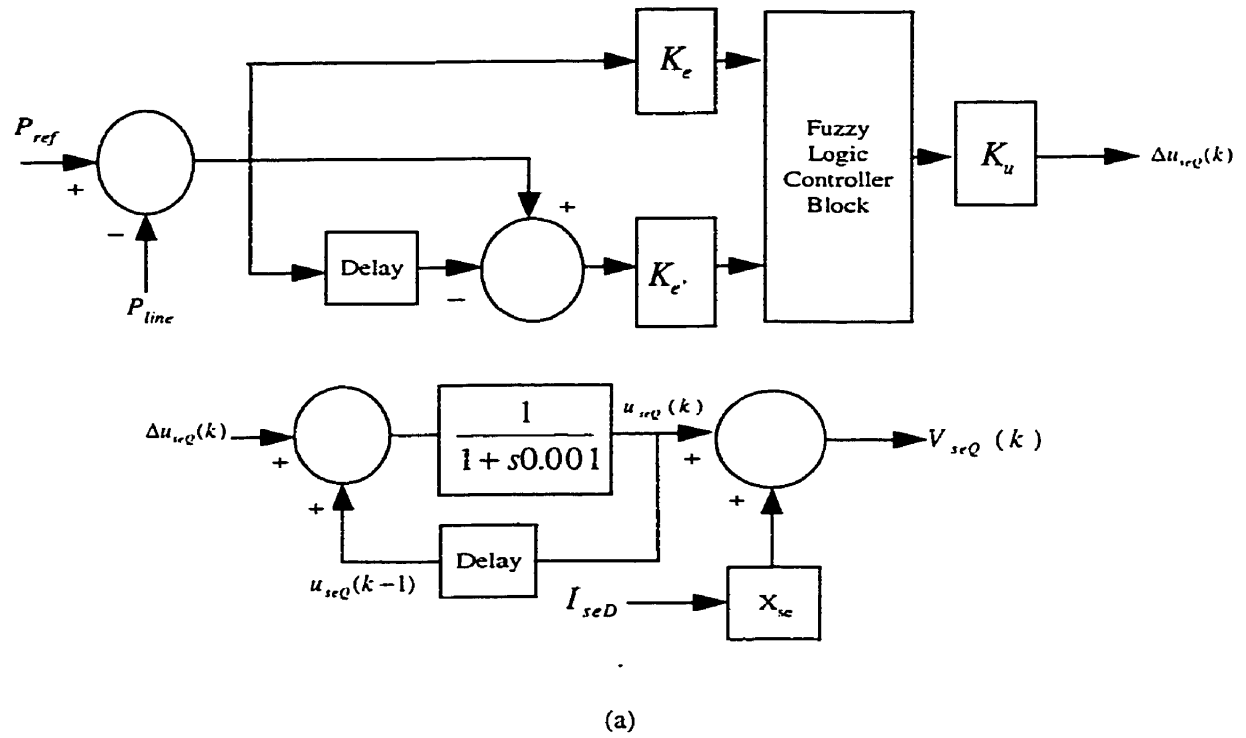


Fig.11.3 Series inverter control system for new control strategy.
 a) Transmission line real power flow controller.
 b) UPFC bus voltage controller.

11.3 Performance of the new control strategy

11.3.1 Step input response: To study the step input response of the power system with the proposed control strategy for UPFC, a power system shown in Fig.11.4 is considered. With the new control strategy, the UPFC controls the UPFC bus voltage ($V_{upfcbus}$), DC link capacitor voltage (V_{dc}), real power flow in the transmission line (P_{line}) and the transmission line reactive power flow (Q_{line}) simultaneously.

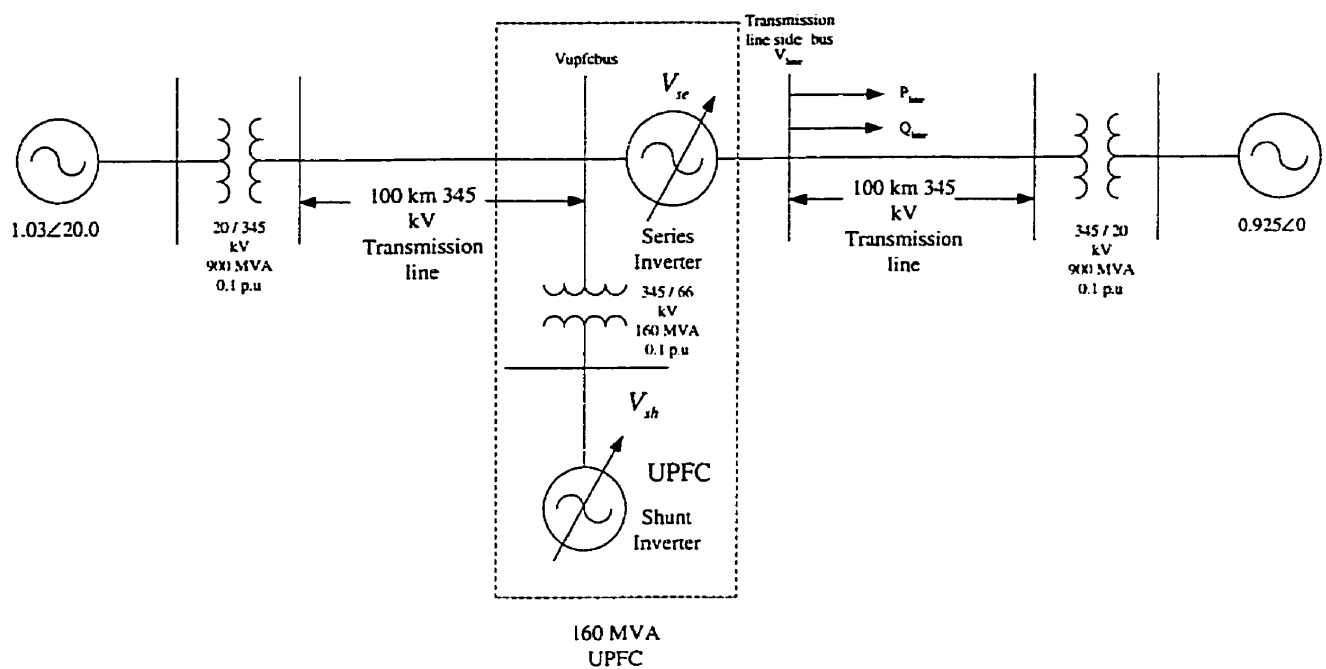


Fig.11.4 Two machine power system with UPFC.

a) Response to step change in transmission line real power flow reference:

The initial operating conditions for this simulation is that the series inverter controls the UPFC bus voltage ($V_{upfcbus}$) at 1.0 p.u and the transmission line real power flow (P_{line}) at 450 MW. The shunt inverter controls the transmission line reactive power flow (Q_{line}) at 125 MVAR and the DC link capacitor voltage (V_{dc}) at 60 kV. Fig.11.5 shows the response to step changes in the transmission line real power flow reference from 450 MW to 290 MW at 10 s and back to 450 MW at 12 s. Plot- 1 through plot-6 of Fig.11.5 shows the transmission line real power flow (P_{line}), transmission line real power flow (P_{line}) around 10 s, transmission line real power flow (P_{line}) around 12 s, transmission line reactive power flow (Q_{line}), UPFC bus voltage ($V_{upfcbus}$) and the DC link capacitor voltage (V_{dc}) respectively.

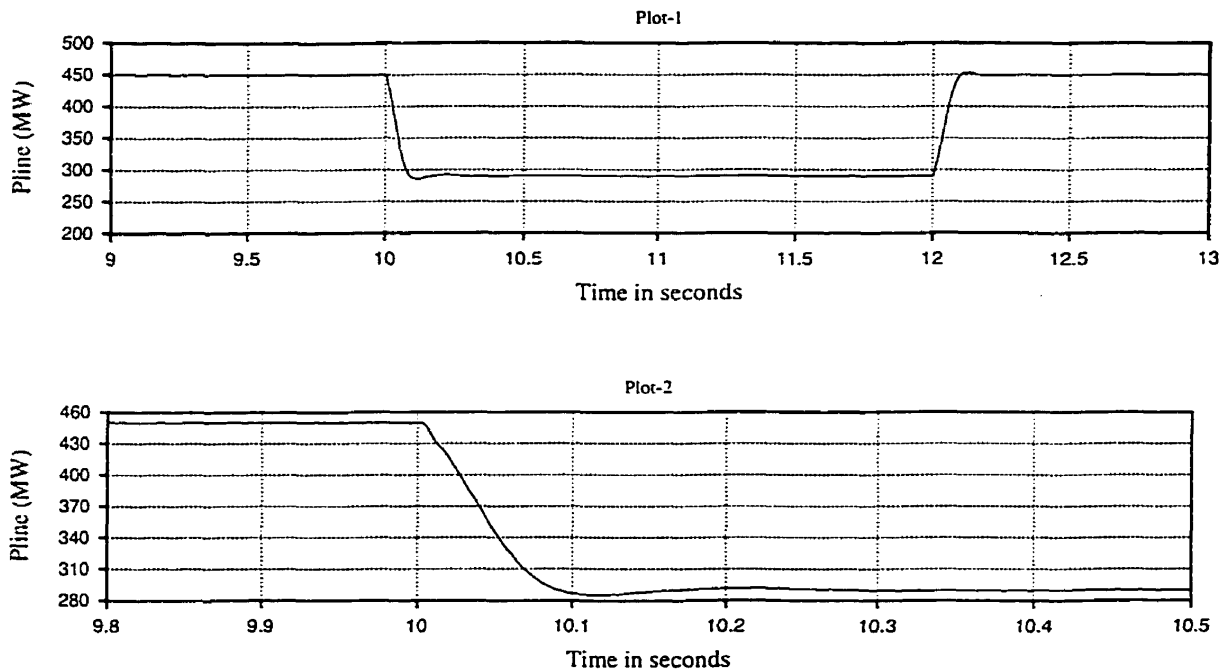


Fig.11.5 Response of the power system to step changes in transmission line real power flow reference.(contd)

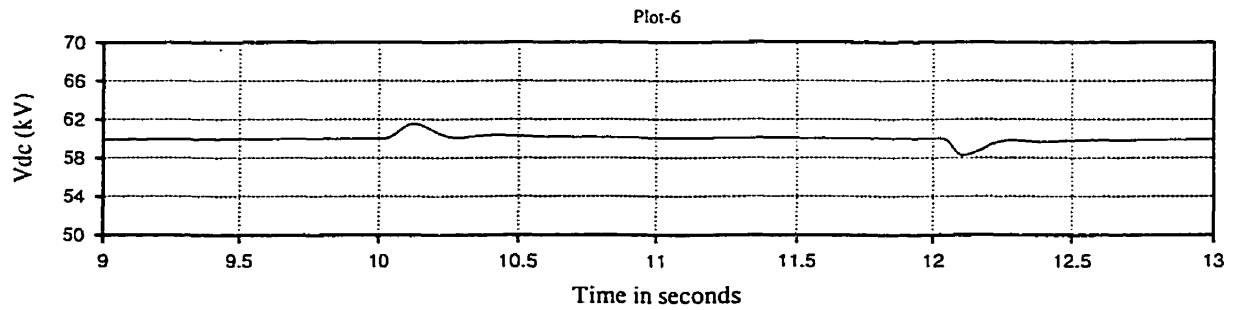
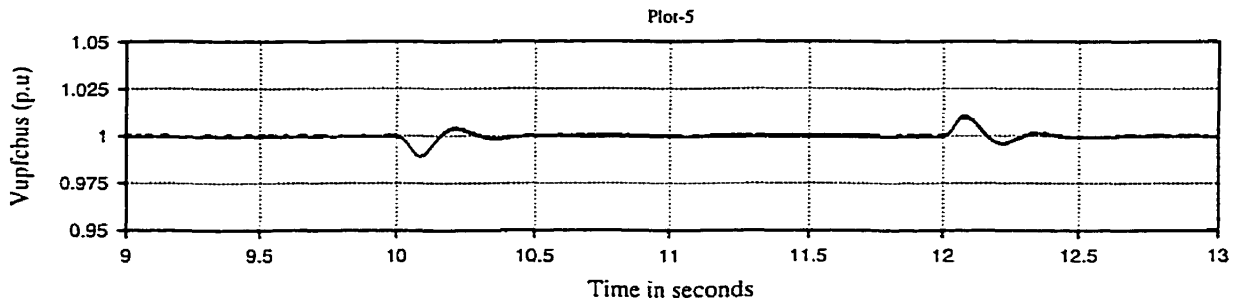
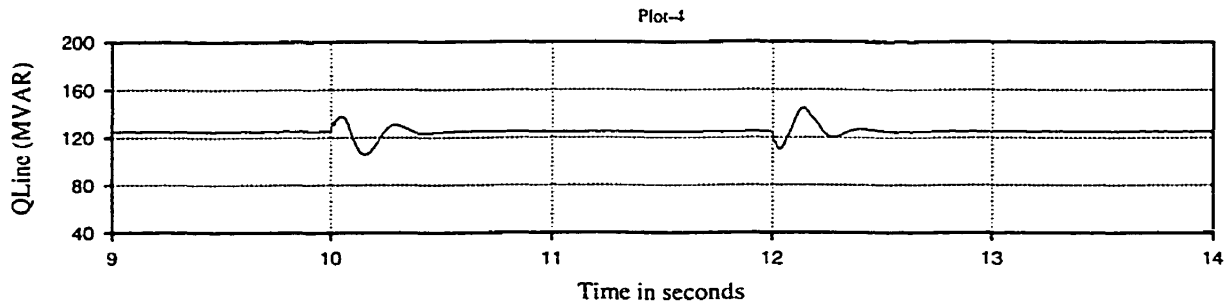
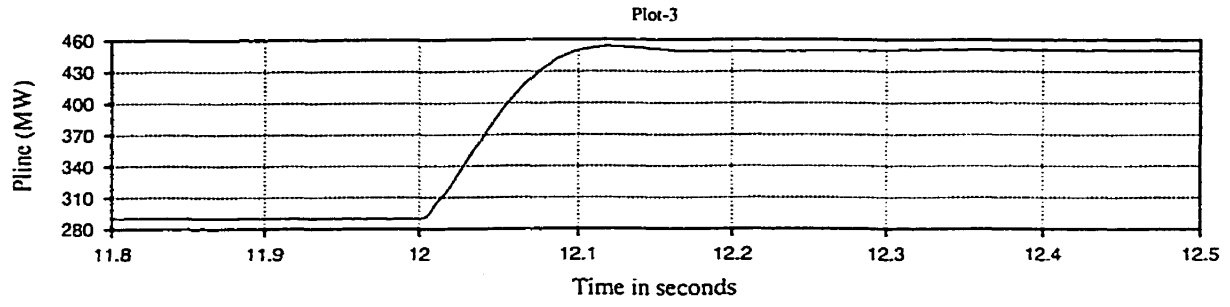


Fig.11.5 Response of the power system to step changes in transmission line real power flow reference.

Step changes were conducted at 10 s and 12 s to the transmission line real power flow reference. At 10 s, the real power flow reference was changed from 450 MW to 290 MW, a drop of 160 MW. Plot-2 of Fig.11.5 shows the transmission line real power flow around 10 s. It is seen that the transmission line real power flow changes from 450 MW to 290 MW in about 100 ms. At 10 s, the transmission line reactive power flow (plot-4 of Fig.11.5) does not deviate significantly from its reference value of 125 MVAR. The change in transmission line reactive power flow is less than 15 MVAR. Also the UPFC bus voltage (plot-5 of Fig.11.5) which is controlled by the series inverter does not deviate significantly from its reference value of 1.0 p.u. In addition, the DC link capacitor voltage (plot-6 of Fig.11.5) is controlled at 60 kV by the shunt inverter. At 12 s, the transmission line real power flow reference is changed from 290 MW to 450 MW, a change in 160 MW. Plot-3 of Fig.11.5 shows the real power flow around 12 s. It is seen that the transmission line real power flow changes from 290 MW to 450 MW in about 100 ms. The reactive power flow profile due to this step change are insignificant. The reactive power flow in the transmission line changes only by 20 MVAR for a step change in 160 MW of real power. Further, the UPFC bus voltage and the DC link capacitor voltage (plot-5 and plot-6) do not vary significantly from their reference values.

This simulation has brought out the decoupled nature of the control strategy. Further, it has also shown that it is possible to control the transmission line reactive power flow through the shunt inverter. In addition, it has also shown that the UPFC bus voltage profile and the DC link capacitor voltage do not significantly deviate much from their reference value.

b) Response to step change in receiving end voltage:

Fig.11.6 shows the response to a step change in receiving end voltage from 0.925 p.u (18.5 kV) to 1.03 p.u (20.6 kV) without UPFC. Plots-1 and plot-2 of Fig.11.6 shows the transmission line real power flow (P_{line}) and the transmission line reactive power flow (Q_{line}) without UPFC. The initial power flow in the transmission line is about 400 MW and 80 MVAR. The step change in receiving end voltage was conducted at 14 s.

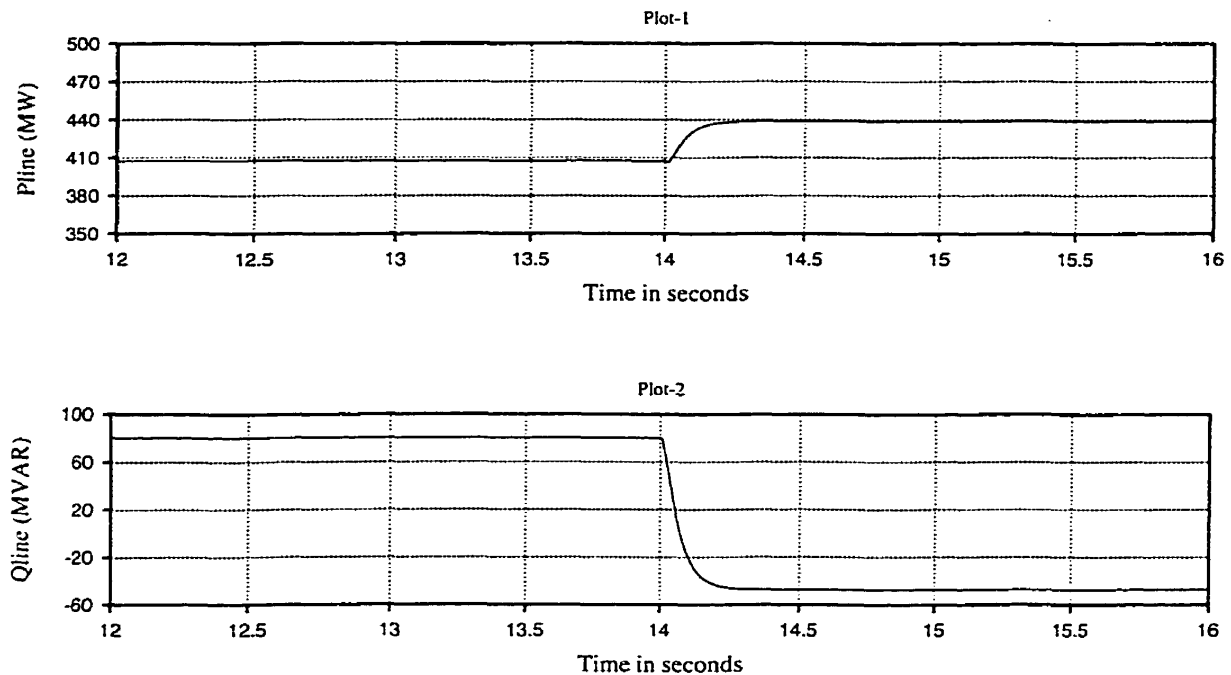


Fig.11.6 Response to step change in transmission line receiving end voltage from 0.925 p.u to 1.03 p.u.

It is observed from plot-1 of Fig.11.6 that the real power changes from 400 MW to 440 MW for a step change in receiving end voltage from 18.5 kV to 20.6 kV. The reactive power flow changes significantly from 80 MVAR to -45 MVAR (a change of 125 MVAR) for a step change in receiving end voltage from 18.5 kV to 20.6 kV. Thus the

above step change in receiving end voltage has significant effect on the transmission line reactive power.

Plot-1 through plot-9 of Fig.11.7 shows the transmission line real power flow (P_{line}), transmission line reactive power flow (Q_{line}), UPFC bus voltage profile ($V_{upfcbus}$), transmission line side bus voltage (V_{line}), DC link capacitor voltage (V_{dc}), shunt inverter reactive power (Q_{sh}), series inverter reactive power (Q_{se}), in-phase voltage component of the series voltage (V_{seD}) and series inverter real power (P_{se}) respectively with UPFC. The initial operating conditions for this simulation is that the series inverter controls the UPFC bus voltage ($V_{upfcbus}$) at 1.0 p.u and the transmission line real power flow (P_{line}) at 400 MW. The shunt inverter controls the transmission line reactive power flow (Q_{line}) at 80 MVAR and the DC link capacitor voltage (V_{dc}) at 60 kV.

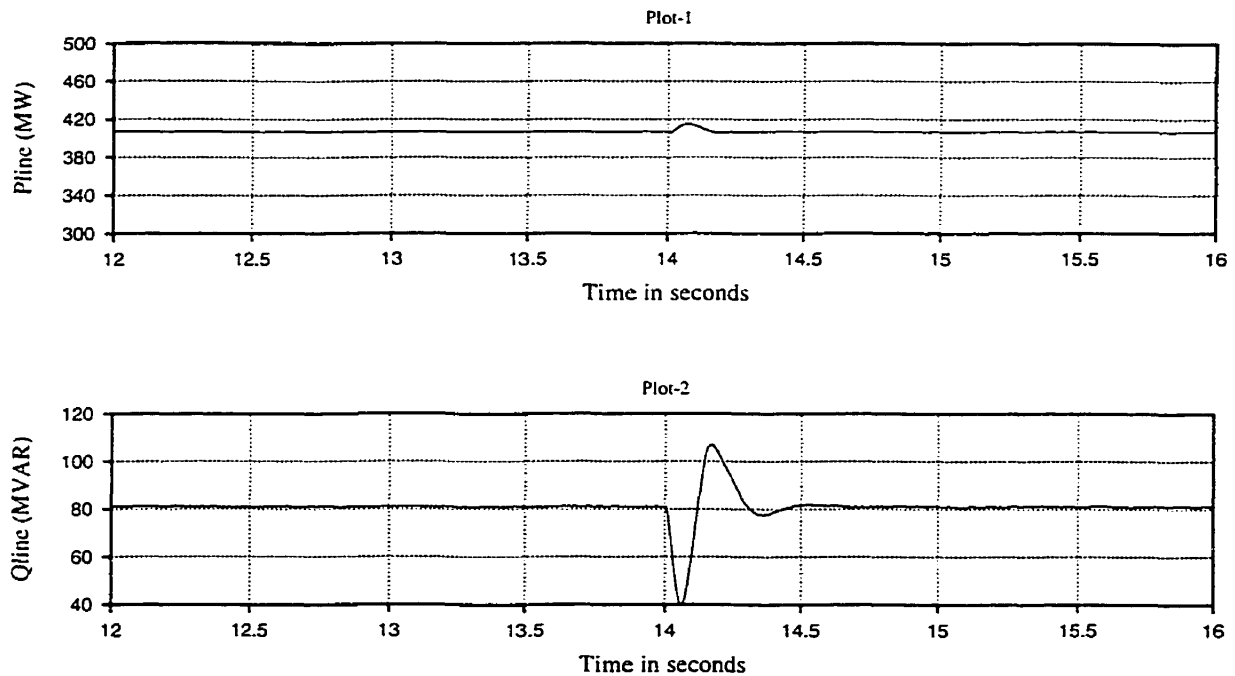


Fig.11.7 Response of the power system to step change in transmission line receiving end voltage from 0.925 p.u to 1.03 p.u. (Contd.)

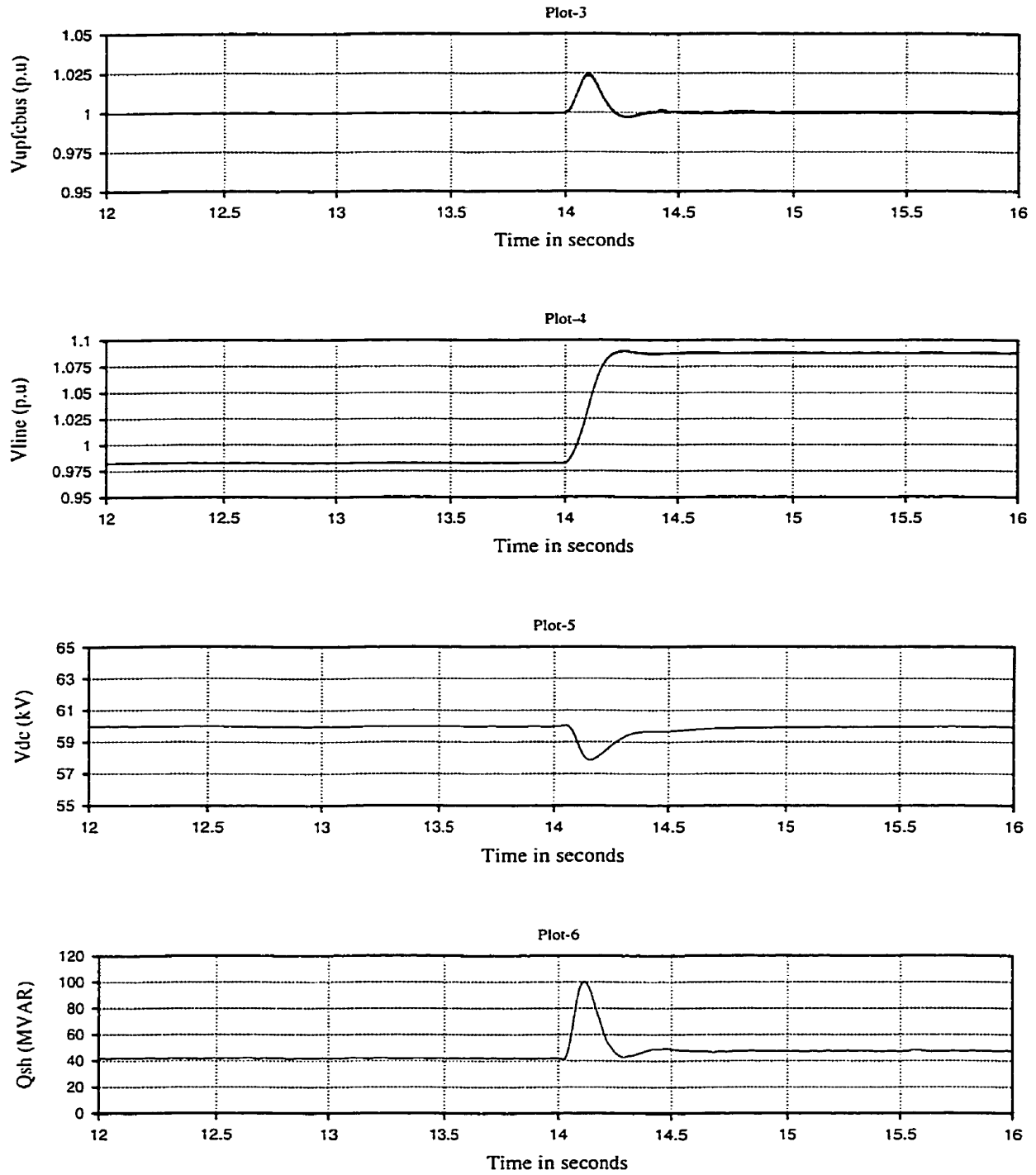


Fig.11.7 Response of the power system to step change in transmission line receiving end voltage from 0.925 p.u to 1.03 p.u. (Contd.)

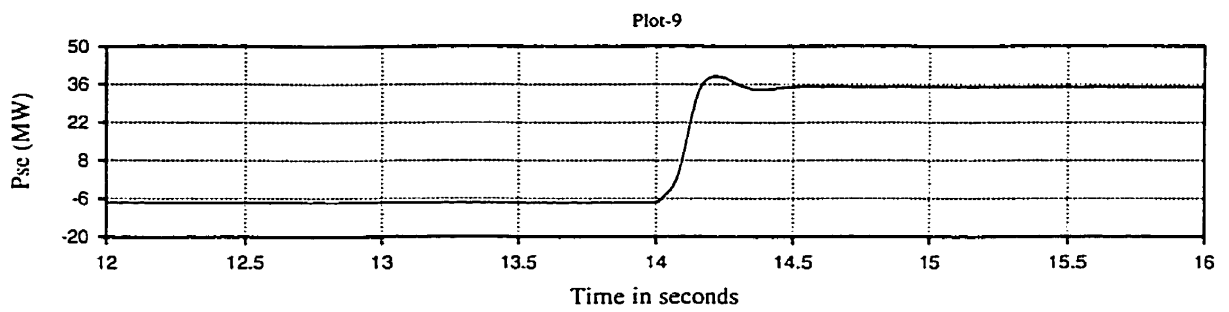
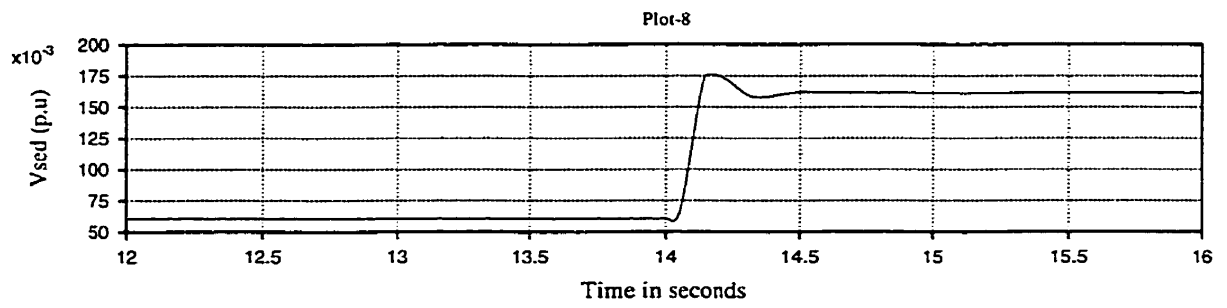
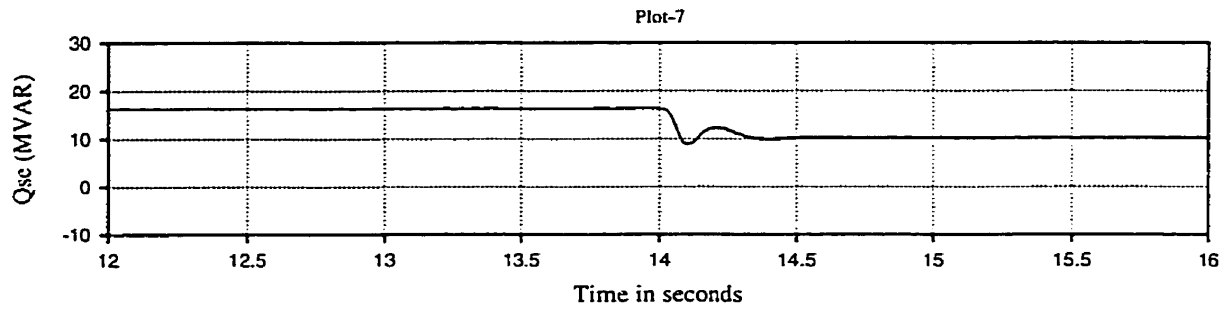


Fig.11.7 Response of the power system to step change in transmission line receiving end voltage from 0.925 p.u to 1.03 p.u.

At 14 s, a step change in receiving end voltage was conducted from 10.8 kV to 20.6 kV (from 0.925 p.u to 1.03 p.u). It is observed from Plot-1 of Fig.11.7 that the transmission line real power flow does not change significantly. On the other hand, the transmission line reactive power flow (plot-2 of Fig.11.7) shows a instantaneous change in transmission line reactive power flow from 80 MVAR to 40 MVAR. With this sudden change in transmission line reactive power, the shunt inverter increases its reactive power (plot-6 of Fig.11.7) instantaneously by about 60 MVAR. This is because the shunt inverter is controlling the transmission line reactive power flow. Subsequently, the transmission line reactive power flow is controlled to 80 MVAR. It should be observed from plot-4 of Fig.11.7 that the transmission line side bus voltage has increased from 0.98 p.u to 1.08 p.u. to keep the transmission line reactive power flow at 80 MVAR. Simultaneously, the in-phase component of the series injected voltage (plot-8 of Fig.11.7) has increased from about 0.06 p.u to 0.16 p.u.. This increase in in-phase series injected voltage has increased the series inverter real power generation from – 6 MW to about 35 MW (plot-9 of Fig.11.7). This is because of the interaction between the in-phase component of the series voltage and the transmission line current. It should also be observed that the series inverter reactive power (plot-7) does not show any significant change. With respect to the UPFC bus voltage (plot-3 of Fig.11.7) it should be seen that a step increase in receiving end voltage of about 0.1 p.u causes the UPFC bus voltage to instantaneously increase to 1.025 p.u from its reference value of 1.0 p.u. Subsequently, the UPFC bus voltage is brought back to 1.0 p.u. With this kind of disturbance, the DC link voltage (plot-5 of Fig.11.7) changes by only 2 kV which is controlled back to 60 kV by the shunt inverter.

This simulation has shown that the real and reactive power flow control has been decoupled. Further, it has also shown that the UPFC can be operated using this new control strategy.

11.4 Power oscillation damping

A two-machine power system with UPFC shown in Fig.11.4 has been considered to study the performance of the UPFC control strategy and its control system under dynamic conditions. This power system was chosen over that in Fig.9.8 for the following reason. Inclusion of the reactive power controller for the UPFC for the power system in Fig.9.8 caused switching problems for the GTO's. The voltage sources shown in Fig.11.4 have been converted into a second order system to model them as generators. This power system model has been chosen to depict a two-area power system. The sending and receiving end voltage source has been modeled as a second order transfer function as given below

$$\frac{Output}{Input} = \frac{\omega_n^2}{1 + 2\zeta\omega_n s + \omega_n^2} \quad (11.1)$$

The sending end voltage source parameters are $\omega_n = 1.5$ Hz and $\zeta = 0.1$. For the receiving end voltage source, the parameters are $\omega_n = 1.3$ Hz and $\zeta = 0.05$. The input and output are phase angle of the sending end voltage source. This is because the second order function only tracks the input signal. For example, a step change of 1.0 p.u causes the output to reach 1.0 p.u based on the parameters ω_n and ζ . As seen the second order function with the above parameters represents an under damped system.

Fig.11.8 shows the response of the power system to a pulse change in the receiving end voltage source phase angle without UPFC. Plot-1 and plot-2 of Fig.11.8 shows the transmission line real and reactive power flow respectively without UPFC. Plot-1 of Fig.11.8 shows the real power flow oscillations (P_{line}) in the transmission line without UPFC. The reactive power oscillations (Q_{line}) without UPFC is shown in plot-2 of Fig.11.8. The real power flow in the transmission line (P_{line}) before the disturbance is 400 MW. The peak of the real power flow in the transmission line (P_{line}) after the disturbance is about 550 MW. The initial reactive power flow in the transmission line (Q_{line}) is 80 MVAR. The positive peak of the reactive power flow (Q_{line}) in the transmission line after the disturbance is about 95 MVAR. The transmission line real and reactive power flows (P_{line}, Q_{line}) exhibit low damping.

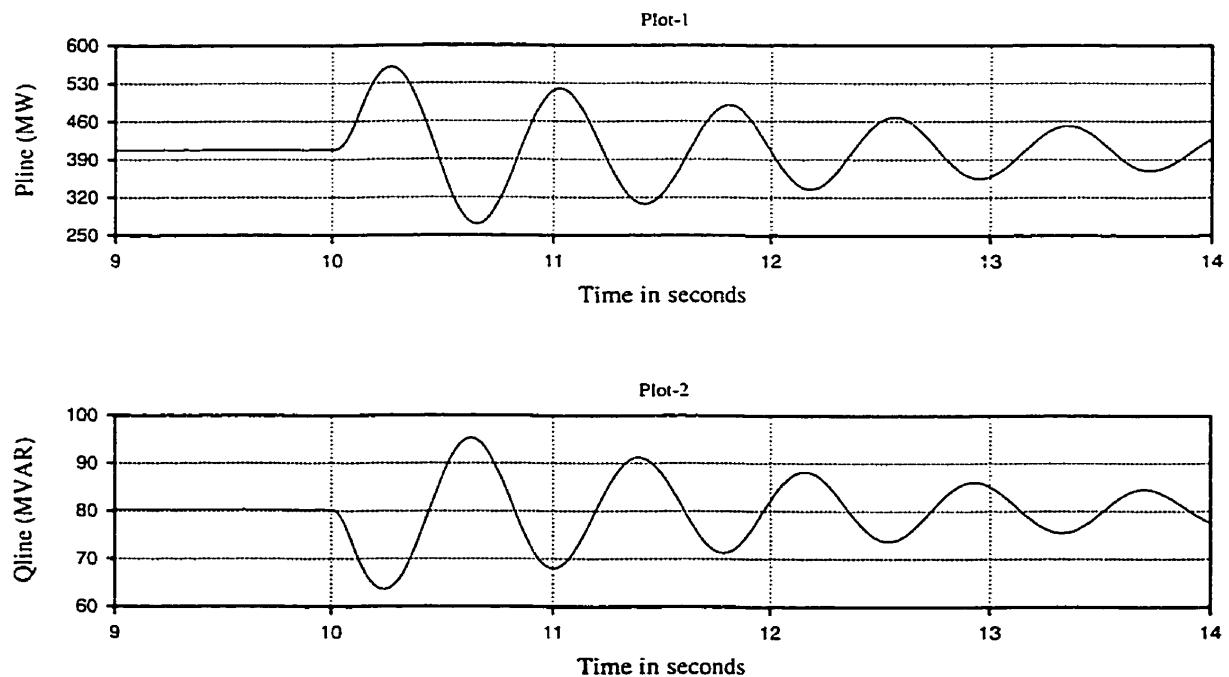


Fig.11.8 Response of the power system to pulse change in receiving end phase angle without UPFC.

Plot-1 through plot-4 of Fig.11.9 shows the response of the power system with UPFC for the above disturbance (pulse change in receiving end phase angle). Plot-1 through plot-4 shows the transmission line real power flow (P_{line}), transmission line reactive power flow (Q_{line}), UPFC bus voltage ($V_{upfcbus}$) and the DC link capacitor voltage (V_{dc}) respectively. It is seen that the UPFC has completely damped the real power oscillations (plot-1 of Fig.11.9) as compared to plot-1 of Fig.11.8. Further, the transmission line reactive power flow (plot-2 of Fig.11.9) shows oscillations which are about 20 MVAR. Eventually, the reactive power oscillations damp out. Plot-3 of Fig.11.9 shows no significant oscillations in the UPFC bus voltage. The DC link capacitor voltage (plot-4 of Fig.11.9) does show oscillations. But these are of small magnitude of less than 2 kV. These are also damped subsequently. This simulation has shown that the new control strategy for UPFC has improved the damping of power oscillations.

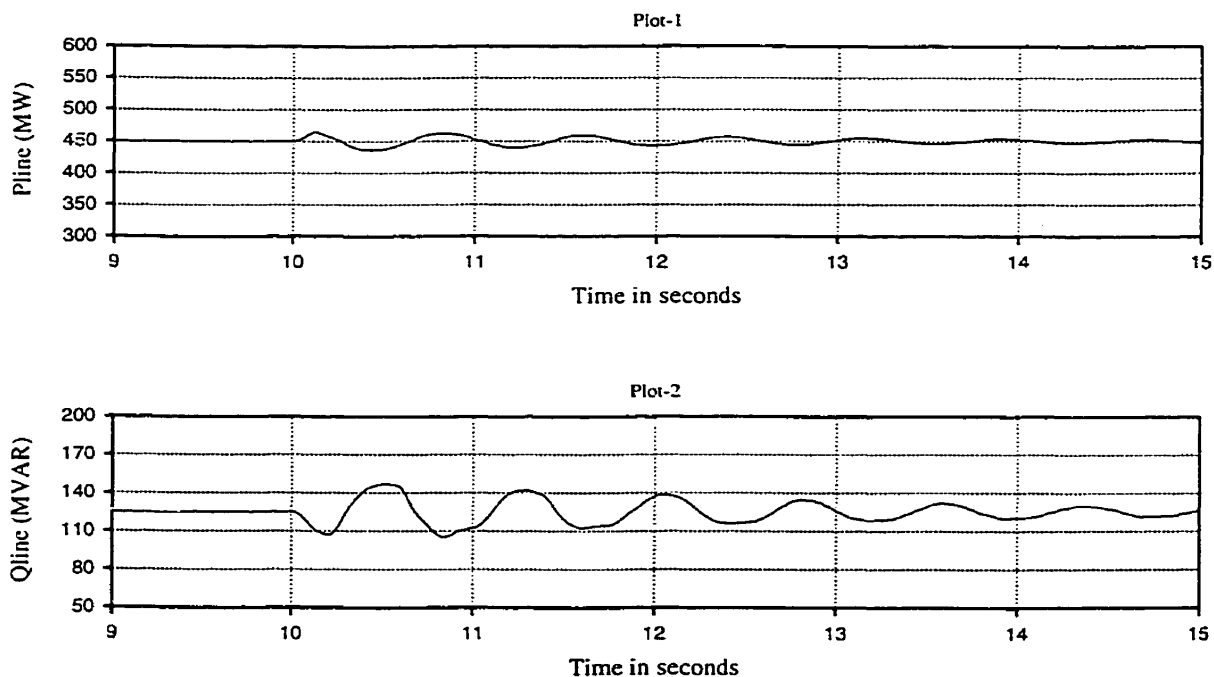


Fig.11.9 Response of the power system to pulse change in receiving end phase angle with UPFC. (Contd.)

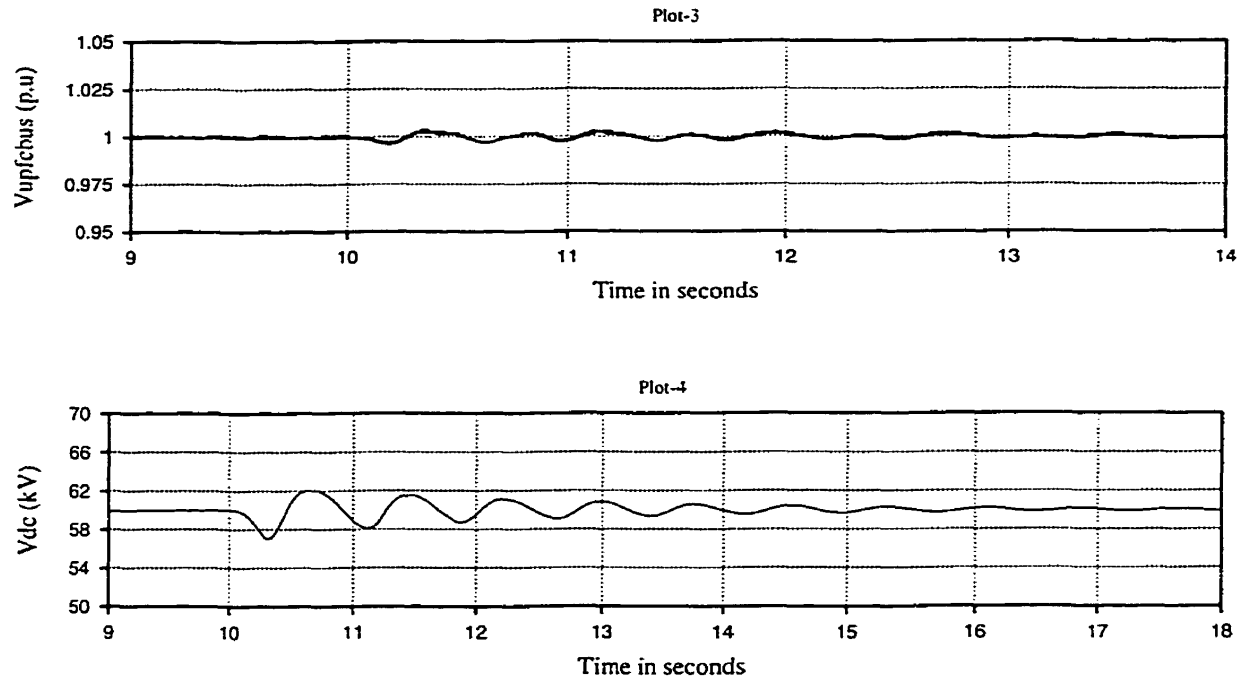


Fig.11.9 Response of the power system to pulse change in receiving end phase angle with UPFC.

11.5 Summary

A new control strategy has been proposed to achieve the simultaneous control of four variables namely, transmission line real power flow (P_{line}), transmission line reactive power (Q_{line}), UPFC bus voltage ($V_{upfcbus}$) and the DC capacitor voltage (V_{dc}). The performance of the UPFC with the new control strategy has been studied based on its ability to track step input changes and provide power oscillation damping.

In the proposed control strategy, the shunt inverter controls the transmission line reactive power flow (Q_{line}) and the DC link capacitor voltage (V_{dc}). The series inverter controls the transmission line real power flow (P_{line}) and the UPFC bus voltage ($V_{upfcbus}$). Simulations conducted have validated the proposed control strategy for UPFC operating under step input disturbances and dynamic conditions by being able to control the UPFC

bus voltage ($V_{UPFCbus}$), real power flow in the transmission line (P_{line}), transmission line reactive power flow (Q_{line}) and DC link capacitor voltage (V_{dc}) simultaneously.

The advantage with this strategy is that by controlling the transmission line reactive power flow directly by the shunt inverter, the need for reactive power coordination controller as designed in chapter-10 is eliminated. Looking from a different perspective, the burden of controlling the real and reactive power flow in a transmission line is split between the series and the shunt inverter respectively. By doing so, the shunt inverter can be used to manufacture and export required quantity of reactive power to the transmission line. The second advantage is that one could replace part of the shunt inverter reactive power capability by inexpensive shunt capacitors and help in reducing the cost of UPFC.

Chapter 12

Conclusions and Future Work

12.0 Conclusions

A control system/control strategy for UPFC has been designed in this thesis. PSCAD-EMTDC computer simulations have been conducted to show the improvement in power system damping with UPFC using the designed control system/control strategy.

A UPFC was constructed using the PSCAD-EMTDC software. The three major components of the UPFC are the shunt inverter and its transformers, series inverter and its associated transformers, and the DC link capacitor. A number of issues and problems have been encountered during the UPFC control system design process. The issues are concerning the ratings of the shunt/series inverters, their transformers and the DC link capacitor. These issues are discussed in this thesis. The operational problems involve the control system design for the integrated control of the real and the reactive power flow on transmission lines while simultaneously controlling the UPFC bus voltage and the DC link capacitor voltage.

The shunt inverter of a UPFC consists of four modules. Each module is a bridge circuit consisting of 6 GTOs. The series inverter consists of a set of two modules. These two modules are for the quadrature series injected voltage and the in-phase series injected voltage. Appropriate switching signals to the shunt inverter and series inverter modules have been implemented. The design process of the UPFC includes quantifying the ratings of the shunt, series inverter/transformers and the DC capacitor. The ratings of the shunt and series transformers/inverters ratings have been based on the SIL rating of the transmission line. A rating of 160 MVA for both series and shunt inverter were used. The design of the DC link capacitor has been based on the amount of energy that can be expended due to the interaction between the series inverter injected voltage and the transmission line current at SIL level. The DC link capacitor was rated at 60 kV, 3000uF for the system studied in this thesis.

To operate the UPFC, proper control strategy needs to be defined to control the transmission line real and reactive power flow while controlling the UPFC bus voltage and the DC link voltage simultaneously. Subsequently, to achieve the control strategy, proper control systems for the series and shunt inverters need to be designed.

In the case of shunt inverter, to control the UPFC bus voltage and the DC link capacitor voltage simultaneously, a de-coupled control system was designed. The de-coupled control system for the shunt inverter provides independent control loops to regulate the UPFC bus voltage and the DC link capacitor voltage. The design process for the de-coupled control system has been presented in this thesis. Proportional-integral controllers were used to control the UPFC bus voltage and the DC link capacitor voltage. The control system design was performed on a system where an inverter was connected

to a constant voltage source. This involved the linearization of the shunt inverter constant voltage system. Subsequently, linear control techniques were used to quantify the control gains. Step response tests were conducted to show the validity of the control system design.

With respect to the series inverter, the problem of low damping associated with the series inverter of a UPFC in controlling the real power flow in a transmission line is solved using a fuzzy controller. The knowledge base for the fuzzy controller has been developed based on a logical process. The logical process includes modeling the UPFC, conducting small-signal studies and subsequently performing time domain simulations. Time domain computer simulations provide a great deal of information on which the rules for the fuzzy controller has been developed. A method has been developed to implement a fuzzy controller in PSCAD-EMTDC software. The complexity in the fuzzy logic controller design for the series inverter of a UPFC is two-fold. The complexity in the design of a fuzzy controller for the series inverter of a UPFC lies in the fact that the fuzzy controller should not only improve the performance of the UPFC but also it should not cause instability. The instability could arise from the non-coordination of the series inverter with the shunt inverter operation. This two-fold problem has been kept in mind while designing the fuzzy logic controller (FLC) for the series inverter of the UPFC. Performance analysis that involves the step response and three-phase fault studies has been conducted to show the validity of the fuzzy control system designed.

DC link capacitor of a UPFC forms a very crucial component of a UPFC. This is because it supplies the necessary DC voltage for the operation of both the shunt and the series inverter. Loss of DC voltage during disturbances could lead to instability and

subsequent removal of UPFC from operation. Further, the real power demand of the series inverter is supplied by the shunt inverter. The real power demand of the series inverter arises due to the interaction between the series inverter injected voltage and the transmission line current. If the operation of the shunt inverter and that of the series inverter are not coordinated with respect to real power demand of the series inverter, it could lead to loss of DC voltage and subsequent removal of UPFC from operation. In order to facilitate proper operation between the series and the shunt inverter control system, a new real power coordination controller has been developed. The coordination controller provides a proper feedback between the series and shunt inverter control system. PSCAD-EMTDC computer simulations for the system under study in this thesis have shown that without the coordination controller, the DC link capacitor voltage drops to 40 kV as compared to 55 kV only with coordination controller for a three-phase fault disturbance. This proves the efficacy of the real power coordination controller designed.

One other problem associated with the operation of a UPFC that has been analyzed in this thesis is associated with transmission line reactive power flow control. All the control strategies found in literature have used the series inverter to control the transmission line reactive power flow. It has been found that the in-phase component of the series injected voltage used for controlling the transmission line reactive power flow in a transmission line, has a significant effect on the shunt inverter operation. Any change in reactive power flow in a transmission line, achieved by injecting an in-phase component of the series inverter voltage, is actually supplied by the shunt inverter. For example, a request for increase in transmission line reactive power flow by 50 MVAR, which is achieved by increasing the in-phase component of the series inverter voltage, is

actually supplied by the shunt inverter. The in-phase component of the series inverter injected voltage actually causes the UPFC bus voltage to decrease instantaneously. Since the shunt inverter is generally used to control the UPFC bus voltage, any decrease in UPFC bus voltage is converted into an equivalent increase in shunt inverter reactive power. The change in shunt inverter reactive power is reflected as a change in transmission line reactive power flow. This means that the cause and the effect are on two different parts of the UPFC. Further, any increase/decrease in transmission line reactive power flow has significant effect on the UPFC bus voltage. PSCAD-EMTDC simulations of the system under study in this research have shown that for an increase in transmission line reactive power of 160 MVAR, the UPFC bus voltage dips to about 0.95 p.u from 1.0 p.u. This could cause power quality problems for customers connected close to the location of UPFC. Based on the two reasons, one being that any increase/decrease in transmission line reactive power flow is actually supplied by the shunt inverter and the other related to power quality problem, a new reactive power coordination controller has been proposed and designed. PSCAD-EMTDC computer simulations have shown that without the reactive power coordination controller, the UPFC bus voltage varies between 1.05 and 0.95 p.u for a step decrease/increase of 160 MVAR in transmission line reactive power flow. With the reactive power coordination controller, the UPFC bus voltage variation has been reduced to 1.01 and 0.98 p.u respectively for a step change in transmission line reactive power of 160 MVAR.

PSCAD-EMTDC computer simulations have been conducted with the shunt inverter controlling the UPFC bus voltage and the DC link capacitor voltage and the series inverter controlling the transmission line real and reactive power flow to show the

improvement in power oscillation damping with and without the UPFC. PSCAD-EMTDC simulations have included the real and the reactive power coordination controller while conducting power oscillation damping studies. It has been found that UPFC enhances power oscillation damping.

Improvement in power oscillation damping has involved the series inverter controlling the real and reactive power flow in the transmission line with the shunt inverter controlling the UPFC bus voltage and the DC link capacitor voltage. With this strategy, it has been mentioned earlier that increase/decrease in the transmission line reactive power achieved by injecting an in-phase voltage by the series inverter is actually supplied by the shunt inverter. Thus the cause and the effect are on two portions of the UPFC. The cause being the injection of in-phase series voltage by the series inverter and the effect is seen as a change in shunt inverter reactive power. This represents an indirect control with respect to transmission line reactive power flow. A new direct control of reactive power flow in a transmission line using the shunt inverter has been proposed in this thesis. In the proposed strategy, the series inverter controls the real power flow in the transmission line and the UPFC bus voltage. On the other hand, the shunt inverter controls the transmission line reactive power flow and the DC link capacitor voltage. By doing so, the burden of controlling the transmission line real power flow and transmission line reactive power flow is split between the series and the shunt inverter of the UPFC respectively. The advantage with this strategy is that one could replace the shunt inverter reactive power capability with inexpensive switched shunt capacitors and reduce the cost of UPFC. Further, with the proposed control strategy, the need for reactive power coordination controller is eliminated. PSCAD-EMTDC computer simulations have been

performed to show the validity of the proposed control strategy and to show the improvement in power oscillation damping.

12.1 Future work

The work completed in this thesis includes a complete control system design for UPFC and studying its performance. All the work done till now assumed that the system is balanced. Power systems in general are never balanced in the sense that the currents and the voltages do have negative and zero sequence components. Very little research has been done in the area of designing a control system and operating a UPFC under unbalanced condition. The future work will include the design of a control system that allows the UPFC to operate reliably under unbalanced power system conditions.

Appendix-1

Table A1-1. Network Data for SMIB

From Bus	To Bus	R	X	$B_c / 2$
2	6	0.0	0.1	0.0
6	3	0.04675	0.4566	0.02178
3	4	0.0	0.1	0.0
4	7	0.0935	0.9132	0.01089
3	5	0.0	0.1	0.0
3	7	0.0935	0.9132	0.01089
7	1	0.0	0.1	0.0

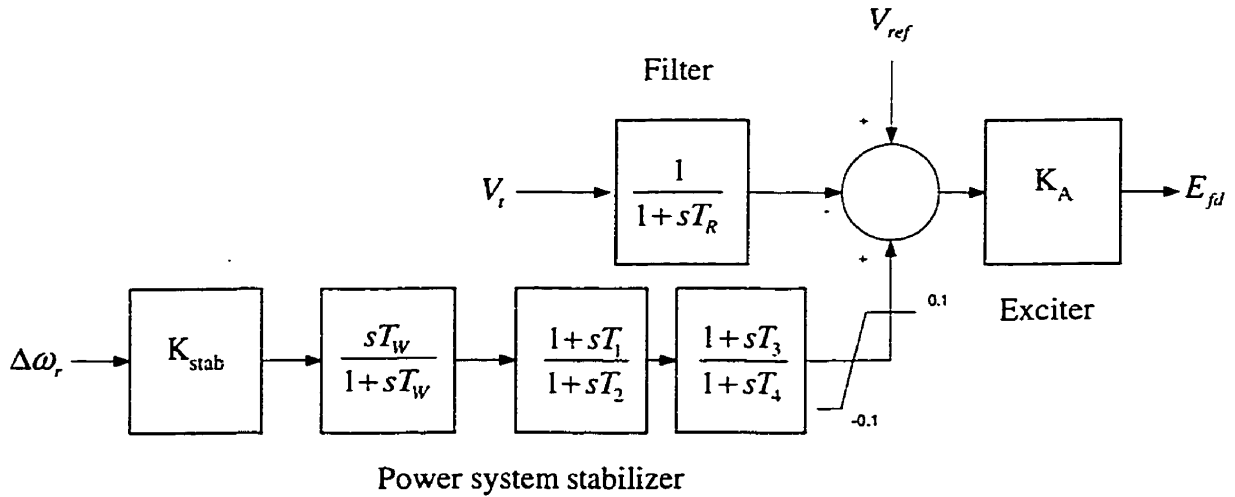
Table A1-2. Bus Data for SMIB

Bus Num/Type	Bus Voltage	Pgen+j Qgen	Pload + j Qload
1 (Infinite Bus)	1.0	0.0 + j 0.0	0.0 + j 0.0
2 (P-V Bus)	1.03	700 + j 0.0	0.0 + j 0.0
3 (Load Bus)	1.0	0.0 + j 0.0	0.0 + j 0.0
4 (Load Bus)	1.0	0.0 + j 0.0	0.0 + j 0.0
5 (Load Bus)	1.0	0.0 + j 150	0.0 + j 0.0
6 (Load Bus)	1.0	0.0 + j 0.0	200 + j 50
7 (Load Bus)	1	0.0 + j 0.0	0.0 + j 0.0

A 1-3. Generator Parameters

$$\begin{aligned}
 L_{adu} &= 1.6 \\
 L_{aqu} &= 1.5 \\
 ll &= 0.2 \\
 L_{ad} &= 0.835 L_{adu} \\
 L_{aq} &= 0.835 L_{aqu} \\
 L_{fd} &= 0.10667 \\
 r_{fd} &= 0.0005658 \\
 L_{1d} &= 0.1 \\
 r_{1d} &= 0.01768 \\
 L_{1q} &= 0.45652 \\
 r_{1q} &= 0.01297 \\
 L_{2q} &= 0.05833 \\
 r_{2q} &= 0.021662
 \end{aligned}$$

A 1-4. Power system stabilizer / Exciter model and parameters



$$K_{stab} = 9.5 \quad T_w = 10.0 \quad T_1 = 0.05 \quad T_2 = 0.02 \quad T_3 = 3.0 \quad T_4 = 5.4$$

A 1-5. UPFC parameters

DC link capacitor = 1000 μ F

Shunt inverter transformer is rated at 200 MVA, 230/66 kV, $X_1 = 0.0222$ per unit.

Series inverter transformer is rated at 44 MVA, 40/69 kV, $X_1 = 0.005$ per unit.

$R_{cap} = 48400 \Omega$.

A 1-6. Small-signal stability analysis

a) **Generator modeling:** The synchronous machine has been modeled in the d-q axis frame on its rotor with two damper windings on the q axis and one dampers on the d-axis. The state variables of the machine along with its algebraic equations are as given in reference [36]. The mechanical equations of the machine are

$$\frac{d\delta}{dt} = \omega_0 \Delta\omega_r$$
$$\frac{d\Delta\omega_r}{dt} = \frac{1}{2H} (T_m - T_e)$$

The rotor voltage equations are given by

$$e_{fd} = p\psi_{fd} + R_{fd}i_{fd}$$
$$0 = p\psi_{1d} + R_{1d}i_{1d}$$
$$0 = p\psi_{1q} + R_{1q}i_{1q}$$
$$0 = p\psi_{2q} + R_{2q}i_{2q}$$

The stator terminal voltage equations are related to the stator fluxes by

$$e_d = -\psi_q \omega_r - R_a i_d$$
$$e_q = \psi_d \omega_r - R_a i_q$$

The stator flux linkage equations are related to the currents by

$$\psi_d = -(L_{ad} + ll)i_d + L_{ad}i_{fd} + L_{ad}i_{1d}$$

$$\psi_q = -(L_{aq} + ll)i_q + L_{aq}i_{1q} + L_{aq}i_{2q}$$

The rotor flux linkages and the electromagnetic torque of the generator are

$$\psi_{fd} = L_{ffd}i_{fd} + L_{f1d}i_{1d} - L_{ad}i_d$$

$$\psi_{fd} = L_{ffd}i_{fd} + L_{f1d}i_{1d} - L_{ad}i_d$$

$$\psi_{1q} = L_{11q}i_{1q} + L_{aq}i_{2q} - L_{aq}i_q$$

$$\psi_{2q} = L_{aq}i_{1q} + L_{22q}i_{2q} - L_{aq}i_q$$

$$T_e = \psi_d i_q - \psi_q i_d \quad (\text{A 1.6.1})$$

The above set of differential and algebraic equations are linearized to obtain the machine state matrix in the form

$$\Delta \dot{X}_G = A_G \Delta X_G + B_G \Delta e_{Mdq} \quad (\text{A 1.6.2})$$

where

$$\Delta X_G = (\Delta \delta, \Delta \omega_r, \Delta \psi_{fd}, \Delta \psi_{1d}, \Delta \psi_{1q}, \Delta \psi_{2q})$$

$$\Delta e_{Mdq} = (\Delta e_d, \Delta e_q)$$

and A_G and B_G are constant matrices.

b) Power system stabilizer model: The power system stabilizer is represented with two lead-lag blocks. The block diagram with the transfer function of the PSS is given in Appendix-1. The linearized equations for the PSS can be put in the form

$$\Delta \dot{X}_{pss} = A_{pss} \Delta X_{pss} + B_{pss} \Delta e_{Mdq} \quad (\text{A 1.6.3})$$

The corresponding state variables for the PSS are

$$\Delta \dot{X}_{pss} = (\Delta V_1, \Delta V_2, \Delta V_3, \Delta V_5)$$

Linearizing equation 5.18 and combining it with equation (A 1.6.2) and (A 1.6.3) we get

$$\Delta \dot{X}_M = A_M \Delta X_M + B_M \Delta e_{Mdq} \quad (\text{A 1.6.4})$$

Where

$$\Delta \dot{X}_M = \left(\Delta \dot{X}_G, \Delta \dot{X}_{pss}, \Delta \dot{V}_{dc} \right)$$

A_M and B_M are constant matrices.

c) Network modeling: The frequency range of interest in this study is between 0.1 Hz and 2.0 Hz. Further, to reduce the complexity of the problem formulation, the network dynamics have been neglected. The loads have been represented as constant shunt admittance and combined into the network admittance matrix. The network is then reduced to include only the machine nodes and the UPFC nodes. At this moment, a simplification regarding the notation of the UPFC bus voltage ($V_{upfcbus}$) and the transmission line side bus voltage (V_{line}) have been made for building the complete state matrix. The UPFC bus voltage ($V_{upfcbus}$) has been represented as V_E and the transmission line side bus voltage (V_{line}) as V_F . Linearizing the network equations we get

$$\begin{aligned} \Delta I_{MDQ} &= K \Delta V_{MDQ} + L \Delta V_{EFDQ} + M \Delta V_{shDQ} \\ \Delta I_{EFDQ} &= O \Delta V_{MDQ} + P \Delta V_{EFDQ} + Q \Delta V_{shDQ} \\ \Delta I_{shDQ} &= R \Delta V_{MDQ} + S \Delta V_{EFDQ} + U \Delta V_{shDQ} \end{aligned} \quad (\text{A 1.6.5})$$

Subscripts D and Q represent the network real and the imaginary axes. The network equations have been put in the following format where subscripts 'M', 'EF', and 'sh' refer to the machine nodes, the nodes between which the series inverter is placed, and the

shunt inverter nodes respectively. Matrices K, L, M, O, P, Q, R, S and U are the corresponding elements of the network admittance matrix.

The connection matrices between the machine d, q axes and the network D, Q axes are given by the following equations.

$$\begin{aligned} e_d &= V_D \sin \delta - V_Q \cos \delta \\ e_q &= V_Q \sin \delta + V_D \cos \delta \end{aligned} \quad (\text{A 1.6.6})$$

Where V_D and V_Q are the network voltages. The transformation matrix can be written as

$$T = \begin{bmatrix} \sin \delta & -\cos \delta \\ \cos \delta & \sin \delta \end{bmatrix} \quad (\text{A 1.6.7})$$

Hence equation (A 1.6.6) can be written as

$$e_{Mdq} = TV_{MDQ} \quad (\text{A 1.6.8})$$

Linearizing equation (A 1.6.8) we can write,

$$\Delta e_{Mdq} = T_0 \Delta V_{MDQ} + T_v \Delta X_M \quad (\text{A 1.6.9})$$

The subscript 0 refers to the operating point at which it is linearised. T_v is a constant matrix.

The machine currents in the d, q axes are related to the network frame of reference by the transformation T .

$$\begin{aligned} i_{Md} &= I_{MD} \sin \delta - I_{MQ} \cos \delta \\ i_{Mq} &= I_{MQ} \sin \delta + I_{MD} \cos \delta \end{aligned} \quad (\text{A 1.6.10})$$

Linearizing equation (A 1.6.10) we get

$$\Delta i_{Mdq} = T_0 \Delta I_{MDQ} + T_i \Delta X_M \quad (\text{A 1.6.11})$$

The subscript 0 refers to the operating point at which it is linearized. T_i is a constant matrix.

Combining equations (A 1.6.4) and (A 1.6.9) relating the machine nodes with the network nodes we can write

$$\Delta \dot{X}_M = A_{MT} \Delta X_M + B_{MT} \Delta V_{MDQ} \quad (\text{A 1.6.12})$$

The shunt inverter voltage (V_{sh}) of the UPFC is also split into two components. One in-phase (V_{shp}) and the other in quadrature (V_{shq}) with the UPFC bus voltage phasor (V_E). The shunt inverter voltage (V_{sh}) can then be expressed in the form

$$\begin{aligned} V_{shD} &= V_{shp} \cos \delta_p + V_{shq} \cos \delta_q \\ V_{shQ} &= V_{shp} \sin \delta_p + V_{shq} \sin \delta_q \end{aligned} \quad (\text{A 1.6.13})$$

δ_p and δ_q are the angles made by the 'p' and the 'q' axis with the network D axis. (Refer Chapter-4, Fig.4.4)

Linearizing equation (A 1.6.13) we get

$$\Delta V_{shDQ} = SH_1 \Delta \delta_{pq} + SH_2 \Delta u \quad (\text{A 1.6.14})$$

The series inverter voltage can be expressed in the form

$$\begin{aligned} V_{seD} &= V_{sep} \cos \delta_p + V_{seq} \cos \delta_q \\ V_{seQ} &= V_{sep} \sin \delta_p + V_{seq} \sin \delta_q \end{aligned} \quad (\text{A 1.6.15})$$

Linearizing equation (A 1.6.15) we get

$$\Delta V_{seDQ} = SE_1 \Delta \delta_{pq} + SE_2 \Delta u \quad (\text{A 1.6.16})$$

where SH_1, SH_2 and SE_1, SE_2 are constant matrices and

$$\Delta u = (\Delta V_{shp}, \Delta V_{shq}, \Delta V_{seq}, \Delta V_{sep})$$

The expression for the variable δ_p and δ_q can be put in the form of

$$\delta_p = \text{angle}(V_E)$$

$$\delta_q = \text{angle}(V_E) + \frac{\pi}{2} \quad (\text{A 1.6.17})$$

where V_E is the voltage of the UPFC bus.

Linearizing equation (A 1.6.17) we get

$$\Delta\delta_{pq} = KPC\Delta V_{EFDQ} \quad (\text{A 1.6.18})$$

where KPC is a constant matrix.

It should be remembered that the variable I_{EFDQ} are the current injections at the buses between which the UPFC is connected. Referring to the Norton equivalent of the UPFC model as given in Chapter-4 Fig.4.3, the current injections at the bus E is given by $jV_{sem}Y_{EF}$ and the current injection at the bus F is given by $-jV_{sem}Y_{EF}$, where Y_{EF} is the admittance between the bus E and F in the Norton equivalent circuit. Y_{EF} is basically the admittance of the series transformer. Thus the expression for the current injection at bus 'E and F' are given by

$$I_{ED} + jI_{EQ} = (V_{seD} + jV_{seQ})jY_{EF} \quad (\text{A 1.6.19})$$

Similarly, the current injection at the bus 'F' is given by

$$I_{FD} + jI_{FQ} = -(V_{seD} + jV_{seQ})jY_{EF} \quad (\text{A 1.6.20})$$

Linearizing equations (A.1.6.19) and 9A.1.6.20) we get

$$\Delta I_{EFDQ} = I_{EFDQ1}\Delta V_{seDQ} \quad (\text{A 1.6.21})$$

Where I_{EFDQ1} is a constant matrix.

Substituting for ΔV_{seDQ} from equation (A 1.6.16) into (A 1.6.21) we get

$$\Delta I_{EFDQ} = I_{EFDQ2}\Delta\delta_{pq} + I_{EFDQ3}\Delta u \quad (\text{A 1.6.22})$$

Where I_{EFDQ2} and I_{EFDQ3} are constant matrices.

From equation (A.1.6.5) we have

$$\Delta I_{EFDQ} = O\Delta V_{MDQ} + P\Delta V_{EFDQ} + Q\Delta V_{shDQ} \quad (\text{A } 1.6.23)$$

Equation (A.1.6.23) can be expressed as

$$\Delta V_{EFDQ} = P^{-1}\Delta I_{EFDQ} - P^{-1}O\Delta V_{MDQ} - P^{-1}Q\Delta V_{shDQ} \quad (\text{A } 1.6.24)$$

Combining equations (A.1.6.14), (A.1.6.22) and (A.1.6.24) we get

$$\Delta V_{EFDQ} = V_{EFDQ1}\Delta\delta_{pq} + V_{EFDQ2}\Delta u + V_{EFDQ3}\Delta V_{MDQ} \quad (\text{A } 1.6.25)$$

where V_{EFDQ1} , V_{EFDQ2} and V_{EFDQ3} are constant matrices.

From equations (A.1.6.1) we can express the machine d-q axis currents as

$$\Delta i_{Mdq} = IN_1\Delta X_M + IN_2\Delta e_{Mdq} \quad (\text{A } 1.6.26)$$

where IN_1 and IN_2 are matrices.

Equating equation (A.1.6.11) with (A.1.6.26) and substituting for Δe_{Mdq} from equation (A.1.6.9) we can write

$$\Delta I_{MDQ} = IN_5\Delta X_M + IN_6\Delta V_{MDQ} \quad (\text{A } 1.6.27)$$

where IN_5 and IN_6 are matrices.

Equating equation ΔI_{MDQ} of (A.1.6.5) with (A.1.6.27) and substituting for ΔV_{EFDQ} and ΔV_{shDQ} from equation (A.1.6.14) and (A.1.6.25) we can write

$$\Delta V_{MDQ} = V_{MDQ1}\Delta X_M + V_{MDQ2}\Delta\delta_{pq} + V_{MDQ3}\Delta u \quad (\text{A } 1.6.28)$$

where V_{MDQ1} , V_{MDQ2} and V_{MDQ3} are matrices.

Substituting for ΔV_{MDQ} from equation (A.1.6.28) in (A.1.6.25) we can write

$$\Delta V_{EFDQ} = V_{EFDQ4}\Delta\delta_{pq} + V_{EFDQ5}\Delta u + V_{EFDQ6}\Delta X_M \quad (\text{A } 1.6.29)$$

where V_{EFDQ4} , V_{EFDQ5} and V_{EFDQ6} are constant matrices.

Substituting for ΔV_{EFDQ} in (A.1.6.18) we can write

$$\Delta\delta_{pq} = DQ_1\Delta u + DQ_2\Delta X_M \quad (\text{A } 1.6.30)$$

where DQ_1 and DQ_2 are matrices.

Substituting for $\Delta\delta_{pq}$ into equation (A.1.6.14) we can write

$$\Delta V_{shDQ} = SH_3\Delta u + SH_4\Delta X_M \quad (\text{A } 1.6.31)$$

where SH_3 and SH_4 are matrices.

Substituting for $\Delta\delta_{pq}$ into equation (A.1.6.16) we can write

$$\Delta V_{seDQ} = SE_3\Delta u + SE_4\Delta X_M \quad (\text{A } 1.6.32)$$

where SE_3 and SE_4 are matrices.

Substituting for $\Delta\delta_{pq}$ from equation (A.1.6.30) into equation (A.1.6.29) we can write

$$\Delta V_{EFDQ} = V_{EFDQ7}\Delta X_M + V_{EFDQ8}\Delta u \quad (\text{A } 1.6.33)$$

where V_{EFDQ7} and V_{EFDQ8} are constant matrices.

Substituting for $\Delta\delta_{pq}$ from equation (A.1.6.30) into equation (A.1.6.28) we can write

$$\Delta V_{MDQ} = V_{MDQ4}\Delta X_M + V_{MDQ5}\Delta u \quad (\text{A } 1.6.34)$$

where V_{MDQ4} and V_{MDQ5} are matrices.

Linearizing equation 5.18 expressing the DC link dynamics we can write

$$\Delta \dot{V}_{dc} = W_1\Delta X_M + W_2\Delta I_{seDQ} + W_3\Delta I_{shDQ} + W_4\Delta V_{seDQ} + W_5\Delta V_{shDQ} \quad (\text{A } 1.6.35)$$

where W_1 to W_5 are constant matrices. I_{seDQ} is the network axis transmission line current.

To find an expression for the transmission line current I_{seDQ} we have,

$$I_{seDQ} = [(V_{ED} + jV_{EQ}) + (V_{seD} + jV_{seQ}) - (V_{FD} + jV_{FQ})](-jY_{EF}) \quad (\text{A } 1.6.36)$$

Linearizing (A.1.6.36) we get

$$\Delta I_{seDQ} = I_{SEDQ1}\Delta V_{EFDQ} + I_{SEDQ2}\Delta V_{seDQ} \quad (\text{A } 1.6.37)$$

Combining equations (A.1.6.32), (A.1.6.33) and (A.1.6.37) we get

$$\Delta I_{seDQ} = I_{SEDQ3} \Delta X_M + I_{SEDQ4} \Delta u \quad (\text{A 1.6.38})$$

where I_{SEDQ3} and I_{SEDQ4} are matrices.

To find an expression for I_{shDQ} we have from equation (A.1.6.5)

$$\Delta I_{shDQ} = R \Delta V_{MDQ} + S \Delta V_{EFDQ} + U \Delta V_{shDQ} \quad (\text{A 1.6.39})$$

Combining equations (A.1.6.31), (A.1.6.33), (A.1.6.34) and (A.1.6.39) we get

$$\Delta I_{shDQ} = I_{SHDQ1} \Delta X_M + I_{SHDQ2} \Delta u \quad (\text{A 1.6.40})$$

where I_{SHDQ1} and I_{SHDQ2} are matrices.

Combining equations (A.1.6.31), (A.1.6.32), (A.1.6.35), (A.1.6.38), (A.1.6.40) we get

$$\Delta \dot{V}_{dc} = W_6 \Delta X_M + W_7 \Delta u \quad (\text{A 1.6.41})$$

where W_6 and W_7 are matrices.

Combining equations (A.1.6.12), (A.1.6.34) and (A.1.6.41) we can write

$$\Delta \dot{X}_M = A \Delta X_M + B \Delta u \quad (\text{A 1.6.42})$$

where A and B are matrices.

d) Output variables: The output variables of interest are the UPFC bus voltage (V_E), the DC link capacitor voltage (V_{dc}), real power flow in the transmission line (P_{line}) and the transmission line side bus voltage (V_F).

$$\Delta Y = [\Delta V_E, \Delta V_{dc}, \Delta P_{line}, \Delta V_F] \quad (\text{A 1.6.43})$$

The expressions for the above variables are as given below. Since ΔV_{dc} is a state variable, there is no need for any expression for it. The expression for the UPFC bus voltage V_E is given by

$$V_E = \sqrt{(V_{ED})^2 + (V_{EQ})^2} \quad (\text{A 1.6.44})$$

Linearizing equation (A.1.6.44) we can write

$$\Delta V_E = \left(\frac{V_{ED0}}{V_{E0}} \right)^2 \Delta V_{ED} + \left(\frac{V_{EQ0}}{V_{E0}} \right)^2 \Delta V_{EQ} \quad (\text{A 1.6.45})$$

The equation (A.1.6.45) can be put in the form

$$\Delta V_E = OP_1 \Delta V_{EFDQ} \quad (\text{A 1.6.46})$$

where OP_1 is a matrix.

Combining equations (A.1.6.33) and (A.1.6.46) we can write

$$\Delta V_E = OP_2 \Delta X_M + OP_3 \Delta u \quad (\text{A 1.6.47})$$

where OP_2 and OP_3 are matrices.

The expression for the real power flow in the line is as given below.

$$P_{line} = V_{FD} I_{seD} + V_{FQ} I_{seQ} \quad (\text{A 1.6.48})$$

Linearizing equation (A.1.6.48) we can write

$$\Delta P_{line} = V_{FD0} \Delta I_{seD} + \Delta V_{FD} I_{seD0} + V_{FQ0} \Delta I_{seQ} + \Delta V_{FQ} I_{seQ0} \quad (\text{A 1.6.49})$$

Equation (A.1.6.49) can be expressed as

$$\Delta P_{line} = OP_4 \Delta I_{seDQ} + OP_5 \Delta V_{EFDQ} \quad (\text{A 1.6.50})$$

where OP_4 and OP_5 are matrices.

Combining equations (A.1.6.33), (A.1.6.38) and (A.1.6.50) we can write

$$\Delta P_{line} = OP_6 \Delta X_M + OP_7 \Delta u \quad (\text{A 1.6.51})$$

where OP_6 and OP_7 are matrices.

The expression for the line side voltage V_F is given by

$$V_F = \sqrt{(V_{FD})^2 + (V_{FQ})^2} \quad (\text{A 1.6.52})$$

Linearizing equation (A.1.6.52) we can write

$$\Delta V_F = \left(\frac{V_{FD0}}{V_{F0}} \right)^2 \Delta V_{FD} + \left(\frac{V_{FQ0}}{V_{F0}} \right)^2 \Delta V_{FQ} \quad (\text{A 1.6.53})$$

The above equation can be put in the form

$$\Delta V_F = OP_8 \Delta V_{EFDQ} \quad (\text{A 1.6.54})$$

where OP_8 is a matrix.

Combining equations (A.1.6.33) and (A.1.6.54) we can write

$$\Delta V_F = OP_9 \Delta X_M + OP_{10} \Delta u \quad (\text{A 1.6.55})$$

where OP_9 and OP_{10} are matrices.

The output equations can be put in the standard form

$$\Delta Y = C \Delta X_M + D \Delta u \quad (\text{A 1.6.56})$$

where C and D are matrices.

e) Controller structure and description: In this control structure, the series inverter controls the real power flow by injecting a controllable magnitude of series voltage (V_{seq}) in quadrature with the UPFC bus voltage i.e V_E . The line side bus voltage (V_F) is controlled by injecting a component of the series voltage (V_{sep}) in phase with the UPFC bus voltage. The shunt inverter controls the DC link capacitor voltage by the variable V_{shq} . The UPFC bus voltage is controlled by adjusting V_{shp} . Four PI controllers have been used to control the UPFC bus voltage, DC link capacitor voltage, real power flow in the transmission line and the transmission line side voltage. The PI controllers have been included while forming the complete state matrix. The PI controller is given by the following equations [37].

$$\begin{aligned} \Delta \dot{X}_c &= \Delta Y - \Delta v \\ \Delta u &= -K_p (\Delta Y - \Delta v) - K_i \Delta X_c \end{aligned} \quad (\text{A 1.6.57})$$

Where Δv is the change in the reference which is zero in our case. K_p and K_i are respectively the proportional and integral constants and are diagonal constant matrices.

f) Closed loop state equation: Combining the following set of equations (A.1.6.42) (A.1.6.56) and (A.1.6.57) we can write

$$\begin{aligned} \Delta \dot{X}_T &= \begin{pmatrix} A - BK_{pi}C & -BK_{ii} \\ MC & -DK_{ii} \end{pmatrix} \Delta X_M + \begin{pmatrix} BK_{pi} \\ -M \end{pmatrix} \Delta v \\ \Delta Y &= (MC \quad -DK_{ii}) \Delta X_M + DK_{pi} \Delta v \end{aligned} \quad (\text{A 1.6.58})$$

where

$$\begin{aligned} \Delta X_T &= (\Delta X_M, \Delta X_c) \\ M &= (I + DK_p)^{-1} \\ K_{pi} &= (I + K_p D)^{-1} K_p \\ K_{ii} &= (I + K_p D)^{-1} K_i \end{aligned} \quad (\text{A 1.6.59})$$

and I is the identity matrix.

Closed loop stability requires that the eigen values of the matrix have negative real parts.

$$\Delta \dot{X}_T = \begin{pmatrix} A - BK_{pi}C & -BK_{ii} \\ MC & -DK_{ii} \end{pmatrix} \Delta X_M \quad (\text{A 1.6.60})$$

Appendix-2

Table A2-1. Network Data for MMPS

From Bus	To Bus	R	X	B_c/2
3	12	0.0	0.15	0.0
12	13	0.0225	0.225	0.0
13	2	0.0	0.15	0.0
13	5	0.009	0.09	0.0
5	6	0.0	0.15	0.0
5	7	0.0	0.15	0.0
5	11	0.09	0.9	0.00972
11	8	0.09	0.9	0.00972
6	14 (1)	0.135	1.35	0.01458
6	14 (2)	0.135	1.35	0.01458
14	8 (1)	0.135	1.35	0.01458
14	8 (2)	0.135	1.35	0.01458
8	10	0.009	0.09	0.0
10	9	0.0225	0.225	0.0
9	1	0.0	0.15	0.0
4	10	0.0	0.15	0.0

Table A2-2. Bus Data for MMPS

Bus Num/Type	Bus Voltage	Pgen+j Qgen	Pload + j Qload
1 (P-V Bus)	1.03	0.0 + j 0.0	0.0 + j 0.0
2 (P-V Bus)	1.01	700.0 + j 0.0	0.0 + j 0.0
3 (P-V Bus)	1.03	700.0 + j 0.0	0.0 + j 0.0
4 (P-V Bus)	1.01	700.0 + j 0.0	0.0 + j 0.0
5 (Load Bus)	1.0	0.0 + j 0.0	967.0 + j 100.0
6 (Load Bus)	1.0	0.0 + j 0.0	0.0 + j 0.0
7 (Load Bus)	1.0	0.0 + j 200.0	0.0 + j 0.0
8 (Load Bus)	1.0	0.0 + j 350.0	1767.0 + j 100.0
9 (Load Bus)	1.0	0.0 + j 0.0	0.0 + j 0.0
10 (Load Bus)	1.0	0.0 + j 0.0	0.0 + j 0.0
11 (Load Bus)	1.0	0.0 + j 0.0	0.0 + j 0.0
12 (Load Bus)	1.0	0.0 + j 0.0	0.0 + j 0.0
13 (Load Bus)	1.0	0.0 + j 0.0	0.0 + j 0.0
14 (Load Bus)	1.0	0.0 + j 0.0	0.0 + j 0.0

A 2-3. Generator Parameters

Each generator has the following parameters :

$$L_{adu} = 1.6$$

$$L_{aqu} = 1.5$$

$$ll = 0.2$$

$$L_{ad} = 0.835 L_{adu}$$

$$L_{aq} = 0.835 L_{aqu}$$

$$L_{fd} = 0.10667$$

$$r_{fd} = 0.0005658$$

$$L_{1d} = 0.1$$

$$r_{1d} = 0.01768$$

$$L_{1q} = 0.45652$$

$$r_{1q} = 0.01297$$

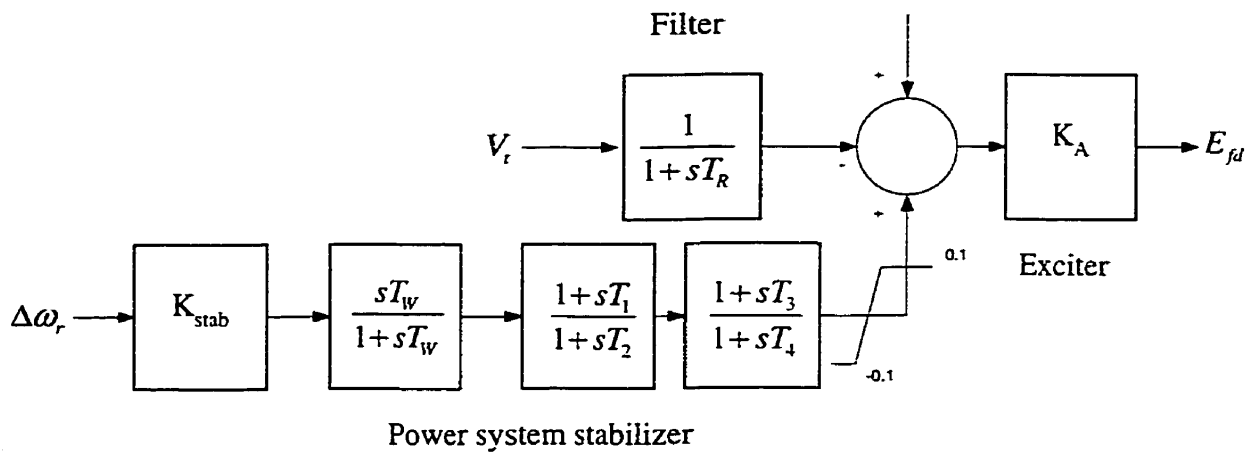
$$L_{2q} = 0.05833$$

$$r_{2q} = 0.021662$$

$$H(1) = 3.175 \quad H(2) = 3.5 \quad H(3) = 3.5 \quad H(4) = 3.175$$

A 2-4. Power system stabilizer / Exciter model and parameters

$$K_{stab} = 9.5 \quad T_W = 10.0 \quad T_1 = 0.05 \quad T_2 = 0.02 \quad T_3 = 3.0 \quad T_4 = 5.4$$



Each of the generators is equipped with an exciter and a PSS.

A 2-5. UPFC parameters

DC link capacitor = 1500 μ F

Shunt inverter transformer is rated at 200 MVA, 230/66 kV, $X_1 = 0.0333$ per unit.

Series inverter transformer is rated at 100 MVA, 40/69 kV, $X_1 = 0.01666$ per unit.

Appendix-3

Complete List of Eigen Values without UPFC for MMPS

Table A3-1

Eigen Number	Real Part	Imaginary Part
1	-55.001541	0.000000
2	-54.689795	0.000000
3	-53.951804	0.000000
4	-53.802533	0.000000
5	-13.200828	20.105156
6	-13.200828	-20.105156
7	-14.582910	16.710678
8	-14.582910	-16.710678
9	-36.409321	0.004691
10	-36.409321	-0.004691
11	-32.010030	0.000000
12	-31.047178	0.000000
13	-16.501603	6.261937
14	-16.501603	-6.261937
15	-16.677649	4.478219
16	-16.677649	-4.478219
17	-1.766684	11.308897
18	-1.766684	-11.308897
19	-1.706468	10.873114
20	-1.706468	-10.873114
21	-0.566010	6.011237
22	-0.566010	-6.011237
23	-3.778084	0.000000
24	-3.601547	0.000000
25	-3.077977	0.000000
26	-3.226662	0.000000
27	-1.048338	0.000000
28	-0.380414	0.000000
29	-0.000003	0.000000
30	-0.182976	0.000000
31	-0.101026	0.000000
32	-0.182533	0.000000
33	-0.101220	0.000000
34	-0.101315	0.000000
35	-0.182309	0.000000
36	-50.000000	0.000000
37	-50.000000	0.000000
38	-50.000000	0.000000
39	-50.000000	0.000000

Complete List of Eigen Values with UPFC for MMPS

Table A3-2

Eigen Number	Real Part	Imaginary Part
1	-54.887022	0.000000
2	-54.645614	0.000000
3	-53.881961	0.000000
4	-53.844345	0.000000
5	-36.491042	0.000000
6	-36.319191	0.000000
7	-32.111936	0.000000
8	-30.926111	0.000000
9	-13.656558	18.831364
10	-13.656558	-18.831364
11	-15.426986	15.771713
12	-15.426986	-15.771713
13	-16.551671	5.277632
14	-16.551671	-5.277632
15	-16.811923	4.505802
16	-16.811923	-4.505802
17	-1.807984	11.401098
18	-1.807984	-11.401098
19	-3.383374	11.095405
20	-3.383374	-11.095405
21	-1.643468	10.724337
22	-1.643468	-10.724337
23	-0.858612	5.896302
24	-0.858612	-5.896302
25	-3.688253	0.000000
26	-3.475911	0.000000
27	-3.110412	0.000000
28	-3.130289	0.000000
29	-0.913055	0.000000
30	-0.372795	0.033815
31	-0.372795	-0.033815
32	0.000000	0.000000
33	-0.193056	0.011402
34	-0.193056	-0.011402
35	-0.182315	0.000072
36	-0.182315	-0.000072
37	-0.097051	0.000000
38	-0.101334	0.000061
39	-0.101334	-0.000061
40	-0.100052	0.000000
41	-50.000000	0.000000
42	-50.000000	0.000000

43	-50.000000	0.000000
44	-50.000000	0.000000

Appendix-4 PSCAD-EMTDC parameters

A 4-1. Generator parameters

$$L_{adu} = 1.6$$

$$L_{aqu} = 1.5$$

$$ll = 0.2$$

$$L_{ad} = 0.835 L_{adu}$$

$$L_{aq} = 0.835 L_{aqu}$$

$$L_{fd} = 0.10667$$

$$r_{fd} = 0.0005658$$

$$L_{1d} = 0.1$$

$$r_{1d} = 0.01768$$

$$L_{1q} = 0.45652$$

$$r_{1q} = 0.01297$$

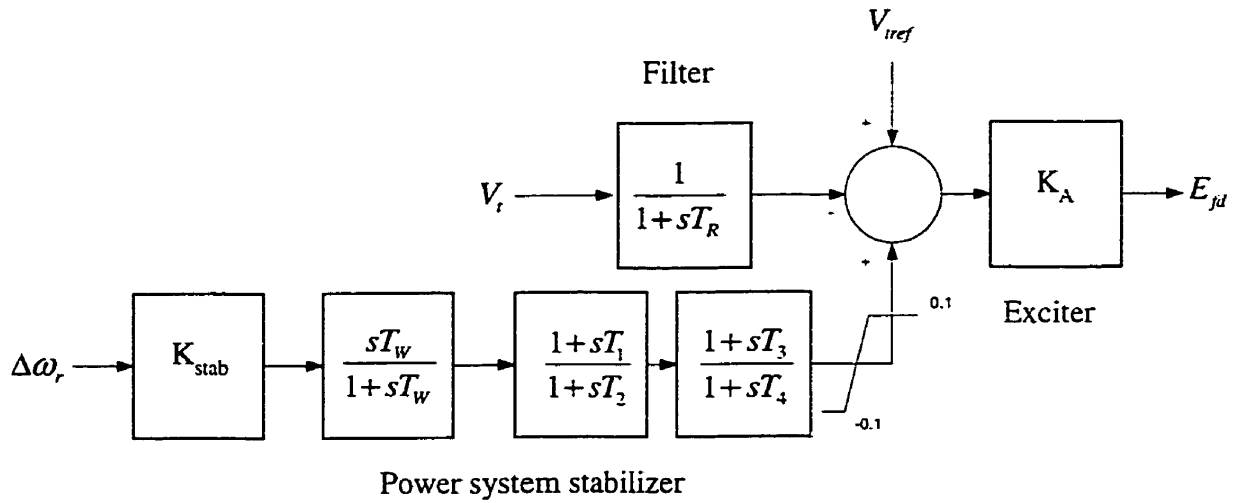
$$L_{2q} = 0.05833$$

$$r_{2q} = 0.021662$$

$$H(1) = 3.15 \quad H(2) = 3.5$$

A4-2. Power system stabilizer / Exciter model and parameters

Each of the generators is equipped with an exciter and a PSS.



$$K_{stab} = 9.5 \quad T_W = 10.0 \quad T_1 = 0.05 \quad T_2 = 0.02 \quad T_3 = 3.0 \quad T_4 = 5.4 \quad T_R = 0.02$$

A 4-3. UPFC parameters

DC link capacitor = 3000 μ F

Shunt inverter transformer is rated at 160 MVA, 345/66 kV, $X_l = 0.2$ per unit.

Series inverter transformer is rated at 160 MVA, 38.1/66 kV, $X_l = 0.04$ per unit.

A 4-4. Synchronous motor parameters

900 MVA, 20 kV Synchronous motor

$$X_{S1} = 0.14$$

$$X_{MDO} = 1.445$$

$$X_{230} = 0.0$$

$$X_{3D} = 0.0437$$

$$X_{2D} = 0.2004$$

$$X_{MQ} = 0.91$$

$$X_{2Q} = 0.106$$

$$R_{S1} = 0.0025$$

$$R_{2D} = 0.00043$$

$$R_{3D} = 0.0051$$

$$R_{2Q} = 0.00842$$

$$H = 1.0$$

References

- [1] N.G.Higorani, "Flexible AC Transmission," *IEEE Spectrum*, April 1993, pp. 40-45.
- [2] L.Gyugyi, "Unified power-flow concept for flexible ac transmission systems," *IEE Proceedings-C*, Vol. 139, No.4, July 1992, pp. 323-331.
- [3] E.Larsen, C.Bowler, "Benefits of thyristor controlled series compensation," *CIGRE*, 1992, 14/37/38-04.
- [4] E.V.Larsen, K.Clark, S.A.Miske, J.Urbaneck, "Characteristics and ratings considerations of thyristor controlled series compensation," *IEEE Transactions on Power Delivery*, Vol.9, No.2, April 1994.
- [5] K.Clark, B.Farannesh, "Thyristor controlled series compensation application study-control interaction considerations," *IEEE Transactions on Power Delivery*, Vol.10, No.2, April 1995, pp. 1031-1036.

- [6] L.G.Lajoie, E.V.Larsen, “ Hydro-qubec multiple SVC application control stability study,” *IEEE Transactions on Power Delivery*, Vol.5, No.3, July 1990, pp. 1543-1550.
- [7] N.Martins, N.J.P.Macedo, “ Control strategies for multiple static var compensators in long distance voltage supported transmission systems,” *IEEE Transactions on Power Systems*, Vol.8, No.3, August 1993, pp. 1107-1117.
- [8] Manzar Rahman, M.Ahmed, R.Gutmna, R.J.O’Keefe, R.Nelson, J.Bian, “ UPFC application on the AEP system: Planning Considerations,” *IEEE Transactions on Power Systems*, Vol.12, No.4. November 1997, pp.1695-1701.
- [9] A.J.F.Keri, X.Lombard, A.A.Edris, A.S.Mehraban, A.Elriachy, “ Unified Power Flow Controller (UPFC): Modeling and Analysis,” *PE-423-PWRD-0-06-1998*.
- [10] A.Arab, P.Kundur, “ A Versatile FACTS Device Model For Powerflow And Stability Simulations,” *IEEE Transactions on Power Systems*, Vol.11, No.4. November 1996, pp.1994-1950.
- [11] A.Nabavi-Niaki, M.R.Iravani, “ Steady-State and Dynamic Model Of Unified Power Flow Controller (UPFC) For Power System Studies”, *IEEE Transactions on Power Systems*, Vol.11, No.4. November 1996, pp.1937-1934.
- [12] C.R.Fuerte-Esquivel, E.Acha, “ Unified Power Flow Controller: A Critical Comparison of Newton-Raphson UPFC Algorithms in Power Flow Studies,” *IEE Proceedings-C Generation, Transmission and Distribution*, Vol.144, No.5. September 1997, pp.437-444.

- [13] K.S.Smith, L.Ran, J.Penman, “ Dynamic Modeling of a Unified Power Flow Controller” *IEE proceedings-Generation, Transmission and Distribution*, Vol.144, No.1, January 1997, pp. 7-12.
- [14] H.F.Wang, “Damping Function of a Unified Power Flow Controller” *IEE proceedings-Generation, Transmission and Distribution*, Vol.146, No.1, January 1999, pp. 81-87.
- [15] S.Limyingcharoen, U.D.Annakage, N.C.Pahalawaththa “Effects of Unified power flow Controller” *IEE proceedings-Generation, Transmission and Distribution*, Vol.145, No.2, March 1998, pp. 182-188.
- [16] R.Mihilac, P.Zunko, D.Povh, “ Improvement of Transient Stability Using Unified Power Flow Controller”, *IEEE Transactions on Power Delivery*, Vol.11, No.1, January 1996, pp. 485-491.
- [17] E.Lerch, D.Povh, R.Witzmann, H.Hlebcar, R.Mihilac “ Simulation and performance analysis of unified power flow controllers”, *CIGRE* 1994, 14-205, pp. 1- 6.
- [18] Wu.S, Z.Xiaoxin, Zhao He, Zhang Wento, “ Analysis and control simulation of unified power flow controller”, *Proceedings of the first international power electronics and motion control conference*, IPEMC-94, pp. 1105-1100.
- [19] K.R.Padiyar, K.Urna Rao, “ Modeling and Control of Unified power flow controller for Transient stability” *Electrical Power & Energy Systems*, Vol.21, 1999, pp.1-11.
- [20] S.Limyingcharoen, U.D.Annakage, N.C.Pahalawaththa “Fuzzy Logic based Unified power flow controllers for transient stability improvement” *IEE*

- proceedings-Generation and Distribution*, Vol.145, No.3, May 1998, pp. 225-232.
- [21] K.K.Sen, E.J.Stacey “ UPFC-Unified power flow controller: theory, Modeling and Applications”, *IEEE Transactions on Power Delivery*, Vol.13, No.4, October 1998, pp. 1453-1459.
- [22] L.Gyugyi, C.D.Schauder, S.L.Williams, T.R.Reitman, D.R.Torgerson, A.Edris “ The Unified Power Flow Controller: A new approach to power transmission control”, *IEEE Transactions on Power delivery*, Vol.10, No.2, April 1995, pp. 1085-1097.
- [23] K.R.Padiyar, A.M.Kulkarni, “ Control design and Simulations of Unified Power Flow Controller”, *IEEE Transactions on Power Delivery*, Vol.13, No.4. October 1998, pp.1348-1354.
- [24] Y.Morioka, M.Kato, Y.Nakachi, M.Asada, K.Tokuhara, “ Implementation of Unified Power Flow Controller and Verification for Transmission capability improvement”, *IEEE Transactions on Power Systems*, Vol.14, No.2. May 1999, pp.575-581.
- [25] M.Toufan, U.D.Annakkage “ Simulations of the Unified Power Flow Controller performance using PSCAD-EMTDC” *Electric Power Systems Research*, Vol.46, 1998, pp. 67-75.
- [26] Z.Huang, Y.Ni, F.Wu, S.Chen, B.Zhang, “ Application of Unified power flow controller in interconnectd power systems-Modeling, interface, control strategy and case study” *IEEE Transactions on Power Systems*, Vol.15, No.2. May 2000, pp.817-824.

- [27] I.Papic, P.Zunko, D.Povh, " Basic Control of Unified Power Flow Controller" *IEEE Transactions on Power Systems*, Vol.12, No.4. November 1997, pp. 1734-1739.
- [28] J.Bian, D.G.ramey, R.J.Nelson, A.Edris " A study of equipment sizes and constraints for a Unified power flow controller" *IEEE Transactions on Power Delivery*, Vol.12, No.3. July 1997, pp. 1385-1391.
- [29] C.D.Schauder, D.M.hamai, A.Edris, L.Gyugyi, T.R.reitman, M.R.Lund, D.R.Torgerson " Operation of the Unified power flow controller (UPFC) under practical constraints", *IEEE Transactions on Power Delivery*, Vol.13, No.2, April 1998, pp. 630-639.
- [30] S.D.Round, Q.Yu, L.E.Norum, T.M.Undeland " Performance of a Unified Power flow controller using a D-Q Control system" *Sixth International Conference on AC & DC Transmission*, No.423. 1997, pp. 357-362.
- [31] A.Daneshpooy, A.M.Gole, D.G.Chapman, J.B.Davies " Fuzzy Logic control for HVDC Transmission" *IEEE Transactions on Power Delivery*, Vol.12, No.4, October 1997, pp. 1690-1697.
- [32] X.Lombard, P.G.Thernod " Control of Unified power flow controller: Comparison of methods on the basis of a detailed numerical model", *IEEE Transactions on Power Systems*, Vol.12, No.2. May 1997, pp.824-830.
- [33] R.J.Nelson, J.Bian, D.G.Ramey, T.A.Lemak, T.R.Reitman, J.E.Hill " Transient Stability enhancement with FACTS controllers" *Sixth International Conference on AC & DC Transmission*, No.423. 1997, pp. 269-273.

- [34] S.A.Al-mawasawi, A.Coonick “ Analysis, Simulation and implementation of PWM based UPFC ” *Sixth International Conference on AC & DC Transmission*, No.423. 1997, pp. 220-225.
- [35] L.Hu, R.E.Morrison “ Simulation study of a transmission system containing two unequally rated parallel lines and a UPFC” *Sixth International Conference on AC & DC Transmission*, No.423. 1997, pp. 346-350.
- [36] P.Kundur, “ Power system stability and control”, EPRI, Power system Engineering series. 1994.
- [37] J.Lunze, “ Robust Multivariable feedback control “, Prentice-Hall.
- [38] C.C.Lee, “ Fuzzy logic in control systems: fuzzy logic controller Part-I and part-II”, *IEEE Transactions on System, Man and Cybernetics*, Vol. 20, No.2, March 1990, pp. 404-435.
- [39] C.Schauder “ Vector analysis and control of advanced static var compensators” *IEE proceedings –C*, Vol.140, 1993, pp. 299-306.
- [40]. Mohan.N, T.M.Undeland, W.P.Robbins, “Power Electronics, Converters, Applications and design”, Second edition 1995.
- [41] K.Sreenivasachar, S.Jayaram, M.M.A.Salama “ Dynamic Stability improvement of multi-machine power system with UPFC” *Electric Power System Research*, Vol.55 (2000), pp. 27-37.
- [42] N.G.Hingorani, L.Gyugyi “Understanding FACTS: Concepts and technology of Flexible AC Transmission systems, *IEEE Press*, 2000.
- [43] C.Schauder, E.Stacey, M.Lund, A.Keri, A.Mehraban, A.Edris, L.Gyugyi, L.Kovalsky “ AEP UPFC Project: Installation, Commissioning and Operation of

- the ± 160 MVA STATCOM (phase I)" *IEEE Transactions on Power Delivery*, Vol.13, No.4, October 1998, pp. 1530-1535.
- [44] P.W.Lehn, M.R.Iravani " Experimental Evaluation of STATCOM Closed Loop Dynamics" *IEEE Transactions on Power Delivery*, Vol.13, No.4. October 1998, pp.1378-1384.
- [45] H.Akagi, Y.Kanazawa, A.Nabae " Instantaneous reactive power compensators comprising switching devices without energy storage components" *IEEE Transactions on Industry Applications*, Vol.20, No.3, May/June 1984, pp. 625-630.
- [46] L.Gyugyi, N.H.Hingorani, P.R.nannery, N.Tai " Advanced static var compensators using gate-turn-off thyristors for utility applications" *CIGRE*, 23-203, 1990 Session.
- [47] E.Uzunovic, C.Canizeres, J.Reeve " Fundamental frequency Model of Unified Power flow controller" *North American Power Symposium (NAPS)*, Cleveland, Ohio, October 1998, pp. 294-299.
- [48] E.Uzunovic, C.Canizeres, J.Reeve " EMTP Studies of UPFC power oscillation damping" *North American Power Symposium (NAPS)*, San Luis Obispo, California, October 1999.
- [49] E.Larsen, N.Miller, " Benefits of GTO-based compensation for electric utility applications", *IEEE Transactions on Power delivery*, Vol.7, No.4, Oct 1992, pp. 2056-2062.

- [50] L.Gyugyi, C.D.Schauder, K.K.Sen “ Static Synchronous Series Compensator: Solid State Approach to the series compensation of transmission lines” *IEEE Transactions on Power delivery*, Vol. 12, No.1, January 1997, pp. 406-417.
- [51] L.Malesani, L.Rossetto, P.Tenti,P.Tomasin “ AC/DC/AC PWM convertor with reduced energy storage in the DC link” *IEEE Transactions on Industry Applications*, Vol.31, No.2, March/April 1995, pp. 287-292.
- [52] M.Klein, G.J.Rogers, P.Kundur “ A Fundamental Study of Inter-area oscillations in power systems” *IEEE Transactions on Power Systems*, Vol.6, No.3, August 1991, pp. 914-921.
- [53] M.R.Iravani, D.Maratukulam, “ Review of semiconductor-controlled (static) Phase shifters for power system applications”, *IEEE Transactions on Power Systems*, Vol.9, No.4, Nov 1994, pp. 1833-1839.
- [54] C.Schauder, M.Gernhardt, E.Stacey, T.W.Cease, A.Edris “ Development of a ± 100 Mvar static condenser for voltage control of transmission systems”, *IEEE Transactions on Power Delivery*, Vol.10, No.3, July 1995, pp. 1486-1496.
- [55] L.Gyugyi, “ Dynamic compensation of AC transmission lines by solid state synchronous voltage sources” *IEEE Transactions on Power Delivery*, Vol.9, No.2, April 1994, pp. 904-911.
- [56] D.N.Kosterev, W.A.Mittelstadt, R.R.Mohler, W.J.Kolodziej, “An Application study for sizing and rating controlled and conventional series compensation” *IEEE Transactions on Power Delivery*, Vol.11, No.2, April 1996, pp. 1105-1111.